**Defining novel mediators and mechanisms of neural microvasculature permeability**

Bridget-Ann Kenny

Thesis submitted in fulfilment for the degree of Doctor of Philosophy

University College London (UCL)

Institute of Ophthalmology

Supervisor: Dr Patric Turowski

Secondary Supervisor: Prof Clare Futter

## DECLARATION

I, Bridget-Ann Kenny, confirm that the work presented in this thesis is my own. Where information has been derived from other sources, I confirm that this has been indicated in the thesis.

# ACKNOWLEDGEMENTS

# ABSTRACT

The microvasculature of the nervous system is exceptionally specialised and its restrictive nature implied by its moniker, blood-brain barrier (BBB), with blood-retinal barrier (BRB) relating to the retinal vasculature. The importance of these barriers is evident during disease states where their functionality is compromised, as in diabetic retinopathy (DR). Due to the complexity of circulating and local mediators with signalling potential at these barriers, and the lack of adequate treatment for some disorders with microvasculature disturbances, there is scope for enriching the knowledge base in this area. With DR as a starting point, it was hypothesised that there were factors other than vascular endothelial growth factor (VEGF) involved in disease progression. It was shown that a bioactive lipid, lysophosphatidylcholine (LPC), enhanced junctional permeability at both the BBB and BRB, doing so via VEGF receptor 2 (VEGFR2) activation thus implicating a transactivation mechanism. It followed that such a mechanism might be involved in the actions of other vascular mediators, bradykinin (BK), lysophosphatidic acid (LPA), thrombin (THR) and TNF-α, and the data shown suggests that this may be the case for more than one of the mediators tested. The former set of data also indicated the presence of transcellular transport across the BBB, the existence of which is highly contested within the literature, and a subsequent aim, investigating the extent of transcytosis for a range of pertinent mediators, was addressed, and for which novel multicellular BBB models were developed and characterised. Finally, in connection with the vesicular process observed for mediators tested, VE-Cadherin (VEC) internalisation, hypothetically to vesicular structures, was tested following ICAM-1 adhesion, as it is key to leukocyte migration via VEC modulation. This cumulative work demonstrates novel roles for LPC-induced permeability, VEGFR2 transactivation by vasoactive stimuli, transcytosis and VEC internalisation at the BBB.

# TABLE OF CONTENTS

**LIST OF FIGURES**

**LIST OF TABLES**

## ABBREVIATIONS

ABC transporters    ATP-binding cassette transporters

AC                  astrocyte

AJs                 adherens junctions

APOE4               astrocyte-secreted apolipoprotein E 4

APS                 ammonium persulfate

ATP                 adenosine tri-phosphate

AVA                 arteriovenous anastomoses

BBB                 blood-brain barrier

bFGF                basic fibroblast growth factor

BK                  bradykinin

BM                  basement membrane

BRB                 blood-retinal barrier

BSA                 bovine serum albumin

$Ca^{2+}$           calcium

CAD                 coronary artery disease

CBF                 cerebral blood flow

| | |
|---|---|
| CD | cluster of differentiation |
| cGMP | cyclic guanosine-3', 5-monophosphate |
| CLEM | correlative light and electron microscopy |
| CMC | critical micelle concentration |
| CNS | central nervous system |
| $CO_2$ | carbon dioxide |
| COP | colloid osmotic pressure |
| CVD | cardiovascular disease |
| DAB | diaminobenzidine |
| DEOX | L-methamphetamine |
| DMEM | Dulbecco's modified eagle's medium |
| DMO | diabetic macular oedema |
| DMSO | dimethyl sulfoxide |
| DNase1 | Deoxyribonuclease 1 |
| DR | diabetic retinopathy |
| DTT | dithiothreitol |
| EC | endothelial cell |

| | |
|---|---|
| ECIS | electric cell substrate impedance sensing |
| ECL | enhanced chemiluminescence |
| EDHF | endothelium-derived hyperpolarising factors |
| EDRF | endothelium-derived relaxing factors |
| EDTA | ethylenediaminetetraacetic acid |
| EGFR | epidermal growth factor receptor |
| EM | electron microscopy |
| eNOS | endothelial NOS |
| EPCR | endothelial protein C receptor |
| F-actin | filamentous actin |
| FBS | foetal bovine serum |
| FCS | foetal calf serum |
| FFA | free fatty acids |
| FFA BSA | bovine serum albumin-fatty acid free |
| FITC | fluorescein isothiocyanate |
| GA-1000 | gentamicin sulphate/amphotericin-B |
| G-actin | globular actin |

| | |
|---|---|
| GFAP | glial fibrillary acidic protein |
| GFP | green fluorescent protein |
| GPCR | G-protein-coupled receptor |
| GPNT | GP8 newly transformed (immortalised rat brain microvascular endothelial cells) |
| GTPase | guanosine triphosphatase |
| $H_2O_2$ | hydrogen peroxide |
| H2S | hydrogen sulphide |
| HBSS | Hank's buffered saline solution |
| hCMEC/D3 | human cerebral microvascular endothelial cell |
| HDL | high density lipoprotein |
| hEGF | human epidermal growth factor |
| HEPES | N-2-hydroxyethylpiperazine-N-2-ethane sulfonic acid |
| hFGF | human fibroblast growth factor |
| HPV | hypoxic pulmonary vasoconstriction |
| HRP | horseradish peroxidase |
| HSPGs | heparan sulfate proteoglycans |

| | |
|---|---|
| HUVEC | human umbilical vein endothelial cell |
| ICAM-1 | intercellular adhesion molecule-1 |
| IGF | insulin growth factor |
| IL | interleukin |
| IP3 | inositol triphosphate |
| JAM | junctional adhesion molecule |
| JNK | c-Jun N-terminal kinase |
| kDa | kilodalton |
| LB | Luria broth |
| LDL | low density lipoprotein |
| LPA | lysophosphatidic acid |
| LPC | lysophosphatidylcholine |
| Lp-PLA$_2$ | lipoprotein-associated PLA$_2$ |
| LPR1 | low-density lipoprotein receptor-related protein 1 |
| LSR | lipolysis stimulated lipoprotein receptor |
| MAPK | mitogen-activated protein kinase |
| MET | methamphetamine |

| | |
|---|---|
| MFSD2A | major facilitator superfamily domain-containing 2a |
| MMP | matrix metalloproteinase |
| MVEC | microvascular endothelial cell |
| NA | noradrenaline |
| NEFA | nonesterified fatty acid |
| NO | nitric oxide |
| NOS | nitric oxide synthases |
| NVU | neurovascular unit |
| OPD | o-phenylenediamine |
| PAI-1 | plasminogen-activator inhibitor type 1 |
| PAR | protease activated receptor |
| PBS | phosphate buffered saline |
| PC | pericyte |
| PCR | polymerase chain reaction |
| PDGFRβ | platelet-derived growth factor receptor-β |
| PET | polyethylene terephthalate |
| PFA | paraformaldehyde |

PFU          plaque formation unit

PGl2          prostacyclin

PI3K/Akt          phosphatidylinositol 3-kinase/Akt

PKC          protein kinase c

$PLA_2$          phospholipase $A_2$

PLNC          peripheral lymph node cells

PTK/ZK          PTK787/ZK

PV-1          plasmalemmal vesicle associated protein-1

PVDF          polyvinylidene difluoride

Rab          Ras-related proteins in brain

Rho          ras homology gene family member

ROS          reactive oxygen species

RTK          receptor tyrosine kinase

SDS          sodium dodecyl sulphate

SDS-PAGE          sodium dodecyl sulphate-polyacrylamide gel electrophoresis

SIM          super-resolution microscopy

SLCs          solute carriers

| | |
|---|---|
| Src | sarcoma tyrosine kinase |
| TAE | tris-acetate-EDTA |
| TAMPs | TJ associated marvel domain containing protein family |
| TBS | tris buffered saline |
| TEER | transendothelial electrical resistance |
| TEM | transendothelial migration |
| TEMED | tetramethylethylene diamine |
| TF | tissue factor |
| TGF-$\beta$ | transforming growth factor-$\beta$ |
| TGF$\beta$R2 | TGF-$\beta$ receptor 2 |
| THR | thrombin |
| TJs | tight junctions |
| TLCK | N$\alpha$-Tosyl-L-lysine chloromethyl ketone hydrochloride |
| TLR | toll like receptor |
| TM | thrombomodulin |
| TNF-$\alpha$ | tumour necrosis factor-$\alpha$ |
| tPA | tissue plasminogen activator |

TSAd            T cell-specific adaptor

TSM             transmembrane

TW              transwell

TX-100          triton X-100

VCAM-1          vascular cell adhesion molecule-1

VEC             vascular endothelial-cadherin

VEGF            vascular endothelial growth factor

VEGFR           vascular endothelial growth factor receptor

VP              virus particle

vWF             von Willebrand factor

XL              cross-linking

ZO              zonula occludens proteins

# Chapter 1   INTRODUCTION

## 1.1   Cardiovascular system

### 1.1.1   The neural microvasculature: one facet of the cardiovascular system

There are many disorders which would benefit from a greater understanding of how the neural microvasculature works, either because the aetiology incorporates a disturbance of the barrier or the disease is rooted within the central nervous system (CNS) and beyond reach of treatment, but it remains incompletely understood. A detailed investigation of neural endothelial function, specifically transport mechanisms, may provide insights which would enhance the current knowledge base and possibly inform relevant therapies. This thesis examines neural microvasculature barriers which, although has specialisms designating it from other microvascular beds, shares some basic characteristics that are found throughout the vasculature. I shall therefore provide an outline of vascular structure and function as a whole before describing specialisations of different beds.

#### 1.1.1.1 The vasculature

The importance of the cardiovascular system is reflected in its early development in the vertebrate embryo, beginning approximately three weeks after conception (Schleich 2002). This ensures tissue viability as the embryo grows, allowing for rapid transport of oxygen, nutrients and waste products throughout, because simple diffusion would no longer sufficiently cover the level of transport required. The vascular half of the cardiovascular system will nevertheless continue to rely on simple diffusion in order to move macromolecules and cells between the parenchyma and the bloodstream (Cines et al. 1998).

The pulmonary and systemic circulations are connected in series, with the right heart perfusing the former and the left heart perfusing the latter. The pulmonary circulation moves through the lungs, bringing oxygenated blood back to the heart for subsequent

ejection to the systemic circulation. It is the systemic circulation which then feeds the tissues of the body, in addition to collecting waste and deoxygenated blood (Stefanovska and Bracic 1999). Regarding both the pulmonary and the systemic circulation, blood flow proceeds through arteries via progressively smaller branching vessels, eventually arriving at the level of the capillary. The decreasing size of the vessel is accompanied by a concomitant increase in the resistance to blood flow, slowing down the blood thereby ensuring sufficient time for exchange of gases, nutrients and wastes within capillaries. Capillaries then converge to form venules, with repeated convergence forming larger veins that return to the heart (Fishman 1982). These are all dynamic vessels which both provide a "nonthrombogenic conduit for blood flow" and continuously adapt to the changing mechanical, haemodynamic, neural or paracrine microenvironment (Martinez-Lemus, Hill and Meininger 2009, Vito and Dixon 2003).

In terms of structure, all levels of blood vessel excluding capillaries, smaller arterioles and venules, consist of three layers, the tunica intima, the tunica media and the tunica adventitia (Jain 2003). The tunica intima, or innermost coat, pertains largely to an endothelial cell monolayer, a flattened sheet of elongated cells that line the lumen of the vessel in the direction of flow (Vito and Dixon 2003). The tunica media, or middle coat, is composed of smooth muscle cells embedded in an elastin-collagen matrix. It generally occupies the greatest proportion of the vessel's size supplying mechanical strength and contractile power (Martinez-Lemus et al. 2009). The tunica adventitia, or outer coat, is a connective tissue sheath responsible for keeping the enclosed vessel in place within the parenchyma. As well as collagen bundles, elastic fibres and fibroblasts, the tunica adventitia frequently contains perivascular nerve endings and, in larger vessels, small blood vessels called vasa vasorum (Majesky et al. 2011).

The mature vasculature functions in part due to the variety of specialized vessels that exist, each usually with auxiliary roles to blood conduction. This specialization arises from a combination of mural cell recruitment, extracellular matrix generation and

vessel wall differentiation (Jain 2003). For example, the pliable nature of the conducting arteries into which the heart ejects blood during systole allows them to temporarily store blood and mechanical energy, ensuring blood flow is then continuous during diastole, hence the term 'elastic arteries' (McEniery, Wilkinson and Avolio 2007).

These larger arteries branch into 'conduit arteries', with a thicker wall relative to the lumen due to additional smooth muscle, conducting blood flow with relatively little resistance towards specific organs (Pugsley and Tabrizchi 2000). On approaching smaller arteries and arterioles, because the lumen narrows and the number of vessels remains relatively low, the resistance to blood flow increases. These 'resistance arteries' regulate blood flow, modulate blood pressure and dictate the regional distribution of blood (Martinez-Lemus 2012). When they dilate, resistance to flow falls and blood flow increases within the tissues they feed. When they constrict, resistance to blood flow increases and the blood flow to the same tissues is decreased (Ellis, Jagger and Sharpe 2005). Even narrower, the terminal arterioles are the last arterial vessels with smooth muscle in the cell wall and their contractile state regulates the number of capillaries that are well perfused. A capillary is 'open' when its upstream arteriole is dilated and 'closed', or flow of blood is slowed, when the same arteriole is constricted. At any one moment in many resting tissues, terminal arterioles may be dilated or constricted and this can produce an uneven distribution of flow to the tissue via the capillaries, a characteristic known as the 'heterogeneity of tissue perfusion' (Pries and Secomb 2009). The term 'exchange vessel' primarily encompasses the capillaries however, as gaseous exchange can occur through the arteriolar wall, and fluid exchange can occur in post-capillary venules, it can also include the microvessels immediately upstream and downstream of the capillaries. Within the exchange vessels there is a very low resistance to flow due to the huge number of capillaries running in parallel enabling a functional transit time for gaseous and nutrient exchange. Finally, venous 'capacitance vessels' act as blood reservoirs, these thin walled vessels exist in such large numbers that they are

responsible for holding approximately two-thirds of the circulating blood at any one time (Rothe 1983, Sugawara et al. 2014).

*1.1.1.2 Intrinsic regulation of vascular tone*

Vascular smooth muscle supplies tension to the blood vessels it surrounds, a characteristic required by the vasodilators and vasoconstrictors which act upon it. As described above, this vascular tone regulates the resistance of the vessel and, as a consequence, the flow of blood through it. Vascular tone is controlled both intrinsically and extrinsically, with intrinsic mechanisms analogous to local mechanisms serving local needs. At the interface between the blood and parenchyma, the endothelium is in a prime local position to modulate vascular tone, as well as general vascular function and homeostasis. The endothelium can both secrete and respond to an array of paracrine factors which elicit vasodilatory or vasoconstrictor effects via smooth muscle cells, the balance of which shapes vascular tone (Sumpio, Riley and Dardik 2002). Vasodilators include nitric oxide (NO) and prostacyclin (PGl$_2$), which are grouped together as endothelium-derived relaxing factors (EDRF), as well as hydrogen peroxide (H$_2$O$_2$) and hydrogen sulphide (H$_2$S) which are grouped together as endothelium-derived hyperpolarising factors (EDHF) (Palmer, Ferrige and Moncada 1987, Bos et al. 2004, Matoba et al. 2002, Mustafa et al. 2011). Vasoconstrictors include endothelin-1, catecholamines, angiotensin II and thromboxanes (Bellomo and Giantomasso 2001, Kim and Iwao 2000, La and Reid 1995, Feletou, Huang and Vanhoutte 2010).

Nitric oxide synthases (NOS) use the amino acid L-arginine and molecular oxygen as substrates for the production of NO and L-citrulline, in the presence of certain cofactors. There are three NOS isoforms, neuronal NOS, inducible NOS and endothelial NOS (eNOS) each with diverse functions such as synaptic plasticity, non-specific immune defense and maintenance of vascular tone respectively. As the predominant isoform expressed in the endothelium, eNOS can be indirectly activated by mediators which trigger a rise in intracellular calcium (Ca$^{2+}$) concentrations (Förstermann and Sessa 2012). The main stimulus for NO production by eNOS is

fluid shear stress resulting in eNOS phosphorylation but there are a number of other mediators including circulating VEGF-A, BK and oestrogen (Schleicher et al. 2009, Fulton et al. 1999, Fleming and Busse 2003, Boo et al. 2002). In relation to basal vascular tone, once NO has been synthesised it diffuses across the endothelial cell (EC) wall into adjacent smooth muscle cells where it activates the soluble pool of guanylate cyclase, increasing production of cyclic guanosine-3', 5-monophosphate (cGMP) and decreasing smooth muscle tension (Sandoo et al. 2010). A combination of these eNOS activation mechanisms continuously operate thus ensuring NO production and maintenance of basal vascular tone.

A second intrinsic regulatory mechanism of vascular tone is the Bayliss myogenic response which describes the change in vessel diameter occurring in response to changes in intravascular pressure (Brozovich et al. 2016). Generally, flow and pressure are linearly related but in arterioles, and occasionally in arteries, venules and veins, after a sharp rise in blood pressure, although the pressure initially distends the vessel, the vessel reacts and undergoes a well-sustained contraction within seconds (Davis and Hill 1999). The opposite occurs for a fall in blood pressure. Such a response can be critically important in certain vascular beds, *i.e.* the brain and heart, but it is absent in the skin, where vascular tone is intrinsically regulated by temperature. The interaction of the myogenic response with the presence of vasoactive mediators enables certain vascular beds to maintain a constant blood flow over a wide range of perfusion pressures, and represents a third intrinsic regulatory mechanism known as autoregulation (Walsh and Cole 2013). Autoregulation allows tissues to ensure even perfusion despite situations of hypotension or hypertension (Brozovich et al. 2016).

*1.1.1.3 Extrinsic regulation of vascular tone*

Extrinsic regulatory mechanisms of vascular tone are directed from outside the tissue, and are delivered by efferent motor neurons and circulating hormones. The sympathetic vasoconstrictor nerves, as opposed to the parasympathetic, are responsible for the bulk of the neural regulation, with postganglionic noradrenergic

fibres innervating the vessels (Brock, Cunnane 1993). Noradrenaline (NA) is released from axon terminals activating $\alpha_1$-adrenoceptors, found on most blood vessels, leading to vasoconstriction. The signal is then swiftly terminated mainly by NA reuptake, but also by NA diffusion into the bloodstream (Sun 1995). Vasodilatation can occur either as the product of reduced sympathetic activity, the activation of $\beta$-adrenergic receptors or via feedback mechanisms at the nerve terminals, reflecting secreted NA levels or the metabolic microenvironment (Levick 1991b). Sympathetic nerves are tonically active, albeit at a low frequency in humans, which means that all of the tissues which they innervate are under some degree of continuous constriction making a significant contribution towards basal vascular tone (Malpas 1998). Importantly it is the arteries, and to a lesser extent the veins, which receive innervation and as the vessels get smaller, *i.e.* with decreasing arteriole size, vessels are more frequently subject solely to intrinsic regulatory mechanisms.

Hormonal regulation of vascular tone is more likely to come into play during pathological or non-physiological situations. Adrenaline circulates at a low basal concentration but its secretion is stimulated during situations of fight or flight, hypotension, hypoglycaemia and exercise. In addition to causing vasoconstriction in the skin and intestinal tissues, and vasodilation in both the skeletal muscle and the heart muscle, adrenaline also results in glucose being released into the bloodstream. Circulating insulin binds the insulin receptor on ECs and produces a vasodilatory effect in healthy people (Kusters and Barrett 2016). Insulin stimulates the phosphatidylinositol 3-kinase/Akt (PI3K/Akt) pathway to activate eNOS and NO production (Zeng and Quon 1996, Jiang et al. 1999, Cardillo et al. 1999). It can also stimulate mitogen activated protein kinase (MAPK) signalling, enhancing production of endothelin-1 producing vasoconstriction (Kusters and Barrett 2016). In people with diabetes, there is either a lack of insulin or a resistance to it and this can lead to atheroma and associated endothelial and vascular disturbances. It has been shown that the PI3K, in diabetic and obese patients, is selectively inhibited by associated low-grade inflammation, free fatty acids (FFA) and oxidative stress (Kusters and Barrett 2016).

**1.1.2 Endothelial cells**

A monolayer of ECs lines the blood-parenchymal interface of the entire cardiovascular system, providing a huge surface area for an array of basal and reactive functions, and is a dynamic, heterogeneous organ. Not only is the endothelium different at a morphological level between different vessels but such differences also exist between different vascular beds (Fishman 1982, Weibel and Palade 1964). This heterogeneity contributes to the maintenance of adaptive processes as well as the development of disorders that are restricted to a particular vascular bed (Cines et al. 1998). Allowing for these variations, ECs are typically flat, approximately 3 µm thick at the nucleus to 0.2 µm thick at the cell periphery, and elongated, approximately 30 µm long by 10 µm wide (Florey 1966). They align in the direction of blood flow along straight passages of arteries but not at branch points (Aird 2007). Particular structural features of ECs will be discussed later on in relation to the neural microvasculature, features such as proteins contributing to junction regulation and transcytosis, as they are of particular relevance to the current thesis.

*1.1.2.1 Structural features*

In its capacity as a barrier, ECs typically organise and maintain robust, yet dynamic, cell-cell and cell-matrix adhesions. These interactions would falter without equally robust, yet dynamic, intracellular scaffolding provided by intermediate filaments, microtubules, actin filaments (Filamentous actin or F-actin) and their myriad of accessory proteins (Revenu et al. 2004). Given the disparity between barrier function within different vascular beds, depending on whether the endothelium is continuous, discontinuous or fenestrated, the role these proteins plays in intracellular organisation can vary a lot (Prasain and Stevens 2009). Generally, intermediate filaments provide mechanical strength while microtubules direct intracellular transport and determine the positions of intracellular organelles. For the present discussion, F-actin is of most importance as it is fundamental for cytoskeletal scaffolds and determining cell shape and movement. F-actin exists in an equal balance with its globular actin (G-actin)

components which polymerise to form double stranded helical polymers of F-actin (Stossel et al. 1985). These polymers then contribute to the organisation of cytoskeletal scaffolds such as the membrane skeleton and stress fibres which, despite being distinct structures, interact through the coordination of intermediary proteins. The actin cytoskeleton associates directly with adhesion proteins at cell-cell junctions, playing a crucial role in adherens junction (AJ) assembly and organisation as well as assembly and stabilisation of tight junctions (TJ) (Prasain and Stevens 2009).

Within continuous endothelium, and mainly at the capillary level, the principal fluid-conducting pathway is via intercellular clefts. The summed cell perimeters of 1 cm$^2$ of endothelium equates to 12-20 m of which 90% is sealed by adhesion proteins. The remaining breaks in this seal are 200-400 nm in length, occur every 2-4 µm and, along the length of the cells, are 14-21 nm wide, providing a tortuous pathway for fluid and plasma proteins (Levick and Michel 2010). The frequency of intercellular clefts is variable between different vessel types and vascular beds for example post-capillary venules, as a prominent site for fluid exchange, have more intercellular clefts while there are no such clefts within the neural microvasculature.

As blood vessels are multicellular, excellent cell-cell communication is important so that they can operate as a unit. Some cell-cell regulatory mechanisms were described earlier; gap junctions are an additional mechanism coordinating direct cell-to-cell communication (Figueroa and Duling 2009). Gap junctions exist between adjacent ECs as well as between ECs and vascular smooth muscle cells allowing passage of ions such as $Ca^{2+}$ and chemical messengers such as inositol triphosphate ($IP_3$). Six connexin proteins, of which there are four: Cx37, 40, 43 and 45, assemble to make a connexon within a cell's plasma membrane and the association of connexons on two opposite cells forms a functional gap-junction intercellular channel (Figueroa and Duling 2009). Connexin expression varies according to vessel type and vascular bed and has been found to be altered in some disorders displaying vascular pathology such as hypertension and diabetes (Figueroa and Duling 2009).

The glycocalyx decorates the luminal surface of the endothelium, including the entrance to intercellular clefts and fenestrations, with a matrix of carbohydrate-rich membrane bound macromolecules which impart a net negative charge. Additional soluble molecules, either blood-borne or produced by the endothelium, are incorporated within this matrix through cationic elements thus extending the structure to form an 'endothelial glycocalyx layer' (Weinbaum, Tarbell and Damiano 2007). Generally, the thickness of the layer varies with vascular diameter, in capillaries it has been measured to be between 0.2 and 0.5 µm thick, while in small arteries it increases to between 2 and 3 µm thick and to 4.5 µm thick in the carotid arteries (van den Berg, Vink and Spaan 2003, Reitsma et al. 2007). Based on electron microscopy (EM) studies, the organisation of the glycocalyx is such that the various polymers are associated in a bush-like tuft at 100 nm intervals, all of which are intracellularly connected to the actin cytoskeleton under the membrane surface as well as to actin stress fibres connecting the luminal surface with the basal (Weinbaum et al. 2007). The combination of a vibrant mix of soluble matrix residents and robust connections to the intracellular EC compartment makes the glycocalyx a powerful force in EC functionality. It contributes to EC permeability as a molecular sieve for plasma proteins, simultaneously creating the forces which direct transcapillary fluid exchange. It operates as a mechano-sensor for fluid shear stress, and when damaged, can contribute to impaired EC regulation *i.e.* NO production. It also functions as a platform for EC sensation of the microenvironment (Weinbaum et al. 2007, Reitsma et al. 2007).

*1.1.2.2 Endothelial functions*

The functions of the endothelium are many and varied, with some restricted to certain vascular beds. The most conspicuous role for the endothelium is that of regulating blood-tissue exchange across its semi-permeable membrane, allowing nutrients to move into the parenchyma and wastes to enter the bloodstream. However, as permeability is of particular relevance to this thesis it will be covered in more detail later on. Regulation of vascular tone is performed, in part, by the endothelium and was described earlier in this section.

In addition to these functions, the endothelium is essential for ensuring haemostasis, that blood is maintained in a fluid state within the circulation and, when a breech occurs, promoting limited clot formation. It expresses a repertoire of pro-coagulant as well as anti-coagulant proteins with any systemic imbalances resulting from congenital or acquired abnormalities contributing to pathology, some of which can prompt catastrophic damage *i.e.* deep vein thrombosis. Natural anti-coagulants include blood flow, non-activated cell surface membranes, thrombomodulin (TM), tissue plasminogen activator (tPA), NO, endothelial protein C receptor (EPCR) and heparin. Natural pro-coagulants include vessel damage, plasminogen-activator inhibitor type 1 (PAI-1), tissue factor (TF), von Willebrand factor (vWF) and protease activated receptors (PARs) (Aird 2007). The localised nature of phenotypic insults despite systemic hypercoagulable states emphasises the role that the endothelium plays in haemostatic balance. The endothelium directs the expression of these proteins in response to the extracellular milieu *i.e.* hypoxia increases PAI-1 expression and decreases tPA expression, VEGF-A increases TM, PAI-1 and tPA expression and TNF-α decreases TM but increases PAI-1 and TF expression (Rosenberg and Aird 1999). At the same time, the expression of these proteins can vary throughout the vascular tree and also over time *i.e.* EPCR is mainly expressed in larger vessels while TM is highly expressed in virtually all vessels of all vascular beds except in the neural vasculature where expression is low (Aird 2007). Similarly, ECs of different vascular beds can respond differently to the same signal for example, increased blood flow increases NO in the aortic endothelium but not in that of the pulmonary artery (Rosenberg and Aird 1999). Endothelial responses to the extracellular milieu are shaped insomuch that ECs are able to transduce the signals.

The endothelium actively participates in immunological responses, initiating a rapid response against pathogens and injuries which is rapidly resolved following pathogen elimination and restoration of the local tissue. EC's ability to mount a response involves a change in phenotype from a 'resting' state, where haemostasis and vascular tone is maintained, permeability is tightly controlled and circulating leukocytes are maintained in a quiescent state, to an 'activated' one (Pober and Sessa

2007). When faced with inflammatory stimuli ECs become activated along two time frames, one which is relatively immediate and another which develops over a few hours as it relies on new gene expression. In response to G-protein-coupled receptor (GPCR) binding, by histamine or thrombin for example, a chain of intracellular signalling is initiated resulting in the alteration of junctional adhesion proteins promoting junctional permeability, the fusion of Weibel-Palade bodies with the cell membrane thus exposing P-selectin to capture passing leukocytes and also upregulated enzyme action increasing production and secretion of vasodilators such as NO and prostaglandin, increasing blood flow and bringing leukocytes to the area. As signals resulting from GPCR binding last 10-20 min before receptors are desensitised, an inflammatory response would be severely limited without other avenues of response. An increase in local cytokine production, TNF-α and interleukin-1 (IL-1), via macrophages and other incoming activated leukocytes extends the time course of the inflammatory response. On cytokine binding, newly formed intracellular signalling complexes trigger transcription factor activation and subsequent gene transcription and translation of pro-inflammatory proteins. Cell surface adhesion molecules, intercellular adhesion molecule-1 (ICAM-1), vascular cell adhesion molecule-1 (VCAM-1) and E-selectin, encourage leukocyte adhesion while enzymes such as COX2 generate chemokines prolonging vasodilatation as described (Pober and Sessa 2007).

Leukocyte binding and subsequent transmigration to the parenchyma to deal with the inflammatory insult primarily occurs in post-capillary venules (Wittchen 2009). As in ECs, this process requires a level of leukocyte activation. Steps in leukocyte activation include integrin activation, podosome probing and subsequent ability to move across the surface of ECs towards sites where they can transmigrate (Sundd et al. 2011, Ley et al. 2007, Carman et al. 2007). P-selectin cell surface exposure, an early event in EC activation, promotes weak, transient interactions with passing leukocytes thus encouraging them to slow down and enable stronger EC-leukocyte interactions providing a firmer adhesion (Patel, Cuvelier and Wiehler 2002). E-selectin exposure, a later event in EC activation, encourages leukocyte rolling

stabilisation (Vestweber 2007). EC expressed ICAM-1 can bind to either leukocyte functional antigen-1 (LFA-1) or macrophage antigen-1 (Mac-1) on leukocytes, thus promoting firm adhesion. This interaction is enriched with additional clustering of ICAM-1, and with intracellular support from the actin cytoskeleton, as the leukocyte migrates to optimal sites for transmigration, evening persisting during transmigration (Muller 2011).

Angiogenesis is the formation of new vessels from pre-existing ones. It is indispensable in developing and growing organisms while in the adult, as blood vessels are typically quiescent, it is essential only at certain times and within certain vascular beds, as in tissue growth, wound repair, cycling uterus and pregnancy. New vessels can either sprout from pre-existing vessels in sprouting angiogenesis or can form when tissue folds insert into the lumen of a pre-existing vessel, as in intussusceptive angiogenesis (De Spiegelaere et al. 2012). The endothelium regulates neovascularisation by angiogenesis in its responses to the pro-angiogenic growth factor VEGF-A, while in the adult other signals can operate such as hypoxia and reactive oxygen species (ROS). In response to VEGF-A, a subset of ECs acquires properties to invade surrounding tissue, they are followed by a second subset which both forms the trunk of the new vessel while maintaining connectivity with the parent vessel (Gerhardt et al. 2003, Blanco and Gerhardt 2013). ECs must be able to transduce the signals to proliferate, resist apoptosis, reorganise the actin cytoskeleton and degrade the extracellular matrix before migrating, differentiating and finally forming a new blood vessel (Muñoz-Chápuli, Quesada and Angel Medina 2004).

### 1.1.3   Vascular bed specialisation

The vascularisation of different organ systems can deviate from the basic principles that apply generally to all vascular beds as vessel specialisations develop within tissues enabling the functions that a particular organ performs. It is the specialisations between vascular beds that can characterise different disease states when function goes awry, and help delineate and define a targeted treatment approach. EC "phenotypes are differentially regulated in space and time" (Aird

2005). In that same review, Aird drew an analogy of a single EC as one adaptive input-output device. The device input is the extracellular microenvironment of a cell while the nature of the output also depends on the context that the device is situated in, the response would vary greatly depending on whether the device is a singular unit or part of a larger population of units. The input would vary greatly between vascular beds, *i.e.* within the coronary endothelium or cerebral endothelium, and also for endothelium within the same organ, *i.e.* the strength and composition of blood flow, due to its nature, is constantly changing. Within any one unit, the coupling between the input and the output gives rise to a unique EC and overall EC heterogeneity. I shall describe three different vascular beds to illustrate this.

### 1.1.3.1 Coronary vasculature

The heart muscle is vascularised by the coronary circulation, the shortest in terms of transit time. It consists of the right and left coronary arteries mainly serving the right and left ventricles respectively with the majority of venous blood returning to the right atrium via the coronary sinus (Levick 1991b). Coronary blood flow is determined by aortic pressure, specifically depending on the pressure gradient that exists between the aortic root and the right atrium, extravascular compression, as most coronary inflow occurs during diastole, myocardial metabolism, and neural control (Schelbert 2010, Feigl 1983). The crucial tasks performed by the coronary circulation include the delivery of oxygen to the myocardium at a rate that matches the basal demand of the tissue and, when cardiac work increases, have the capacity to concomitantly increase blood flow to match energy requirements. The coronary circulation is structurally specially adapted in its very high capillary density, with approximately one capillary for each myocyte. This provides a large endothelial surface area and reduces the diffusion distance from lumen to myocyte. With exercise, coronary artery width and capillary number both increase to accommodate blood flow requirements (Duncker and Bache 2008).

The coronary circulation's basal flow is very high to match the high metabolic demand of the myocardium. The production of NO by the endothelium aids this high

flow and the capacity for oxygen extraction from the blood by the myocardium is extremely high, extracting over twice as much oxygen from circulating blood as the rest of the body (Feigl 1983, Laughlin et al. 2011). Any oxygen requirements beyond that gained by high oxygen extraction rates is achieved by an increase in blood flow through the coronary circulation, increasing the level of available oxygen. This hyperaemia can be achieved through the integration of a number of processes, the production of vasodilators, such as adenosine, NO and prostanoids; the involvement of adenosine tri-phosphate (ATP)-sensitive $K^+$ channels and $K^+$-sensitive $Ca^{2+}$ channels (which both result in decreased amounts of intracellular $Ca^{2+}$ prompting vasodilation); hypoxic vasodilation, as a mechanism limiting coronary artery disease (CAD) damage; and adrenaline production, as adrenaline acting on $\beta_1$-adrenoceptors increases cardiac work thus activating $\beta_2$-adrenoceptors causing vasodilation (Duncker and Bache 2000).

Regardless of scale, problems arising in the coronary circulation can be very serious as they are functional end arteries with ineffectual anastomoses. This means that any obstruction occurring upstream has the potential to cause a large zone of myocardial ischaemia, leading to an area of infarct and a peripheral area of partial ischemia depending on collateral circulation, the type of occlusion, preconditioning and the sensitivity of the myocytes to ischemia; this is exceptionally serious as the heart generates the perfusion pressure for the entire circulation (Levick 1991b, Feigl 1983, Thygesen et al. 2012). In addition, the coronary circulation is a hotbed for atherosclerosis whereby atheroma, a cholesterol rich, subintimal plaque, narrows the lumen of coronary arteries thus limiting blood flow, straining the system and causing angina. Atherosclerosis can also contribute to the formation of blood clots and if a coronary artery is completely obstructed by a thrombus it can cause a heart attack, a major cause of death and disability worldwide (Thygesen et al. 2012).

*1.1.3.2 Cutaneous vasculature*

The skin is vascularised by the cutaneous circulation, specifically the dermis as the epidermis is avascular. Depending on circumstances, cutaneous blood flow speed

ranges over 100 fold in difference but as the skin has a relatively constant, low metabolic rate its oxygen demands are generally fulfilled by the lower end of these values (Levick 1991b). The crucial task performed by the cutaneous circulation is ensuring tight regulation of the temperature of the core organs (the brain, thorax and abdominal organs) to between 37°C and 37.5°C by matching heat loss through the skin to core heat production (Johnson, Minson and Kellogg 2014). Dissipation of heat in this way is via three processes, radiation, as rate of heat loss is proportional to the difference between ambient temperature and skin temperature; conduction-convection, with heated skin warming adjacent air which is removed by local air currents; or the evaporation of sweat, and all three are determined by the speed of cutaneous blood flow (Shibasaki, Wilson and Crandall 2006, Nilsson 1987). Structurally the cutaneous circulation is adapted for this role as in regions of skin with a high surface area to volume ratio (*i.e.* acral or glabrous skin) there are specialised, direct coiled connections between the dermal arterioles and venules responding directly to ambient temperature called arteriovenous anastomoses (AVAs). AVAs are innervated by sympathetic vasoconstrictor nerves, are thick-walled and low resistance allowing high flow rates, and substantial changes in blood flow can occur depending on whether the AVAs are open or closed (Johnson et al. 2014, Braverman 1989).

Both ambient and core temperature affects cutaneous basal flow. Vascular tone is inversely related to ambient temperature in that local warming causes vasodilatation, in conjunction with increased eNOS activity, while local cooling causes vasoconstriction, and occurs alongside decreased eNOS activity and the increased action of $\alpha_2$-adrenoceptors. It follows that warmth induced vasodilatation promotes heat loss and flushed skin, while cold induced vasoconstriction promotes heat conversion and pallor. The reverse happens under situations of extreme ambient cold, when initial vasoconstriction gives way to dilatation as a way to help prevent skin damage during prolonged cold exposure (Charkoudian 2003). Core temperature influences sympathetic vasomotor activity of the cutaneous circulation whereby the hypothalamus, sensing any rise in core temperature, signals to the skin via the

brainstem to promote vasodilatation and sweating (Boulant 2006, Mallette et al. 2016). Under certain dire circumstances, such as acute cardiac failure or shock, arterial and central venous blood pressures are supported by an intense constriction and increased resistance of the cutaneous arterioles and venules promoted by angiotensin, vasopressin, adrenaline and increased sympathetic vasomotor activity (Levick 1991b, Johnson et al. 2014).

Problems localised to the cutaneous circulation include pressure ulcers in those that are elderly or unable to move themselves, as they are unable to relieve vascular compression by easily shifting position. When compressed, vasodilatation is induced to delay the onset of ischaemia, it is also helpful that the skin is able to withstand a certain level of ischemia better than most other tissues, but if compression prolonged discomfort prompts a shift in position, compression is relieved and blood flow is increased for a period of time (Braverman 1989). With excessive ambient heat, vasodilatation of cutaneous veins reduces central venous pressure and can lead to fainting while vasodilatation of cutaneous resistance vessels increases capillary filtration pressure and can lead to tissue swelling. The combination of cutaneous and muscular vasodilatation reduces peripheral resistance in conjunction with decreased cardiac output during heavy exercise and can lead to heat exhaustion (Levick 1991b).

*1.1.3.3 Pulmonary vasculature*

The pulmonary circulation is a short, low pressure circuit running deoxygenated blood from the right ventricle for gaseous exchange at the level of the alveoli before returning to the left heart replete with oxygen. As the crucial task performed by the pulmonary circulation, gaseous exchange requires both the blood of the lumen equilibrating with the gas phase of the alveolar sac and for each alveolus to be perfused with blood in proportion to its ventilation (Dupuis, Harel and Nguyen 2014). The pulmonary circulation is structurally adapted to ensure this as there is a very high number of capillaries in the alveolar wall and a very short diffusion distance, approximately 0.2-0.3 µm, comprised of endothelial barrier, basement membrane and epithelial barrier, thus allowing optimal oxygen transfer rates as it is

limited only by blood flow, or cardiac output (West and Mathieu-Costello 1999). Another structural specialisation is that the arteries and arterioles of the pulmonary vasculature are shorter and thinner resulting in less resistance to blood flow. Ultimately this, in combination with a low pressure gradient and thin right ventricle wall, contributes to a pulmonary capillary pressure which is midway between the pressure found in the arteries and veins on either side, and helps reduce tension in the alveolar-endothelial membrane precluding rupture (Maina and West 2005).

A functional specialisation of the pulmonary vasculature is vasoconstriction resulting from local hypoxia, unlike other vascular beds whereby vasodilatation occurs. This is an adaptive phenomenon known as hypoxic pulmonary vasoconstriction (HPV) but is not yet fully understood. HPV ensures that there is less under-oxygenated blood returning to the systemic vasculature as blood flow is diverted away from hypoxic alveoli. It is partially mediated by the endothelium upstream of the small, muscular, resistance arteries, and downstream by $Ca^{2+}$ sensitisation of Rho kinase. The core mechanism is believed to be deployed by the arterial smooth muscle cells, as a redox-based oxygen sensor (mitochondria of the smooth muscle cells) generates diffusible ROS which then contributes, in some unknown way, to HPV (Sylvester et al. 2012). The specialised pulmonary endothelium also plays a metabolic role in that it produces, activates, modifies and degrades circulating vasoactive agents that can affect the underlying smooth muscle cells as well as having systemic actions (Dupuis et al. 2014).

Similar to that seen in the coronary circulation, a pulmonary embolism occurs when a thrombus formed elsewhere in the body becomes detached and travels back to the heart and is fed directly into the narrowing pulmonary vasculature. Depending on the size of the blockage, vascular resistance in the area is raised, followed by an increase in pulmonary arterial pressure causing right ventricular afterload. The subsequent decrease in right ventricular output has a direct effect on left ventricular output and can lead to symptoms such as collapse, shortness of breath and rapid breathing; after CAD and stroke, pulmonary embolism is the third most common type of CVD and

can be a life threatening condition, especially if not treated soon after it occurs (Bělohlávek, Dytrych and Linhart 2013). Under circumstances where the blood-alveoli barrier is subjected to undue stress, in patients with certain heart conditions for example, the barrier can rupture, leading to pulmonary oedema and haemorrhage (Levick 1991b).

## 1.2 Blood-brain and blood-retinal barriers

### 1.2.1 Cerebral vascular bed

The cerebral circulation supplies the brain, at 2% of body weight, with 12% of cardiac output as the high metabolic demands of neuronal activity requires 20% of resting oxygen consumption and 25% of total glucose (Bolduc, Thorin-Trescases and Thorin 2013, Williams and Leggett 1989). These large energy requirements indicate that the brain has little energy reserve and relies on excellent cerebral perfusion to function normally (Faraci 2011). Cerebral blood flow is extremely well regulated, local perfusion must instantly adapt to local changes in neural activity, and this regulation involves a number of coordinated mechanisms. Due to a high demand for oxygen neurons are very sensitive to hypoxia and any mismatch between blood flow and metabolic needs can be catastrophic, leading to astrocytic and neuronal stress and ultimately put cell survival at risk (Faraci 2011, Bolduc et al. 2013).

Blood is delivered to the brain via two pairs of large arteries, the left and right internal carotids, mainly serving the cerebrum, and the left and right vertebral arteries, mainly serving the cerebellum and brain stem as the merged basilar artery. These vessels anastomose at the base of the brain, forming the Circle of Willis, before giving rise to three main pairs of arteries, the anterior, middle and posterior cerebral arteries which subsequently perfuse the brain on their gradual subdivision into smaller vessels (Cipolla 2009). This specialisation enables some preservation of cerebral perfusion in the event that a carotid artery becomes obstructed. An additional structural specialisation that optimises oxygen transport is the very high capillary density within the cerebrum (the total capillary length is approximately 400

miles) as this creates a large surface area for diffusion and reduces the diffusion distance to less than 10 µm (Begley and Brightman 2003).

Regulation of cerebral blood flow is chiefly intrinsic, and can be subdivided into four parts, autoregulation, neurovascular coupling, and cerebrovascular carbon dioxide ($CO_2$) and oxygen reactivity (Meng et al. 2015). To secure optimal metabolic supply, cerebral capillaries are perfused with blood at all times and have a very high basal rate of blood flow (Zlokovic 2008). This is achieved by the pressure gradient between pre-capillary arterioles and post-capillary venules, with flow increasing when arterioles dilate (Cipolla 2009). Upstream of the micro-vessels, larger cerebral arteries and arterioles on the brain's surface account for over half of the total cerebral resistance while local intravascular pressure before vessels enter the parenchymal tissue is about half the systemic blood pressure in the cortex indicating the importance of the contribution these vessels make towards regulating local perfusion pressure (Faraci and Heistad 1990). A further third of cerebral vascular resistance is partitioned to the parenchymal arterioles and capillaries, as well as their local cell population interactions, thus arranging control of cerebral blood flow across a wider playing field (Faraci 2011). Regional neuronal activity initiates regional increases in metabolic blood flow through the coordinated action of neurons and glia, as they generate vasodilatory signals directed at ECs, pericytes (PCs) and smooth muscle cells which then collectively trigger the necessary vascular changes (Girouard and Iadecola 2006, Hall et al. 2014). The cerebral vasculature maintains the required level of blood flow during instances of increased arterial $CO_2$ via hydrogen ion action on vessels, and a fall in oxygen tension, both through arterial vasodilatation (Meng et al. 2015, Kety and Schmidt 1948). There are further specialisations in the cerebrovascular vessels at a microvascular level, and problems localised to the cerebral circulation which will be described in more detail in later sections.

## 1.2.2   Specialised endothelial cell phenotype

*1.2.2.1 Neural microvasculature*

The neural microvascular endothelium, as the main site for blood-tissue exchange within the CNS, is highly specialised when compared with endothelial barriers in other vascular beds. Specialisations ensure that the CNS can operate within an elaborately controlled microenvironment without which neuronal signalling could not exist (Abbott et al. 2010). Restrictive transport mechanisms across the neural microvascular endothelium is the predominant characteristic responsible and led to it being known as the blood-brain barrier, or BBB. As an extension of the CNS the retina also has an inner blood-retinal barrier, or BRB, which functions similarly to the BBB (London, Benhar and Schwartz 2013). Some of the transport mechanisms involved are partly founded in interendothelial junction assembly and maintenance. This separates the luminal from abluminal surfaces with accompanying distinct partitioning of receptors and transporters, providing the BBB with exceptional apico-basal polarisation. This contributes to the establishment of essential biochemical concentration gradients and makes transport directional despite these gradients (Worzfeld and Schwaninger 2015). The physical barrier, operating at the level of the microvascular ECs and the interendothelial junctions between them, is enhanced by additional physiological and chemical elements (Saunders et al. 2013).

The neural microvascular endothelium is approximately 40% thinner, when measured from luminal to abluminal surfaces, compared with those of other vascular beds (Coomber and Stewart 1986). This is thought to enable a shortened transport time across the barrier as an adaptation to restricted BBB permeability (Stamatovic, Keep and Andjelkovic 2008). Furthermore, the neural microvascular endothelium is continuous and without fenestrae and, under healthy conditions, non-specific, fluid-phase transcytosis occurs at very low levels (Prasain and Stevens 2009, Daneman 2012). Alongside the distinctive interendothelial junctions, these characteristics contribute to the membrane's semi-permeable, size-selective nature.

The efficacy of the BBB is enhanced by the glycocalyx and two contiguous basement membranes (BM). These structures provide additional filtration properties as physical and enzymatic barriers. The glycocalyx limits the access of circulating macromolecules to the BBB luminal surface by steric hindrance, size exclusion and electrostatic charge (Van Teeffelen et al. 2007). The first BM covers the abluminal surface of neural microvascular ECs embedding adjacent PCs, and is secreted by both of these cell types. The second BM encloses the first BM, running alongside the perimeter of the brain parenchyma, and is secreted by astrocytic endfeet. Although there are differences, both BMs comprise four major components, type IV collagens, laminins, nidogen, and heparan sulfate proteoglycans (HSPGs). This specialised double BM limits both macromolecular and cellular movement as well as directing immune cell infiltration to targeted locations (Sorokin 2010, Daneman 2012).

Under basal conditions, junctions between neural microvascular ECs operate like molecular sieves and severely attenuate movement through intercellular spaces with exclusion descending to the level of ions (Saunders et al. 2008). This similarly supports biochemical gradients by enabling polarised transport systems and is exemplified by experimental measurements of electrical resistance across the barrier (Abbott et al. 2010). Across neural microvascular ECs there are five transport mechanisms for different molecules, proteins and cells: passive diffusion, ATP-binding cassette transporters (ABC transporters), solute carriers (SLCs), transcytosis, and transendothelial migration (TEM) of leukocytes (Abbott et al. 2010). Lipid soluble and lipophilic molecules, as well as gaseous molecules such as $CO_2$ and oxygen, can passively diffuse across the BBB down concentration gradients in an unrestricted manner. ABC transporters, such as P-glycoprotein and other multidrug resistance associated proteins, function as active efflux pumps which use ATP to transport lipid soluble compounds out of the CNS. These transporters are the predominant force preventing efficient delivery of lipid soluble therapies to the CNS. They can be expressed on either the luminal or abluminal membranes, or both. Carrier mediated influx via SLCs transports many of the essential polar nutrients, such as glucose, amino acids, monocarboxylic acids and ions including iron, copper

and magnesium, into the CNS. SLCs can be polarised in their membrane expression, they may be bi-directional, unidirectional, require an exchange of one substrate for another, or be driven by an ion gradient. Larger molecular weight proteins and peptides are transported into the CNS by transcytosis within vesicles of which there are two types. Receptor-mediated transcytosis usually moves peptides and proteins while adsorptive-mediated transcytosis usually moves positively charged macromolecules but does so in a non-specific manner (Abbott et al. 2010, Turowski and Kenny 2015, Saunders et al. 2013, Stamatovic et al. 2008). Lastly, leukocytes appear to migrate through both the healthy and diseased vascular BBB via a membrane-intensive, largely transcellular pathway (Bamforth, Lightman and Greenwood 1997, von Wedel-Parlow et al. 2011, Wolburg, Wolburg-Buchholz and Engelhardt 2005).

*1.2.2.2 Interendothelial junction proteins*

There are two groups of proteins which are responsible for the stature of the interendothelial junctions of the neural microvascular ECs, TJs and AJs, comparable to those found in epithelial cells (Dejana 2004). In contrast to epithelial cells, where they are organised in distinct bands, TJs and AJs of ECs are intermingled in their organisation and functionally interdependent (Fig. 1.1A) (Tietz and Engelhardt 2015). Furthermore, when comparing junctional complexes of the BBB with those of other vascular beds, differences in expression and molecular signature go hand in hand with broader differences in junction complexity and continuity (Tietz and Engelhardt 2015). There are other adhesive proteins located along the intercellular face of membranes such as PECAM-1, CD99, CD99L and CD146 but they are removed from areas containing TJs and AJs (Dejana and Orsenigo 2013). As the BBB is subject to a variety of physiological situations requiring spatial adjustments whilst maintaining a fully operational barrier, the junctional complexes between individual ECs must be dynamic in their interactions, and dynamically regulated (Steed, Balda and Matter 2010).

**(A)**

Epithelial cells           Endothelial cells

Tight junctions

Adherens junctions

**(B)**

ZO-1/-2/-3    PAR-3/-6
AF-6          MAGI
MUPP1       Cingulin

4-TSM

Actin

JAM

AF-6
ZO-1
ZO-2

VEC

SHP2
DEP1
α-actinin

**Figure 1.1. Interendothelial junctions: TJs and AJs**
Schematic representation of interendothelial junctions in epithelial and endothelial cells.
While TJs (yellow) are located apically to AJs (red) in epithelial cells, they are intermingled
in ECs and functionally interdependent (A). Overview of interendothelial junction protein
complex organisation between neural microvascular endothelial cells, highlighting
transmembrane proteins and intracellular partners. TJ four-pass TSM (4-TSM) proteins
include claudins, occludin and tricellulin whose intracellular partners include ZO proteins
(Z) amongst others. JAM, a TJ single-pass TSM protein, is also known to interact with ZO
proteins (Z) and AF-6. The key AJ protein, VEC, interacts with p120 catenin (p), α catenin
(α), β catenin (β), vinculin (V) and eplin (E) intracellularly, amongst others (B). Adapted (in
conjunction with Hirst, A) from "Tight junctions: from simple barriers to multifunctional

molecular gates" and "Endothelial cell-cell junctions: Happy Together" (Zihni et al. 2016, Dejana 2004).

TJs have three important functions. They regulate the flow of ions, solutes and cells through the paracellular space, they help establish and maintain apico-basal polarity and thirdly, they are pillars within signalling pathways controlling gene expression, cell differentiation and proliferation (Guillemot et al. 2008). The structure of a TJ is characterised by the presence of integral and peripheral membrane proteins (Tsukita, Furuse and Itoh 2001, Aijaz, Balda and Matter 2006). The integral proteins span the membrane and are classified according to the number of transmembrane (TSM) domains they have, being either four-pass TSM proteins such as the claudins, occludin and tricellulin, or single-pass TSM proteins, such as junctional adhesion molecule (JAM) (Fig. 1.1B).

The claudins, a family of more than 20 members, are the core protein components of TJs, with selective expression observed at the BBB (Dejana, Tournier-Lasserve and Weinstein 2009). They provide support via homophilic and heterophilic *cis* and *trans* interactions and, depending on the isoform, contribute to the formation of pores or fences along the intercellular cleft (Turowski and Kenny 2015). To date, three claudins which contribute to fence formation, 3, 5, and 12, have been identified within neural microvascular ECs (Gunzel and Yu 2013, Tietz and Engelhardt 2015). Claudin-2 has been found to contribute to pore formation regulating paracellular ion and water flow (Tietz and Engelhardt 2015). PDZ domains enable interactions between claudins, excluding claudin-12, with the peripheral membrane scaffold proteins, such as the zonula occludens proteins (ZO), thus connecting junctional complexes with the actin cytoskeleton (Van Itallie and Anderson 2014).

Both occludin and tricellulin are members of the TJ associated marvel domain containing protein family (TAMPs). Occludin has been shown to regulate size selective diffusion through the interendothelial junction (Balda et al. 2000). Specifically, the phosphorylation of occludin has been shown to regulate TJ protein interactions and transendothelial electrical resistance (TEER) in vitro (Raleigh et al.

2011). It has also been shown to contribute to $Ca^{2+}$ transport across the BBB, tricellulin localisation and provide a link between TJs and the actin cytoskeleton via positively charged surfaces interacting with ZO proteins and not PDZ domains (Tietz and Engelhardt 2015). Tricellulin expression is enriched in neural microvascular ECs and is localised to tricellular junctions assisted by lipolysis stimulated lipoprotein receptor (LSR), also enriched within this vascular bed. Tricellulin's function within the BBB has not yet been fully elucidated but may be critical for BBB formation (Van Itallie and Anderson 2014, Daneman 2012).

Peripheral membrane proteins are located on the cytoplasmic side of the membrane and together form large cytoplasmic plaques, providing dynamic links between the membrane TJ complexes, the actin cytoskeleton and other intracellular partners. A number of peripheral membrane proteins have been identified, including the zona occludens proteins ZO-1, ZO-2 and ZO-3, cingulin, binding partitioning defective proteins PAR-3 and PAR-6, MAGI and MUPP1 and AF-6 (Abbott et al. 2010). This network also associates with proteins of other TJs and with those of AJs, contributing to the correct organisation of junctional proteins, the regulation of junction assembly and function, and cell signalling (Fig. 1.1B) (Steed et al. 2010, Daneman 2012).

AJs are cell-cell adhesion complexes and, like TJs, are linked to the actin cytoskeleton. They are essential for embryogenesis and tissue homeostasis. They maintain vascular integrity and transfer intracellular signals needed for functions including apico-basal polarity and lymphocyte TEM. They are indispensable in cell processes such as contact inhibition of cell growth, prevention of apoptosis via PI3K/Akt, endothelial-mesenchymal transition and cytoskeletal organisation (Dejana 2004). The structure of an AJ is signified by the presence of VEC, a type II cadherin; there are two types of classic cadherins and both have five extracellular cadherin domains with a highly conserved cytoplasmic domain (Hulpiau and van Roy 2009). VEC, also known as cadherin-5 and CD144, is only expressed in ECs (Gavard 2013). Like other type I and II cadherins, it has five extracellular domains, the first of which (EC1) is responsible for $Ca^{2+}$ dependent homophilic cadherin recognition and

binding (Pokutta and Weis 2007, Leckband and Prakasam 2006). The physical basis for adhesive binding is the formation of a 'strand exchange dimer' whereby the opposing EC1 domains secure themselves within the hydrophobic grooves of their partners (Harris and Tepass 2010). This association is insufficient as a sole contributor to the adhesive forces that exist between cells and it is the remaining four extracellular domains which provide additional adhesive strength through the promotion of lateral cadherin clustering (Leckband and Prakasam 2006, Tsukasaki et al. 2007). VEC's cytoplasmic tail enables molecular interactions with a host of supporting cytoskeletal and signalling proteins within the cell including SHP2, DEP1, α-actinin and the catenins, namely α-, β-, γ- and p120 catenins (Tietz and Engelhardt 2015). The catenins coexist as molecular hubs, integrating and disseminating signals that provide a direct line for interplay between the cytoskeleton and AJs while stabilising them (Perez-Moreno and Fuchs 2006, Tietz and Engelhardt 2015). While β- and p120-catenins bind directly with VEC, α-catenin, vinculin and eplin bind the actin cytoskeleton thus mediating interactions between AJs and the cytoskeleton (Fig. 1.1B) (Gavard 2013).

### 1.2.3 Ancillary non-neuronal cells

*1.2.3.1 Pericytes*

PCs are the mural cells of microvessels, including neural microvessels, and they reside embedded within the BM on the abluminal side of ECs. PC surface coverage at the BRB and BBB is the highest of all vascular beds, equivalent to at least 30% coverage, or a 1:1-3:1 ratio of ECs to PCs, compared with 100:1 in striated muscles (Armulik, Genove and Betsholtz 2011, Allt and Lawrenson 2001). They project elongated, finger-like processes which surround the capillary wall (Winkler, Bell and Zlokovic 2011). Where opposing PC-neural microvascular EC surfaces are not buffered by a shared BM, PCs make direct contact with the EC surface via N-cadherin peg and socket junctions and connexin-43 hemi-channels (Li et al. 2011, Winkler et al. 2011). These form gap junctions between the cells allowing direct transfer of molecules. Connexin-43 hemi-channels also exist between ECs-astrocytes

(ACs) and between ACs-neurons (Chew et al. 2010). Although there are discrepancies between models used to investigate the BBB, the influence of PCs on the BBB appears to be manifold, being essential for both BBB formation and function (Armulik et al. 2011, Sweeney, Ayyadurai and Zlokovic 2016). With respect to the latter role, PCs appear to inhibit the expression of genes that lead to transcellular permeability and leukocyte infiltration in the periphery (Daneman et al. 2010, Armulik et al. 2010). They also contribute to regulation of "BBB permeability, angiogenesis, clearance, cerebral blood flow (CBF), neuroinflammation and stem cell activity" (Sweeney et al. 2016).

PCs have been found to suppress plasmalemmal vesicle associated protein-1 or PV-1 (also known as PLVAP), first identified as a caveolar protein, at the healthy BBB (Shue et al. 2008). The only known component of the diaphragm which bridges the fenestrae of fenestrated capillaries is PV-1, and so is normally only found in vascular beds other than neural microvascular ECs (Daneman 2012). PCs also appear to regulate major facilitator superfamily domain-containing 2a (MFSD2A), a protein expressed exclusively in neural microvascular ECs and a sodium-dependent long-chain fatty acid transporter (Nguyen et al. 2014). MFSD2A was found to suppress transcytosis in neural microvascular ECs of the BBB indicating a role in formation and maintenance of the BBB (Ben-Zvi et al. 2014). However, a recent study investigating MFSD2A at the BRB and BBB using MFSD2A KO mice found the complete opposite and did not observe any leakiness at either barrier (Wong et al. 2016).

*1.2.3.2 Astrocytes*

ACs are specialised glial cells that regulate neuronal function and have the capacity to coordinate and administer multitudinous signals from both neurons and the BBB. They are the most abundant glial cell type in the brain, a ramified star shape with many fine processes and specialised endfeet (Rosenegger and Gordon 2015). This allows a single AC to contact thousands of synapses while nearly entirely wrapping around a microvessel, either directly or via the BM, making them ideal for

conducting information between themselves and other cells (Bushong et al. 2002, Filosa et al. 2016). Specifically, ACs form "a continuous membranous network around the vessels called the glia limitans" which organises AC-PC-EC signalling and on top of which ACs produce glycoproteins contributing to the BM (Boulay, Cisternino and Cohen-Salmon 2016).

The ability of ACs to influence CNS-neural microvascular crosstalk is aided by a number of structural components expressed on cell-cell membranes including gap junction proteins such as connexin-43, integrins and specialised ion channels such as aquaporin 4, potassium channels and transient receptor potential channels (Filosa et al. 2016). Aquaporin 4 is a water channel enriched at the perivascular endfeet of ACs which facilitates the redistribution of water (Boulay et al. 2016). Aquaporin 4 expression correlates with the expression of a glycoprotein on the BM, a HSPG called agrin. Agrin, in conjunction with other glycoproteins, is required for aquaporin 4 localisation to AC perivascular endfeet (Abbott, Ronnback and Hansson 2006). As in EC-PCs, connexin-43 hemi-channels contribute to channel functions (described earlier) as well as channel-independent functions involving protein interactions and intracellular signalling, immune quiescence, regulation of neuronal signalling and cell stability (Boulay et al. 2016). ACs also strongly influence both BBB TJs and transport properties with factors secreted by ACs increasing TJ expression and TEER in cultured ECs, presumably by inducing sustained barrier protective cAMP signalling within the EC (Rist et al. 1997, Perriere et al. 2005, Abbott et al. 2010). ACs contribute to BBB integrity, the glymphatic system, CNS-immune homeostasis, modulate synaptic transmission, and, as well as vasodilatation, have been reported to cause vasoconstriction and regulate vascular tone all contributing to functional hyperaemia and neurovascular coupling (Filosa et al. 2016, Jessen et al. 2015).

*1.2.3.3 CNS immune cells*

CNS immune cells include microglia, also known as the brain macrophages, and a heterogeneous group of cells that have origins systemically, collectively termed the perivascular macrophages (Boulay et al. 2016). Microglia are highly ramified,

phagocytic cells found throughout the CNS and continually survey the tissue. They contribute to innate immune responses, can initiate adaptive immune responses and also have important roles in neural development, neuronal plasticity, synaptic stripping and wound healing (Gomez-Nicola and Perry 2015). Perivascular macrophages reside in the perivascular space of the BBB, between the BM and astrocytic foot processes, ideally positioned for first line CNS immune surveillance and antigen presentation (Daneman 2012). When activated, these cells produce chemotactic factors which contributes to increased BBB permeability and leukocyte infiltration (Deneiffe *et al.*, 2013).

### 1.2.4   Neurovascular unit

In line with the description that EC "phenotypes are differentially regulated in space and time", the neural microvascular endothelium performs functions according to a combination of innate EC characteristics and the microenvironment of individual ECs (Aird 2005). One key element contributing to the neural EC microenvironment is the neurovascular unit (NVU). This is the functional association of neural microvascular ECs with neurons and non-neuronal cells including PCs, ACs, microglia and perivascular macrophages, and also the BM (Winkler et al. 2011, Abbott and Friedman 2012). The close proximity of these cells has been illustrated and, in the context of the NVU, enables effective paracrine interactions, as well as contact signalling (via gap junctions for example) between unit members (Zlokovic 2008, Winkler et al. 2011).

There are many signalling pathways between cells of the NVU contributing to BBB functions (Sweeney et al. 2016). Between PCs and ECs, platelet-derived growth factor receptor-β (PDGFRβ) is expressed on PCs and, when PDGF secreted by ECs binds, PDGFRβ dimerises, auto-phosphorylates and activates. A variety of intracellular partners can interact with activated PDGFRβ and differentially proceed to regulate PC survival, migration, attachment, apoptosis, proliferation and differentiation and leukocyte trafficking. These activities help to promote vessel development and stabilisation (Sweeney et al. 2016, Betsholtz 2004, Winkler et al.

2011). Transforming growth factor-β (TGF-β) is expressed by PCs and ECs as well as neurons and glial cells. It activates TGF-β receptor 2 (TGFβR2) expressed on both PCs and ECs promoting cell differentiation, maturation, proliferation, migration and EC-PC attachment as well as correct BBB formation (Sweeney et al. 2016, Winkler et al. 2011). Notch signalling in both PCs (Notch3) and ECs (Notch1 and 4) contributes to BBB stability working in conjunction with TGF-β-TGFβR2 activity. The Wnt-β-catenin pathway also regulates Notch signalling contributing to BBB development and maturation via TJ complex establishment (Zhou et al. 2014, Artus et al. 2014, Liebner et al. 2008). Both PCs and ECs secrete VEGF-A which can activate VEGF receptors located on the apical (VEGFR1) and basal (VEGFR2) EC membranes contributing to either BBB cytoprotection or permeability respectively (Hudson et al. 2014, Franco et al. 2011, Dore-Duffy and LaManna 2007). MFSD2A, described earlier, is expressed exclusively on ECs but it has been found that its expression is influenced by PCs (Ben-Zvi et al. 2014). Angiopoietin-1 is constitutively secreted by PCs and binds Tie2 receptor tyrosine kinase (RTK) expressed on ECs maintaining the BBB; during hypoxic events angiopoietin-2 secretion increases and competes for Tie2 binding thus destabilising the BBB (Dore-Duffy and LaManna 2007, Sweeney et al. 2016).

ACs secrete many of the same factors as PCs and ECs described above, including TGF-β, VEGF-A and angiopoietin-1, with associated outcomes (Abbott et al. 2006). Secreted by ACs, astrocyte-secreted apolipoprotein E 4 (APOE4) binds low-density lipoprotein receptor-related protein 1 (LRP1) on PCs activating cyclophilin A, NFκB and matrix metalloproteinase 9 (MMP-9). MMP-9 contributes to the degradation of the EC TJ and BM leading to BBB breakdown (Sweeney et al. 2016). Raised intracellular $Ca^{2+}$, via neuronal activation of glutamate receptors, can raise levels of arachidonic acid following phospholipase $A_2$ (PLA$_2$) activation. Arachidonic acid metabolites can cause vasodilatation, if metabolised to prostaglandin $E_2$ then binding receptor EP4 on the PC membrane, or vasoconstriction, if transferred to PCs and metabolised to 20-HETE (Attwell et al. 2010, Sweeney et al. 2016).

The NVU provides a higher level of complexity to the functionality of the BBB. However, although the BBB evolved to provide a regulated CNS microenvironment, when the cellular players are unable to rectify disturbances, the problems arising from a dysfunctional BBB can become additive, severe and difficult to treat. Next I will discuss principles and physiology of vascular permeability in order to follow with a discussion on pathophysiological permeability.

## 1.3 Permeability

### 1.3.1 Physiological

The nature of the exchange vessels as a semi-permeable, size selective membrane is essential to fulfil vascular bed specific roles regarding gaseous, water, ion and solute exchange between the blood and parenchyma. Different approaches which set out to understand vascular permeability have provided theoretical frameworks relating functional parameters but they have not been fully reconciled with vessel structure and solute composition. In the following passages I will describe some of the observations and assumptions, or theories, which led to the development of vascular permeability parameters and concepts.

An early model of vascular permeability, called 'pore theory', developed following the observation that the capillary permeability of lipophobic solutes falls faster than the free diffusion coefficient as their radius increases. Presuming that this was due to steric exclusion and restricted diffusion, 'pore theory' proposed that the "capillary walls are pierced with numerous ultramicroscopic openings which are in general too small to allow the passage of plasma protein molecules, but are of sufficient size and number to account for the observed rates of passage of water and nonprotein constituents of the plasma" (Pappenheimer, Renkin and Borrero 1951). However, the permeability of molecules larger than albumin deviated from this model, as their movement across the barrier fell only slightly with increasing radius. A follow up 'two-pore theory' proposed two sets of water-filled channels in exchange vessel walls, one set mediated permeability of small molecules akin to those proposed

earlier (pore radius 3-5 nm), and a second set mediated permeability of larger plasma proteins (pore radius 22-60 nm), which were located at the venous ends of capillaries (GROTTE, KNUTSON and BOLLMAN 1951, Rippe and Haraldsson 1994, Michel and Curry 1999). While the small pores have been generally accepted to have a morphological equivalent in the interendothelial junctions, the cellular nature of the large pores has yet to be fully resolved (Mehta and Malik 2006, Levick and Michel 2010, Fraser, Dallas and Davies 1990). An additional modification of pore theory proposed a greater role for the glycocalyx in vascular permeability, the fibre-matrix model. It suggested that the molecular sieving properties of the vessel was determined by an endocapillary layer at the entrance to cell-cell junctions rather than though large and small pore sizes or cell-cell junctions (Curry and Michel 1980).

In relation to the identity of the large pores, early EM studies of blood capillary structure in different vascular beds revealed a large number of small vesicles concentrated immediately under continuous EC membranes of both the lumen and parenchymal space (Palade 1953). Further experiments in the muscle of rat diaphragm suggested that these vesicles were the structural equivalent of the large pores postulated by the two-pore theory and were involved in transcellular transport, or 'transcytosis' (Bruns and Palade 1968, Michel and Curry 1999). Later studies similarly investigating transport of large pore sized tracers estimated that the radius of the neck region of these vesicles approximated the large pore radius (25 nm), providing further support for vesicles constituting the large pore system (Predescu and Palade 1993, Mehta and Malik 2006). It has been estimated that the theoretical small pores contribute to 95% of hydraulic permeability while the large pores contribute to, at most, 5% (Levick and Michel 2010). Depending on the vascular bed this can translate into ratios of small to large pores ranging from 19000-1 to less than 1000-1 (Michel and Curry 1999, Levick and Michel 2010).

There have been disparities relating to the interpretation of experiments investigating transcellular, vesicular transport (Rippe et al. 2002). It has been suggested that the appearance of tracer on the parenchymal side of the vessel wall, or even in

58

cytoplasmic vesicles, may be due to the movement of the tracer paracellularly and back-filling vesicles from the abluminal membrane. The frequent lack of free vesicles observed within the cytoplasm was another argument against transcytosis (Michel and Curry 1999). In contrast, EM experiments using continuous thin serial sections in the vasculature of the eel illustrated the intracellular presence of a large tracer far removed from cell-cell junctions as well as tracer deposits in parenchymal areas "bounded and limited to regions of the capillary wall devoid of interendothelial associations" (Wagner and Chen 1991). Numerous experiments targeting specific vesicular components, *i.e.* caveolae, have also demonstrated transcellular vesicular movement (Mehta and Malik 2006). Caveolin-1 is integral to caveolae formation. Caveolin-1 knockout mice have profound vascular dysfunctions with aberrant capacity for endothelium relaxation, contraction and maintenance of vascular tone (Predescu, Predescu and Malik 2007). Studies using caveolin-1 knockout mice demonstrated no caveolae and no vesicular transport but displayed increased overall leakage via cell-cell junctions (Lin et al. 2007). This could indicate an unknown contribution of caveolae towards the regulation of interendothelial junctions and paracellular permeability (Mehta and Malik 2006). Supporting this, it has been found that caveolae sense mechanical pressure and form important signalling platforms for proteins such as eNOS (Cheng et al. 2015, Duran, Breslin and Sanchez 2010). Lower levels of permeability were measured in these mice in response to VEGF-A suggesting that, rather than basal permeability, pathological permeability was dependent on caveolae (Chang et al. 2009).

Across a thin, semi-porous membrane, such as in the exchange vessels, water flows bi-directionally according to pressure gradients while low molecular weight solutes, ions and dissolved gases diffuse according to concentration gradients. It is also possible for larger or intermediate-sized solutes to be transported within flowing water, in a much slower process called convection (Michel and Curry 1999). Fick's law describes diffusion in a body of fluid, without a membrane, whereby the mass of solute transferred per unit time depends on four factors, concentration gradient, diffusion distance, surface area and diffusion coefficient, or the ease with which a

solute dissolves within a solvent (Nagy et al. 2008). However, when this diffusion occurs via the pores of a membrane, as in the exchange vessels, it is slowed down in three ways. Firstly, by a reduction in area available for diffusion, from the size of the membrane decreasing to the cumulative pore sizes. Due to steric exclusion the pore size through which a solute can travel is decreased further. Secondly, a reduction in the diffusion coefficient occurs within the pore space, called restricted diffusion. Thirdly, because the path across the exchange vessel is not generally direct, the length of the path is increased beyond the width of the vessel wall. These factors describe diffusion without a pressure gradient. Within a pressurised system, solute transport occurs partly by diffusion and partly by filtration. An additional parameter is required in order to take this into account, the reflection coefficient. It corresponds to the difficulty a solute particle has in passing through a pore when compared with water (Nagy et al. 2008, Levick 1991b).

A single parameter better encapsulates these effects, permeability. Permeability of a membrane is the rate of the diffusion of solute across unit area of membrane, per unit concentration difference across the membrane, in the absence of fluid filtration (Levick 1991b). Along the length of the exchange vessel, macromolecular composition of the blood can vary at any point. This, in addition to barrier filtration properties, hydrostatic pressure and available exchange vessel surface area, determines permeability (Fig. 1.2) (Levick and Michel 2010). Relating to pore theory, EC permeability is dependent on both pore structure and the properties of the solute travelling through the pores, whether they are lipid soluble or not, and how small or large they are. Lipid soluble solutes, such as gases and general anaesthetics, have a greater area for diffusion than the lipid insoluble solutes confined to travel via the pores and so the exchange vessels are highly permeable to them. Small lipid insoluble molecules are restricted to travel through the membrane via cell-cell junctions or fenestrae (depending on vascular bed) and this greatly reduces the permeability of the exchange vessel to them, when compared with lipid soluble solutes. Differences in permeability between vascular beds are due to differences in the number of available cell-cell junctions or fenestrae along which solutes can

travel, and not due to their size. In addition, the size-selective properties of these vessels are also supported by the luminal glycocalyx, with some extension into cell-cell junctions, acting as a molecular sieve. It has been shown that the enzymatic removal of the glycocalyx increased the permeability of the exchange vessels (Michel and Curry 1999). Larger lipid insoluble molecules like plasma proteins, those rising in size above the diameter of the 'small pores', have less ingress to the opposite side of the membrane due to reduced permeability of the exchange vessel for them. As mentioned earlier, vessel permeability to such larger molecules does not stop completely but peters off and is dependent on both the size of the molecule and its charge, due to the approximate circumscribed pore size and negative charge of the glycocalyx (Levick and Michel 2010).
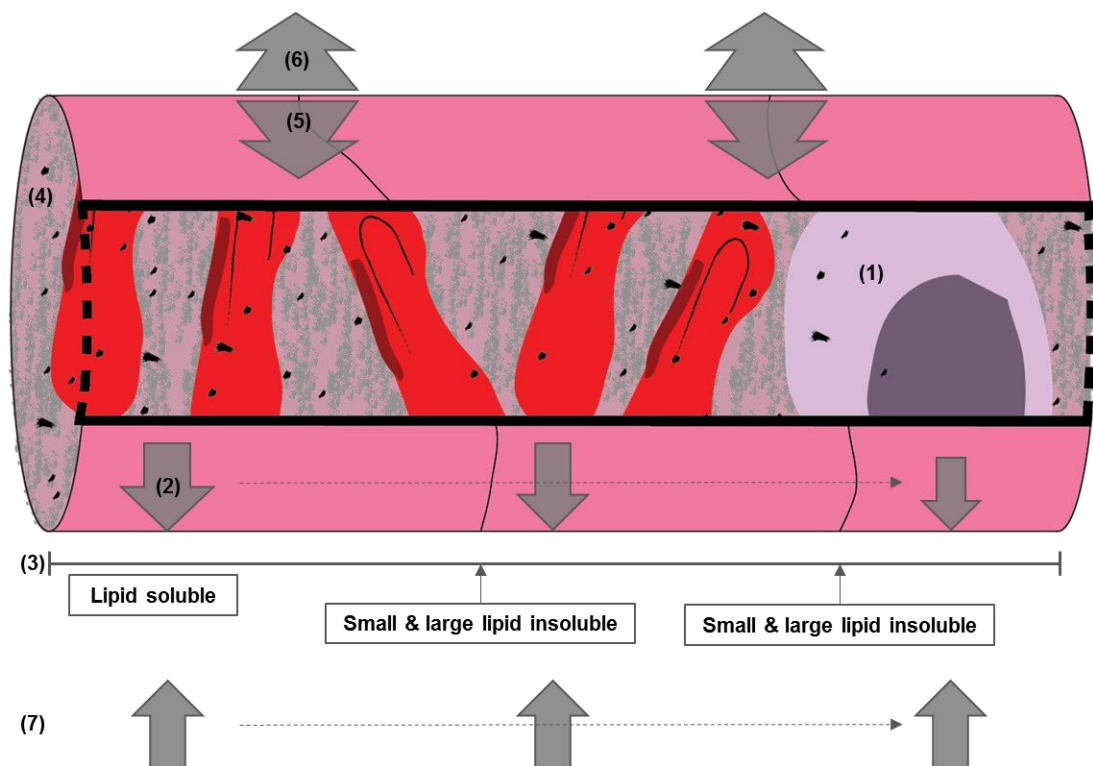


**Figure 1.2. Main parameters regulating fluid exchange in capillaries/post-capillary venules**
Schematic representation of a neural micro-vessel with cutaway to illustrate the interconnected mechanisms which influence vascular permeability (prepared with Hirst, A). Macromolecular blood composition varies along the length of the exchange vessel thus

61

continuously altering the vessel's local permeability response (1). Local capillary BP decreases along the length of the vessel, and is the main driving force behind filtration (2). Available exchange vessel surface area varies depending on the properties of crossing solutes *i.e.* lipid soluble solutes have a greater area for diffusion than lipid insoluble solutes confined to crossing via cell-cell junctions (3). Both the sieving and exclusion charge properties provided by the glycocalyx contribute to filtration across the vessels, specifically effecting larger lipid insoluble molecules *i.e.* plasma proteins (4). COP provided by the circulating plasma proteins is the main force opposing local capillary BP (5). Interstitial fluid osmotic pressure also opposes COP (6). While interstitial fluid pressure (which doesn't decrease along the length of the vessel) also opposes local capillary BP (7).

Filtration (mediated by the glycocalyx) has a significant impact on the flux of larger lipid insoluble molecules, mainly plasma proteins, across the exchange vessels. The main driving force behind this filtration is the local blood pressure in the capillary and the main force opposing this is the pressure supplied by the plasma proteins. Starling first described the parameters regulating this in 1896 proposing that the exchange vessel walls were semi-permeable membranes and that the plasma proteins (colloids) exert an absorptive, sucking force called the colloid osmotic pressure (COP) across it (Levick and Michel 2010). "Starling's principle of fluid exchange states that the rate of fluid movement across a short segment of exchange vessel of unit area is proportional to the net pressure difference across the vessel wall" (Levick 1991a). The net pressure difference is governed by four pressures, local capillary BP driving filtration (regulation of which described earlier), interstitial fluid pressure opposing it, COP and interstitial fluid osmotic pressure, which oppose each other. An additional term is required which takes into account the exchange vessel membrane's leakiness, the reflection coefficient (Nagy et al. 2008). Structural characteristics of the neural microvasculature, where basal levels of permeability are comparatively very low, would have an impact on the parameters described. Hydraulic conductivity, the ease with which water passes across the exchange vessel, is much lower at neural-vascular barriers when compared with vasculature of the muscle, while the reflection coefficient is maximal here (Fraser et al. 1990). Here, the

continuous endothelium directs water and lipid insoluble molecules either to cell-cell junctions, with highly complex junctional complexes enhancing sieve properties, or towards transport mechanisms directly through the cell, of which there is little fluid-phase transcytosis, in order to cross the vessel wall (Daneman 2012). Regardless, the Starling equation has been proven in single capillaries and has been extremely useful in understanding disorders with a pathophysiological permeability component (Nagy et al. 2008, Michel and Curry 1999, Levick 1991b).

### 1.3.2 Pathophysiological

Increased microvascular permeability is a feature of many pathophysiological disorders (Levick and Michel 2010). The vasculature and surrounding parenchyma must maintain volume homeostasis and avoid the accumulation of unfiltered plasma within the interstitial space. The lymphatic system plays a role draining fluid delivered from the microvasculature via the interstitium, which can function as a reservoir for the microvasculature thus contributing to maintenance of volume homeostasis (Zawieja 2005). The degree of increased permeability, and the time frame over which it occurs, reflects the intensity and variety of insult. In addition, the impact EC heterogeneity has on the response to permeability mediators can be significant, even within the same microvascular bed. Early EM studies demonstrated that pathophysiological leakage mainly occurs in post-capillary venules (Majno, Shea and Leventhal 1969, MAJNO, PALADE and SCHOEFL 1961). Unlike in arterial ECs, ECs of the post-capillary venules were also shown to not be closely coupled in relation to changes in intracellular $Ca^{2+}$ resulting from pathophysiological leakage. This has been postulated to indicate a self-preservation mechanism, reducing the spread of injury responses along the length of the vessel segment (Michel and Curry 1999).

Permeability changes can occur on a larger scale under acute or chronic insult, can result in generalised smaller increases in a number of systemic disorders and minimal variations can occur in physiological vascular haemostasis (Michel and Curry 1999, Nagy et al. 2008). Acute permeability changes are immediate and self-limiting *i.e.*

they are complete within 30 min or so. Following exposure to permeability mediators there is a swift influx of unfiltered plasma, called exudate, into the parenchyma. The composition of exudate differs from the standard filtrate, which is mainly water with small solutes, as it contains much higher levels of plasma proteins and is very similar to circulating plasma. On the other hand, chronic exposure to permeability mediators can lead to profound changes in the structure and function of the exchange vessels as well as abnormal growth of new vessels. This contributes to prolonged irregularities in barrier function and extensive fluid leakage into the parenchyma (Nagy et al. 2008).

Increased exudate within the parenchyma occurs when the capillary filtration rate is greater than the lymphatic drainage rate for a sufficient length of time. Different circumstances lead to an imbalance between compartments including raised capillary pressure, reduced osmotic pressure of plasma proteins and impairment of lymphatic drainage. Most relevant for the current discussion is increased microvascular permeability, when the endothelial barrier breaks down following aberrations in both paracellular and transcellular pathways as well as glycocalyx disruption (Levick and Michel 2010). Physiologically, both hydraulic conductance and protein permeability increase while protein reflection coefficient falls permitting enhanced flux of water and larger solutes (Zawieja 2005). Critically, relatively minute changes in vascular barrier properties can contribute to substantial pathology (Levick and Michel 2010).

At the cellular level, changes to neural exchange vessels resulting in increased permeability include disruption of TJ and AJ complexes, an increase in transcytosis, changes in transport properties, upregulation of proteases such as MMPs and increased leukocyte infiltration (Daneman 2012). The dynamic reorganisation of the actin cytoskeleton which results can disrupt centrifugal tensions and contribute to the formation of junctional disruption and paracellular permeability (Mehta and Malik 2006, Stamatovic et al. 2008). Cytoskeletal rearrangements are mediated by Rho GTPase signalling followed by downstream signalling of kinases such as ROCK and MLCK (Sit and Manser 2011). Due to their links with TJs and AJs, underlying

cytoskeletal rearrangements may also directly disrupt the extracellular adhesive nature of junctional complexes, such as the *cis* and *trans* interactions between AJs dimers (Brasch et al. 2012). Occurring concomitantly with modifications elicited by cytoskeletal rearrangements, reversible changes in the phosphorylation status of TJ and AJ complexes also facilitates junctional disruption, with subsequently altered adhesive properties, complex interactions and localisation, all contributing to increased paracellular permeability (Tietz and Engelhardt 2015). More starkly, TJ expression has been found to be decreased by transcriptional down-regulation, post-translational modifications (such as phosphorylation) or as a consequence of protease action, thus contributing towards increased paracellular movement during neurovascular disorders, as observed in experimental models of multiple sclerosis and stroke (Kim et al. 2015, Murakami, Felinski and Antonetti 2009, Orsenigo et al. 2012, Daneman 2012, Taddei et al. 2008, Yuan et al. 2012). Other intracellular mediators contributing to enhanced BBB permeability include Src kinases, PKC isoforms and NO and ROS operating via eNOS and NADPH oxidase respectively; while Akt promotes barrier integrity at the BBB, contrary to its permeability-inducing role in peripheral vascular beds (Fraser 2011, Spyridopoulos et al. 2002, Harhaj et al. 2006, Stamatovic et al. 2008, Perriere et al. 2005, Liu, Zhou and Yuan 2014). It is possible to perform experiments in cultured cells distinguishing between permeability affecting either paracellular or transcellular routes as paracellular permeability results in changes in TEER, affecting the movement of ions across the exchange vessel, while transcellular permeability does not.

A number of different factors have been identified as vasoactive mediators of neural microvasculature permeability including kinin peptides, phospholipids, neurotransmitters, coagulant serine proteases, inflammatory mediators, MMPs, ROS and growth factors (Mehta and Malik 2006, Stamatovic et al. 2008). THR is a coagulant serine protease which, as well as regulating haemostasis, mitogenesis and smooth muscle contraction, causes extended opening of the neural microvasculature via cytoskeletal changes. Due to its short half-life THR's primary site of action is in the locality in which it was generated but, as it can be concentrated within fibrin

clots, THR's actions can be magnified when coupled with thrombosis (van Hinsbergh and van Nieuw Amerongen 2002, Mehta and Malik 2006). BK is an inflammatory neuro-peptide, an end product of the kallikrein-kinin system, which is generated at sites of tissue injury and inflammation and is rapidly degraded with a half-life shorter than THR's (Dobrivojevic, Spiranec and Sindic 2015). BK degradation is mediated by a number of different proteases which are highest in concentration in the vicinity of BK receptors. BK contributes to smooth muscle contraction and relaxation (depending on the vascular bed), pain mediation and modulation of inflammation (Emerich et al. 2001). It is known that on binding BK receptor type 2, BK increases intracellular $Ca^{2+}$, activates eNOS and releases NO, prostacyclins and activates Janus kinase/STAT pathways which contributes to EC permeability (Dobrivojevic et al. 2015). LPA is a phospholipid produced in activated platelets without any detectable membrane-perturbing effects other than receptor activation. It functions as a growth factor, induces cell proliferation, migration and survival but also gap junction closure (Moolenaar, van Meeteren and Giepmans 2004). LPA has also been found to mediate EC permeability at the BBB by disruption of the TJ complexes, enhancing paracellular permeability (On et al. 2013).

When the focal role of the BBB is jeopardised and enhanced exudate within the neural parenchyma results, neurotoxic products are generated that compromise synaptic and neuronal functions, and can ultimately lead to their degeneration (Zlokovic 2008). Opposing this is the possibility that a partially accessible BBB, under pathological circumstances, can provide better access for leukocyte infiltration thus contributing to resolution of the pathology (Daneman 2012). In either case disruption of the BBB is critical in the pathogenesis of a range of vascular, neuronal and cerebrovascular disorders (Stanimirovic and Friedman 2012). On the whole, whether or not BBB dysfunction precedes a neurological disorder, develops in response to a neuronal aetiology, or whether BBB dysfunction and neurological disease arise as a comorbidity, is not yet clear (Zlokovic 2008). Regardless, acute, chronic or systemic BBB disruption is a facet of a number of disorders including metabolic disorders such as diabetes; cancer, primary CNS inflammatory conditions

such as meningitis or multiple sclerosis; secondary CNS inflammatory conditions such as stroke; epilepsy and neurodegenerative disorders such as Alzheimer's disease, Parkinson's disease and motor neuron disease (Stamatovic et al. 2008, Drozdzik et al. 2003, Lo, Dalkara and Moskowitz 2003, Jeynes and Provias 2011, Montagne et al. 2015, Argaw et al. 2012, Alvarez, Cayrol and Prat 2011). As it is relevant for the current thesis I will briefly discuss diabetes and its neural microvasculature dysfunctions.

Diabetes is a systemic disease with well-recognised microvascular complications such as nephropathy and retinopathy but is also a known risk factor for ischemic stroke (Beckman, Creager and Libby 2002, Hawkins et al. 2015). As in the retinal microvasculature, diabetes has been associated with increased vascular permeability at the BBB and decreased occludin at TJs (Chehade, Haas and Mooradian 2002). The breakdown of the inner BRB can be a consequential progressive event for those afflicted by diabetes (Klaassen, Van Noorden and Schlingemann 2013). The DR which results is the most common microvascular complication of diabetes and is classified as either non proliferative or proliferative based on the extent of damage to the microvasculature and its associated cells (Stitt et al. 2016). DR pathology is manifested by retinal haemorrhages, microanuerysms, neovessels and ischemia, with the vascular leakage (of plasma solutes) leading to oedema and the formation of hard exudates within the retinal interstitium (Klaassen et al. 2013). Occurring at any stage of DR, although more prevalent in later stages, the primary cause of vision loss in diabetes is diabetic macular oedema (DMO) whereby the retinopathy extends to include that area of the eye with which we have the greatest visual acuity, the macula (Curtis, Gardiner and Stitt 2009). The diabetic environment preceding DR pathogenesis is multifaceted and complicated, including an altered haemodynamic state and cellular dysautoregulation on account of metabolic abnormalities, an increase in inflammation and ROS production, with subsequent dysfunction and death of retinal ECs and PCs in conjunction with disturbances in neurovascular coupling (Klaassen et al. 2013, Stitt et al. 2016). Loss of occludin from TJs for example is a hallmark of DR (Barber and Antonetti 2003). These vast and varied

67

changes are accompanied by the induction of an array of growth factors and related cytokines and kinin peptides such as VEGF-A, BK, TGF-β, TNF-α and MCP-1 (Klaassen et al. 2013).

Upregulation of VEGF-A occurs early in DR with levels remaining consistently high thereafter (Curtis et al. 2009, Simo, Sundstrom and Antonetti 2014). As VEGF-A is crucial for both angiogenesis and permeability responses, when the ischemic conditions of early DR kick-starts HIF-α function, a cycle of neovascularization and pathological permeability is initiated (Shima et al. 1995, Stitt et al. 2016). Notwithstanding the central role VEGF-A plays in the cardiovascular system at large, VEGF-A's evident role in DR pathogenesis makes it a key target for therapeutic approaches aimed at its inhibition, with prospective clinical trials also supporting this strategy (Simo et al. 2014, Miller et al. 2013). Recognizing three recent anti-VEGF strategies, bevacizumab is a monoclonal antibody that targets all VEGF isoforms although it is licensed for use in colorectal cancer. Ranibizumab was subsequently developed for use in the eye, with a design based on bevacizumab's structure but consisting of a Fab fragment and therefore a third of bevacizumab's size but with greater affinity for VEGFs (Simo et al. 2014, Ford et al. 2013). Aflibercept or VEGF-TRAP is a protein composed of the fused extracellular ligand binding domains of VEGFR1 and VEGFR2 attached to the Fc fragment of human IgG1, it also targets all VEGF isoforms, as well as PlGF, but with a much better affinity than its predecessors (Holash et al. 2002, Simo et al. 2014). Despite a VEGF neutralization strategy providing significant improvements for many DR patients the approach is not effective in all and, over time, has become refractory in some (Ford et al. 2013, Ciulla et al. 2015).

## 1.4    Aims of this study

The overarching aim of this PhD was to explore different aspects of transport across the neural microvasculature, as measured in response to different vasoactive mediators thus characterising various BBB and BRB microenvironments. As the specialisations inherent to the neural microvasculature are critical in order to fully realise BBB and BRB function, establishing and maintaining a highly controlled CNS microenvironment, the *in vitro* model systems chiefly used in pursuit of this aim are closely representative of the *in vivo* setting. Furthermore, while paracellular and transcellular transport are traditionally considered disparate and studied in isolation, both processes were of great interest to the current study.

Breakdown of the inner BRB, and aberrant permeability, can be an aggravating step leading to blindness in those with diabetes (Klaassen et al. 2013). While anti-VEGFs are the mainstream treatment for the DR which results, this approach does not work for all patients (Ford et al. 2013, Ciulla et al. 2015). Moreover, the diabetic microenvironment to which the microvasculature is exposed is complicated and incompletely characterised. Collaborators observed the protective effect of lipoprotein-associated $PLA_2$ (Lp-$PLA_2$) inhibition on the BRB in two *in vivo* models used for diabetic research (Canning et al. 2016). My first aim, using functional assays and measurements of protein activation in *in vitro* models, was to determine whether the product of this enzyme reaction (Lysophosphatidylcholine, LPC) played a role in inner BRB breakdown (see **Chapter 3**). To augment the findings of this chapter, as neural microvascular disruption is a feature of several disorders, my second aim was to similarly investigate the role played by certain vasoactive mediators of the circulating milieu, THR, BK, LPA and TNF-α, on some of the same *in vitro* models used previously (see **Chapter 4**).

Non-specific, fluid-phase transcytosis occurs at very low levels at the neural microvascular endothelium under healthy conditions. However, this is not the case following pathological disturbances (Daneman 2012). In fact, the presence of both

paracellular and transcellular transport had been observed following LPC treatment (see **Chapter 3**). Therefore, my third aim was to investigate the role of certain endogenous and exogenous mediators, MET, DEOX, BK, LPA and VEGF-A, on levels of transcellular transport in relevant *in vitro* models using functional assays and EM analysis. I further investigated the contribution of different components of the vascular unit to these observations by developing multicellular models (see **Chapter 5**).

Finally, I examined VEC internalisation, expanding ongoing work within the lab investigating the effect of ICAM-1 signalling at cell-cell junctions. My aim was to better characterise the location and dynamics of VEC internalisation in brain MVECs employing both quantitative and qualitative methods (see **Chapter 6**).

# Chapter 2   MATERIALS AND METHODS

## 2.1     Materials

### 2.1.1   General Laboratory Materials

All reagents were purchased from Sigma Aldrich, unless stated otherwise in the relevant section. Glassware was purchased from VWR International.

### 2.1.2   General Laboratory Solutions

Water used was purified by a Milli-Q reagent grade water ultrafiltration system from Millipore.

### 2.1.3   Tissue Culture

Polycarbonate transwells of 0.4 μM pore-size and diameter 6.5, 12, or 24 mm, were purchased from Corning. Electric cell substrate impedance sensing (ECIS) polyethylene terephthalate (PET) grids, both 8W1E and 8W10E, were purchased from Applied Biophysics via Ibidi. All other plastic-ware was from Nunc. Foetal calf serum (FCS: heat inactivated, European origin), foetal bovine serum (FBS: certified, US origin), Hank's buffered saline solution (HBSS) both with, and without, $Ca^{2+}$ and magnesium ($Mg^{2+}$), Dulbecco's phosphate buffered saline (PBS) without $Ca^{2+}$ and $Mg^{2+}$, Ham's F-10 nutrient mix with Glutamax™, Dulbecco's modified eagle's medium (DMEM: high glucose), N-2-hydroxyethylpiperazine-N-2-ethane sulfonic acid (HEPES), penicillin-streptomycin were all purchased from Invitrogen. EBM®2 and EGM®2 MV Single Quots® were purchased from Lonza-Biowhittaker. Deoxyribonuclease 1 from bovine pancreas (DNase 1), puromycin dihydrochloride from *Streptomyces alboniger* powder, Percoll, Collagenase/Dispase®, basic fibroblast growth factor (bFGF: basic, human), Nα-Tosyl-L-lysine chloromethyl ketone hydrochloride (TLCK), trypsin (from porcine pancreas), collagen IV (from human placenta), BK, THR, TNF-α, LPA, bovine serum albumin-fatty acid free, low

71

endotoxin, lyophilized powder (FFA BSA), dynasore hydrate, methamphetamine (MET), L-methamphetamine (DEOX), trypsin inhibitor from *Glycine max* (soybean), SU1498 and fibronectin (from bovine plasma) were purchased from Sigma. 22% bovine serum albumin (BSA) in PBS was purchased from First Link and collagen-1 (high concentration, rat tail) from BD Biosciences. LPC was purchased from Cambridge Biosciences. Recombinant rat VEGF 164 was purchased from R&D Systems. SB202190 was purchased from Tocris. SP600125 was purchased from Merck. PTK787/ZK (PTK) was kindly supplied by Christiana Ruhrberg.

### 2.1.4   Molecular Cell Biology

All kits were purchased from Qiagen unless stated otherwise. XL-1 Blue® competent cells were purchased from Agilent Technologies. 1kb DNA ladder was purchased from Invitrogen. shRNA oligos were purchased from Eurofins MWG Operon. Gene cleaning was performed using plates purchased from Genetix. Restriction enzymes used were either from Roche or New England Biolabs. The pRNAT-H1.1/Shuttle vector was purchased from GenScript.

## 2.1.5 Antibodies

**Table 2.1 Primary antibodies and dilutions. FITC is fluorescein isothiocyanate**

| Primary Antibody | Species | Raised against | Dilution | Company |
|---|---|---|---|---|
| ZO-1 | Rabbit | Human, rat | 1:50 (IF) | Thermo Fisher Scientific |
| Occludin | Mouse | Human, rat | 1:50 (IF) | Thermo Fisher Scientific |
| Claudin-5 | Mouse | Human, rat | 1:100 (IF) | Thermo Fisher Scientific |
| α-catenin | Rabbit | Human, rat | 1:50 (IF) | Sigma |
| β-catenin | Rabbit | Human, rat | 1:50 (IF) | Sigma |
| γ-catenin | Mouse | Human, rat | 1:50 (IF) | BD Biosciences |
| p120 | Mouse | Human | 1:50 (IF) | BD Biosciences |
| p-glycoprotein | Mouse | Human, rat | 1:20 (IF) | Genetex Inc |
| Transferrin receptor | Mouse | Human | 1:50 (IF) | Serotec |
| vWF | Rabbit | Human | 1:50 (IF) | Dako |
| VEC (CD144), C-terminus (C-19) | Goat | Rat, human | 1:20 (IF) | Santa Cruz |
| VEC (CD144), extracellular domain (TEA 1.31) | Rabbit | Human | 1:50 (IF) | Serotec |
| VEC (CD144) FITC conjugated, extracellular domain | Rabbit | Human | 1:20 (IF) | Serotec |
| Affinity purified VEC (CD144), extracellular domain | Rabbit | Mouse, rat | 1:500 (IB) | Patric Turowski UCL |
| Phosphorylated VEGF2 (Y1175) | Rabbit | Human, mouse | 1:500 (IB) | Cell Signalling |
| VEGF2 (clone 55B11) | Rabbit | Human, mouse | 1:1000 (IB) | Cell Signalling |
| Tubulin | Mouse | Human, rat | 1:10000 (IB) | Sigma |

| Anti-VEGF monoclonal (DMS1529) | | Rat | 10 µg/mL | GSK |
|---|---|---|---|---|
| p38 | Rabbit | Human, rat | 1:1000 (IB) | Cell Signalling |
| Phosphorylated p38 (T180/Y182, clone 9212) | Rabbit | Human, rat | 1:500 (IB) | Cell Signalling |
| ICAM-1 (CD54, clone 1A29) | Mouse | Rat | 1:200 | Serotech |
| ICAM-1 (CD54) | Mouse | Human | 1:200 | Serotech |
| PDGFRβ | Rabbit | Human, rat | 1:300 (IF) | New England Biolabs |
| Anti-Glial Fibrillary Acidic Protein (GFAP) Cy3 conjugated | Mouse | Human, rat | 1:200 (IF) | Sigma |

**Table 2.2 Secondary antibodies and dilutions**

| Secondary antibody | Species | Dilution | Company |
|---|---|---|---|
| Anti-rabbit horse-radish peroxidase (HRP) | Donkey | 1:5000 (IB) | GE Healthcare |
| Anti-mouse HRP | Sheep | 1:10000 (IB) | GE Healthcare |
| Anti-rabbit Cy3 | Donkey | 1:200 (IF) | Stratech Scientific Ltd |
| Anti-rabbit Cy5 | Donkey | 1:200 (IF) | Life Technologies |
| Anti-rabbit Cy3 | Goat | 1:200 (IF) | Stratech Scientific Ltd |
| Anti-goat Cy3 | Rabbit | 1:1000 (IF) | Stratech Scientific Ltd |
| Anti-goat Cy3 | Donkey | 1:400 (IF) | Stratech Scientific Ltd |

**Table 2.3 Cell stains and dilutions**

| Secondary stains | Dilution | Company |
|---|---|---|
| Hoechst | 1:100 | Sigma |
| Cell Tracker™ CMAC | 1 µm | Thermo Fisher Scientific |
| Cell Tracker™ CMFDA | 1 µm | Thermo Fisher Scientific |

### 2.1.6   Electron Microscopy reagents

Kindly provided by Clare Futter.

## 2.2   Methods

### 2.2.1   Cell Culture

Several different cell lines and primary cells were used to investigate the aims, the reasons for which are manifold. For example, functional experiments measuring TEER across a cell barrier required the use of cells which form robust cell-cell interactions comparable with *in vivo* physiology. Therefore, when investigating the effect of an agent on functional inner BRB breakdown it was ideal to use rat retinal MVEC primaries but, as it is difficult to derive a prolific amount of these cells from source material, basic principals were illustrated in both rat retinal and brain MVEC primaries before extensive experiments were continued in brain MVEC primaries (see **Chapter 3**). Then, as cell lines will most usually express a repertoire of proteins akin to primary cells, experiments investigating the activation of certain proteins, or movement of certain proteins within a cell, were performed in relevant cell lines. For example, a rat retinal MVEC line was used to investigate VEGFR2 activation rather than rat retinal MVEC primaries, as the former provides more material to work with (see **Chapter 3**). As rats were the source of primary cells, rat cell lines (retinal or brain) were frequently used. However, there were some instances when a human brain MVEC line was used and this was to enable flexibility within Ab constraints

but also allowed for extrapolation of results to a human model. For example, a FITC-conjugated Ab directed against extracellular VEC was used to track VEC internalisation but the Ab was raised to target human VEC, thus requiring the use of a human brain MVEC line (see **Chapter 6**). Additional rat primary cells, PCs and ACs, were used alongside rat brain MVEC primaries to create multicellular models of the NVU (see **Chapter 5**).

### 2.2.1.1    *Immortalised rat brain microvascular endothelial cells*

Growth medium: F-10 supplemented with 10% FCS, 2 μg/mL bFGF, 80 μg/mL heparin, 100 i.u/mL penicillin, 100 μg/mL streptomycin

GPNTs were derived from an immortalised Lewis rat brain microvascular endothelial cell line by GP8 by lipofectin-mediated transfection with a vector containing the puromycin resistance gene (Regina et al. 1999). GPNTs were maintained in growth medium at 37°C and 5% $CO_2$ and grown on collagen 1 coated plastic-ware. Collagen 1 (25 mg/mL) was added to 22.5 mL of filtered water containing 0.1 mM acetic acid before addition to 500 mL of HBSS ($Ca^{2+}/Mg^{2+}$). This coat was was left on plastic-ware to be used for at least 2 h. The coating was then aspirated and the remaining collagen film polymerised by alkalisation in a box containing ammonia vapour. This plastic-ware was then washed twice with HBSS ($Ca^{2+}/Mg^{2+}$) before cells were plated.

When confluent, GPNTs were passaged by trypsinisation. Cells were washed twice with PBS before addition of trypsin solution. Excess trypsin was aspirated and plastic-ware was returned to incubator until cells had detached. Cells were gathered by two successive washes with 10 mL growth medium and a single cell suspension produced by syringing with a 23G needle. Cells were plated at a density of 31,250/cm$^2$ on collagen 1 coated plastic-ware.

When preparing cell stocks for long-term storage, cells were suspended in ice-cold medium containing 10% dimethyl sulfoxide (DMSO) and aliquoted to cryotubes (usually at $1\text{-}5 \times 10^6$/mL) for slow freezing at -20°C for 2 h and -80°C overnight before transfer to liquid nitrogen.

When thawing cell stocks, cryotubes were held for 20-30 s in a 37°C water bath, until a slight thaw was observed. Cells were then transferred to coated plastic-ware containing media using a p1000 pipette. Cells were allowed to adhere to plastic-ware for 2-3 h and media was then changed. Media was changed again the following morning.

*2.2.1.2*        *hCMEC/D3 human brain microvascular endothelial cells*

Growth medium: EBM®-2 MV supplemented with 5% FBS, gentamicin sulphate/amphotericin-B (GA-1000) and growth factors (human fibroblast growth factor (hFGF), VEGF, ascorbic acid, human epidermal growth factor (hEGF), insulin growth factor ($R^3$-IGF-1) and hydrocortisone) at 25% of the volume as suggested by manufacturers.

hCMEC/D3s are "derived from human temporal lobe microvessels isolated from tissue excised during surgery for control of epilepsy. The primary isolate was enriched in CECs. In the first passage, cells were sequentially immortalised by lentiviral vector transduction with the catalytic subunit of human telomerase and SV40 large T antigen, following which CEC were selectively isolated by limited dilution cloning, and clones were extensively characterised for brain endothelial phenotype" (Weksler, Romero and Couraud 2013). hCMEC/D3s were cultured and passaged as described for GPNTs (See 2.2.1.1).

### 2.2.1.3    *PT2 rat retinal microvascular endothelial cells*

Growth medium: EBM®-2 MV supplemented with 5% FBS, hFGF, VEGF, ascorbic acid, hEGF, $R^3$-IGF-1, hydrocortisone and GA-1000 according to manufacturer's instructions.

PT2s were derived from freshly isolated rat retinal microvascular endothelial cells immortalised using a retrovirus coding for temperature sensitive large T. PT2s were cultured and passaged as described for GPNTs (See 2.2.1.1) save cells were plated on plastic-ware coated with a solution of 100 μg/mL collagen IV and 50 μg/mL fibronectin in tissue-culture water as described for primary rat brain microvascular endothelial cells (See 2.2.1.4).

### 2.2.1.4    *Primary rat brain microvascular endothelial cell isolation*

Growth medium: EBM®-2 MV supplemented with 5% FBS, hFGF, VEGF, ascorbic acid, hEGF, $R^3$-IGF-1, hydrocortisone and GA-1000 according to manufacturer's instructions.

Working buffer: 100 mL HBSS ($Ca^{2+}$/$Mg^{2+}$) containing 2.25 mL of 22% (w/v) BSA in PBS, 10 mM HEPES and 100 i.u/mL penicillin, 100 μg/mL streptomycin

Complete digest medium: 100 mL HBSS (without $Ca^{2+}$/$Mg^{2+}$) containing 0.5 mg/mL collagenase and dispase (Roche), 10 mM HEPES, 100 i.u/mL penicillin, 100 μg/mL streptomycin sterile-filtered followed by addition of 20 U/mL DNase 1 (Sigma) and 0.147 μg/mL TLCK (Sigma). Stored at -20°C.

Percoll density gradient: For a 50% solution, 50 mL Percoll (GE Healthcare), 5 mL 10X HBSS ($Ca^{2+}/Mg^{2+}$) and 45 mL HBSS ($Ca^{2+}/Mg^{2+}$) combined. Stored at 4°C.

Protocol was adapted from Abbott et al (1992) using the cells from one brain to plate 15 $cm^2$ of plastic-ware or 7.5 $cm^2$ of transwell inserts (Abbott et al. 1992). All dissection instruments were sterilised in 70% IMS. Female 6-8 week old Wistar rats were killed by $CO_2$ asphyxiation followed by cervical dislocation. For each rat, the head was removed and dissected to reveal the entire brain. The brain was collected in ice-cold working buffer. Fine dissection was performed on sterile lint moistened with working buffer. For each brain, cerebellum was removed and one hemisphere dissected at a time, with the second returned to ice-cold working buffer. Meninges and choroid plexus were picked off using fine forceps before visible white matter was removed from the hind and mid brain. Hemisphere was transferred to dry sterile lint and briefly rolled to remove leptomeningeal cells. It was then returned to moistened lint where curved forceps were used to pinch off any remaining white matter. Dissected hemispheres were collected in fresh ice-cold working buffer. All dissected hemispheres were chopped together using a scalpel and then centrifuged for 5 min at 4°C at 1800 rpm. Buffer was aspirated and 15 mL complete digest medium (per three brains) was added before tissue digested for 1 h at 37°C in water bath. Digests were agitated every 15 min.

Digests were then removed to ice. A plugged Pasteur pipette was used to triturate the cell digests for approximately 2.5 min and further triturated with a narrower ended pipette for a similar time. The digests were centrifuged for 5 min at 4°C at 1800 rpm and supernatant removed. 20 mL of 22% (w/v) BSA in PBS was added to the pellet,

resuspended by tapping and centrifuged for 20 min at 4°C at 3000 rpm. The resulting myelin plug was rolled away and collected for further processing. Remaining supernatant was discarded and the pellet held inverted on sterile tissue to prevent myelin contamination. The pellet was resuspended in 5 mL working buffer and centrifuged for 5 min at 4°C at 1800 rpm. The supernatant was discarded, the pellet resuspended in 5 mL complete digest buffer and the suspension digested for 3 h at 37°C in a water bath. The myelin plug was re-triturated as described earlier, 22% (w/v) BSA in PBS was added to the fill line and the suspension centrifuged for 20 min at 4°C at 3000 rpm. Both the myelin plug and supernatant were discarded and the pellet held inverted on sterile tissue as before. The pellet was resuspended in 5 mL working buffer and centrifuged for 5 min at 4°C at 1800 rpm. The supernatant was discarded and the pellet added to the suspension of digest medium already held at 37°C in a water bath. This was all then returned to 3 h incubation.

Plastic-ware was coated with a solution of 100 μg/mL collagen IV and 50 μg/mL fibronectin in tissue-culture water. This coat was left on plastic-ware to be used for at least 1 h at 37°C in a humidified incubator. Before use, the coating was aspirated and the plastic-ware washed twice with PBS before cells were plated.

Percoll gradients were prepared in 10 mL Du Pont centrifuge tubes sterilised with 70% IMS. Tubes were coated with working buffer for at least 1 h before 7 mL of 50% Percoll gradient solution was added and then centrifuged for 1 h at 4°C at 14,500 rpm. Tissue digests were centrifuged for 5 min at 4°C at 1800 rpm, supernatant removed and pellet resuspended in 1 mL working buffer. This was layered onto the pre-equilibrated 50% Percoll gradient solution by pipetting down the wall of the tube and then centrifuged for 20 min at 4°C at 3000 rpm.

Capillary fragments were removed using a plugged Pasteur pipette and washed with working buffer (20 mL), centrifuged for 5 min at 4°C at 1800 rpm. Pellets were resuspended in appropriate volume of growth medium before plating.

The next day, medium was changed for 0.22 μM filtered media containing 5 μg/mL puromycin. Cells were washed with PBS and returned to normal growth medium three days later.

### 2.2.1.5 *Primary rat brain pericyte isolation*

Growth medium: DMEM supplemented with 10% foetal bovine serum (FBS, US origin) and 100 i.u/mL penicillin, 100 μg/mL streptomycin.

Working buffer: 100 mL HBSS ($Ca^{2+}/Mg^{2+}$) containing 2.25 mL of 22% (w/v) BSA in PBS, 10 mM HEPES and 100 i.u/mL penicillin, 100 μg/mL streptomycin

Collagenase digest medium: 100 mL HBSS (without $Ca^{2+}/Mg^{2+}$) containing 1 mg/mL collagenase (Worthington), 10 mM HEPES, 100 i.u/mL penicillin, 100 μg/mL streptomycin sterile-filtered followed by addition of 20 U/mL DNase 1 (Sigma) and 0.147 μg/mL TLCK (Sigma). Stored at -20°C.

Protocol was adapted from Maria Deli's lab and closely resembles section 2.2.1.4 using the cells from one brain to plate 15 cm$^2$ of uncoated plastic-ware (Nakagawa et al. 2009). Dissection was carried out as per section 2.2.1.4 and, once all dissected hemispheres were chopped and centrifuged for 5 min at 4°C at 1800 rpm, buffer was aspirated and 15 mL of collagenase digest medium (per three brains) added before tissue digested for 1 h at 37°C in water bath with agitation every 15 min. Digests were then removed to ice, titurated

and subjected to a 22% (w/v) BSA spin as per 2.2.1.4. The pellet was then resuspended in 5 mL complete digest buffer and digested for 1 h at 37°C in a water bath while the myelin plug was re-triturated and added to the digest as per 2.2.1.4. Percoll gradients were prepared as per 2.2.1.4 and tissue digests added and then centrifuged for 20 min at 4°C at 3000 rpm. Capillary fragments were removed using a plugged Pasteur pipette and washed with working buffer by centrifugation for 5 min at 4°C at 1800 rpm. Pellets were resuspended in appropriate volume of growth medium before plating and media changed every 3 days. No puromycin selection was used.

2.2.1.6    *Primary rat brain astrocyte isolation*

Growth medium: DMEM supplemented with 10% FBS (US origin) and 100 i.u/mL penicillin, 100 μg/mL streptomycin.

Working buffer: 100 mL HBSS ($Ca^{2+}/Mg^{2+}$) containing 2.25 mL of 22% (w/v) BSA in PBS, 10 mM HEPES and 100 i.u/mL penicillin, 100 μg/mL streptomycin

Trypsin digest medium: 1.25 mg/mL trypsin in working buffer

Protocol was adapted from the approaches of two labs, using the cells from six pups to plate 250 cm$^2$ of uncoated plastic-ware (Nakagawa et al. 2009, Abbott et al. 1992). All dissection instruments were sterilised in 70% IMS. Wistar rat pups (postnatal day 0-2) were killed by cervical dislocation. For each pup, the head was removed and dissected to reveal the entire brain similar to procedure outlined in 2.2.1.4. The brain was collected in ice-cold working buffer. Fine dissection was performed as described in 2.2.1.4. All dissected hemispheres were chopped together using a scalpel and centrifuged for 5 min at 4°C at 1800 rpm. Buffer was aspirated and 5 mL trypsin

digest medium (per three brains) was added before tissue digested for 30 min at 37°C in water bath. The trypsin was inactivated by adding astrocyte medium (5 mL), centrifuged for 5 min at 4°C at 1800 rpm and resuspended in astrocyte medium (2 mL). A narrowed plugged Pasteur pipette was used to triturate the tissue for 2 min and the cell suspension then filtered through a sterile 70 μM pore size nylon cell strainer. Cells were plated on uncoated plastic-ware and media changed every three days. Cell contaminants were separated from astrocytes seven days later by shaking on an orbital shaker for 24 h at 37°C and 5% $CO_2$.

### 2.2.1.7    *Primary rat retinal microvascular endothelial cell isolation*

Growth medium: EBM®-2 MV supplemented with 5% FBS, hFGF, VEGF, ascorbic acid, hEGF, $R^3$-IGF-1, hydrocortisone and GA-1000 according to manufacturer's instructions.

Working buffer: 100 mL HBSS ($Ca^{2+}/Mg^{2+}$) containing 2.25 mL of 22% (w/v) BSA in PBS, 10 mM HEPES and 100 i.u/mL penicillin, 100 μg/mL streptomycin

Complete digest medium: 100 mL HBSS (without $Ca^{2+}/Mg^{2+}$) containing 0.5 mg/mL collagenase and dispase (Roche), 10 mM HEPES, 100 i.u/mL penicillin, 100 μg/mL streptomycin sterile-filtered followed by addition of 20 U/mL DNase 1 (Sigma) and 0.147 μg/mL TLCK (Sigma). Stored at -20°C.

Percoll density gradient: For a 50% solution, 50 mL Percoll (GE Healthcare), 5 mL 10X HBSS ($Ca^{2+}/Mg^{2+}$) and 45 mL HBSS ($Ca^{2+}/Mg^{2+}$) combined. Stored at 4°C.

Protocol closely resembles section 2.2.1.4 using the cells from twelve eyes to plate up to 1.5 cm$^2$ of plastic-ware. Before the head was removed, eyes were cut out and collected in ice-cold working buffer. One at a time, an eye was disinfected briefly in ethanol (70%), transferred to fresh working buffer to rehydrate and moved to sterile lint moistened with working buffer for dissection. The eye was pierced under the lens and a circular incision made to flip the eye open, removing the lens, and the retinae plucked out and collected in ice-cold working buffer (5 mL). Retinae were spun twice in 20 mL working buffer (5 min at 4°C at 1800 rpm), clearing the pellet from the associated vitreous. Pellet was resuspended in complete digest medium (5 mL) and digested for 2 h at 37°C in water bath. Digests were gently shaken twice during this time.

Percoll gradients were prepared as outlined in section 2.2.1.4. Tissue digests were centrifuged for 5 min at 4°C at 1800 rpm, supernatant removed and pellet resuspended in 1 mL working buffer. This was layered onto the pre-equilibrated 50% Percoll gradient solution by pipetting down the wall of the tube and then centrifuged for 20 min at 4°C at 3000 rpm. Capillary fragments were removed using a plugged Pasteur pipette and washed with working buffer (20 mL), centrifuged for 5 min at 4°C at 1800 rpm. Pellets were resuspended in appropriate volume of growth medium before plating on plastic-ware coated with a 100 μg/mL collagen IV and 50 μg/mL fibronectin in tissue-culture water, as per section 2.2.1.4.

The next day, medium was changed for 0.22 μM filtered media containing 5 μg/mL puromycin. Cells were washed with PBS three days later and returned to normal growth medium.

## 2.2.2 Nucleofection

Subconfluent cells were trypsinised and pelleted at $3 \times 10^6$ cells per nucleofection and one reaction carried out at a time. Supernatant was aspirated and the pellet resuspended in 100 µL of Amaxa's Nucleofector™ solution V*. The suspension was added to an electrocuvette containing 10-20 µg (in a maximum volume of 5 µL) of DNA and directly nucelofected using programme U-013 of the Nucleofector device (Amaxa). Cells were then covered with the appropriate media, plated and maintained at 37°C and 5% $CO_2$ before further analysis 24-48 h later.

## 2.2.3 Sample preparation

Lysis buffer 4X: 250 mM Tris pH 6.8, 8% SDS, 35% glycerol, 10 mg/mL bromophenol blue

Lysis buffer was used at 2X by dilution with water, and prepared with 100 mM dithiothreitol (DTT). Samples to be lysed were washed with HBSS ($Ca^{2+}/Mg^{2+}$), residual liquid removed and lysis buffer added to the centre of the dish. Cells were scraped and collected into eppendorfs. Lysates were syringed 4-5 times with a 25G needle and then boiled at 95°C for 5 min. Lysates were spun at 16,000 rcf before running on a gel or storage at -20°C.

For phosphorylated proteins, samples were washed twice with ice-cold PBS supplemented with pervanadate (1 mM) and lysed with lysis buffer supplemented with pervanadate. Samples were stored at -80°C and boiled at 95°C for 5 min and pelleted at 16,000 rcf before running on a gel.

## 2.2.4 Gel electrophoresis

Running buffer: 25 µM Tris, 0.1% sodium dodecyl sulphate-polyacrylamide gel electrophoresis (SDS), 192 mM glycine

Separating and stacking gels were prepared according to the stoichiometry outlined in Table 2.4. Wells were flushed with running buffer before assembling within gel tank system and loading the molecular weight ladders (GE Healthcare), low (97, 66, 45, 30, 20.1 and 14.4 kDa) or high (220, 170, 116, 76 and 53 kDa), and designated boiled and pelleted lysates. The system was filled with running buffer and run at constant amperage of 25 mA through the stacking gel and 50 mA through the separating gel using a Power Pac 300 from Bio-Rad.

**Table 2.4: Separating and stacking gel solutions. APS is ammonium persulfate and TEMED is tetramethylethylenediamine**

| Separating gel (for two gels) | | | | Stacking gel (for two gels) | |
|---|---|---|---|---|---|
| | 7.5% | 10% | 12% | | |
| | 80 kDa | 55 kDa | 35 kDa | | |
| Acrylamide | 2.5 mL | 3.34 mL | 4 mL | Acrylamide | 0.75 mL |
| 1.5 M Tris pH 8.8 | 2.5 mL | 2.5 mL | 2.5 mL | 1 M Tris pH 6.8 | 0.63 mL |
| Water | 4.85 mL | 4 mL | 3.35 mL | Water | 3.4 mL |
| 10% SDS | 100 μL | 100 μL | 100 μL | 10% SDS | 50 μL |
| 10% APS | 80 μL | 80 μL | 80 μL | 10% APS | 75 μL |
| TEMED | 4 μL | 4 μL | 4 μL | TEMED | 10 μL |

## 2.2.5 Electroblotting

### 2.2.5.1 Semi-dry transfer

Transfer buffer: 25 mM Tris, 192 mM glycine, 20% methanol

Amido black stain: 40% methanol, 10% acetic acid, 0.1% (w/v) amido black

TBS (Tris buffered saline) 10X: 0.5 M Tris Base, 1.5 M NaCl, pH 7.5

For those with a molecular weight under 100 kDa, proteins were transferred from gel to polyvinylidene difluoride (PVDF, from GE Healthcare) membrane using a semi-dry transfer cell (Bio-Rad). While gels equilibrated in transfer buffer (at least 10 min), PVDF was primed in methanol (15 s), transferred to deionised water (2 min) and equilibrated in transfer buffer (5 min) before use. To assemble, transfer buffer soaked filter paper (5 sheets) was lain out on the transfer cell, followed by membrane, gel and topped with more transfer soaked filter paper (5 sheets), ensuring no bubbles between layers. The assembly was run at a constant voltage (12) for the required length of time, with 1 min of transfer roughly corresponding to 1 kDa of protein transferred. Once complete, amido black stain was applied to the membrane, agitated and removed, and followed by methanol (100%) for 15 s, removing excess stain, before equilibrating in TBS 1X and then drying between filter paper.

*2.2.5.2 Wet transfer*

Transfer buffer: 25 mM Tris, 192 mM glycine, 20% methanol from National Diagnostics

For those with a molecular weight over 100 kDa, proteins were transferred from gel to PVDF membrane using using a Power Pac 200 from Bio-Rad. Gels and PVDF membrane were prepared for transfer as in 2.2.5.1 with a honeycomb clamp used to contain the assembled sandwich. Transfers were performed within the same gel tank system as gel electrophoresis containing transfer buffer at 4°C and at a constant amperage of either 100 mA overnight or 350-400 mA for 3-4 h. An amido black stain was performed as described in 2.2.5.1.

## 2.2.6  Immunoblotting

BSA blocking solution: 1% (w/v) BSA, TBS 1X, 0.1% Tween-20

Milk blocking solution: 5% milk powder, TBS 1X

Secondary antibody solution: 1% (w/v) BSA, PBS 1X, 0.1% Tween-20

TBS with Tween (TBST): TBS 1X, 0.1% Tween-20

PBS with Tween (PBST): PBS 1X, 0.1% Tween-20

PVDF, after marking ladders with pen, was activated with methanol and equilibrated in TBS 1X. Membrane was blocked overnight at 4°C (or 2 h at room temperature) to block non-specific binding. Primary antibody solution was prepared in blocking solution and added to the membrane for 2 h (or overnight at 4°C). Membrane was washed twice with blocking solution and once with secondary antibody solution before addition of secondary antibody dilution for 1 h at room temperature. Membrane was washed once with secondary antibody solution, twice in TBST and once in TBS. Enhanced chemiluminescence (ECL, from Roche) was prepared at 1:1 and the membranes added for 5 min agitation on a shaker. Excess solution was removed, the membranes exposed to film and developed. When probing for phosphorylated proteins, a milk-based blocking solution was used instead.

### 2.2.7   Assessment of VEC internalisation by cell surface trypsinisation

Following treatment, as designated in the text, cells were washed three times with ice-cold PBS and incubated on ice (4°C) with trypsin (1 mg/mL) for 30 min. The reaction was stopped by the addition of soybean trypsin inhibitor (50 mg/mL). Cells were gently collected with soft sterile scrapers, centrifuged for 5 min at 4°C at 500 rpm and supernatant aspirated. Dishes were washed again with ice-cold PBS, the washings added to the lysates and spun a second time. The supernatant was aspirated and the pellet lysed as normal.

## 2.2.8 Immunofluorescence

Formalin fix: PBS 1X, 3.7% formaldehyde

Paraformaldehyde (PFA) 4% fix: PBS 1X, 4% (w/v) prilled PFA

Methanol fix: 3.7% formaldehyde, 50 mM HEPES prepared in methanol, held at -20°C

Acetone extraction: 100% acetone, held at -20°C

Triton permeabilisation: PBS 1X, 0.1% Triton X-100 (TX-100)

Blocking solution: PBS 1X, 0.02% sodium azide, 5% (w/v) BSA

Mounting solution: prepared as per Cold Spring Harbour protocol using Mowiol and DABCO

Cells to undergo immunofluorescence were plated on 35 mm plastic-ware as normal. Dishes were fixed and permeabilised as required and filled with blocking buffer while antibody dilutions were prepared in blocking buffer and centrifuged at 10,000 rcf for 5 min. A dry ring was formed around a central patch of adherent cells using folded tissue. Antibody dilution (95 μL) was added to the central patch and dishes incubated for 30-45 min within a humidified chamber inside a 37°C oven. Dishes were washed with blocking buffer and any additional staining carried out as described. Dishes were washed with blocking buffer, twice with PBS 1X and once with water before a dry ring formed, mounting solution (10 μL) added to the central patch of adherent cells, a coverslip placed on top and secured. Dishes stored at 4°C.

### 2.2.9   Assessment of VEC internalisation by cell surface acid wash

Basal media buffer: EBM2, 1% BSA, 300 μM chloroquine

Acid wash: 25 mM glycine, 154 mM NaCl, pH 1.9

Cells were washed with ice-cold HBSS ($Ca^{2+}/Mg^{2+}$) and a VEC-FITC tagged antibody directed at the extracellular tail of VEC and diluted in ice-cold basal media buffer was added to the cells for 1 h, on ice (4°C) and covered with tin foil. Cells were then washed with ice-cold basal media buffer and stimulated as designated in warmed basal media buffer. Cells were then washed with HBSS ($Ca^{2+}/Mg^{2+}$) and either fixed directly or subjected to acid wash for 15 min before fixation.

### 2.2.10   Molecular Biology

#### 2.2.10.1        *shRNA oligomer design and plasmid used*

Three shRNA oligomers were designed for each target protein. Three (21 nucleotide) sequences were pulled from three independent search engines applicable for use in both rat and mouse species (Table 2.5). pRNAT-H1.1/Shuttle (GenScript) was an adenoviral shuttle vector used for cloning. It contains a GFP marker under CMV promoter control that was used to track transfection efficiency (Fig. 2.1).

**Table 2.5: Sequences generated targeting VEGFR1 or VEGFR2**

| Gene | Accession number | Designation in text | Target sequence | Start | End |
|------|-----------------|---------------------|-----------------|-------|-----|
| VEGFR1 | NM_010228 | VR1.1 | GCGGTCTTCTTCC GAAGTAAA | 2609 | 2629 |
| | | VR1.2 | CCACATCGGCCAT CATCTGAA | 2906 | 2926 |
| | | VR1.3 | GAAACAGTGGCT TCACATACT | 3787 | 3807 |
| VEGFR2 | NM_010612 | VR2.1 | CCATGTTCTTCTG GCTCCTTC | 2578 | 2598 |
| | | VR2.2 | GACCTGGCAGCA CGAAACATT | 3336 | 3356 |
| | | VR2.3 | ATTGAGCTATCTG CCGGAGAA | 966 | 986 |
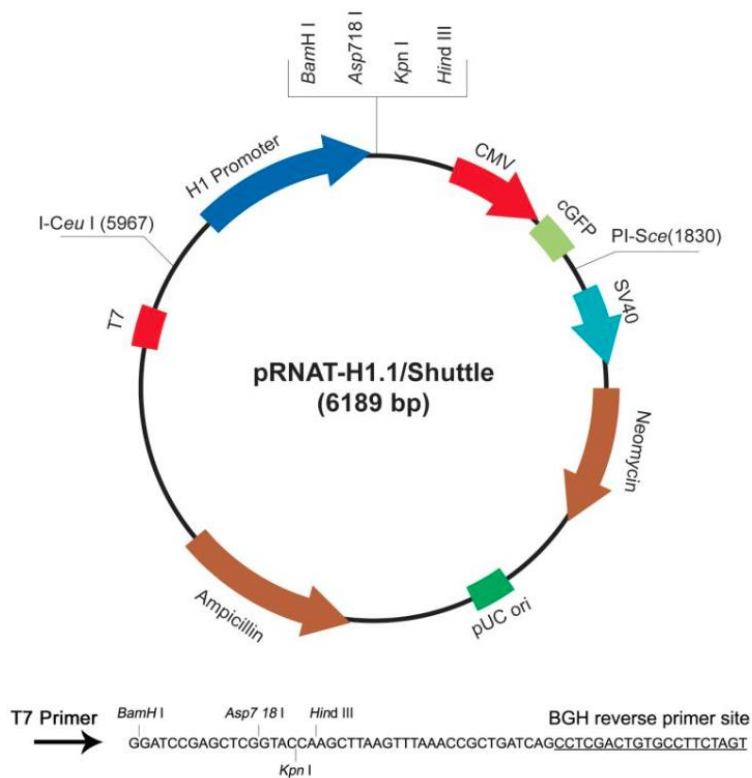


**Figure 2.1. pRNAT-H1.1/Shuttle vector map**

## 2.2.10.2 Transformation of XL1-Blue® supercompetent cells

For each reaction, 1.42 M β-mercaptoethanol (1.7 μL) was added to a sterile pre-chilled polypropylene round-bottom falcon tube (BD Biosciences) on ice. XL-1 Blue® supercompetent cells (100 μL), taken directly from -80°C and held on ice, were added to the β-mercaptoethanol and falcon swirled gently on ice. Falcon was swirled every 2 min over 10 min, next, 1μL of plasmid was added and the falcon swirled before incubation on ice for 30 min. LB broth was pre-warmed in 42°C water bath and LB agar plate containing appropriate antibiotic was pre-warmed in 37°C oven. Falcon was heat shocked in 42°C water bath for 45 s exactly and then moved to ice for 2 min to quench. LB broth (900 μL) was added to the transformation product and, once secured at an angle, incubated in 37°C rotary shaker at 225 rpm for 45 min. The resulting transformation mixture (100 μL) was added to the centre of the agar plate and spread with a sterile spreader, once all of the mixture absorbed plates moved to 37°C oven overnight.

## 2.2.10.3 Maxi preparation using Qiagen Endo-free plasmid maxi-kit

For each sample, a starter culture of LB broth (2 mL) containing appropriate antibiotic (*i.e.* 100 μg/mL of ampicillin) and a single colony of transformed XL-1 Blue® supercompetent cells was, once secured at an angle, incubated in 37°C rotary shaker at 225 rpm for 8 h. 200 μL of this starter culture was added to an overnight culture of LB broth (200 mL), again containing appropriate antibiotic (*i.e.* 100 μg/mL of ampicillin), incubated in 37°C rotary shaker at 225 rpm.

DNA was prepared, for the most part, according to the protocol accompanying the Endo-free plasmid maxi-kit (Qiagen). Overnight culture was pelleted by centrifugation for 15 min at 4°C at 6,000 rcf. The pellet was resuspended in Buffer P1 supplemented with RNase A (10 mL). Buffer P2 (10 mL) added and mixed by inverting 4-6 times and then incubated for 5 min at room temperature. Chilled Buffer P3 (10 mL) was added, mixed by inverting 4-6 times and the lysate then poured into the barrel of a prepared QIAfilter Cartridge and incubated for 10 min at room

temperature. The lysate was filtered through the Cartridge, Buffer ER (2.5 mL) added, mixed by inverting 10 times and then incubated for 30 min on ice. During this time a QIAGEN-tip 500 was prepared by equilibrating with Buffer QBT (10 mL), allowing the column to empty by gravity flow. The filtered lysate was similarly added to the QIAGEN-tip 500 and emptied by gravity flow; this was followed by two washes of Buffer QC (30 mL). The DNA was eluted with Buffer QN (15 mL), precipitated by the addition of 0.7 volumes of isopropanol, mixed and immediately centrifuged for 40 min at 4°C at 8,000 rcf. The supernatant was decanted and the pellet washed with endotoxin-free 70% ethanol (5 mL) by centrifugation for 20 min at 4°C at 8,000 rcf. The supernatant was decanted and the pellet air-dried before resuspension in either PCR water or Buffer TE. DNA concentration and purity was measured using the spectrophotometer at 260 nm and 280 nm respectively.

### 2.2.10.4    *Restriction enzyme digest*

DNA was digested with restriction enzymes, sourced from either Roche or New England BioLabs, in a total volume of 20 µL. A master mix containing the correct 10X buffer (2 µL), restriction enzyme/s (0.5 µL), RNAse (1 µL) and PCR water (to 20 µL final volume) was added to each DNA product (5 µL) and incubated for 1 h in 37°C oven. Reactions were stopped by heat inactivating restriction enzymes for 15 min in 65°C heat block and products analysed by 1% (w/v) agarose (BDH Electran) gel electrophoresis.

### 2.2.10.5    *Agarose gel electrophoresis*

Loading dye 6X: 30% (w/v) glycerol, 0.25% xylene cyanol

DNA fragments were analysed by separation on 1% (w/v) agarose gel (BDH Electran). Agarose was dissolved in Tris-acetate-EDTA (TAE) buffer by melting and, before pouring into appropriate gel tray with comb to set, 2 µL of nucleic acid staining solution (RedSafe from iNtRON) was added. Samples, and a 1 kb DNA ladder (Invitrogen), were prepared by addition of loading dye 6X before loading on the gel and visualisation by electrophoresis in TAE buffer at a constant voltage of

80-140 (dependant on gel size). The separated DNA fragments were visualised at 320 nm under a UV illuminator (Gene Genius Bio Imagine System, Syngene).

## 2.2.10.6 *Annealing oligomers*

Annealing buffer 10X: 100 mM Tris-Cl (pH 8), 10 mM EDTA, 1 M NaCl

Upper and lower oligomers were annealed in a total reaction volume of 20 μL. Annealing reactions were prepared in the following order with PCR water (8 μL), annealing buffer 10X (2 μL) and then the upper and lower oligomers (5 μL, at 200 μM for final concentration of 50 μM), added to tubes on ice. Tubes were incubated for 8 min in 95°C heat block and then entire block removed to bench so that the annealing reactions cooled down slowly to room temperature (approximately 45 min-1 h). Tubes then moved to ice.

## 2.2.10.7 *Ligation of oligomers into plasmid vector*

Annealed oligomers were ligated into plasmid vector in a total reaction volume of 10 μL. Plasmid vector (6 μL), oligomer (2 μL), 10X buffer (1 μL) and DNA ligase (1 μL) were added to reaction tubes and incubated for 40 min at room temperature. Tubes were then incubated for 10 min in 65°C heat block. To test that the linearised plasmid vector has taken the oligomer and re-ligated to form a ring, a diagnostic restriction digest was carried out.

## 2.2.10.8 *Small scale preparation of plasmid DNA*

Lysing buffer: 50 mM Tris-Cl (pH 7.5), 62.5 mM EDTA, 0.4% TX-100, 2.5 M LiCl

A single colony from a transformation reaction was added to LB broth (2 mL) containing appropriate antibiotic (*i.e.* 100 μg/mL of ampicillin) and, once secured at an angle, incubated in 37°C rotary shaker at 225 rpm overnight. The following morning, starter culture moved to ice and 1.5 mL transferred to pre-chilled eppendorfs. Culture pelleted for 2 min at 4°C at 12,000 rcf and supernatant aspirated.

Pellet resuspended in lysing buffer (250 μL) and incubated for 5 min on ice. Freshly prepared lysozyme (25 μL, and 10 mg/mL) was added and tube vortex for 3 s. Tube boiled for 1 min, 20 s in 100°C water bath and incubated for 5 min on ice. Cell debris pelleted for 10 min at room temperature at 12,000 rcf and the pellet removed using an autoclaved toothpick in one motion. 100% ethanol (500 μL) added to supernatant and mixed before leaving to stand for 15 min at room temperature. Tube spun for 10 min at room temperature at 12,000 rcf and 70% ethanol (500 μL) added before another 10 min at room temperature at 12,000 rcf. Ethanol aspirated and the pellet allowed to air dry before resuspension in appropriate solution.

### 2.2.10.9 *Polymerase Chain Reaction*

DNA amplification using either forward or reverse primers directed at the sequence of interest was carried out in a total reaction volume of 10 μL. Primers were dissolved in PCR water to a concentration of 0.25 μM. A master mix of big dye reaction mix (0.5 μL), big dye buffer (2 μL) and either forward or reverse primer (2.5 μL) was prepared and added to 1 μL of DNA. Amplification was carried out in an Eppendorf Mastercycler Gradient starting with 1 min at 96°C to denature the samples, 25 cycles of 10 s at 96°C, 5 s at 50°C and 4 min at 60°C then followed before the products were held at 4°C.

### 2.2.10.10 *Sequencing*

Amplification products were cleaned before sequencing using genCLEAN 96-well spin plates (Genetix). PCR water (10 μL) was added to each sample (total volume of 20 μL) and a genCLEAN plate prepared, first by centrifugation for 5 min at 910 rcf to remove storage liquid and then washed with PCR water (100 μL) for 5 min at 910 rcf. Diluted amplification products (20 μL) were added to the prepared genCLEAN plate and collected in fresh plate by centrifugation for 5 min at 910 rcf. Contents were transferred to sequencing plate and run on a Hitachi 3730 DNA analyser (Applied Biosystems). Sequencing data analysed using Chromas Lite programme (free download) and identified using Blast.

### 2.2.10.11    *DNA precipitation*

DNA precipitated by ethanol precipitation, 3 M sodium acetate added to sample at 10% total volume and mixed well. Ethanol (100%) added at 2.5 volumes and sample incubated for 10 min on ice. Sample centrifuged for 10 min at 4°C at 16,400 rpm and then washed with ethanol (70%) for 5 min at 4°C at 16,400 rpm. Ethanol was aspirated and pellet allowed to air dry before resuspension in appropriate volume of water or buffer.

### 2.2.10.12    *Recombinant adenovirus production*

Two adenoviral stocks per protein of interest were generated, scaled up and purified by Vector BioLabs. Characterisation profile including virus particle (VP) and plaque formation unit (PFU) titres in Table 2.6.

**Table 2.6: Characteristics of adenoviruses**

| Name | Volume | VP titre | PFU titre |
|------|--------|----------|-----------|
| Ad-H1-shVEGFR1(#1)-CMV-cGFP | 10 x 200ul | 5.0 x1012 VP/ml | 2.1 x1011 IFU/ml |
| Ad-H1-shVEGFR1(#2)-CMV-cGFP | 10 x 200ul | 5.0 x1012 VP/ml | 1.9 x1011 IFU/ml |
| Ad-H1-shVEGFR2(#1)-CMV-cGFP | 10 x 200ul | 5.0 x1012 VP/ml | 1.6 x1011 IFU/ml |
| Ad-H1-shVEGFR2(#2)-CMV-cGFP | 10 x 200ul | 5.0 x1012 VP/ml | 1.6 x1011 IFU/ml |

## 2.2.11  Measuring TEER across cell barriers

For measurements using either the volt-ohmmeter or ECIS device the rationale is similar whereby an alternating current is produced by an electrode and the voltage which results is measured by the device which derives an impedance value (resistance equivalent in AC) using Ohm's law (Impedance is the voltage divided by the current). With greater barrier properties of the cells under investigation, the

greater the TEER value. It follows that, when measuring the effect of a vasoactive mediator on barrier function for example, a drop in TEER indicates a disruption in barrier function.

### 2.2.11.1 *Measuring TEER within transwells*

An epithelial volt-ohmmeter (WPI Inc.), with mode knob set to R for resistance, was used to measure the TEER of primary rat brain microvascular endothelial cells (BMVECs) plated on transwells (of diameter 12 mm or larger). STX2 chopsticks (WPI Inc.) were sterilized with ethanol (70%), allowed to dry and then equilibrated with potassium chloride (0.1 M) before taking measurements. The electrode was placed into the well so that the tips (which are of two different lengths to accommodate the difference in depth between the bottoms of the transwell and well) just touch the bottom of the transwell/well without bending the electrode. The electrode was held in this position while measurement taken by pressing test button, with the value appearing on a digitised panel on the device. The value of a blank transwell was taken from raw resistance values before use.

### 2.2.11.2 *Measuring TEER using ECIS*

Cells were grown on 12 mm gold-coated ECIS grids (8W1E and 8W10E) at 37°C and 5% $CO_2$ and real time impedance was acquired using a 1600R device and firm software (Applied Biophysics) to derive TEERs. Once grids clamped to device, appropriate parameters selected using software and initial values checked. At the start of experiments, TEER values were approximately 25,000 $\Omega$ and 15,000 $\Omega$ for brain and retinal BMVECs, respectively. Measurements were taken for approximately 1 h, or until the baseline stabilised, after which time the device was paused and additions were made to wells, without removing the grid/s from the incubator. Additions were made to both minimize changes in hydrostatic pressure and ensure optimal mixing, by taking up a quarter of the grid volume (400 µL) and transferring it to a companion Eppendorf containing the designated treatment, mixing, and then returning the solution back to the grid. This was repeated for all

grid wells before restarting measurements. Once experiment was complete, data was visualised and analysed using Excel.

### 2.2.12  Fluorescein flux assay

FITC-dextran 4 kDa (1 mg/mL) was added to the apical side of primary rat BMVECs plated on transwell filters (12 mm), cultured overnight in starvation medium. A sample of media from the basal side of each transwell (50 µL) was removed to a black 96-well plate, which was kept covered from light, and the loss replenished with fresh starvation media (50 µL), this was repeated every 20 min for at least 1 h when designated treatments were then added. Measurements were continued for at least another 2 h. PBS (50 µL) was added to each well of black 96-well plate, a trio of blank wells prepared using starvation media and PBS prepared and the fluorescence was measured in a FLUOstar OPTIMA microplate reader (excitation 490 nm, emission 520 nm). Fluorescence for samples was plotted against time and dextran flux was determined from linear slope changes before and after addition of treatments.

### 2.2.13  HRP assay

HRP (5 mg/mL) was added to the apical side of primary rat BMVECs plated on transwell filters (12 mm) with the designated treatment, and incubated for 1 hour at 37°C and 5% $CO_2$. Cells were washed six times with HBSS ($Ca^{2+}/Mg^{2+}$) and fresh medium was added. Samples (100 µL) were then removed from the basal transwell side to eppendorfs kept at 4°C, every 20 minutes, and the loss replenished with fresh media (100 µL). This was continued for at least 2 hours following which time samples were reacted with 100 µL of 1 mg/mL o-phenylenediamine (OPD) with 30% hydrogen peroxide. Once the relevant and timed colour change was observed, the reaction was stopped with 100 uL of hydrochloric acid (1N) and absorbance measured in a FLUOstar OPTIMA microplate reader. HRP activity was plotted against time and rates determined by linear regression (Martins *et al.*, 2013).

### 2.2.14  HRP uptake assay

Uptake of HRP was studied similarly to transport, primary rat BMVECs were grown in 96-well plates and treated with the designated treatment before the addition of HRP (1 mg/mL). Cells were washed three times with HBSS ($Ca^{2+}/Mg^{2+}$) and lysed with 1% TX-100 in PBS (50 µL) before proceeding with a stoichiometric OPD and hydrogen peroxide reaction and analysis as described above 2.2.15.

### 2.2.15  Triple culture preparation

For a transwell (12 mm) model, $50,000/3.8$ $cm^2$ primary rat astrocytes were plated 48 h before assembly of triple cultures. Using primary rat BMVECs prepared on separate transwells and with a corrected TEER of at least 300 $\Omega$ (approximately $30,000/cm^2$), media was aspirated and either $20,000/cm^2$ or $100,000/cm^2$ primary rat brain pericytes were applied to inverted transwells in 100µL volumes and the preparation moved to 37°C and 5% $CO_2$ for 2 h. Transwells were transferred to plastic-ware containing astrocytes and returned to incubator for 48 h at 37°C and 5% $CO_2$ before TEER measured and preparations used once TEER over 300 $\Omega$.

### 2.2.16  NVU spheroid preparation

Suspension media: 4% methylcellulose in EBM®2 without supplements

Triple cultured spheroids of an equal ratio of primary rat brain astrocytes, pericytes and microvascular endothelial cells were generated by suspension in 30 µL droplets on the lids of 60 mm plastic-ware for 48 h at 37°C and 5% $CO_2$. Neurospheres were collected by gravity and fixed with 4% PFA. Before assembly, astrocytes and pericytes were stained with CellTracker™ dyes (Thermo Fisher Scientific), CMAC (blue) and CMFDA (green) as designated in the text, while microvascular endothelial cells were immunostained for the endothelial marker, VEC, post-fixation.

### 2.2.17  Electron microscopy

Wash buffer: 0.1% BSA in PBS

Antibody solution: 4 μg/mL digitonin, 0.25% BSA *i.e.* permeabilisation buffer at 1:10

Full fix: 2% PFA, 2% glutaraldehyde, 0.1 M cacodylate

#### 2.2.17.1      *HRP loading for EM analysis*

Cells were prepared and treated as outlined in 2.2.14 (HRP transport) and, once washes complete, cells were fixed in full fix for 2 h and kept in PBS until ready to proceed to diaminobenzidine (DAB) reaction and embedding.

#### 2.2.17.2      *DAB reaction*

PBS removed to waste, DAB reaction prepared and added. Cells covered with tin foil, incubated at RT for 30 min and then washed twice with 0.1 M Tris, twice with deionised water.

#### 2.2.17.3      *Embedding*

Cells were incubated on ice with a solution of 1.5% potassium ferricyanide and 1% osmium tetroxide at a 1:1 ratio, covered with tin foil for 1 h. The solution was discarded to a designated waste container, and the first wash with deionised water also discarded to the designated waste container. Cells were washed twice more and waste discarded to the fume hood sink. Cells then underwent dehydration steps, deionised water was aspirated and 70% ethanol applied for 5 minutes. This was aspirated and replaced with 90% ethanol for a further 5 minutes. Finally, the 90% ethanol was replaced with 100% and left to incubate for 10 minutes. This was followed by a second incubation with 100% ethanol. After 10 minutes, a 1:1 propylene oxide and Epon mixture was applied and incubated for 20 minutes at room

temperature. Coverslips were then placed, cell side facing down, onto the top of an Epon resin stub that was prepared separately. These stubs were baked in a 60°C oven overnight. The following day, a heat block was used to aid the removal of the coverslip from the top of the stubs. Slivers of Epon containing sample were chipped from the stub using a blade and transferred to coffins containing appropriate labels. Free Epon was added to the coffins, ensuring the slivers were ideally positioned and left to bake in the 60°C oven overnight.

### 2.2.17.4 Sectioning and imaging

Specimens were sectioned at 70nm and visualized on a JEOL 1010 transmission electron microscope.

## 2.2.18 Confocal microscopy

CLSM 700 (Carl Zeiss) was used to take Z-stack images from which maximum intensity projections were generated using Image J software.

## 2.2.19 Quantification and statistics

Data are expressed as mean ± standard error of the mean (SEM) using Excel. Statistical calculations were performed using IBM SPSS statistics 22 and significance was considered acceptable when $P < 0.05$. The statistical tests implemented in this thesis are as follows; 1) One-way ANOVA followed by Bonferroni's post-hoc tests, 2) Unpaired student's T-test. Box plots were generated using BoxPlotR (Spitzer et al. 2014).

# Chapter 3   Results

**Luminal LPC induces microvascular permeability at the blood brain and blood retinal barriers via VEGFR2 signalling**

## 3.1    Contribution of authors

**Figure 3.1. LPC enhances macromolecular flux across rat brain MVECs**

Hudson, N

**Figure 3.2. LPC enhances junctional permeability in both brain and retinal MVECs**

(A) Kenny, BA

(B) Kenny, BA

**Figure 3.3. Luminal LPC enhances permeability of a fluorescent tracer from an occluded rat pial microvessel**

(A) Sarker, MH

(B) Sarker, MH

(C) Sarker, MH

(D) Sarker, MH

**Figure 3.4. Apical (luminal) LPC enhances macromolecular flux across rat brain MVECs**

Kenny, BA

**Figure 3.5. Characterisation of retinal cell line, PT2**

(A) Shams, F

(B) Shams, F

(C) Turowski, P

**Figure 3.6. LPC activates p38 and VEGFR2 in PT2 cells**

(A) Kenny, BA

(B) Kenny, BA

(C) Kenny, BA

(D) Kenny, BA

**Figure 3.7. LPC induced junctional permeability prevented by chemical inhibitors targeting VEGFR2 in both brain and retinal MVECs**

(A) Kenny, BA

(B) Kenny, BA

**Figure 3.8. LPC enhanced macromolecular flux across rat brain MVECs prevented by VEGFR2 inhibition but not by VEGF sequestration**

(A) Hudson, N

(B) Kenny, BA

**Figure 3.9. Development and characterization of VEGFR2 targeting adenovirus using GPNTs**

(A) Kenny, BA

(B) Kenny, BA

(C) Kenny, BA

**Figure 3.10. Representative visualisation of GFP expression following infection of rat brain MVECs with adenovirus**

(A) Kenny, BA

(B) Kenny, BA

**Figure 3.11. LPC induced junctional permeability prevented by adenovirus targeting VEGFR2 in brain MVECs and LPC induced permeability *in vivo* prevented by VEGFR2 chemical inhibition**

(A) Kenny, BA

(B) Kenny, BA

**Figure 3.12. Indications that LPC's capacity to alter MVEC permeability extends to transcellular transport**

Kenny, BA and Turowski, P (analysis)

## 3.2    Introduction

As detailed in the introduction, diabetes is a systemic disease with well recognized microvascular complications one of which is inner BRB breakdown. This contributes to the development of DR, the prevalence of which is about one third among those with diabetes and the leading cause of blindness among the working population across the world (Guo et al. 2016, Yau et al. 2012). Furthermore, risk of DR increases with longer disease duration and presence of hypertension (Stitt et al. 2016). Currently, a key therapeutic target is to counteract the effect of VEGF-A within the retina but treatments do not fully resolve manifestations of DR, such as oedema, in a significant proportion of patients and could possibly harm retinal neuroglia and resident macrophages (Stitt et al. 2016).

Thus, there is justification to identify other mediators in the pathogenesis of DR, one of which could be LPC. In healthy subjects, the serum concentration of LPC (140-150 µM) is much higher than the maximal concentrations (10-50 µM) which have been found to elicit LPC's biological activities (McIntyre, Zimmerman and Prescott 1999). In diabetic patients, LPC is elevated even more; lipids extracted from the total plasma of control, type-1 or type-2 diabetes patients were separated, visualised and compared using inorganic phosphorus level analysis revealing that average levels of LPC in these groups were $143\pm22$, $237\pm45$ and $208\pm41$ µmol $P_i$/l respectively (Iwase et al. 2008, Rabini et al. 1994). LPC has been shown to induce permeability responses in endothelial cells (of dermal and pulmonary origin) *in vitro* (Huang et al. 2005). In addition, an upregulation of adhesion molecule expression, cytokine and superoxide production and NF-κB binding, all contributing to a pro-inflammatory EC phenotype, has also been found to result from LPC activity *in vitro* (Huang et al. 2005). An amphiphilic phospholipid, LPC is generated alongside oxidized nonesterified fatty acids (NEFAs) when lipoprotein-associated $PLA_2$ (Lp-$PLA_2$) hydrolyzes the phosphatidylcholine of oxidized low density lipoprotein (LDL) (Matsumoto, Kobayashi and Kamata 2007). Increased levels of oxLDL coincide with an increasingly oxidative diabetic milieu in a way commensurate to the increased

oxidative status seen in atherosclerosis, where it has been known for many years that oxLDL plays a significant role in its pathogenesis (Steinberg 1997). First detected in snake venom, very high concentrations of LPC theoretically can be powerfully cytolytic but LPC levels are very well controlled in terms of both its catabolism and its reversible sequestration by albumin in the plasma (Weltzien 1979, Matsumoto et al. 2007). Moreover, although LPC can exist as a monomer, within a micelle or as both versions simultaneously when in a fluid, it has been shown that LPC's specific effects are exerted when in monomeric form, while micelles are responsible for nonspecific damage such as cell lysis (Bergmann, Ferguson and Sobel 1981). Crucially, the critical micelle concentration (CMC) for LPC micellar formation is relatively high (40-50 µm for LPC monomers, when present without albumin), and the CMC increases further when albumin presence is taken into account, an evolutionary safeguard against rampant LPC cellular destruction (Bergmann et al. 1981).

In this chapter the effect of LPC on neural and retinal microvascular endothelium was explored using a novel retinal cell line, PT2, primary brain MVECs, primary retinal MVECs and occluded rat pial microvessels as models. Here the data indicates that LPC induces vasopermeability via transactivation of VEGFR2 in a manner separate from VEGF's activity. This work pinpoints an alternative, or complementary, target for the treatment of diabetes-induced retinal vasopermeability.

## 3.3 Results

### 3.3.1 LPC triggers permeability changes in both neural and retinal microvascular endothelium

The potential functional effect of LPC on neural and retinal microvasculature was initially investigated using highly purified cultures of primary cells isolated from rat brain and retina. While a high yield of primary MVECs can be isolated with well-preserved inter-endothelial junctions, apico-basal polarity and barrier properties for use at passage zero, the equivalent culture of primary retinal MVECs required an additional round of culturing by trypsinisation before use at passage one. The apical to basal macromolecular flux of a 4 kDa dextran tracer conjugated to FITC (FITC-dextran flux) across brain MVECs plated on polycarbonate transwells was measured in response to the addition of LPC to the apical chamber. LPC addition promoted a dose-dependent, significant increase in tracer flux across brain MVECs (Fig. 3.1A), indicating a change in permeability.
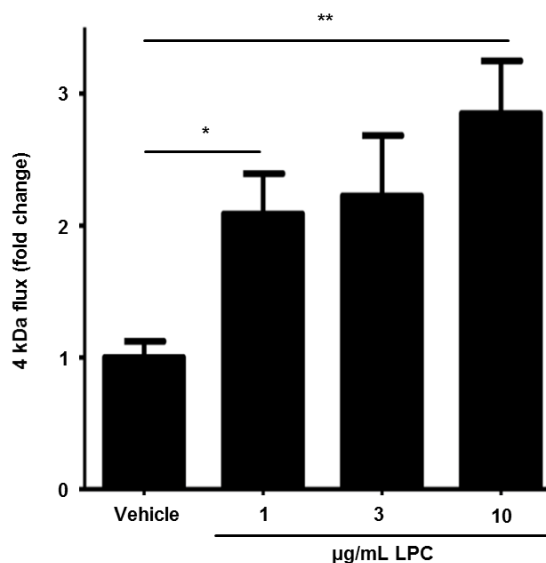


**Figure 3.1. LPC enhances macromolecular flux across rat brain MVECs**
4 kDa dextran flux across primary rat brain MVECs grown to confluence measured before and after the addition of LPC at the concentrations indicated. Shown are means ± SEM (n =

8 for vehicle, n = 4 for 1 µg/mL LPC, n = 5 for 3 µg/mL LPC, n = 10 for 10 µg/mL LPC) of averaged 2 h flux with measurements following treatment additions divided by baseline measurements. One-way ANOVA (p = 0.022) with Bonferroni post-hoc tests: *, p < 0.05, **, p < 0.01.

TEER measurements provide another approach for characterizing physiological barrier function by which a drop in TEER reflects an increase in junctional permeability. A dose-dependent decrease in TEER was recorded in response to the apical addition of increased concentrations of LPC to brain MVECs, this change was significant and peaked within 10 minutes of LPC addition (Fig. 3.2A). In retinal MVECs, LPC (10 µg/mL) similarly induced a transient decrease in TEER measurements but the change was slightly delayed and slightly less potent (Fig. 3.2B). The disparity between vascular beds in this regard could be due to limitations in primary retinal MVEC preparation requiring the use of passaged cultures.
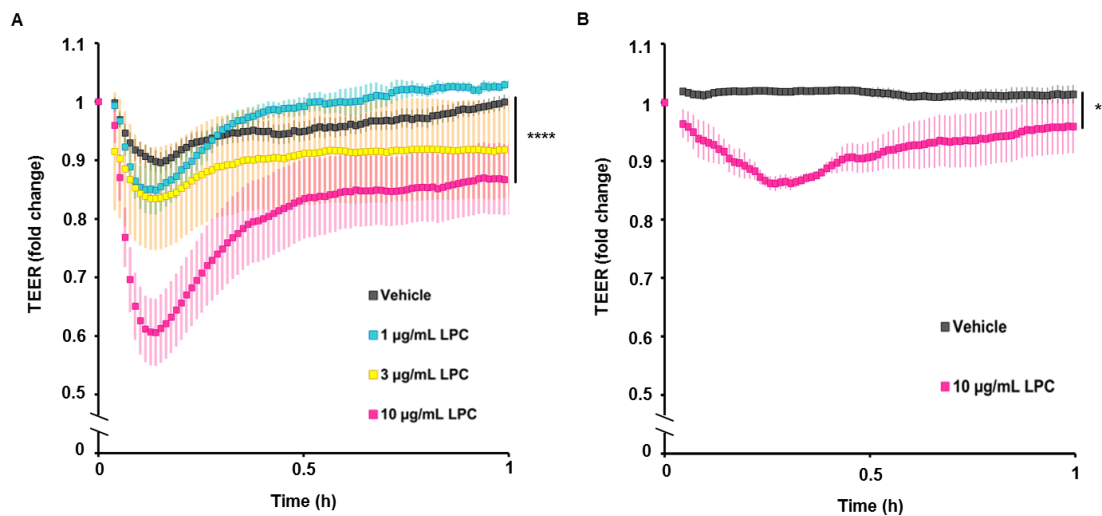


**Figure 3.2. LPC enhances junctional permeability in both brain and retinal MVECs**
Primary rat brain (A) and retinal (B) MVECs were grown to confluence and full electrical barrier (TEER of ca. 25,000 Ω and 15,000 Ω respectively). LPC at the concentrations indicated added at time 0. Shown are means ± SEM of normalised resistance changes. Brain and retinal MVEC differences: ****, p < 0.0001 and *, p < 0.004 respectively. Bonferroni

post-hoc tests indicate significant differences between vehicle and 10 μg/mL LPC (brain: ****, p < 0.0001; retina: *, p < 0.05).

The effect of LPC on tracer loss (sulforhodamine B, 580 Da) from occluded pial microvessels of Wistar rats (age 25-30 days) was used to confirm whether *in vitro* results translated to an *in vivo* model. Vessels in the area of interest were filled with tracer before one microvessel on the pial surface was occluded using a glass probe and LPC delivered either through the carotid artery (luminal) or via application to a cranial window (abluminal). Video microscopy was used to record time-dependent tracer loss from the vessel, with any loss solely due to permeability changes. Intensity mapping enabled calculations of vessel permeability and time-dependent changes using $C_t = C_0.e^{-kt}$; where $k = 4P/d$, and where $C_t$ and $C_0$ are the dye concentrations at time $t$ and 0, respectively; $P$ is the permeability and $d$ is the diameter of the vessel (Hudson et al. 2014). Following luminal injection of LPC (30 μg/mL to account for dilution within the circulation and concentration assumed to be 10-15 μg/mL in the area of interest), the level of sulforhodamine B within the single occluded microvessel decreased approximately 40 s later (Fig. 3.3A upper image sequence and Fig. 3.3B). When LPC (10 μg/mL) was applied abluminally through a cranial window at 20 s there were no changes in sulforhodamine B levels (Fig. 3.3A lower image sequence and Fig. 3.3C). The increase in microvascular permeability seen with luminal LPC application was significant when compared with abluminal LPC application within this *in vivo* model (Fig. 3.3D).

The sidedness in LPC's effect on opposing sides of the pial microvessel wall was further examined by FITC-dextran flux across brain MVECs in response to LPC addition to either the apical or basal compartments, corresponding to the luminal or abluminal aspect of a microvessel respectively. Apical LPC addition promoted a significant increase in tracer flux when compared with the level of tracer flux measured on basal LPC addition (Fig. 3.4A).
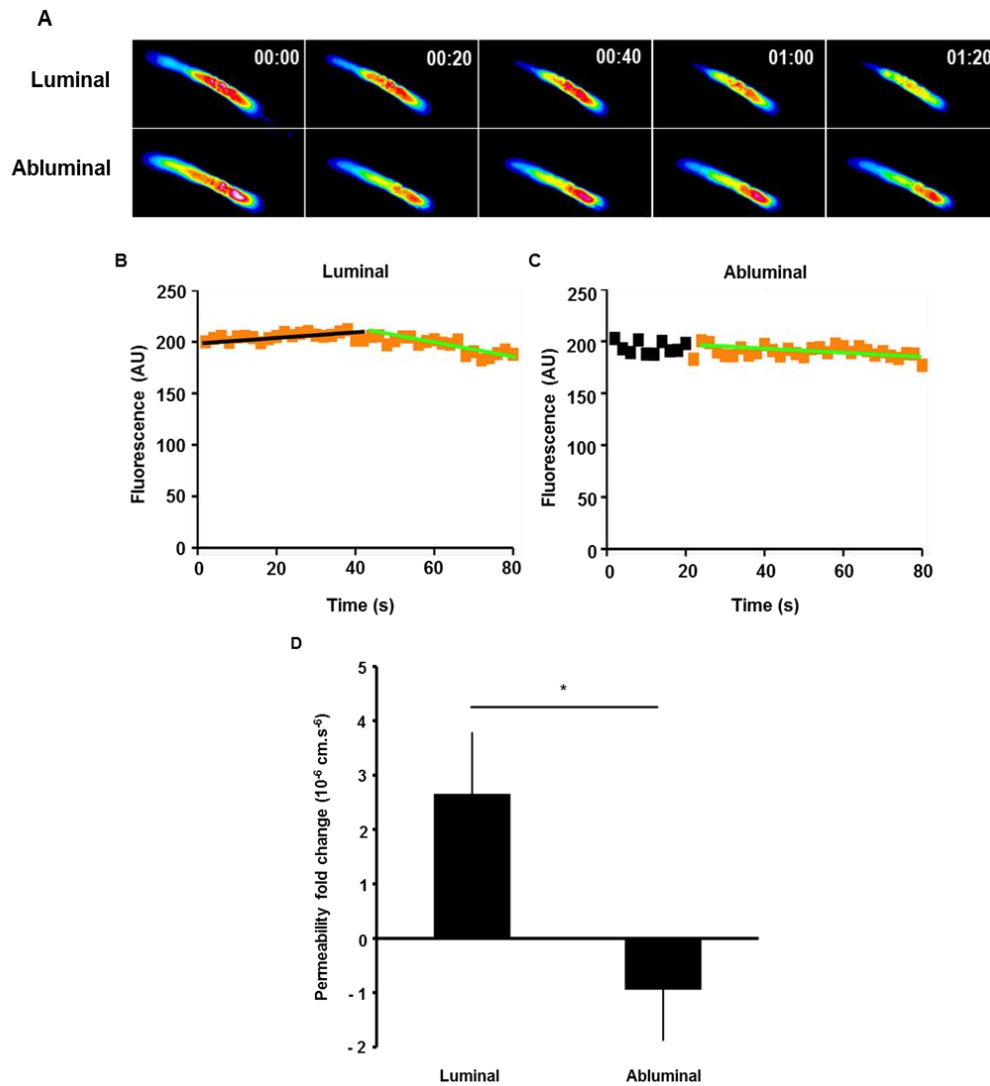
**Figure 3.3. Luminal LPC enhances permeability of a fluorescent tracer from an occluded rat pial microvessel**

Real time recording of sulforhodamine B (580 Da) loss from single occluded rat pial microvessels *in vivo*. Luminal injection of 30 μg/mL LPC via intracarotid (assumed diluted to 10-15 μg/Ll final LPC in brain vasculature) produced strong decrease of sulforhodamine B after ca. 40 s (A, upper panel). Abluminal application of 10 μg/ml LPC via cranial window at 20 s did not lead to changes in permeability (A, lower panel). Representative micrographs of pseudo-coloured microvessels at indicated times (min). Mean densitometric fluorescent intensities in microvessels plotted against time for luminal (B) and abluminal (C) where data was fitted to the equation $C_t = C_0 e^{-kt}$ (black and green trend lines, pre- and post-LPC addition respectively). Mean permeability changes (D) following luminal LPC (n = 8 for assumed 10-

15 μg/mL final) and abluminal LPC (n = 4 for 10 μg/mL) ± SEM (*, p < 0.05, Student's T-test).
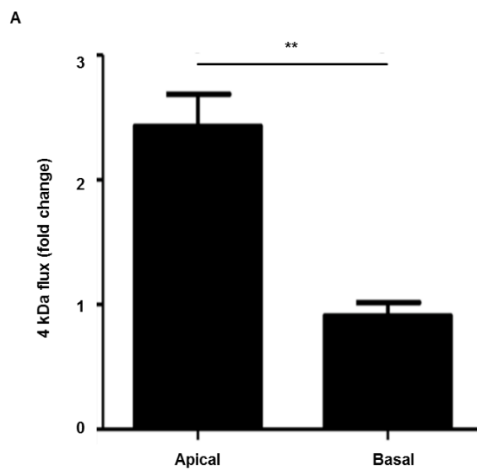


**Figure 3.4. Apical (luminal) LPC enhances macromolecular flux across rat brain MVECs**
4 kDa dextran flux across primary rat brain MVECs grown to confluence measured before and after the addition of LPC (10 μg/mL) either apically or basally. Shown are means ± SEM (**, p < 0.01, Student's T-test).

### 3.3.2    LPC induced vasopermeability operates via VEGFR2 signalling

VEGF-A activates VEGFR2 promoting increased permeability via p38 MAP kinase signalling within brain MVECs (Hudson et al 2014). To investigate any functional interaction of LPC signalling and VEGF-A signalling, it was convenient to utilize a relevant cell line. PT2s are a rat retinal MVEC line that is morphologically comparable with primary retinal MVECs, from phase contrast images (Supplementary Fig. 3.1A). Although functionally, and not unusually for a cell line, the average TEER of the former, 33.6 (-/+ 7) $\Omega cm^2$, is five times less than the latter, 150 (-/+ 10) $\Omega cm^2$ (Fig. 3.5A). Regardless, PT2 cells stain for endothelial cell markers including VE-Cadherin, PECAM-1 and von Willebrand factor; blood brain barrier markers including transferrin receptor and p-glycoprotein; and also for junctional markers including ZO-1, occludin, p120, claudin-5, α-catenin,

**A**

Primary RMVEC    RMVEC cell line PT2

**B**

VE-Cadherin    PECAM-1    VWF    Transferrin receptor

P – glycoprotein    ZO-1    Occludin    Claudin – 5

α – catenin    β – catenin    γ – catenin    p120

**C**
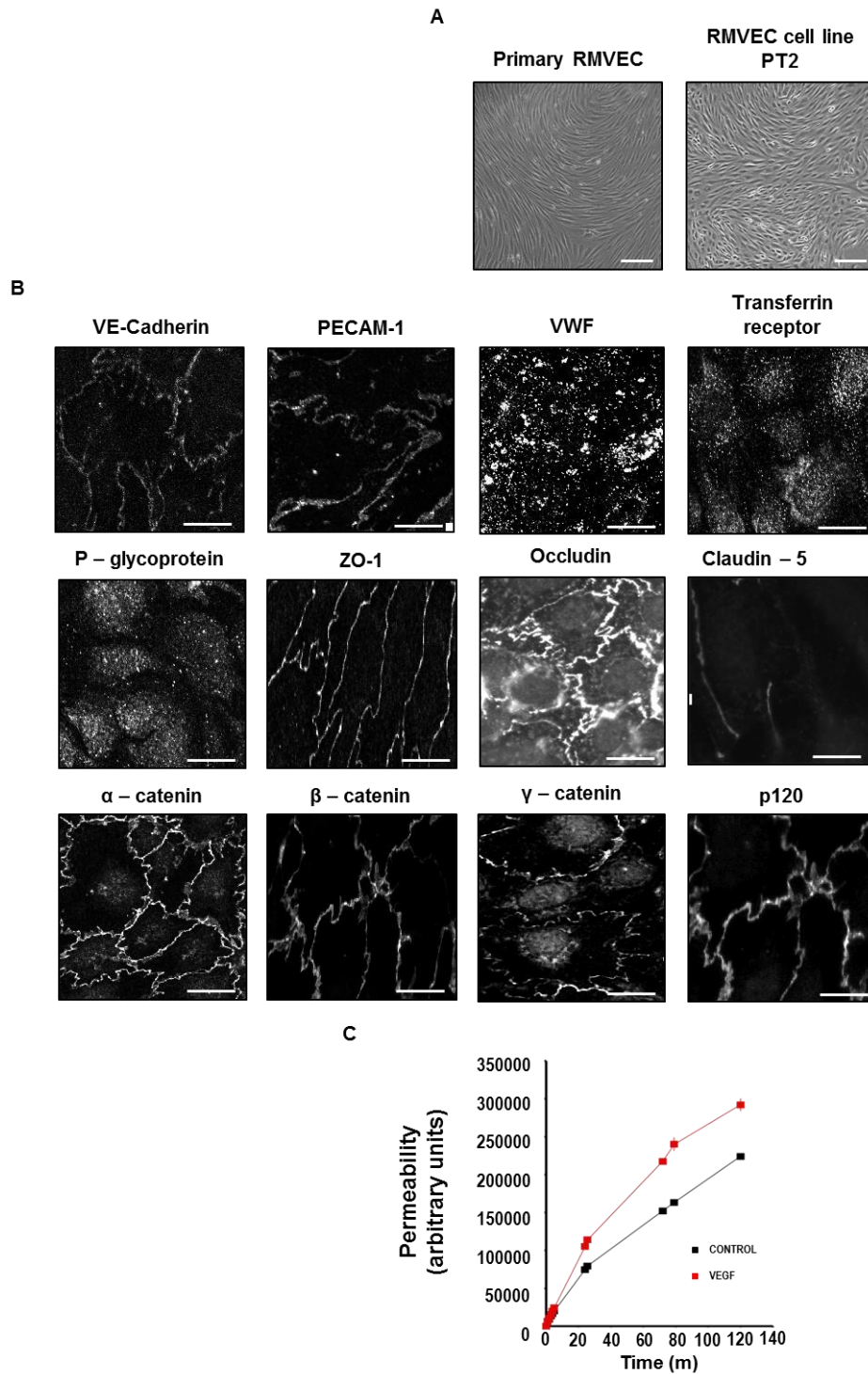
**Figure 3.5. Characterisation of retinal cell line, PT2**

Primary retinal MVECs were isolated and immortalized using a retrovirus coding for temperature-sensitive large T and immortalised clones were then isolated and characterized by immunofluorescence. Phase contrast of primary rat retinal MVECs, with an average

112

TEER of 150 ($\pm$ 10) $\Omega$ cm2 measured by STX-2 chopstick electrodes (A, left panel). Scale bar 50 $\mu$M. Phase contrast of rat retinal MVEC line, PT2, with an average TEER of 33.6 ($\pm$ 7) $\Omega$ cm2 (A, right panel). Scale bar 50 $\mu$M. 4 kDa FITC coupled dextran flux and 70 kDa rhodamine coupled dextran flux across PT2 was measured by spectrophotometer. The permeability coefficient obtained for 4 kDa FITC-dextran was 0.001289 ($\pm$ 0.000361) cm/min (n = 3) and 0.000083347 ($\pm$ 0.00000214) cm/min (n = 3) for 70 kDa rhodamine-dextran. The permeability coefficients obtained for experiments on brain primary MVECs were 0.000232 cm/min for 4 kDA FITC-dextran (Ockrim, 2010, Thesis). Scale bar 50$\mu$M. PT2s were fixed and stained for EC markers including VEC, PECAM-1 and vWF; blood brain barrier markers including transferrin receptor and p-glycoprotein, and junctional markers including ZO-1, occludin, claudin-5, $\alpha$-catenin, $\beta$-catenin, $\gamma$-catenin and p120 (B). Scale bar 10$\mu$M. PT2s grown on permeable transwell supports for 40 kDa dextran flux measured after the addition of control or VEGF (50 ng/mL) (C).

$\beta$-catenin and $\gamma$-catenin (Supplementary Fig. 3.5B). When measured by dextran flux (4 kDa), PT2 cells were shown to be responsive to VEGF, as VEGF addition caused increased levels of permeability (Fig. 3.5C).

Treatment of PT2 cells with LPC resulted in significant p38 activation, as measured by phosphorylation of T180/Y182 on p38, within 5 min of LPC addition (Fig. 3.6A, B). VEGFR2 was also significantly activated within 5 min of LPC addition, with phosphorylation on Y1175, and in a manner akin to activation observed following 5 min of VEGF-A treatment (Fig. 3.6C, D). Phosphorylation on Y1175 following treatment with either VEGF-A, or LPC, was prevented by pre-treatment with the VEGFR2 specific kinase antagonist SU1498 for 1 h (Fig. 3.6C, D). As it has been shown that VEGFR2 distribution on brain MVECs predominates on the abluminal side of vessel walls, yet LPC's functional effects are exerted from the luminal side, it is possible that LPC transactivates VEGFR2 (Hudson et al. 2014).

To determine whether VEGFR2 inhibition translated to a reduction in the functional effects of LPC on MVECs, pharmacological inhibitors, PTK/ZK and SU1498, were employed in assays recording TEER measurements of brain and retinal MVECs in

response to LPC addition (Fig. 3.7A, B). For both brain and retinal MVECs, SU1498 significantly reduced the effect of LPC on TEER measurements (Fig. 3.7A, B). A second VEGFR2 tyrosine kinase antagonist called PTK/ZK, with different specificity for VEGFR2 than SU1498, was similarly employed and found to have a greater
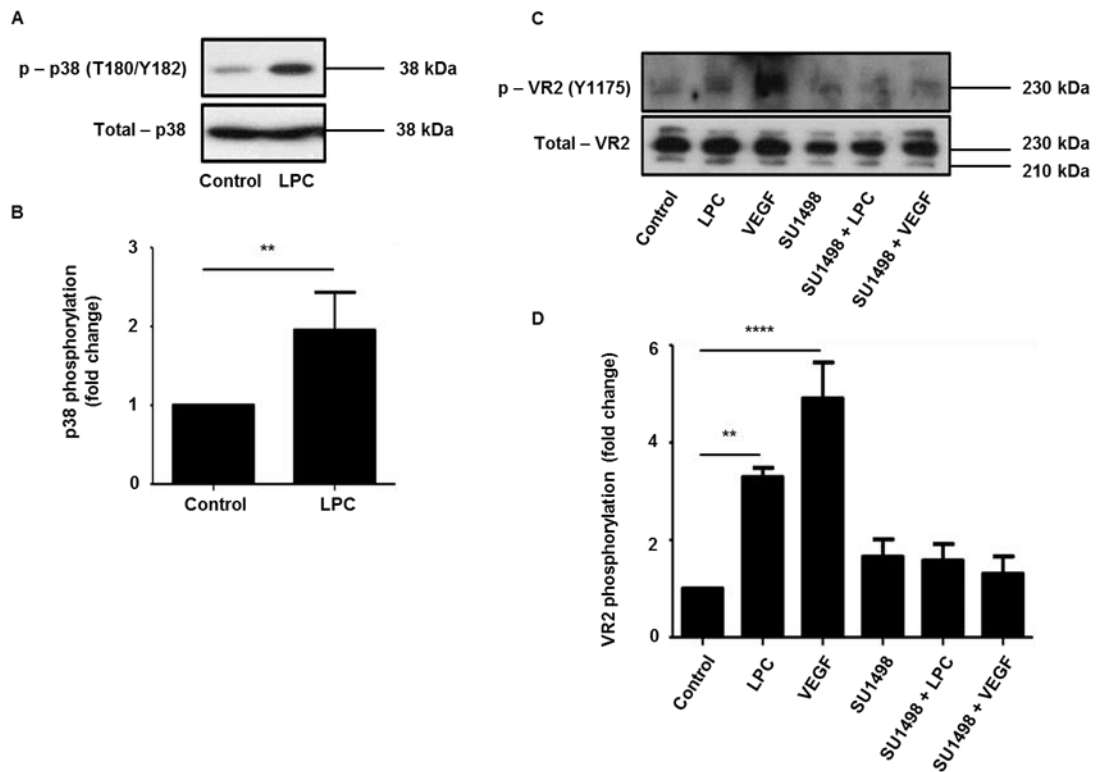


**Figure 3.6. LPC activates p38 and VEGFR2 in PT2 cells**
PT2s treated with LPC (10 μg/mL) for 5 min and levels of phosphorylated p38 (pT180/Y182) determined by western blotting. Representative blot (A) and normalized densitometric quantifications (B) shown (means ± SEM, n = 3, **, p < 0.01, Student's t-test). PT2s were pre-treated with SU1498 (10 μM) for 1 h where indicated and then with either LPC (10 μg/mL) or VEGF-A (50 ng/mL) for 5 min and levels of phosphorylated VEGFR2 (Y1175) determined by western blotting. Representative blot (C) and normalised densiometric quantifications (D) shown (means ± SEM, n = 3). One-way ANOVA (p < 0.0001) with Dunnett's post-hoc test indicates significant differences between vehicle and both LPC and VEGF (**, p < 0.01 and ****, p < 0.0001, respectively).

impact in the reduction of LPC mediated TEER changes than SU1498 (Fig. 3.7A, B). The functional effect of VEGFR2 inhibition through SU1498 pre-treatment was also examined by FITC-dextran flux across brain MVECs, with VEGFR2 inhibition significantly preventing an LPC mediated increase in tracer flux (Fig. 3.8A).
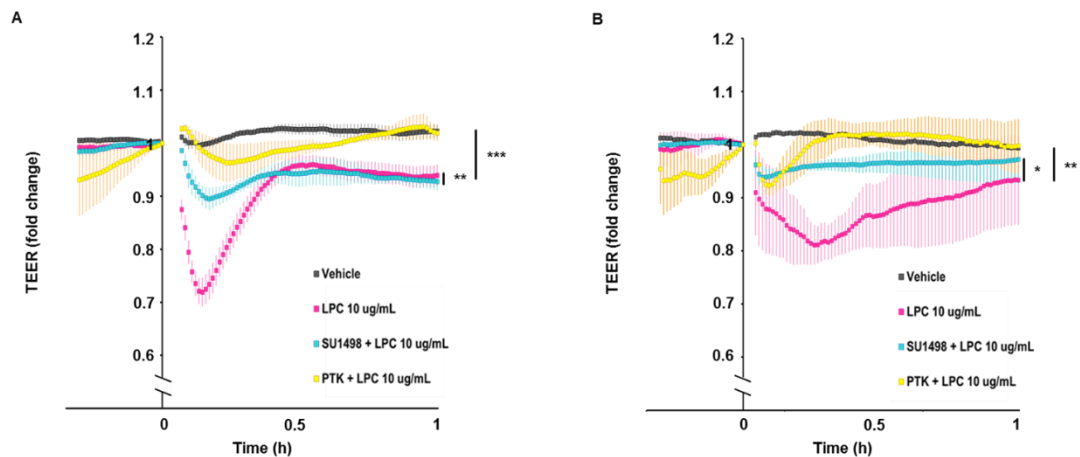


**Figure 3.7. LPC induced junctional permeability prevented by chemical inhibitors targeting VEGFR2 in both brain and retinal MVECs**
Primary rat brain MVECs were grown to confluence and full electrical barrier. At time -1 h cells were pre-treated with SU1498 or PTK/ZK (both at 10 μM) as indicated and LPC (10 μg/mL) added at time 0 h. Shown are means ± SEM of normalized resistance changes (A). One-way ANOVA ($p < 0.01$) with Bonferroni post-hoc test indicates significant differences between vehicle and LPC (****, $p < 0.01$), LPC and LPC + PTK (***, $p < 0.001$) and also LPC and LPC + SU1498 (**, $p < 0.01$). Primary rat retinal MVECs were grown to confluence and full electrical barrier. At time -1 h cells were pre-treated with SU1498 or PTK/ZK (both at 10 μM) as indicated and LPC (10 μg/mL) added at time 0 h. Shown are means ± SEM of normalized resistance changes (B). One-way ANOVA ($p < 0.01$) with Bonferroni post-hoc test indicates significant differences between vehicle and LPC (*, $p < 0.05$), LPC and LPC + PTK (**, $p < 0.01$) and also LPC and LPC + SU1498 (*, $p < 0.05$).

115

### 3.3.3 VEGF secretion is not required for LPC induced vasopermeability via VEGFR2

As autocrine VEGF-A is required for homeostasis of the vasculature, as reported by VEGF deletion within the endothelium leading to vasculature regression, it was important to determine whether VEGF-A could be implicated in LPC's effects in the microvasculature (Lee et al. 2007). To discern the key player, any potential involvement of VEGF-A was negated by pre-treatment with DMS1529 (an anti-VEGF domain antibody) in an assay measuring FITC-dextran flux across brain MVECs in response to LPC addition. DMS1529 pre-treatment had no impact on the action of LPC in this setting (Fig. 3.8A). The use of aflibercept (EYLEA™) pre-treatment to sequester any existing VEGF decimated what were significant levels of flux induced by the addition of VEGF-A (Fig. 3.8B). At the same time, aflibercept did not alter the enhanced flux induced by the addition of LPC (Fig. 3.8B). These data further substantiate LPC's action on MVEC is via transactivation of VEGFR2.
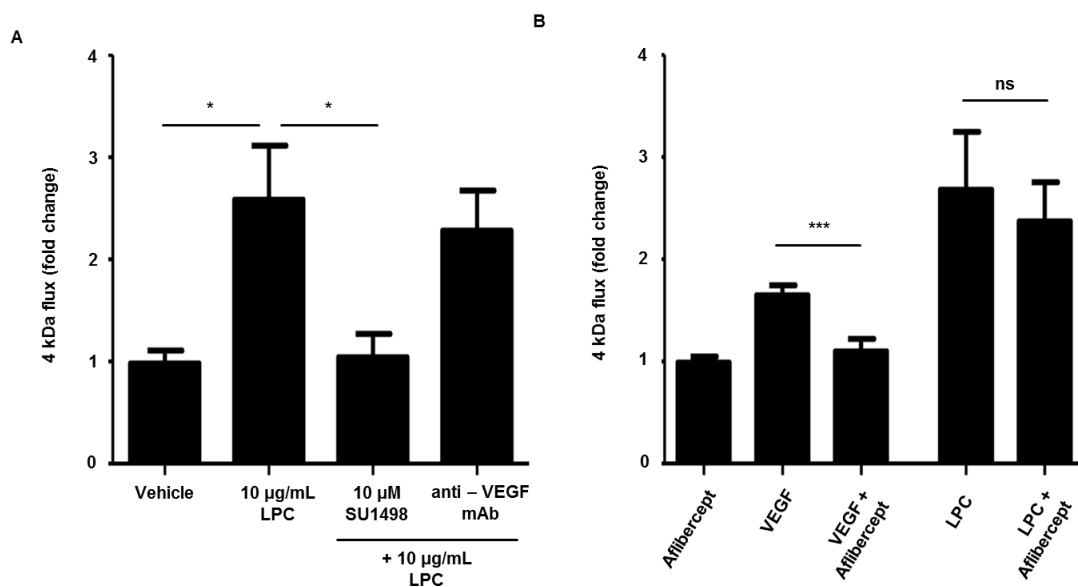


**Figure 3.8. LPC enhanced macromolecular flux across rat brain MVECs prevented by VEGFR2 chemical inhibition but not by VEGF sequestration**

Primary rat brain MVECs grown to confluence were pre-treated with SU1498 (10 μM) or DMS1529 (10 μg/mL) as indicated and 4 kDa dextran flux was measured before and after

the addition of LPC (10 μg/mL). Shown are means ± SEM (n = 8 for vehicle, n = 8 for LPC, n=8 for SU1498 + LPC, n = 4 for DMS + LPC) (A). One-way ANOVA with Dunnett's post-hoc test indicates significant differences between vehicle and LPC (*, $p < 0.05$) and between LPC and LPC + SU1498 (*, $p < 0.05$). Primary rat brain MVECs grown to confluence were pre-treated with Aflibercept (EYLEA™, 25 μg/mL) as indicated and 4 kDa dextran flux was measured before and after the addition of either VEGF-A (50 ng/mL) or LPC (10 μg/mL). Significant increases in flux induced by VEGF-A were reversed by Aflibercept (***, $p<0.01$, Student's T-test). Aflibercept did not reverse the increase in flux induced by LPC (not significant, Student's T-test).

### 3.3.4   Development and characterization of VEGFR2 targeting adenovirus

VEGFR2 involvement in LPC induced vasopermeability on primary brain MVEC was confirmed using adenovirus packaged with shRNA targeting VEGFR2, rather than siRNA and associated transfer methods. This circumvented the inherent limitations in siRNA delivery to the primary cells used in the current study as trypsinisation depletes the intrinsic characteristics secured in the preparation of non-passaged MVECs, and these same intrinsic characteristics make it difficult to achieve sufficient transfection levels in non-passaged MVECs.

As detailed in the methods (2.2.10), three shRNA oligomers were designed targeting VEGFR2 (with a further three targeting VEGFR1 as a control) and ligated into a pRNAT-H1.1/Shuttle containing a GFP reporter. A rat brain MVEC line, GPNT, was used to test both the level of receptor knockdown and transfection efficiency of these constructs by nucleofection. Of the three constructs, VR2.1 and VR2.2 significantly decreased the level of VEGFR2 protein levels as measured by immunoblot and when normalised to control plasmid levels following densiometric quantification (Fig. 3.9A, B). Relating levels of protein knockdown directly to the average level of transfection efficiency, *i.e.* the number of GFP expressing cells as a percentage of total number of cells, the level of VEGFR2 knockdown was greatest in cells treated with construct VR2.1 (Fig. 3.9C). For preparation within adenovirus, VR2.1

construct was selected to target VEGFR2 while an equivalent construct targeting VEGFR1 knockdown was also selected for preparation within adenovirus.
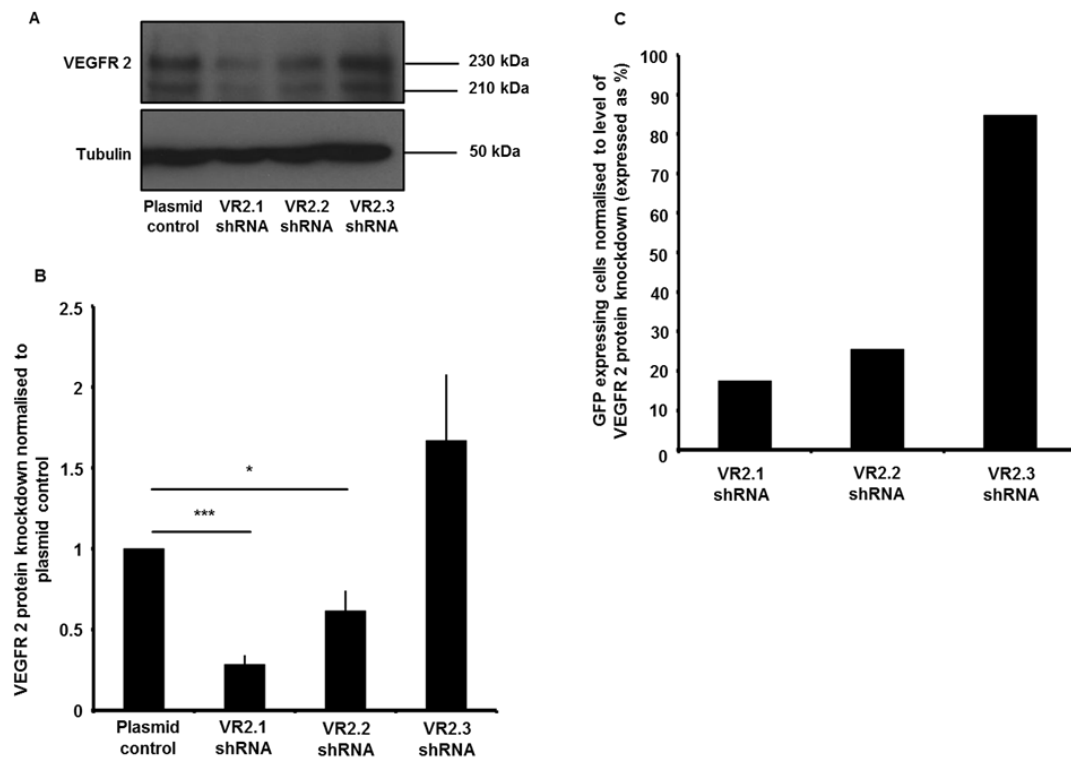


**Figure 3.9. Development and characterization of VEGFR2 targeting adenovirus using GPNTs**

Rat brain MVEC line, GPNT, were nucleofected either with shRNA variants designed to target VEGFR2 (VR2.1 shRNA, VR2.2 shRNA, VR2.3 shRNA) ligated into a plasmid backbone containing GFP reporter or a plasmid control (all at concentration of 10 μg). Lysates were prepared 48 h after nucleofection and levels of VEGFR2 protein knockdown determined by western blotting. Representative blot (A) and normalized densitometric quantifications (B) shown with means ± SEM (n = 3). Significant differences between plasmid control and VR2.1 shRNA (***, $p < 0.001$) and between plasmid control and VR2.2 shRNA (*, $p < 0.05$), Student's T-test. Transfection efficiency measured by relating number of GFP expressing cells to total number of cells, by nuclear stain. The transfection efficiency was related directly to protein knockdown for each construct by determining the product of both values, expressed as a percentage (C).

Following 24 h incubation with shRNA encoding adenovirus (at 400 m.o.i) phase contrast and fluorescence images were taken in which increased GFP expression was seen for both VEGFR1 (VR1.2) and VEGFR2 (VR2.1) targeting adenoviruses (Fig. 3.10A). GFP expression levels remained the same a further 24 h later and protein levels were compared at this time. While VEGFR1 targeting adenovirus had a slight effect on VEGFR2 levels (not surprising as VEGFR2 can exist in heterodimers with VEGFR1), VEGFR2 targeting adenovirus significantly decreased VEGFR2 levels (Fig 3.10B).
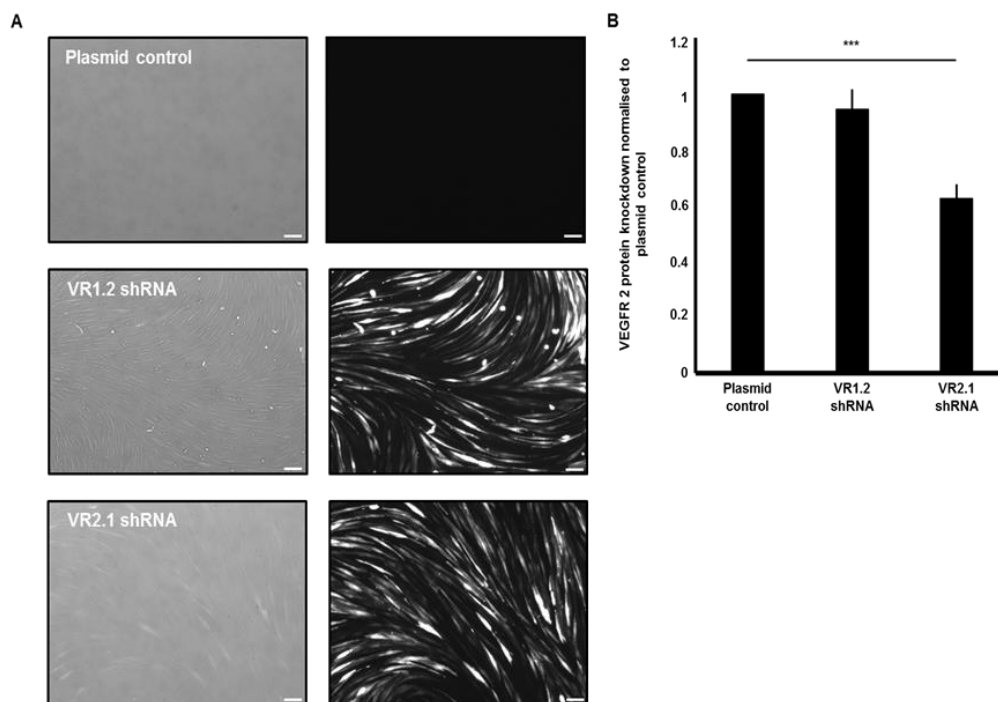


**Figure 3.10. Representative visualisation of GFP expression following infection of rat brain MVECs with adenovirus**

Primary rat brain MVECs grown to confluence were infected with shRNA encoding adenovirus targeting either VEGFR1 (shVR1.2) or VEGFR2 (shVR2.1) at 400 m.o.i. 24 h post-infection phase contrast and fluorescence images were taken (A). Scale bar 10μM. Lysates were prepared a further 24 h later and levels of VEGFR2 protein knockdown determined by western blotting. Normalized densitometric quantifications (B) shown with means ± SEM (n = 3). Significant differences between plasmid control and VR2.1 shRNA encoding adenovirus (***, $p < 0.001$).

These adenoviruses were subsequently employed in assays recording TEER measurements in primary brain MVECs, with cells infected 48 h before LPC addition. Infection with VEGFR1 targeting adenovirus did not significantly affect the characteristic LPC induced drop in TEER (Fig.3.11A). Adenovirus targeting VEGFR2 significantly inhibited LPC's ability to decrease brain MVEC's TEER, bringing resistance levels back strikingly close to control addition levels (Fig.3.11A). These data indicate LPC's requirement for VEGFR2 kinase activity to affect the vasopermeability of brain MVEC.

### 3.3.5 LPC induced vasopermeability operates via VEGFR2 signalling: by *in vivo* pharmacology approach

The *in vivo* permeability model using occluded pial microvessels was used to confirm *in vitro* results indicating VEGFR2 involvement in LPC's actions on vasopermeability. The VEGFR2 selective kinase inhibitor, SU1498, significantly suppressed the ability of LPC to increase sulforhodamine B's loss from occluded pial microvessels corroborating *in vitro* evidence (Fig.3.11B).

### 3.3.6 Indications that LPC's capacity to alter MVEC permeability extends to transcellular transport

Considering that the action LPC exerts on the MVEC barrier resolves within an hour, when measured by distinctive TEER changes, it was unexpected that LPC's action, when measured by FITC-dextran tracer flux across brain MVECs, did not resolve within a timeframe extending beyond 2 h (Fig.3.12). This could indicate that the initial MVEC response to LPC is a junctional component which proceeds to a transcellular form of macromolecular flux over extended periods of time.
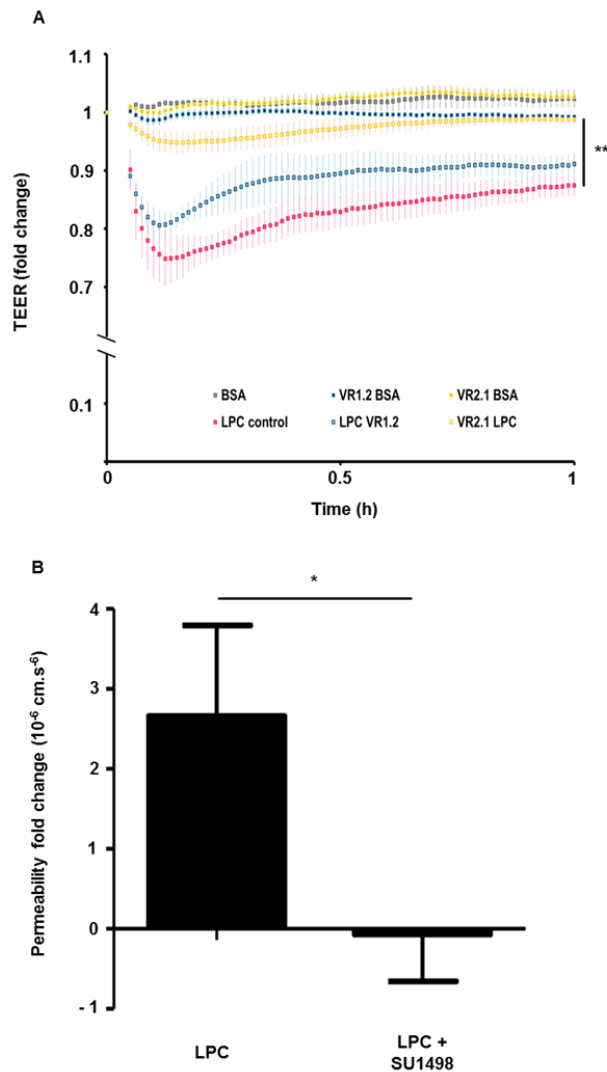
**Figure 3.11. LPC induced junctional permeability prevented by adenovirus targeting VEGFR2 in brain MVECs and LPC induced permeability *in vivo* prevented by VEGFR2 chemical inhibition**

Primary rat brain MVECs grown to confluence and full electrical barrier were infected with shRNA encoding adenovirus targeting either VEGFR1 (shVR1.2) or VEGFR2 (shVR2.1) at 400 m.o.i. 48 h post-infection LPC (10 µg/ml) added at time 0 h (A). One-way ANOVA ($p < 0.0001$) with Bonferroni post-hoc test indicate significant differences between BSA and LPC (***, $p < 0.001$) and between LPC and VR2.1 + LPC (**, $p < 0.01$) but not between LPC and VR1.2 + LPC. Shown are means ± SEM ($n = 4$). Real time recording of sulforhodamine B (580 Da) loss from single occluded rat pial microvessels *in vivo*. Luminal injection of LPC (10-15 µg/mL final) produced strong decrease of sulforhodamine B after ca. 40 s (B). Pre-treatment with SU1498 (20 µM) for 15 min preceded luminal injection of LPC (10-15 µg/mL

121

final) produced no change in sulforhodamine B levels (B). Shown are mean permeability changes ± SEM (* $p<0.05$, Student's T-test).
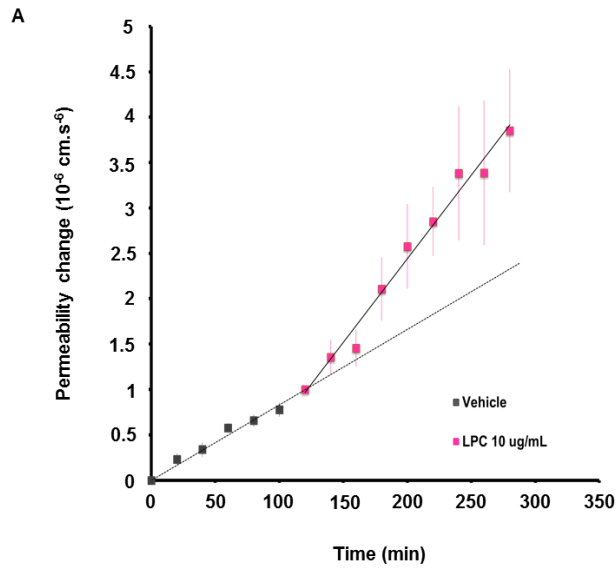


**Figure 3.12. Indications that LPC's capacity to alter MVEC permeability extends to transcellular transport**

Primary rat brain MVECs grown to confluence and 4 kDa dextran flux was measured before and after the addition of LPC (10 μg/mL) at 120 min (grey and pink data points respectively). Trend line fitted to data points following LPC addition indicate no stoppage in macromolecular flux over 2 h later.

## 3.4    Discussion

Elevated LPC levels have been noted to feature in a number of disorders including type-1 and type-2 diabetes (Iwase et al. 2008, Oresic et al. 2008), early coronary atherosclerosis (Lavi et al. 2007), non-alcoholic fatty liver (Lehmann et al. 2013), asthma (Mehta et al. 1990) and ischemia (McHowat and Corr 1993) amongst others (Matsumoto et al. 2007). Within the realm of these disorders, the observed pathophysiological activities LPC is implicated in include the promotion of an inflammatory environment, atherogenicity and related endothelial dysfunction. The majority of the work presented in this chapter was recently published alongside complementary *in vivo* work which found that inhibition of Lp-PLA$_2$ was able to protect the BRB within a diabetic animal model and within an animal model displaying retinal vascular leakage (Canning et al. 2016). Lp-PLA$_2$ is a Ca$^{2+}$ independent enzyme, four-fifths of which is transported on circulating LDL, while the remainder associates with high density lipoprotein (HDL) (Matsumoto et al. 2007). It is produced by haematopoietic cells particularly macrophages, and elevated levels of Lp-PLA$_2$ could be a potential predictive biomarker for stroke, atherosclerosis and coronary heart disease (Stafforini 2009, Oei et al. 2005, Katan et al. 2014, Thompson et al. 2010). Previously, in diabetic, hypercholesterolemic pigs, both atherosclerosis was reduced and BBB dysfunction prevented when such an inhibitor was used (Wilensky et al. 2008, Acharya et al. 2013). Furthermore, this inhibition reduced atherosclerosis in ApoE-deficient mice (Wang et al. 2011).

The collaborative work found that the preventative use of a rodent specific Lp-PLA$_2$ inhibitor (10 mg/kg) reduced Lp-PLA$_2$ activity to 19.1% when compared with plasma collected before treatment in a diabetic rat model. Within the same timeframe, diabetic rats without this treatment had Lp-PLA$_2$ activity levels elevated approximately three fold when compared with non-diabetic controls (Canning et al. 2016). Measured using Evans Blue leakage (corresponding to both paracellular and transcellular transport), BRB integrity was significantly compromised in diabetic controls not receiving Lp-PLA$_2$ inhibition while those receiving the inhibitor (10

mg/kg) had significantly attenuated levels of BRB vasopermeability (Canning et al. 2016). The former group also had significantly increased levels of parenchymal albumin staining within retinal sections when compared with non-diabetic controls, with levels nearly completely reversed by inhibitor treatment. Albumin leakage, which corresponds more specifically to transcellular transport, occurred primarily in areas that appeared strongly dilated and did not occur regularly along the lengths of vessels (Canning et al. 2016). Therapeutic treatment with Lp-PLA$_2$ inhibition similarly improved BRB integrity as measured by albumin presence in the parenchyma when comparing the same diabetic rats with or without inhibitor (Canning et al. 2016). As anti-VEGFs are currently a mainstream treatment for DR, the effect of Lp-PLA$_2$ inhibition was analysed in combination with an anti-VEGF therapy, a neutralising antibody, using the same diabetic rat model. While both therapies used in isolation required higher concentrations to achieve significant levels of BRB breakdown prevention, a combination therapy was found to achieve the same BRB breakdown prevention but at half the concentration required as mono-therapies (Canning et al. 2016).

In this chapter I provided functional evidence for LPC, a product of Lp-PLA$_2$ activity, as a novel permeability mediator at both the BBB and BRB. LPC's capacity for causing a change in permeability has been previously shown to exist within other vascular beds, in experiments using dermal MVECs and pulmonary MVECs (Huang et al. 2005). Together, this indicates that LPC is a general permeability factor and there is a potential for changes in LPC levels to have various impacts systemically.

LPC's role as a general permeability factor was further defined by experiments (performed either by myself or Sarker, MH) discerning a sidedness to the action. Lp-PLA$_2$ has been shown to both be present in the human CNS and its activity detected in cerebrospinal fluid, a separate Lp-PLA$_2$ population from that found in circulating plasma (Huiban et al. 2017). Thus there exists a population of LPC generated from neural membrane phospholipids by Lp-PLA$_2$ within the CNS, 'behind' the BBB (Farooqui and Horrocks 2006). However, LPC evoked a permeability response when

present luminally and not abluminally, although polarity at EC membranes is not unusual (Lizama and Zovein 2013). At the BBB, transporter systems are exceptionally polarised, thus contributing to the establishment and maintenance of essential biochemical gradients (Worzfeld and Schwaninger 2015). Again, at the BBB, it was found that highly polarised receptor distribution contributed to distinct VEGF-A signalling patterns. While VEGFR1 localisation was predominantly luminal, with VEGF-A signalling contributing to cytoprotection, VEGFR2 localisation was predominantly abluminal, with VEGF-A signalling contributing to increased permeability (Hudson et al. 2014). This sidedness to the VEGF-A response was the complete opposite to what was found for LPC in the current study. This finding, of luminal LPC's permeability response, draws together elevated plasma LPC levels measured in diabetes patients with a direct repercussion in potential pathological permeability leading to DR.

At present there is no confirmed endothelial LPC permeability effector protein but LPC is known to interact with a number of proteins and, specifically in relation to neuronal cells, alter protein conformation by incorporating into phospholipid bilayers (Maingret et al. 2000). LPC has been shown to upregulate LOX-1 expression in both macrophages and T-cells, with upregulation of CXCR4 and CCR5 expression also increased by LPC in T-cells (Schaeffer et al. 2009, Hara et al. 2008). Of these, LOX-1 is expressed at the BBB and could be a potential LPC receptor, especially considering LOX-1 is oxLDL's cognate receptor (Chen, Masaki and Sawamura 2002, Pirillo, Norata and Catapano 2013). CD36 is also expressed at the BBB and a known oxLDL receptor (Ueno et al. 2016). One of the direct precursors to LPC (1-palmitoyl-2-(5'-oxo-valeroyl)- *sn* -glycero-3-phosphocholine) is recognised by CD36 and, as LPC triggered a more powerful biogenic effect within the same study, CD36 could be another potential LPC receptor, notwithstanding a lack of data indicating a direct interaction between LPC and CD36 (Vladykovskaya et al. 2011). In conjunction with CD36, TLR2 and TLR4 could also mediate LPC's effector functions as CD36 has been shown to regulate the assembly of a heterodimer of TLR2 and TLR4 through which oxLDL, amyloid-β and LPC signal in macrophages

(Stewart et al. 2010, Carneiro et al. 2013). Both TLR2 and TLR4 are expressed at the BBB (Nagyoszi et al. 2010). Yet none of these receptors are known to mediate fast permeability changes as they have been shown within the present work. A novel G protein-coupled receptor, GPR4, could be the putative LPC receptor as it has been implicated in mediating LPC's permeability effect on endothelial cells, although any subsequent research has been relatively limited (Qiao et al. 2006).

As mentioned, the polarity of LPC's permeability response contrasted with what was found for VEGF-A within the same vascular bed, whereby abluminally located VEGFR2 mediated abluminally located VEGF-A's permeability response via p38 (Hudson et al. 2014). Here, I provided evidence for LPC mediated activation of both p38 and VEGFR2 – if it was transactivated VEGFR2 could be the LPC permeability effector protein. LPC mediated VEGFR2 transactivation had previously been shown to occur within HUVECs, although the work focused on atherosclerosis rather than EC permeability (Fujita et al. 2006). I was unable to measure a sufficient phosphorylation signal for the VEGFR2 residue most consistently activated during a permeability response, Y951 (Olsson et al. 2006, Manni et al. 2014). The measurement of increased Y1175 phosphorylation nevertheless indicated receptor activation in this instance. As activation is only an indication of function, I also confirmed the functional role of VEGFR2 in LPC induced permeability using chemical inhibitors and VEGFR2 targeting adenovirus (with contributions from Hudson, N and Sarker, MH). These results further substantiate that VEGFR2 transactivation is responsible for mediating LPC induced permeability.

The intermediaries between LPC signalling and VEGFR2 mediated permeability have not yet been investigated in the present context. However, VEGFR2 transactivation has been found to occur in response to ROS generated from hyperglycemia, as seen in diabetes, and also in response to fluid shear stress (Warren et al. 2014, Jin et al. 2003). In the case of ROS, VEGR2 phosphorylation occurs in the Golgi when exposed to high glucose, this impedes the movement of the receptor to the cell surface thus making less VEGFR2 available for mediation of vasoactive

responses (Warren et al. 2014). VEGFR2 has also been reported to function as a mechanotransducer resulting in flow mediated activation of eNOS via PI3K and Akt producing NO. In this instance, flow rapidly activated Src kinases, which then activated VEGFR2. This study also highlighted the reported ligand independent activation of VEGFR2 by integrins suggesting that, as the activation of integrin receptors is associated with Src kinase activation, Src kinases operate as transducers of signals from mechanosensors such as integrins (Jin et al. 2003, Wang et al. 2002). Furthermore, ligand independent activation of VEGFR2 in this context, and subsequent activation of Akt and eNOS, was sustained for far longer than activation by VEGF, indicating a disparity in phosphorylation and de-phosphorylation induced by different mechanisms (Jin et al. 2003). VEGFR2 transactivation within neural microvascular beds was explored further in the next chapter and is where additional discussion on this topic can be found.

When permeability data relating LPC-induced macromolecular flux in brain MVECs was represented linearly versus time instead of as a fold change, it was evident that flux had not resolved 2 h after treatment addition. In comparison, an LPC-induced decrease in TEER had nearly fully resolved within 30 min of treatment addition. With a clear discrepancy between two different representations of the same experiment, and the fact that assays measuring macromolecular flux represents both paracellular and transcellular transport, there is a possibility that LPC's actions in relation to permeability are more complex than originally thought. Perhaps LPC's initial actions at the neural microvasculature, triggering junctional flux which resolves, is an early event in a permeability cascade that progresses to some kind of vesicular flux. The presence of transcellular transport within neural microvasculature was explored further in a subsequent chapter and is where additional discussion on this topic can be found.

# Chapter 4   Results

**Transactivation of VEGFR2 is involved in the permeability actions of other vasoactive mediators**

## 4.1   Contribution of Authors

**Figure 4.1. Junctional permeability triggered by endogenous mediators in brain MVECs**

(A) Kenny, BA

(B) Kenny, BA

(C) Kenny, BA

(D) Kenny, BA

**Figure 4.2. LPA and THR-induced junctional permeability prevented by VEGFR2 chemical inhibition in brain MVECs**

(A) Kenny, BA

(B) Kenny, BA

(C) Kenny, BA

**Figure 4.3. LPA and THR-induced junctional permeability prevented by VEGFR2 adenoviral inhibition in brain MVECs**

(A) Kenny, BA

(B) Kenny, BA

(C) Kenny, BA

**Figure 4.4. BK, LPA and THR-induced junctional permeability prevented by p38 chemical inhibition in brain MVECs**

(A) Kenny, BA

(B) Kenny, BA

(C) Kenny, BA

**Figure 4.5. BK, LPA, THR and and TNF-α activate p38 in PT2 cells**

(A) Kenny, BA

(B) Kenny, BA

**Figure 4.6. p38 activation by BK, LPA, THR and TNF-α not prevented by VEGFR2 chemical inhibition in PT2 cells**

(A) Kenny, BA

(B) Kenny, BA

**Figure 4.7. BK, THR and TNF-α activate VEGFR2 in PT2 cells**

(A) Kenny, BA

(B) Kenny, BA

**Figure 4.8. VEGFR2 activation observed in response to BK, THR and TNF-α prevented by VEGFR2 chemical inhibition in PT2 cells**

(A) Kenny, BA

(B) Kenny, BA

**Figure 4.9. VEGFR2 activation observed in response to BK, THR and TNF-α prevented by p38 chemical inhibition in PT2 cells**

(A) Kenny, BA

(B) Kenny, BA

**Figure 4.10. Disruption of clathrin coated vesicle formation, via dynamin inhibition, prevents VEGFR2 activation in PT2 cells**

(A) Kenny, BA

(B) Kenny, BA

**Figure 4.11. Disruption of clathrin coated vesicle formation, via dynamin inhibition, does not prevent p38 activation in PT2 cells**

(A) Kenny, BA

(B) Kenny, BA

## 4.2    Introduction

Our work on LPC indicated a role for VEGFR2 transactivation contributing to permeability changes at the neural microvasculature. As detailed in the introduction, disruption of the BBB is critical in the pathogenesis of a range of disorders and there are numerous factors which operate as vasoactive mediators within the neural microvasculature. Given the increased expression of VEGF-A within hypoxic/ischemic tissues and VEGFR2's polarized expression on the parenchymal membrane of exchange vessels it would be interesting to determine whether other mediators similarly exploited a path to permeability via VEGFR2 (Hudson et al. 2014). If so, this would indicate a more common function for VEGFR2 as a conduit for permeability responses and better inform therapeutic targets for disorders which share VEGFR2 mediated permeability as a feature of its pathogenesis. Although not known to involve VEGFR2, there are many disorders displaying BBB dysfunction which have been frequently found to have comorbidities such as type-2 diabetes and Alzheimer's disease; cerebral small vessel disease and depressive disorders; and vascular dysfunction and epilepsy (Luchsinger and Gustafson 2009, Direk et al. 2016, Stanimirovic and Friedman 2012).

In this chapter, the previous findings involving VEGFR2 transactivation by a vascular mediator were extended to include other pertinent vascular mediators namely, BK, LPA, THR and TNF-α. Functional approaches were used to establish those mediators relevant to VEGFR2 mediated permeability, employing the VEGFR2 specific kinase antagonist, SU1498, and a VEGFR2 targeting adenovirus as before. Subsequently, analysis by immunoblot using a variety of chemical mediators further elucidated the nature of their involvement. This work highlights the dynamic intricacy of neural microvascular cellular responses to vasoactive mediators and strongly indicates the involvement of VEGFR2 transactivation in thrombin mediated permeability at neural microvascular barriers, also indicating a plausible role for VEGFR2 transactivation in LPA's mechanism of action.

## 4.3 Results

### 4.3.1 Acute permeability change triggered in neural microvascular endothelium by endogenous mediators

The functional effect of BK, LPA, THR and TNF-α was tested on primary brain MVECs using TEER measurements, as first described in chapter three. For BK and THR treated cells, the observed permeability change was immediate, acute and transient, resolving within 30 min (Fig. 4.1A and B). When compared to control, this change in permeability produced by both mediators, BK and THR, was highly statistically significant. The change in permeability for LPA treated cells was also immediate and acute, dropping to half the level of control barrier cells, a statistically significant change, but persisted for longer than 1 h (Fig. 4.1C) and did not resolve fully for 10 h (data not shown). No acute permeability changes were seen within the first hour of TNF-α treatment and further functional data using TNF-α was not pursued (Fig. 4.1D).

### 4.3.2 LPA and THR-induced vasopermeability operates via VEGF2 signalling

The VEGFR2 specific kinase antagonist, SU1498, was used to determine whether observed permeability changes for BK, LPA and THR in primary brain MVECs operated via VEGFR2. Cells were either pre-treated with SU1498 or left untreated for 1 h. On BK addition, a similar drop in barrier function was observed for both non-inhibited and VEGFR2 inhibited cells (Fig. 4.2A). Both parameters were statistically different from control cells, with no significant difference between BK treated cells and BK treated cells pre-treated with SU1498 (Fig. 4.2A). For both LPA and THR treated cells, SU1498 pre-treatment reduced the effect on TEER measurements, decreasing the severity of the response by more than half and attenuating the duration of the response to three quarters of an hour and a quarter of an hour respectively (Fig.
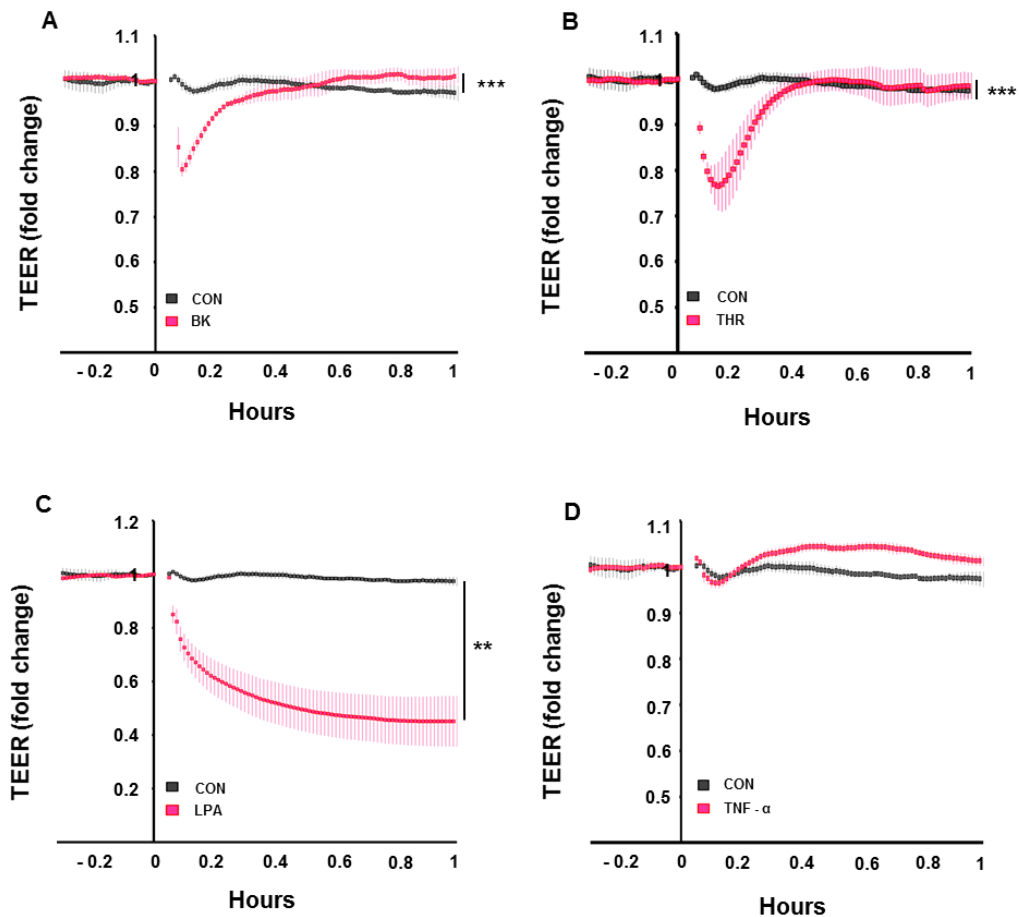
**Figure 4.1. Junctional permeability triggered by endogenous mediators in brain MVECs**

Primary rat brain MVECs were grown to confluence and full electrical barrier (TEER of ca. 25,000 $\Omega$). BK at 1 µm (A), THR at 1 U/mL (B), LPA at 10 µm (C) and TNF-$\alpha$ at 1 µm (D) were added at time 0. Shown are means $\pm$ SEM of normalised resistance changes (n = 4). One-way ANOVA with Bonferroni post-hoc test indicates significant differences between control and BK (***, $p < 0.001$) (A), between control and THR (***, $p < 0.001$) (B) and between control and LPA (**, $p < 0.01$) (C).

**Figure 4.2. LPA and THR-induced junctional permeability prevented by VEGFR2 chemical inhibition in brain MVECs**

Primary rat brain MVECs were grown to confluence and full electrical barrier. At time -1 h cells were pre-treated with SU1498 (10 µm) as indicated and either BK at 1 µm (A), LPA at 10 µm (B) or THR at 1 U/mL (C) then added at time 0. Shown for each panel are means ± SEM of normalised resistance changes (n = 4). One-way ANOVA with Bonferroni post-hoc test indicates significant differences between control and BK (**, $p < 0.01$) and control and SU1498 + BK (*, $p < 0.05$) (A). One-way ANOVA with Bonferroni post-hoc test indicates significant differences between control and LPA (***, $p < 0.001$) and LPA and SU1498 + LPA (*, $p < 0.05$) (B). One-way ANOVA with Bonferroni post-hoc test indicates significant differences between control and THR (***, $p < 0.001$) and THR and SU1498 + THR (**, $p < 0.01$) (C).

4.2B and C). While, LPA treated cells caused a highly significant permeability change when compared with control, LPA treated cells pre-treated with SU1498

133

were not significantly different from control cells but were significantly different from LPA treated cells, indicating a role for VEGFR2 in LPA's effects on permeability change (Fig. 4.2B). THR's effect on primary BMVEC was inhibited by SU1498 in a manner similar to LPA, with highly significant differences between THR treated cells and both control cell and cells pre-treated with SU1498 followed by THR addition (Fig. 4.2C). This result also points to a role for VEGFR2 signalling in THR's effects on permeability change.

The VEGFR2 targeting adenovirus described in chapter three was subsequently employed to confirm the role of the receptor in LPA and THR mediated permeability changes using primary brain MVECs. It was first used to confirm the observed lack of involvement of VEGFR2 in BK mediated permeability changes, where no significant difference existed between BK treated cells and BK treated cells pre-treated with VEGFR2 targeting adenovirus (Fig. 4.3A). Both parameters were highly significantly different from control treated cells, resembling the trend seen for SU1498 (Fig. 4.3A). For LPA treated cells, VEGFR2 targeting adenovirus reduced the severity of the permeability change but not to the same extent as chemical inhibition with SU1498 (Fig. 4.3B). While the change between LPA treated cells and control was highly significant, there was no significance between LPA treated cells and the adenovirus targeting VEGFR2 and significance was reached between LPA treated cells pre-treated with VEGFR2 targeting adenovirus and control (Fig. 4.3B). VEGFR2 targeting adenovirus also reduced the severity of the permeability response of primary brain MVEC to THR treatment but in a manner resembling that seen for SU1498 pre-treatment (Fig. 4.3C). THR treated cells elicited a significant permeability change from control, pre-treatment with VEGFR2 targeting adenovirus had a significant effect on THR's action, halving its response (Fig. 4.3C). There was no significance between control treated cells and cells pre-treated with VEGFR2 targeting adenovirus followed by THR treatment (Fig. 4.3C). These data indicate a clear role for VEGFR2 kinase activity in THR mediated permeability within primary brain MVEC and a likely level of involvement of VEGFR2 within LPA's capacity to elicit a permeability response in the same vascular bed.
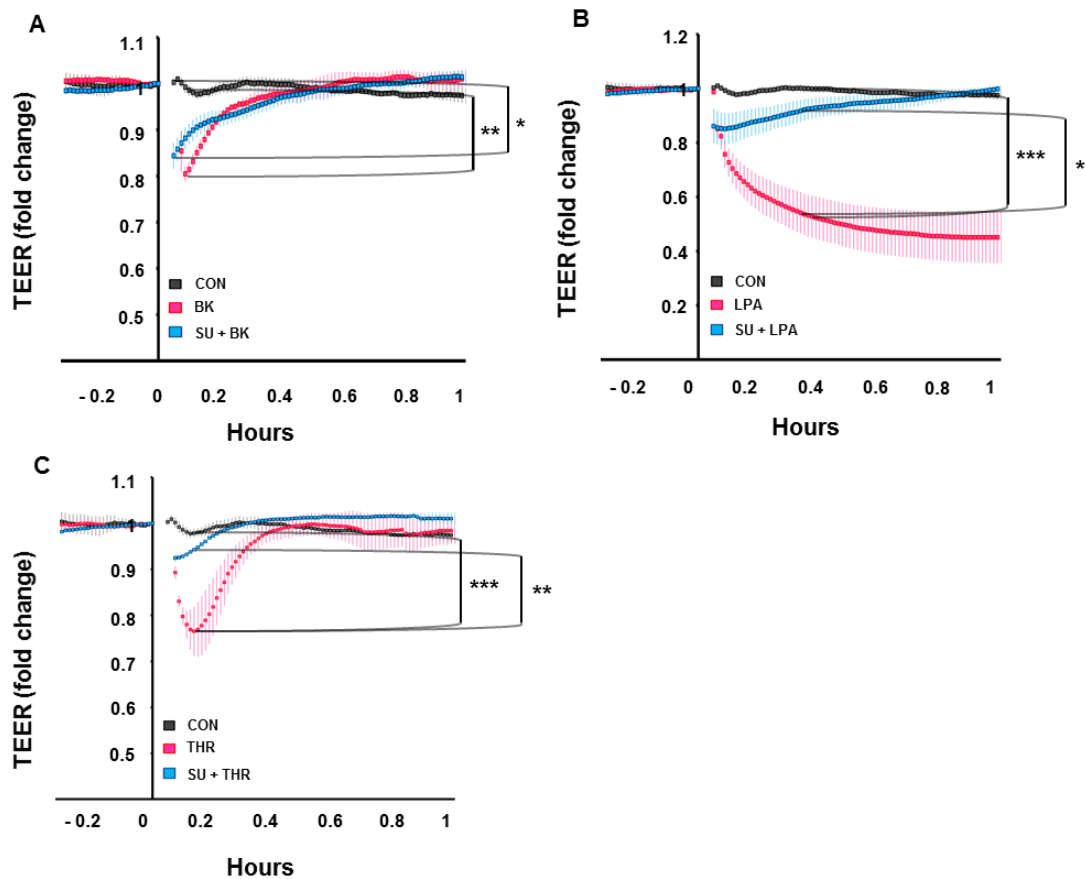
**Figure 4.3. LPA and THR-induced junctional permeability prevented by VEGFR2 adenoviral inhibition in brain MVECs**

Primary rat brain MVECs grown to confluence and full electrical barrier were infected with shRNA encoding adenovirus targeting VEGFR2 (VR2.1) at 400 m.o.i. 48 h post-infection either BK at 1 µm (A), LPA at 10 µm (B) or THR at 1 U/mL (C) were added at time 0. Shown for each panel are means ± SEM of normalised resistance changes (n = 4). One-way ANOVA with Bonferroni post-hoc test indicates significant differences between control and BK (****, $p < 0.0001$) and control and VR2.1 + BK (****, $p < 0.0001$) (A). One-way ANOVA with Bonferroni post-hoc test indicates significant differences between control and LPA (****, $p < 0.0001$), between control and VR2.1 + LPA (****, $p < 0.0001$) and between LPA and VR2.1 + LPA (****, $p < 0.0001$) (B). One-way ANOVA with Bonferroni post-hoc test indicates significant differences between control and THR (**, $p < 0.01$) and THR and VR2.1 + THR (*, $p < 0.05$) (C).

### 4.3.3 BK, LPA and THR-induced vasopermeability operates via p38 signalling

As p38 activity is instrumental in mediating VEGF-A-induced permeability within a number of vascular beds, the highly selective and potent p38 inhibitor, SB202190, was used to determine whether permeability changes observed for BK, LPA and THR in primary brain MVECs operated similarly (Takahashi and Shibuya 2005). For all three mediators, BK, LPA and THR, p38 inhibition completely prevented a drop in barrier function (Fig. 4.4A, B and C). BK's effect on permeability was highly significant when compared with both control cells and also with BK treated cells pre-treated with SB202190 while there was no significant difference between the latter (Fig. 4.4A). Similarly, for LPA, the highly significant difference seen between LPA treated cells and control treated cells was also seen for LPA treated cells pre-treated with SB202190, with no significant difference between control treated cells and LPA treated cells pre-treated with SB202190 (Fig. 4.4B). For THR, significant differences were evident between both control cells and THR treated cells as well as between THR treated cells pre-treated with SB202190 and THR treated cells, while no significance was seen between control cells and THR treated cells pre-treated with SB2020190 (Fig. 4.4C). These data indicate an integral role for p38's involvement in BK, LPA and THR mediated vasopermeability.
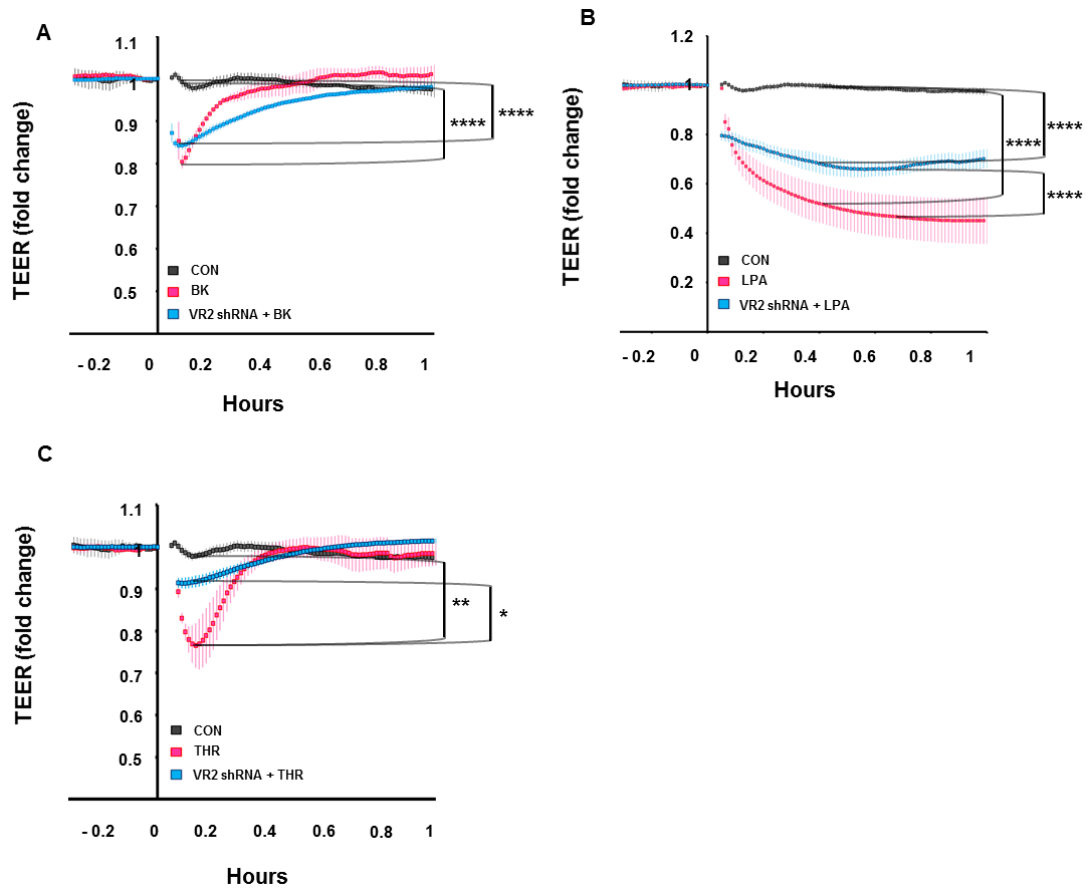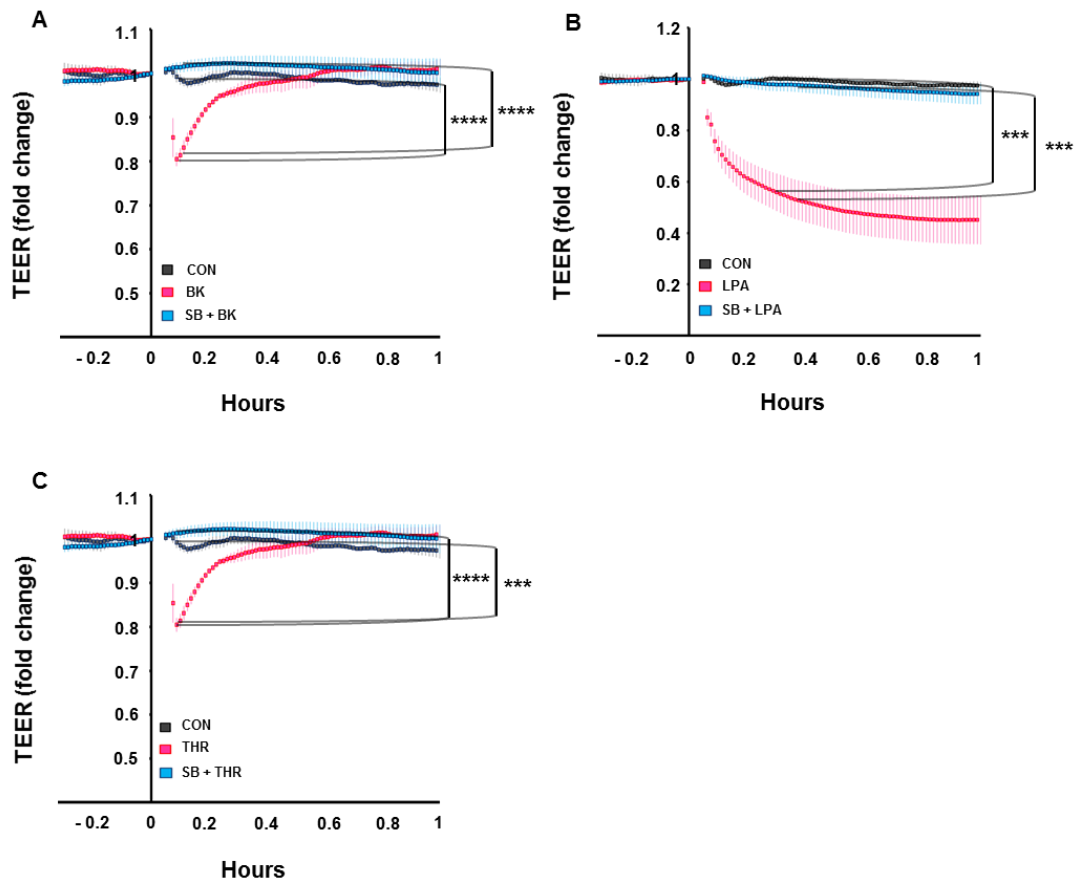
**Figure 4.4. BK, LPA and THR-induced junctional permeability prevented by p38 chemical inhibition in brain MVECs**

Primary rat brain MVECs were grown to confluence and full electrical barrier. At time -1 h cells were pre-treated with SB202190 (50 µm) as indicated and either BK at 1 µm (A), LPA at 10 µm (B) or THR at 1 U/mL (C) then added at time 0. Shown for each panel are means ± SEM of normalised resistance changes (n = 4). One – way ANOVA with Bonferroni post-hoc test indicates significant differences between control and BK (****, p < 0.0001) and BK and SB202190 + BK (****, p < 0.0001) (A). One-way ANOVA with Bonferroni post-hoc test indicates significant differences between control and LPA (***, p < 0.001) and LPA and SB202190 + LPA (***, p < 0.001) (B). One-way ANOVA with Bonferroni post-hoc test indicates significant differences between control and THR (***, p < 0.001) and THR and SB202190 + THR (****, p < 0.0001) (C).

To accompany functional data, p38 activation in PT2 cells was analysed. Following 5 min of mediator treatment, levels of T180/Y182 phosphorylation was detected by

immunoblot and compared with total p38. PT2s were treated with either BK, LPA, THR or TNF-α and the level of p38 activation measured by immunoblot. BK, LPA and THR all activated p38, as measured by its phosphorylation, to a similar extent (Fig. 4.5A). When quantified from n=3, BK, LPA and THR treatment all significantly increased p38 phosphorylation from control levels (Fig. 4.5B). On the other hand, TNF-α more than doubled the level of p38 phosphorylation from control levels and this was highly significant, when compared with control (Fig. 4.5A and B).
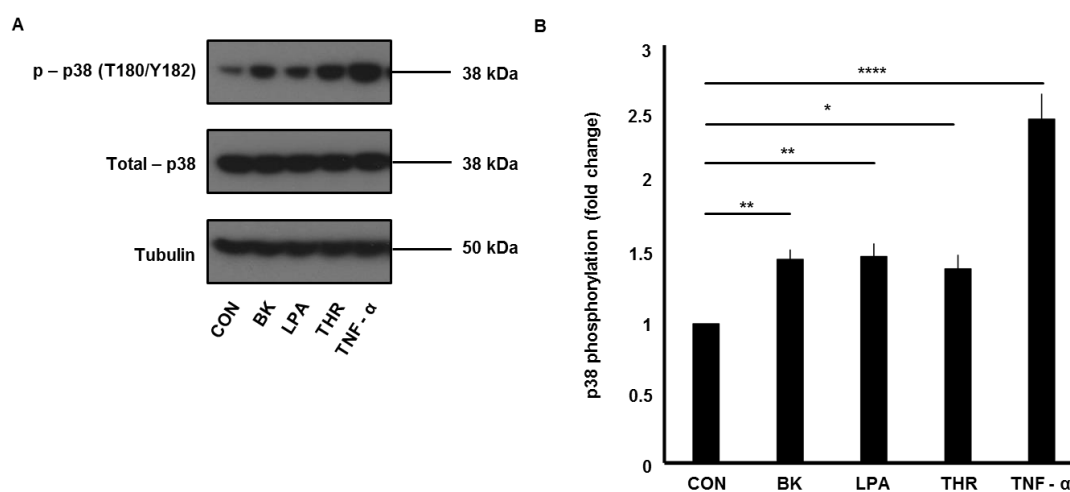


**Figure 4.5. BK, LPA, THR and TNF-α activate p38 in PT2 cells**
PT2s treated with either BK (1 µm), LPA (10 µm), THR (1 U/mL) or TNF-α (1 µm) for 5 min and levels of phosphorylated p38 (T180/Y182) determined by western blotting. Representative blot (A) and normalised densitometric quantifications (B) shown (means ± SEM, n = 3). One-way ANOVA ($p < 0.0001$) with Bonferroni's post-hoc test indicates significant differences between control and BK (**, $p < 0.01$), between control and LPA (**, $p < 0.01$), between control and THR (*, $p < 0.05$) and between control and TNF-α (****, $p < 0.0001$).

When SU1498, the VEGFR2 specific kinase antagonist, was used to determine whether p38 activation was downstream of VEGFR2, no significant differences were

seen between any of BK, THR, LPA or TNF-α treated cells and their counterpart with SU1498 pre-treatment, again as measured by p38 activation (Fig. 4.6A and B).



**Figure 4.6. p38 activation by BK, LPA, THR and TNF-α not prevented by VEGFR2 chemical inhibition in PT2 cells**

PT2s were pre-treated with SU1498 (10 µm) for 1 h where indicated and then with either BK (1 µm), LPA (10 µm), THR (1 U/mL) or TNF-α (1 µm) for 5 min and levels of phosphorylated p38 (T180/Y182) determined by western blotting. Representative blot (A) and normalised densitometric quantifications (B) shown (means ± SEM, n = 3). One-way ANOVA (p < 0.0001) with Bonferroni's post-hoc test indicates no significant differences.

### 4.3.4  VEGFR2 activation observed in response to BK, THR and TNF-α

The level of VEGFR2 activation in PT2s following 5 min treatment with either BK, LPA, THR or TNF-α, as measured by Y1175 phosphorylation using immunoblot, was analysed to further inform earlier functional data. Quantified from n=3, VEGFR2 activation was observed following treatment with BK, THR and TNF-α, while LPA-induced activation of VEGFR2 was negligible (Fig. 4.7A and B). VEGFR2 activation by TNF-α treatment was highly significant when compared with control levels of activation (Fig. 4.7B). Activation of VEGFR2 by either BK or THR treatment were also both significant, but both to a lesser extent than TNF-α, with THR's capacity for VEGFR2 induced activation slightly less again than BK's capacity for VEGFR2 induced activation (Fig. 4.7B).
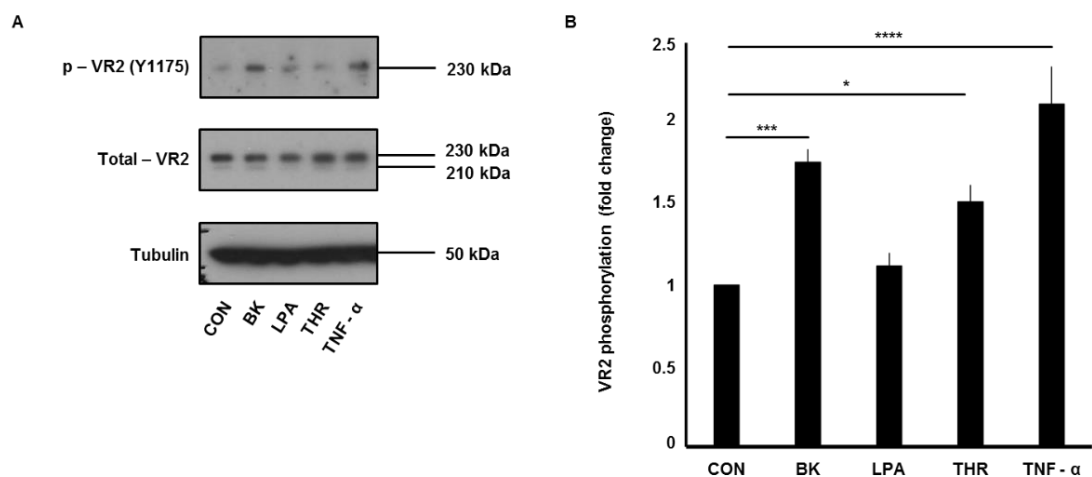


**Figure 4.7. BK, THR and TNF-α activate VEGFR2 in PT2 cells**
PT2s treated with either BK (1 µm), LPA (10 µm), THR (1 U/mL) or TNF-α (1 µm) for 5 min and levels of phosphorylated VEGFR2 (Y1175) determined by western blotting. Representative blot (A) and normalised densitometric quantifications (B) shown (means ± SEM, n = 3). One-way ANOVA (p < 0.0001) with Bonferroni's post-hoc test indicates significant differences between control and BK (***, p < 0.001), between control and THR (*, p < 0.05) and between control and TNF-α (****, p < 0.0001).

The VEGFR2 specific kinase antagonist, SU1498, was used to inhibit VEGFR2 activation in PT2s, as measured by Y1175 phosphorylation using immunoblot, following 5 min treatment with either BK, LPA, THR or TNF-α. Quantified from n=3, a highly significant difference was seen for VEGFR2 activation when comparing TNF-α treated cells with TNF-α treated cells pre-treated with SU1498, with SU1498 completely inhibiting TNF-α mediated VEGFR2 activation (Fig. 4.8A and B). Similarly, VEGFR2 activation by both BK treated and THR treated cells was completely inhibited by SU1498 pre-treatment, albeit to a slightly lesser level of significance (Fig. 4.8A and B). It is clear from the figure that LPA induced VEGFR2 activation is also diminished by SU1498 pre-treatment but the comparison did not reach statistical significance (Fig, 4.8A and B).

The highly selective and potent p38 inhibitor, SB202190, was next used to determine whether VEGFR2 activation in BK, THR and TNF-α treated PT2s operated via p38, to parallel functional studies described earlier, by measuring Y1175 phosphorylation using immunoblot. Inhibition of p38 significantly prevented VEGFR2 activation for all three mediators, BK, THR and TNF-α, when compared with their non-inhibited counterparts (Fig. 4.9A and B).

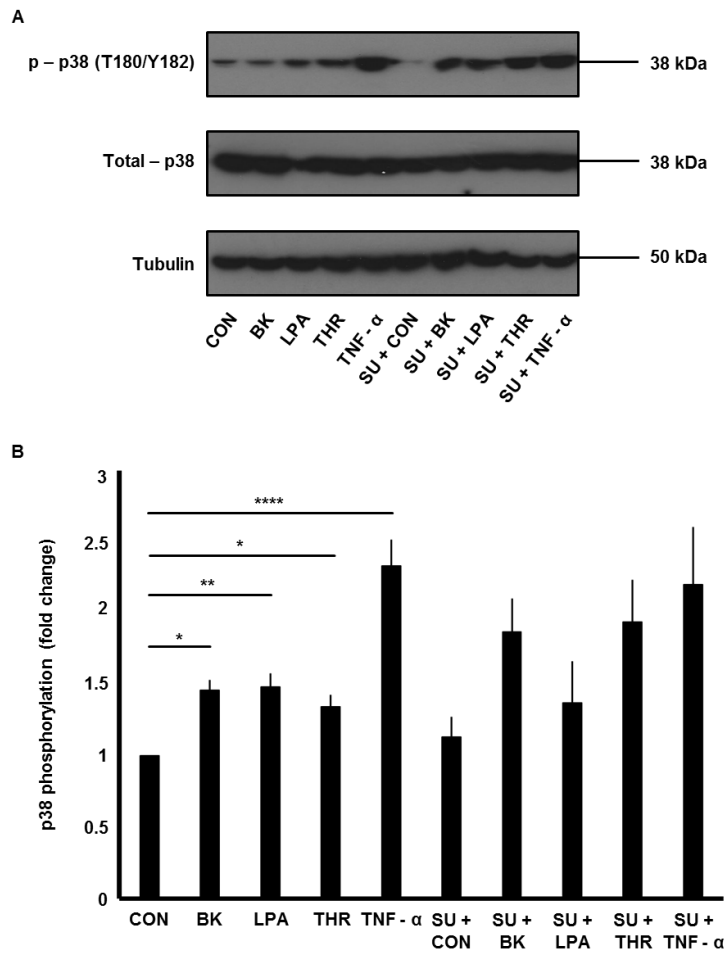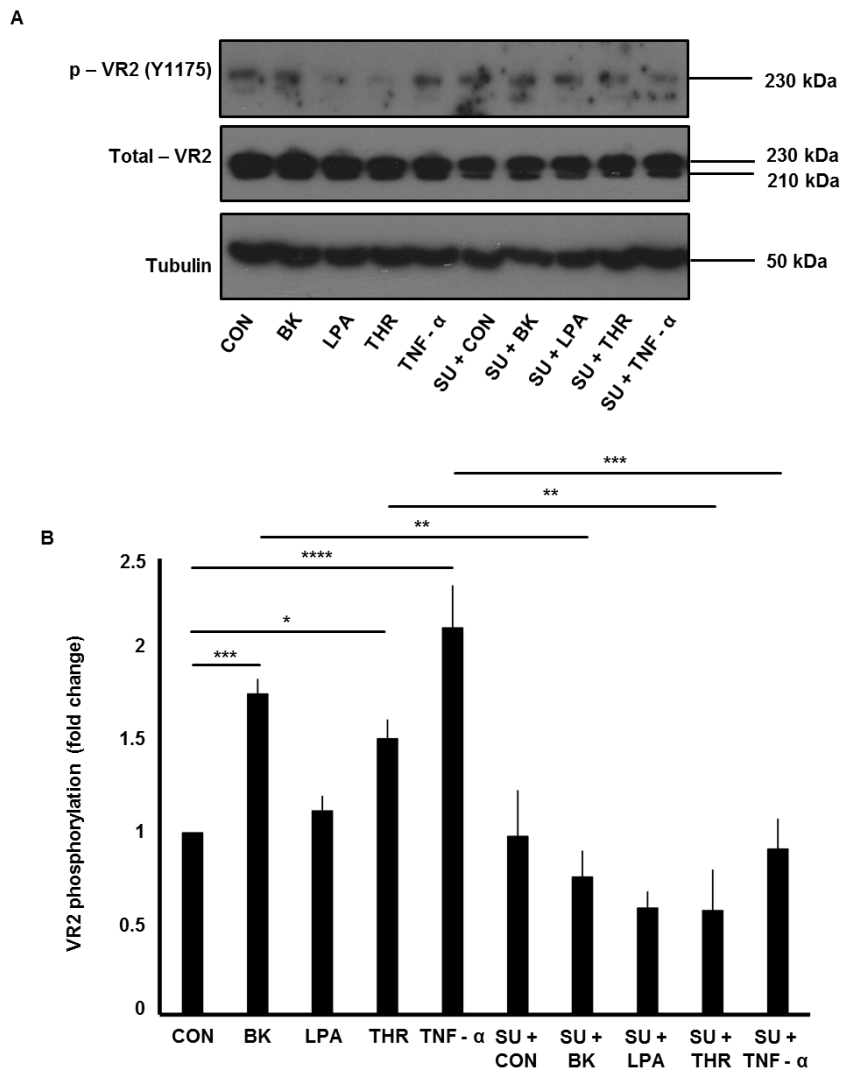**Figure 4.8. VEGFR2 activation observed in response to BK, THR and TNF-α prevented by VEGFR2 chemical inhibition in PT2 cells**

PT2s were pre-treated with SU1498 (10 µm) for 1 h where indicated and then with either BK (1 µm), LPA (10 µm), THR (1 U/mL) or TNF-α (1 µm) for 5 min and levels of phosphorylated VEGFR2 (Y1175) determined by western blotting. Representative blot (A) and normalised densitometric quantifications (B) shown (means ± SEM, n = 3). One-way ANOVA (p < 0.0001) with Bonferroni's post-hoc test indicates significant differences between BK and SU1498 + BK (**, p < 0.01), between THR and SU1498 + THR (**, p < 0.01) and between TNF-α and SU1498 + TNF-α (***, p < 0.001).
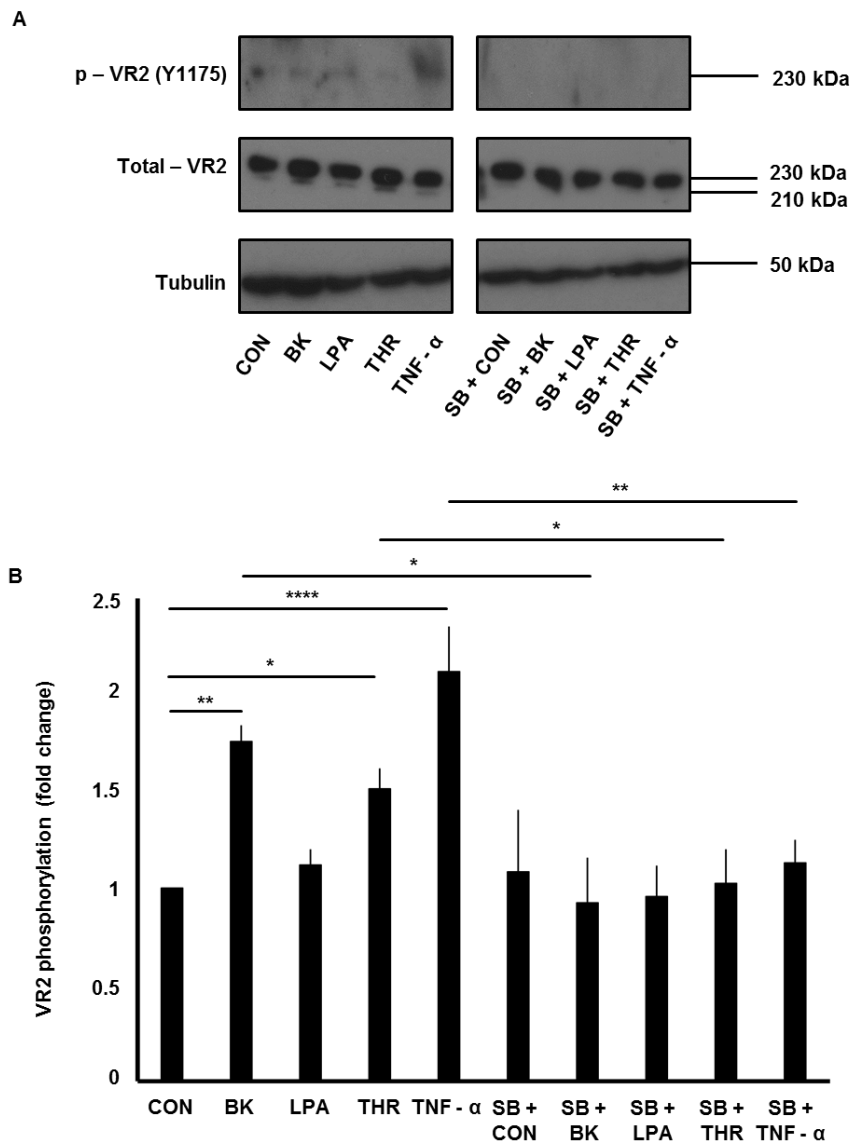
**Figure 4.9. VEGFR2 activation observed in response to BK, THR and TNF-α prevented by p38 chemical inhibition in PT2 cells**
PT2s were pre-treated with SB202190 (50 µm) for 1 h where indicated and then with either BK (1 µm), LPA (10 µm), THR (1 U/mL) or TNF-α (1 µm) for 5 min and levels of phosphorylated VEGFR2 (Y1175) determined by western blotting. Representative blot (A) and normalised densitometric quantifications (B) shown (means ± SEM, n = 3). Faint bands were visible and quantifiable in the original digital image. One-way ANOVA (p < 0.0001) with Bonferroni's post-hoc test indicates significant differences between BK and SB202190 + BK (*, p < 0.05), between THR and SB202190 + THR (*, p < 0.05) and between TNF-α and SB202190 + TNF-α (**, p < 0.01).

143

### 4.3.5 Disruption of clathrin coated vesicle formation, via dynamin inhibition, prevents VEGFR2 activation but not p38 activation

As the literature surrounding VEGFR2's required location for activation has been divisive, a dynamin inhibitor which disrupts clathrin coated vesicle formation, called dynasore, was used to investigate the spatial relation of VEGFR2 activation in PT2s. This was measured by Y1175 phosphorylation using immunoblot, following 5 min of BK, LPA, THR or TNF-α treatment, with or without dynasore. All of BK, THR and TNF-α treated cells pre-treated with dynasore had significantly inhibited levels of VEGFR2 activation when compared to their non-dynasore pre-treated counterparts (Fig. 4.10A and B). On the other hand, p38 activation by 5 min treatment with either BK, LPA, THR or TNF-α in PT2s, as measured by T180/Y182 phosphorylation using immunoblot, was not at all prevented by pre-treatment with dynasore (Fig. 4.11A and B).
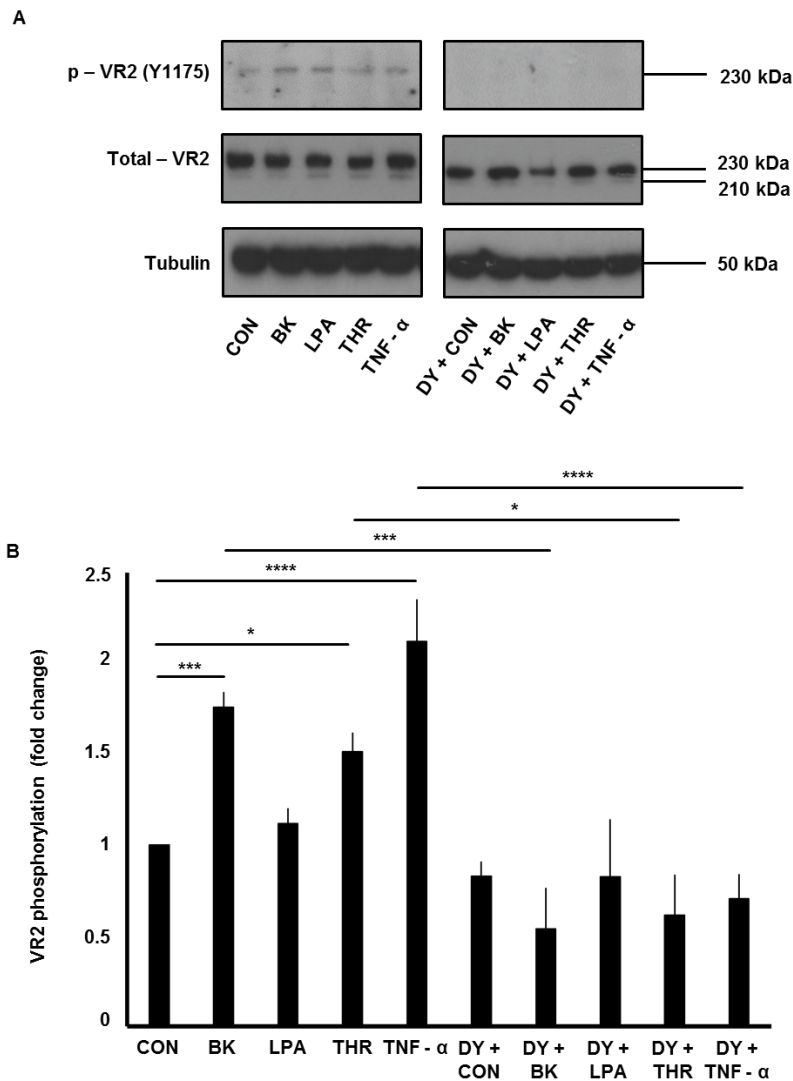
**Figure 4.10. Disruption of clathrin coated vesicle formation, via dynamin inhibition, prevents VEGFR2 activation in PT2 cells**

PT2s were pre-treated with dynasore (80 µm) for 30 min where indicated and then with either BK (1 µm), LPA (10 µm), THR (1 U/mL) or TNF-α (1 µm) for 5 min and levels of phosphorylated VEGFR2 (Y1175) determined by western blotting. Representative blot (A) and normalised densitometric quantifications (B) shown (means ± SEM, n = 3). Faint bands were visible and quantifiable in the original digital image. One-way ANOVA (p < 0.0001) with Bonferroni's post-hoc test indicates significant differences between BK and dynasore + BK (***, p < 0.001), between THR and dynasore + THR (*, p < 0.05) and between TNF-α and dynasore + TNF-α (****, p < 0.0001).
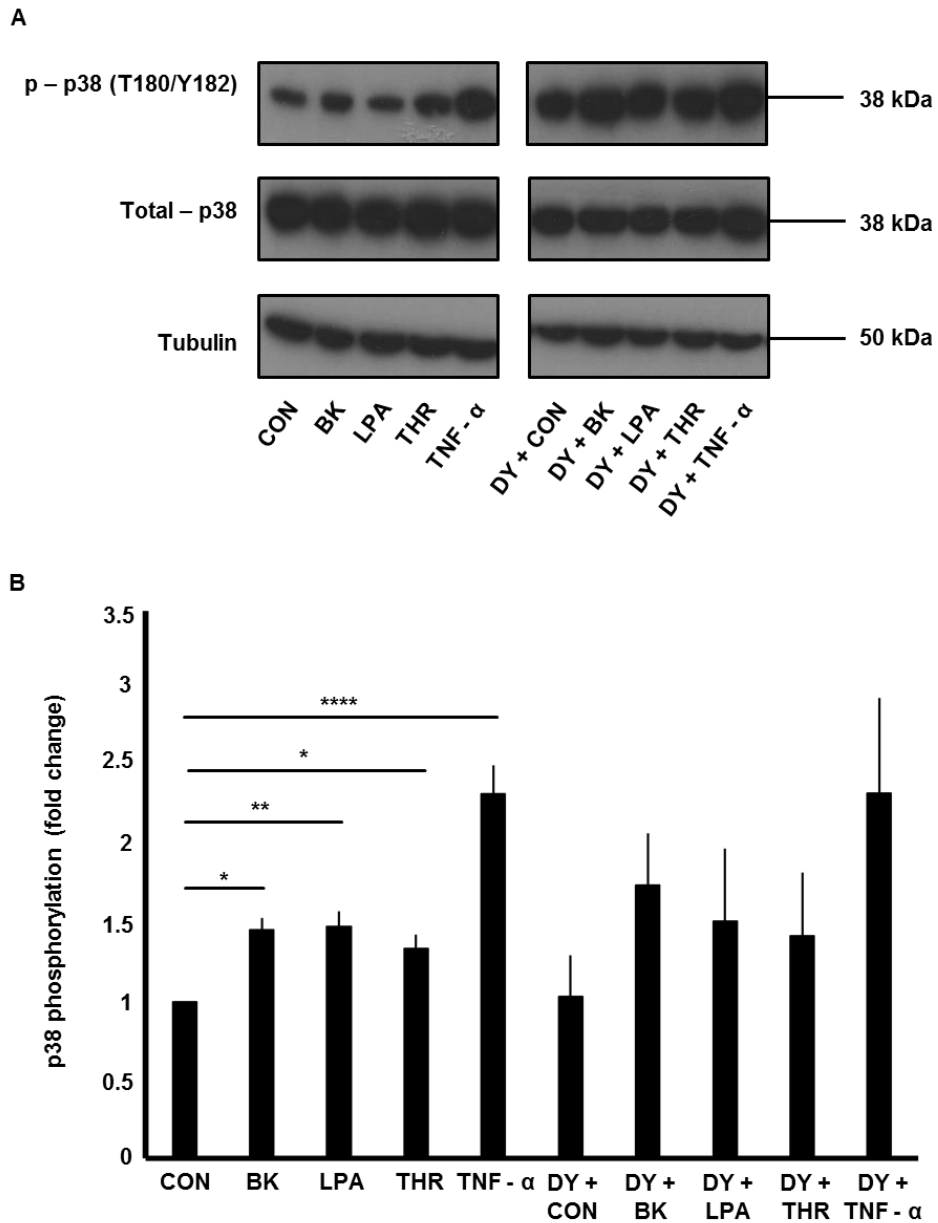
**Figure 4.11. Disruption of clathrin coated vesicle formation, via dynamin inhibition, does not prevent p38 activation in PT2 cells**

PT2s were pre-treated with dynasore (80 µm) for 30 min where indicated and then with either BK (1 µm), LPA (10 µm), THR (1 U/mL) or TNF-α (1 µm) for 5 min and levels of phosphorylated p38 (T180/Y182) determined by western blotting. Representative blot (A) and normalised densitometric quantifications (B) shown (means ± SEM, n = 3). One-way ANOVA with Bonferroni's post-hoc test indicates no significant differences.

## 4.4    Discussion

Although transactivation of VEGFR2 has been found to operate within multiple vascular beds and in relation to a number of VEGFR2 mediated functions, following results from the previous chapter, it was evident that VEGFR2's transactivation as a pathway for triggering acute permeability responses at the BBB and BRB has not yet been explored (Fujita et al. 2006, Warren et al. 2014, Petreaca et al. 2007, Thuringer, Maulon and Frelin 2002, Tanimoto, Jin and Berk 2002). Cross talk between different signalling systems can be critical for coordinating cellular responses to stimuli and cell surface transmembrane proteins are particularly integral in facilitating diverse cell response (Cattaneo et al. 2014). These cell surface proteins are typically either RTKs, such as VEGFR2, or GPCRs. Given the wide variety of vasoactive mediators that are implicated in a permeability response, and the potential increase in pathway complexity given VEGFR2 transactivation exists at the BBB, it was of great interest to expand on the findings from our work on LPC. Four stimuli with known vasoactive characteristics, a kinin peptide (BK), another phospholipid (LPA), a serine protease coagulant factor (THR) and a cytokine (TNF-α) were provisionally tested to see whether VEGFR2 transactivation was a mechanistic feature in a pilot study.

Firstly, I defined the acute permeability response for these four vasoactive mediators within primary brain MVECs using TEER measurements. BK and THR had similar profiles that resolved within 30 min of treatment, in comparison LPA had a prolonged response and TNF-α did not appear to have a comparable response (Fig. 4.12). While BK has been shown to cause a decrease in TEER for both *in vitro* and *in vivo* BBB models, the current result is interesting as earlier *in vitro* work was performed in a HUVEC related cell line cultured with glioma cells. This co-culture would thereby imbue the ECs with BBB properties and a similar magnitude of TEER decrease was found (Easton and Abbott 2002, Butt 1995, Raymond, Robertson and Dinsdale 1986). The response within the current model resolves more quickly however and this could be due to differences between the model systems used. LPA

147

has been previously shown to cause a decrease in TEER *in vitro* within a BBB primary cell model, and also *in vivo* (Schulze et al. 1997, Sarker, Easton and Fraser 1998, Sarker, Hu and Fraser 2010). While data could only be found for THR-induced decrease in TEER at the BBB *in vivo*, *in vitro* data showing a THR-induced decrease in TEER exists for pulmonary artery ECs and dermal MVECs. The decrease in TEER is prolonged and of greater magnitude when compared with brain MVECs, but this could be due to innate differences between vascular beds (Borbiev et al. 2003, Lee et al. 1997, Tiruppathi et al. 2000). TNF-α has been frequently investigated as a permeability mediator at the BBB where it has been found to trigger a strong immediate decrease in TEER that resolves within 4 h *in vitro*, and my findings contradict this. When comparing the baseline resistance measurements used, previous studies have proceeded when the barrier was relatively low for brain MVECs and this could explain the discrepancy (Deli et al. 2005, de Vries et al. 1996).

I then provided functional evidence for VEGFR2 transactivation triggering a permeability response within brain MVECs by inhibiting VEGFR2 function, firstly using a chemical inhibitor and then a VEGFR2 targeting adenovirus to confirm. In both instances, VEGFR2 inhibition did not prevent BK from generating a decrease in TEER. There is substantial evidence for BK's mode of action, that BK activates receptor $B_2$ mediating a rise in intracellular $Ca^{2+}$ possibly leading to tight junction opening through phospholipase $A_2$ (Deli 2009). On the other hand, VEGFR2 inhibition had a significant impact on both LPA and THR's capacity for generating a decrease in TEER indicating VEGFR2 involvement, a novel finding for both mediators (Table 4.1). LPA is known to activate RhoA leading to stress fibre formation, a morphological feature of altered junctions and increased permeability (Burridge and Wittchen 2013). It is the ligand for six known GPCRs $LPA_{1-6}$ which signal though coupled $G_\alpha$ proteins but there is no literature indicating that VEGFR2 is involved in mediating LPA's effects (Yung, Stoddard and Chun 2014). Similarly, thrombin has not been connected to VEGFR2 in the literature to date in relation to a permeability response, rather its receptors are the PARs (1-4) of which PAR1, PAR3

and PAR4 are directly activated by thrombin, while PAR2 is transactivated by activated PAR1 (Zhao, Metcalf and Bunnett 2014, Lin and Trejo 2013). PAR1 is expressed in the cerebral vasculature and thrombin has also been found to activate RhoA (Junge et al. 2004, van Nieuw Amerongen et al. 2000).

As p38 activity is integral for VEGF-A mediated permeability at the BBB, I next analysed whether it is also implicit in the actions of BK, LPA and THR on permeability, considering two out of three utilise VEGFR2 to some extent (Hudson et al. 2014). Unlike VEGFR2 inhibition, I found that all three mediators were completely prevented from triggering a permeability response when p38 was inhibited (Table 4.1). While all three mediators have been found to activate p38 within other vascular beds, and in relation to other processes such as cytokine induction, apoptosis and gene expression, the result, while hinting at a complex signalling pathway, suggests the possibility that some elements of the pathways may either converge at common points, or utilise similar pathways (Maeda et al. 2004, Hayashi et al. 2000, Shimada and Rajagopalan 2010, Brault et al. 2007, Rahman et al. 2001, Borbiev et al. 2004). In support of this functional result, I measured p38 activation via western blotting T180/Y182 phosphorylation and found a similar level of activation for all three mediators that was significantly higher than control treated cells (Fig. 4.12).

I then sought to provide VEGFR2 activation data to support the functional results and trialled blotting for three different phosphorylated residues, Y951, Y1214 and Y1175, but Y1175 was the only residue for which I could detect a signal. I demonstrated VEGFR2 activation at Y1175 following BK, THR and TNF-α treatment but relatively little activation was observed with LPA treatment (Fig. 4.12). The fact that VEGFR2 is phosphorylated following BK, THR and TNF-α treatment is a general indicator of receptor activation but the pattern observed does not correlate with earlier functional data. The implications from this are twofold. Firstly, VEGFR2 is activated by THR in this context and in support of VEGFR2's functional involvement in THR's mediated actions, while LPA's signalling through VEGFR2

remains to be confirmed, although it is likely when VEGFR2's clear functional involvement is considered. Secondly, the data I've presented reveals a potential flaw in using Y1175 phosphorylation alone as an indicator of VEGFR2 permeability, as has been a feature of a number of studies (Olsson et al. 2006). Modulation of residue Y951, on the other hand, is considered to be the principal residue implicated in vascular leakage. Specifically, it was recently found that signalling initiated by phosphorylated Y951 of VEGFR2 regulates dynamic c-Src and VEC phosphorylation (Li et al. 2016). Prior to this it had been known that Y951 interacted with T cell-specific adaptor (TSAd) which then regulated c-Src's signalling at EC junctions through the formation of a VEGFR2-TSAd-c-Src-VEC complex (Sun et al. 2012).
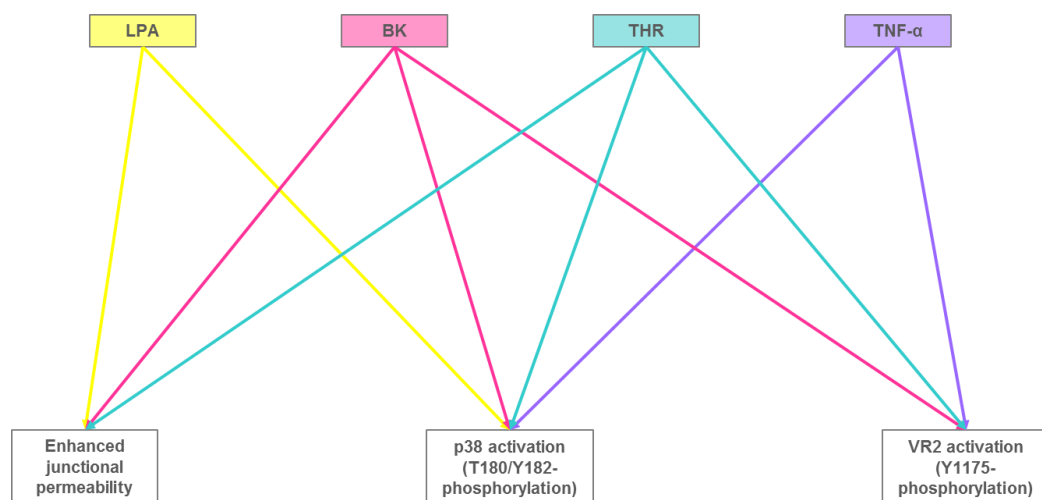


**Figure 4.12. Effect of LPA, BK, THR and TNF-α on junctional permeability, p38 and VR2 phosphorylation in neural microvascular endothelium**

Some RTKs, such as EGF receptor (EGFR) and VEGFRs, are known to be internalised following activation and signalling so as to regulate receptor activity (Jones and Rappoport 2014, Sorkin and Goh 2009, Ballmer-Hofer et al. 2011, Scott and Mellor 2009). It was recently shown that EGFR when alternatively activated, *i.e.* by a stressor, was internalised to a different compartment and activated once internalised (Tomas et al. 2015). For VEGFR2, there is a lot of conflicting literature

150

in relation to its required location for activation, whether it is connected to internalisation or whether presence at the plasma membrane is sufficient (Lampugnani et al. 2006, Lanahan et al. 2010, Sawamiphak et al. 2010, Jakobsson et al. 2006). Most recently, VEGFR2 was found to be activated (on residue Y1175) despite being prevented from internalisation in HUVECs when stimulated with VEGF (Gourlaouen et al. 2013). I was curious as to whether the outcome would be similar within the neural microvasculature. To test whether VEGFR2 internalisation is important in relation to its activation, at least at residue Y1175, a dynamin inhibitor was used to prevent clathrin-mediated endocytosis. In the present study, I found that preventing VEGFR2 internalisation prevented its activation following treatment with any of BK, THR and TNF-α (Table 4.1). However, activation of p38, downstream of VEGFR2 and key in mediating VEGF-A permeability, was not prevented by the same inhibitor. This latter result could indicate that, although dynamin inhibition antagonises trafficking of VEGFR2 and its phosphorylation, it does not prevent receptor activation, reflecting the unsuitability of this VEGFR2 residue as an indicator of permeability.

**Table 4.1: Summary of main findings in relation to effects of LPA, BK, THR and TNF-α on junctional permeability, p38 and VR2 phosphorylation on neural microvascular endothelium**

|  | p38 inhibition prevents | VR2 inhibition prevents | Clathrin inhibition prevents |
|---|---|---|---|
| LPA | Enhanced junctional permeability | Enhanced junctional permeability | |
| BK | Enhanced junctional permeability and VR2 phosphorylation on Y1175 | VR2 phosphorylation on Y1175 | VR2 phosphorylation on Y1175 |
| THR | Enhanced junctional permeability and VR2 phosphorylation on Y1175 | Enhanced junctional permeability and VR2 phosphorylation on Y1175 | VR2 phosphorylation on Y1175 |
| TNF-α | VR2 phosphorylation on Y1175 | VR2 phosphorylation on Y1175 | VR2 phosphorylation on Y1175 |

# Chapter 5　Results

**Transcellular transport across an *in vitro* blood-brain barrier model is differentially enhanced by a variety of mediators**

## 5.1　Contribution of Authors

**Figure 5.1. Uptake of macromolecular tracer to brain MVECs is enhanced by a range of endogenous and exogenous mediators**

(A) Kenny, BA

(B) Kenny, BA

**Figure 5.2. MET does not disturb the interendothelial junctions of brain MVECs**

(A) Martins, T

(B) Martins, T

(C) Burgoyne, T

**Figure 5.3. A range of endogenous and exogenous mediators enhances macromolecular flux across brain MVECs**

Kenny, BA

**Figure 5.4. A range of endogenous and exogenous mediators enhances macromolecular flux across brain MVECs and, on visualisation using EM, incorporates a transcellular process**

(A) Kenny, BA

(B) Kenny, BA

(C) Kenny, BA

(D) Kenny, BA

(E) Kenny, BA

(F) Kenny, BA

**Figure 5.5. Development and preliminary characterization of multicellular *in vitro* blood-brain barrier models**

(A) Kenny, BA and Hirst, A

(B) Kenny, BA and Hirst, A

**Figure 5.6. Characterisation of brain MVECs, PCs and ACs for use in multicellular *in vitro* blood-brain barrier models**

(A) Kenny, BA

(B) Kenny, BA

**Figure 5.7. Preliminary characterisation of multicellular *in vitro* co-culture blood-brain barrier model**

(A) Kenny, BA

(B) Kenny, BA

**Figure 5.8. Preliminary characterisation of multicellular *in vitro* spheroidal blood-brain barrier model**

Kenny, BA

## 5.2 Introduction

Our work on LPC also indicated the presence of both paracellular and transcellular transport when acting on neural MVECs, with an initial response directed towards the junctions and, as this resolves, a subsequent or continuation of the response which operates transcellularly. As detailed in the introduction, vascular permeability can occur via both routes. Although the healthy BBB has very low levels of specific, fluid-phase transcytosis, apparently lacking the vesicular structures required, the abnormal BBB (and inner BRB) displays characteristics of utilizing such transcellular transport with increased numbers of vesicles observed (Simionescu et al. 1988, Bouchard, Ghitescu and Bendayan 2002, Hirano, Kawanami and Llena 1994, Thompson et al. 2010). Here, I was interested in the role, if any, that transcellular transport played in the permeability effects mediated by different endogenous and exogenous factors, some with known paracellular or transcellular effects.

As there have been many studies reporting permeability enhancing effects of MET on the BBB both *in vitro* and *in vivo*, although with discrepancies in their execution and thus more difficult to directly compare, MET and its chiral enantiomer DEOX were both tested (Turowski and Kenny 2015). MET is a highly addictive CNS stimulant with known neurotoxic features. It can damage nerve terminals of monoaminergic neurotransmitters by eliciting excitotoxicity, mitochondrial dysfunction and increased ROS production (Quinton and Yamamoto 2006). It is unclear whether or not MET acts on membrane receptors of the BBB but, as a small lipid soluble molecule, it readily crosses the BBB and is known to bind a variety of proteins expressed in neurons (Turowski and Kenny 2015). In addition, it appears as though MET evades BBB efflux pumps as it rapidly accumulates within the CNS parenchyma of rodents (Martins et al. 2013).

A monoculture model of primary brain MVECs with well-preserved inter-endothelial junctions, apical-basal polarity, barrier properties and highly predictive of the intact

BBB was used to assess the effects of mediators (Hudson et al. 2014). However, studies investigating gene and protein expression analyses of the BBB have indicated that brain MVECs lose some of their properties *in vitro*, in a manner termed 'phenotypic drift' (Obermeier, Daneman and Ransohoff 2013, Urich et al. 2013). As mentioned in the introduction, PCs have been found to suppress PV-1, a caveolar protein, at the healthy BBB as well as regulating MFSD2A, a protein which transports long-chain fatty acids across the BBB. This could mean that results using monoculture models are not representative of the BBB *in vivo* and that structural and functional observations are artefacts. Models making use of multiple supporting cells of the NVU are being used more frequently to promote physiological cell-cell interactions which would exist *in vivo* (Urich et al. 2013).

In this chapter, the effect of endogenous and exogenous mediators on the level of transcellular transport was assessed within an established single culture BBB model. When evident that transcellular transport was differentially enhanced by the mediators tested, an additional aim was included, exploring the contribution of the different components of the neurovascular unit to this flux enhancement. This led to the development and preliminary characterization of two multicellular *in vitro* BBB models however further experiments using the models were not carried out due to restrictions on time and a decision to focus on other elements of this thesis.

## 5.3   Results

### 5.3.1   Uptake of macromolecular tracer to brain MVECs is enhanced by a range of endogenous and exogenous mediators

The circulating concentration of MET in users of the drug is approximately 1 µm, with concentrations exceeding 30 µm considered toxic (Turowski and Kenny 2015, Melega et al. 2007). A concentration curve was established to test whether a range of values, including 1 µm, would cause effects of interest *in vitro*. An assay measuring the uptake of a 40 kDa macromolecular tracer, HRP, within primary brain MVECs was used. Starting at 0.03 µm, concentrations up to 1 µm led to an increase in HRP uptake to cells following 1 h pre-treatment, with a significant maximal effect seen for 1 µm MET (Fig. 5.1A). Concentrations higher than 1 µm led to a drop in HRP uptake. For subsequent experiments, 1 µm MET was used and, as it is the chiral enantiomer, 1 µm was used for DEOX.

Analysing the potential for a range of mediators, MET, DEOX, BK (1 µm) and LPA (10 µm), to enhance HRP uptake within cells, the same non-directional assay measuring HRP uptake was used and results were normalized to non-treated control measurements. For all four mediators, following 1 h of pre-treatment, HRP uptake to primary brain MVECs was significantly enhanced (Fig. 5.1B). While MET, DEOX and LPA enhanced HRP uptake nearly five times higher than control, BK enhanced uptake approximately 3.5 times higher.
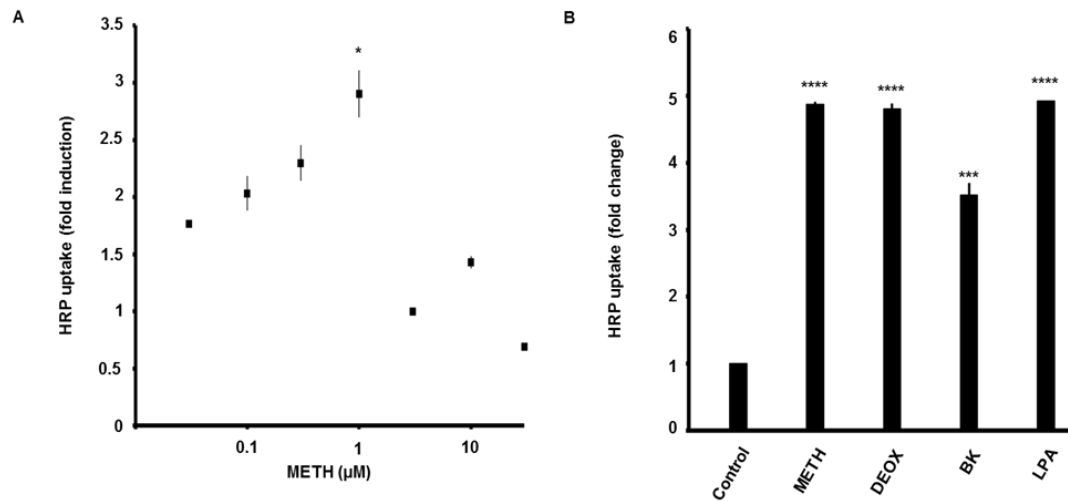
**Figure 5.1. Uptake of macromolecular tracer to brain MVECs is enhanced by a range of endogenous and exogenous mediators**
Primary rat brain MVECs were grown to confluence on a 96-well plate, MET was added at various concentrations, as indicated, for 1 h before the addition of HRP (1 mg/mL) for 5 min (A). Cells were washed extensively, lysed and a stoichiometric OPD and hydrogen peroxide reaction performed and analysed, shown are means ± SEM of HRP activity (n = 3) (A). Primary rat brain MVECs were grown to confluence on a 96-well plate and either MET (1 µm), DEOX (1 µm), BK (1 µm) or LPA (10 µm) was added with HRP (1 mg/mL) for 1 h (B). Cells were washed extensively, lysed and a stoichiometric OPD and hydrogen peroxide reaction performed and analysed, shown are means ± SEM of HRP activity (n = 3) (B).

### 5.3.2 MET does not disturb the interendothelial junctions of brain MVECs

Endothelial junction organization in response to BK, LPA and VEGF has been well characterized in the literature therefore it was equally important to ascertain MET's effects (Sarker et al. 2010, Hudson et al. 2014, Weis and Cheresh 2005, Schulze et al. 1997, Abbott 2000). First, the functional effect of MET (1 µm) on interendothelial junctions of brain MVECs was measured by TEER as described in chapter three. Baseline measurements were taken for 2 h and then either cells were left untreated (NT) or MET was added at time indicated (Fig. 5.2A). Compared with NT, TEER values were not altered by addition of MET indicating no major effect on

interendothelial junctions. Immunofluorescence staining was then used to compare the organization of major junctional proteins between NT primary brain MVECs and those treated with either 2 h or 6 h of MET (1 µm). For NT cells, VEC, occludin and ZO-1 staining were all confined to cellular junctions while claudin-5 was found both at the junctions and also within internal vesicles and apical membranes (Fig. 5.2B upper panels). For MET treated cells, at both 2 h and 6 h treatment, the staining for all four junctional proteins was the same as that seen in NT cells (Fig. 5.2B lower panels). To compare the ultrastructure of the cell-cell junctional areas between primary brain MVECS treated with NT and MET (1 h), cells grown on TW filters were prepared for EM analysis. Representative images show that there were no observable changes between the cell-cell junctions of NT and MET (1 h) treated cells (Fig. 5.2C).
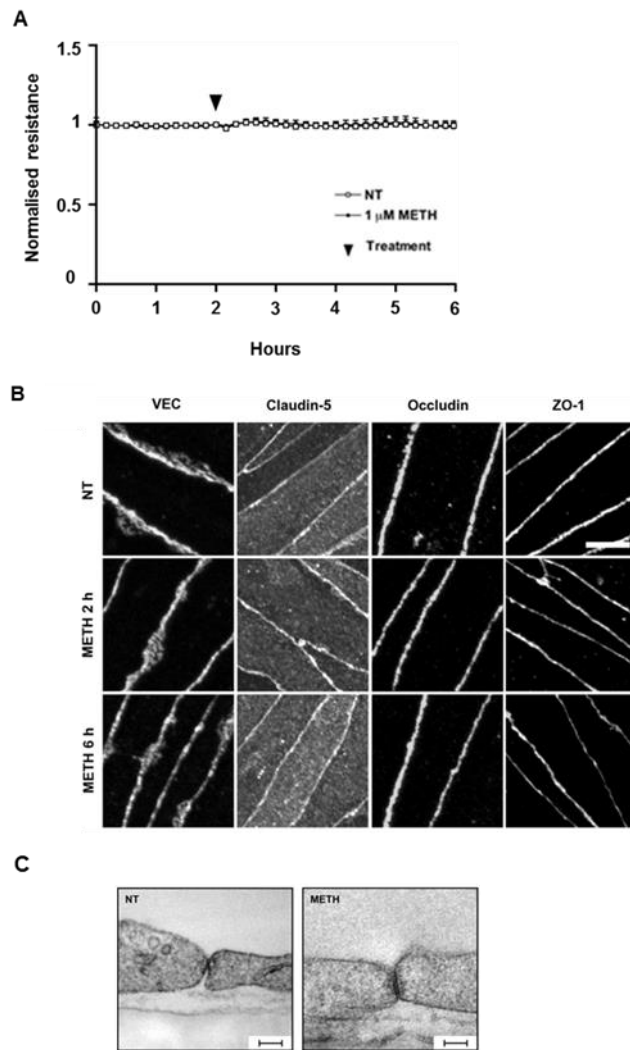
**Figure 5.2. MET does not disturb the interendothelial junctions of brain MVECs**

Primary rat brain MVECs were grown to confluence and full electrical barrier before proceeding with measurements. Measurements were recorded for 2 h before either being left untreated (NT) or MET (1 µm) was added as indicated (A). Shown are means ± SEM of normalised resistance changes (at least n = 3). Primary rat brain MVECs were grown to confluence and either untreated (NT) or treated with MET (1 µm) for 2 h or 6 h (B). Cells were then fixed and stained for VEC, claudin-5, occludin and ZO-1 and analysed by confocal microscopy. Shown are representative projections of overlapping 0.35 µm sections spanning the thickness of the cell (B). Scale bar = 5 µm. Primary rat brain MVECs were grown to confluence and either untreated (NT) or treated with MET (1 µm) for 1 h before processing for transmission EM (C). Shown are representative images of endothelial contact areas (C). Scale bar = 100 nm.

159

### 5.3.3 Macromolecular flux across brain MVECs is enhanced by a range of endogenous and exogenous mediators and incorporates a transcellular process

To determine whether the enhancement in HRP uptake to brain MVECs extended to the transcellular flux of HRP, an assay that measures unidirectional transcellular transport was used. Primary brain MVECs plated on transwells (TWs) were apically loaded with HRP and either NT, MET (1 µm), DEOX (1 µm), BK (1 µm), LPA (10 µm) or VEGF (50 ng/mL) treated for 1 h before both sides of the TWs were washed and the rate of basal HRP efflux measured and compared. For all five mediators tested, the rate of HRP transcellular was significantly increased when compared to normalized control but to a different extent (Fig. 5.3). Unlike earlier HRP uptake experiments, BK enhanced HRP flux to the greatest extent, over three times higher than the normalized control. MET, DEOX and VEGF approximately doubled HRP flux compared with the normalized control while LPA increased HRP flux by half.
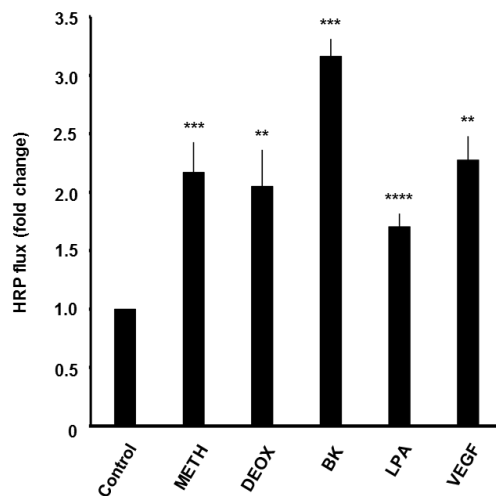


**Figure 5.3. A range of endogenous and exogenous mediators enhances macromolecular flux across brain MVECs**
Primary rat brain MVECs were grown to confluence and full electrical barrier on TWs before treatment in the apical compartment with either MET (1 µm), DEOX (1 µm), BK (1 µm), LPA (10 µm) or VEGF-A (50 ng/mL) in the presence of HRP (1 mg/mL) for 1 h, or in

the presence of HRP (1 mg/mL) for 1 h alone as control. Cells were washed extensively and the rate of transport from apical to basal side determined and compared. Shown are means ± SEM of HRP activity (n = 3). **, $p < 0.01$, ***, $p < 0.001$, ****, $p < 0.0001$ (Student's T-test), significant when compared to CON.

Primary brain MVEC samples corresponding to those used in the HRP transcellular flux functional assay were prepared for EM analysis. DAB staining revealed HRP containing structures within primary brain MVECs for all five mediator pre-treatments, although as indicated by the HRP flux assay, the number of these structures differed depending on the mediator, as shown in representative images. When compared with NT (Fig. 5.4A), BK, with the highest enhancement in HRP flux, had many small HRP containing vesicular structures (Fig. 5.4B). Both MET and DEOX (Figs. 5.4C and D respectively), had less HRP-containing structures overall, when compared with BK, but these were a mix of both small and large HRP containing vesicular structures. Within the LPA representative image (Fig. 5.4E), while there were comparably less HRP containing structures, a high number of non-HRP containing structures were seen, both vesicular and pit shape along both the apical and basal sides of the cell resembling caveolae. In a way similar to MET and DEOX treatment, VEGF treated primary brain MVECs had a mixture of small and large HRP containing vesicles, but a slightly less amount overall (Fig. 5.4F).
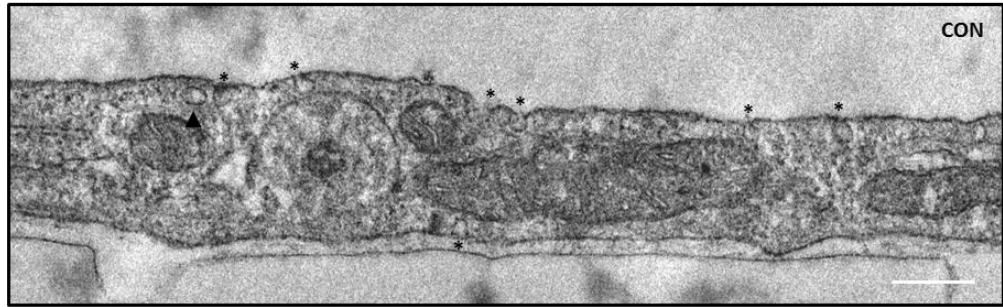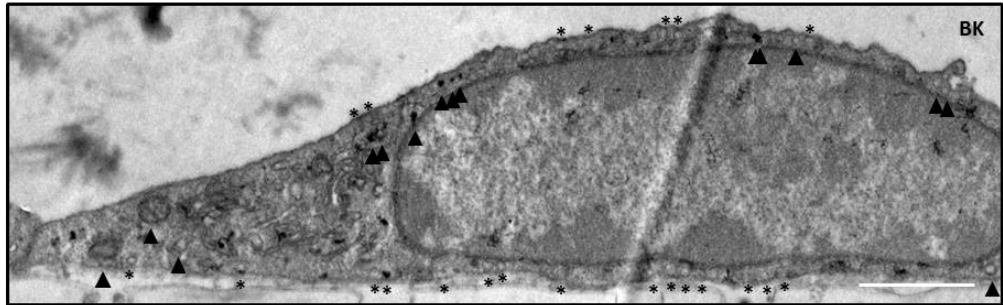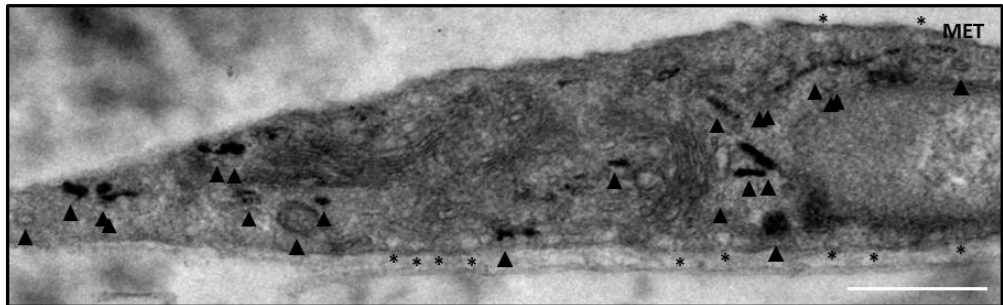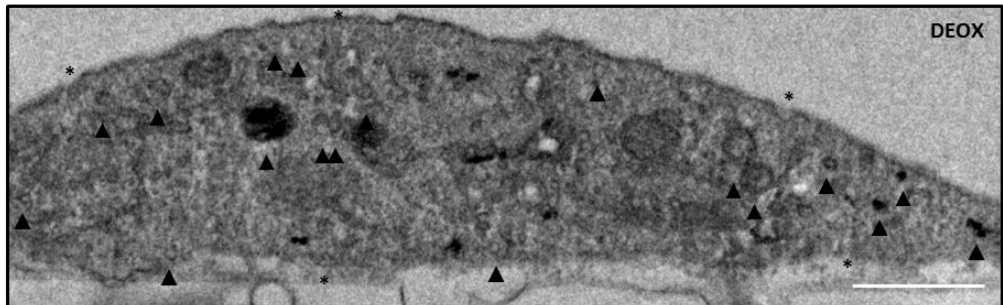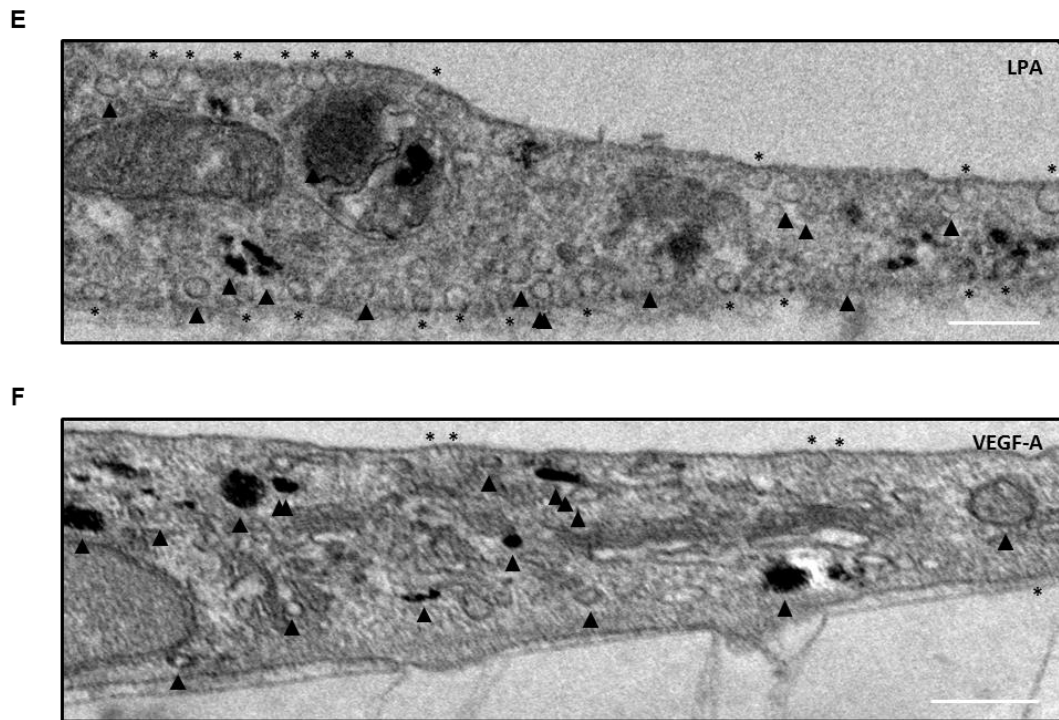
**Figure 5.4. A range of endogenous and exogenous mediators enhances macromolecular flux across brain MVECs and, on visualisation using EM, incorporates a transcellular process**

Primary rat brain MVECs were grown to confluence and full electrical barrier on TWs before treatment in the apical compartment with either MET (1 µm), DEOX (1 µm), BK (1 µm), LPA (10 µm) or VEGF-A (50 ng/mL) in the presence of HRP (1 mg/mL) for 1 h, or in the presence of HRP (1 mg/mL) for 1 h alone as control. Cells were washed extensively, processed for HRP visualisation using DAB and transmission EM. Shown are representative images in which electron dense DAB reaction products reveal the presence (or absence) of HRP-containing compartments, CON (A), BK (B), MET (C), DEOX (D), LPA (E) or VEGF-A (F). Asterisk indicates pits, triangle indicates compartments (HRP-containing and not). Scale bar = 100 nm.

## 5.3.4   Development and preliminary characterization of multicellular *in vitro* BBB

As the literature regarding the existence of physiological transcellular transport at the BBB has been contentious, in that some parties regard an *in vitro* monoculture model

insufficient, it was decided to reinforce the earlier results of this chapter by determining the effect these mediators had within multicellular *in vitro* BBB models (Helms et al. 2016). Achieving this aim required establishing these models within the lab, a co-culture model similar to the TW model used already in the lab, and a spheroidal model (Nakagawa et al. 2009, Urich et al. 2013). The co-culture model consists of primary brain MVECs cultured on the apical side of a TW filter, primary brain PCs cultured on the basal side of the same TW and primary brain ACs cultured within the multi-well plate holding the TWs (Fig. 5.5A). The potential benefits of this model were that it could provide a direct comparison with earlier results and, once it was possible to prepare good primary pericyte and astrocyte cultures, would be relatively easy to assemble and then characterize. The spheroid model consists of the same three cell types, primary brain MVECs, PCs and ACs, but their organization does not require a material support and the cells instead freely assemble based on their intrinsic properties. PCs are key in this as they have the greatest capacity to interact with both MVECs and ACs and naturally drive the desired NVU spheroid layering. What results is in the spontaneous formation of a spheroid shape with the MVECs encasing a layer of PCs and a denser core of ACs, with the inner core representing the CNS parenchymal side of the BBB and the outer facing MVECs represent the luminal side of the BBB (Fig. 5.5B). This model would provide a truer reproduction of the NVU *in vivo* as the three cell types would be in direct contact with each other.
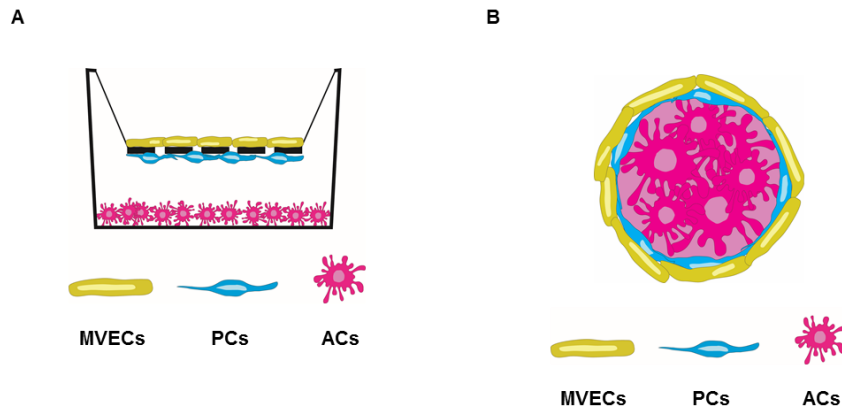
**Figure 5.5. Development and preliminary characterization of multicellular *in vitro* blood-brain barrier models**

Schemas are illustrated for both co-culture model (A) and a spheroidal model (B) of the *in vitro* BBB developed within this study. The co-culture model consists of primary rat brain MVECs grown to confluence and full electrical barrier on TWs within the apical chamber, primary rat brain PCs grown on the reverse side of the TW and primary rat brain ACs grown within the bottom of the lower chamber (A). The spheroidal model consists again of primary rat brain MVECs, PCs and ACs but without a supportive scaffold material, the cells freely assemble according to their cell type so that the ACs form a core layer (or parenchymal space), PCs line the space between the ACs and an outer cell layer of MVECs (facing the luminal space) producing a spheroidal shape (B).

For both models, in addition to the primary brain MVECs routinely used in the lab, primary PCs and primary ACs also needed to be isolated and cultured. Cells were prepared as described in the methods and samples fixed and stained by immunofluorescence. The preparation methods for primary brain MVECs and PCs are closely related as are the cell types, being closely associated during embryonic development in the rat, and cell samples were stained for both an endothelial marker, VEC, and a pericyte marker, platelet-derived growth factor receptor-β (PDGFR-β). Representative images of primary brain MVECs show morphologically appropriate cells that were elongated and grew in monolayers without overlapping despite being in close apposition. There was no visible staining for PDGFR-β but clear junctional staining for VEC was seen, in addition to cytoplasmic background staining (Fig.

165

5.6A). For primary brain PCs, there is clear intracellular punctate staining for PDGFR-β and the morphology was also appropriate, with cells spreading more and with irregular projections and overlapping, unlike primary brain MVECs. Despite this, there was also a low level of apparent VEC staining, as this was not junctional and appeared to correlate with PDGFR-β staining it is possible that there was a certain amount of cytoplasmic background staining similar to MVECs (Fig. 5.6B). Finally, the preparation method for primary brain ACs was disparate from those of primary brain MVECs and PCs. ACs, cells that are not generated *in vivo* until after birth in the rat, are typically identified by their expression of GFAP as they are morphologically very heterogeneous. The primary brain ACs cultured had both strong GFAP staining and a typical morphological feature, long cell processes (Fig. 5.6C).
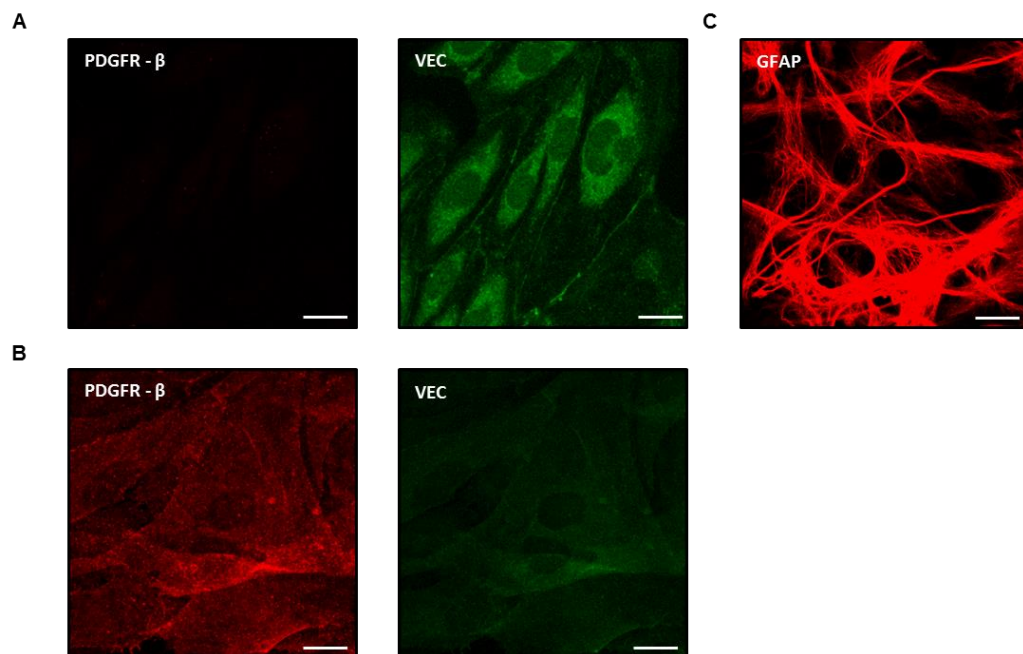


**Figure 5.6. Characterisation of brain MVECs, PCs and ACs for use in multicellular *in vitro* blood-brain barrier models**
Primary rat brain MVECs, PCs or ACs were grown to confluence (MVECs and PCs) or sub-confluence (ACs) and fixed and stained for either PDGFR-β and VEC (MVECs and PCs) or GFAP (ACs) and analysed by confocal microscopy. Shown are representative projections of

overlapping 0.35 µm sections spanning the thickness of the cell for MVECs (A), PCs (B) and ACs (C). Scale bar = 10 µm.

To determine the effect co-culturing might have on an *in vitro* BBB, four different cellular combinations were assembled at the same time and compared longitudinally by TEER measurement. These combinations included a monoculture model of primary brain ECs plated in the TW apical chamber (EC), a dual culture model of primary brain ECs as before plus primary brain ACs plated in the multi-well plate holding the TWs (EC AC), the third and fourth combinations added primary brain PCs to the basal side of the TWs at a density expected to correspond to approximately a third of the number of ECs on the opposite side of the filter, or five times this number of PCs (EC AC PC1 and EC AC PC5 respectively). To prepare the co-culture model, media was aspirated from the inner chamber of TWs plated with primary brain MVECs that had reached a TEER (corrected for resistance of filter) of at least $285 \pm 7.5$ (for EC AC), and as high as $408 \pm 18$ (for EC), and inverted on to a sterile culture dish assembly, with moisture reservoir. Counted PCs were added in 100 µL volumes to the underside of the TWs (now inverted) designated for PCs and returned to 37°C and 5% $CO_2$ for 2 h. TWs were subsequently transferred to culture plates either plated or without ACs seeded 48 h previously. Cultures were left undisturbed for 48 h at 37°C and 5% $CO_2$ before TEER was measured (time 0 h in Fig. 5.7A), TEER was measured in the same way over the following two weeks to ascertain effects of additional cell types on primary brain EC barrier function.

As the cell culture media used for the *in vitro* monoculture model contains the key components that enable brain MVECs to function as the intact BBB, it would not be expected for additional NVU cellular components to alter the barrier greatly. Over a two-week time-frame, and using EC as a baseline, there was little deviation in TEER of the co-culture combinations, EC AC and EC AC PC1, from the baseline (Fig. 5.7A). This is not to say that the presence of ACs and PCs are not having effects on the barrier which are not being taken into account using this functional test. However, using an expected number of PCs that was far greater than that which is

found *in vivo*, EC AC PC5, did cause the TEER to deviate from the EC baseline values (Fig. 5.7A). It appears as though the ideal time at which to use prepared co-cultures would be approximately five days following assembly of the cultures.

For comparative purposes, images of the upper sides of TWs from each of the four different cellular combinations stained with nuclear DAPI stain, provided a representative view of their cellular landscape. For EC and EC AC, only crisply stained morphologically accurate primary brain MVECs were seen (Fig. 5.7B upper panels). For EC AC PC1 and EC AC PC5, while primary brain MVECs were seen as in the upper panels, the number of ECs appeared to be a little less in ECACPC5, perhaps the cause of the lower TEER values. At the same time, for both EC AC PC1 and EC AC PC5, the blurred profile of PCs, also stained with DAPI, were seen adherent to the opposite side of the TWs, with a far greater number seen for ECACPC5 (Fig. 5.7B lower panels).



**Figure 5.7. Preliminary characterisation of multicellular *in vitro* co-culture blood-brain barrier model**

Multicellular co-culture BBB models were assembled with varying PC densities and the TEER of the four different assembled models measured over 10 days using STX-2 chopstick electrodes (A). MVECs were used at ca. $30000/cm^2$ (EC), ACs at ca. $50000/3.8\ cm^2$ (AC) or none at all, and PCs either at ca. $20000/cm^2$ (PC1), ca. $100000/cm^2$ (PC5) or none at all. Shown are mean TEER values minus blank TW measurement $\pm$ SEM (n = 6) for the four assembled models, EC, EC AC, EC AC PC1 and EC AC PC5 (A). TWs from (A) were fixed

and stained on both sides with nuclear DAPI stain (B). Shown are representative images of the apical TW chamber for the four assembled models, EC (i), EC AC (ii), EC AC PC1 (iii) and EC AC PC5 (iv), MVECs clearly visible in all four models while PCs obscured by the TW filter can be seen in the two models containing PCs, being plated on the TW side opposite to MVECs (B). Scale bar = 30 µm.

After testing a series of combination ratios, NVU spheroids were prepared by combining equal numbers of primary brain MVECs, PCs and ACs and dispensing them in aliquoted droplets (maximum volume 30 µL), evenly spaced, to upturned sterile cell culture lids. These lids were placed over a liquid reservoir and returned to 37°C and 5% $CO_2$ for 48 h following which time they were collected by gravity. Spheroids were fixed and stained for an endothelial cell marker, VEC, and imaged by confocal; PCs and ACs had been stained with live cell dyes before assembly. A combination of embedding techniques and microscopy approaches were trialled and shown is an image of a representative NVU spheroid showing three distinct layers of a well-defined multicellular structure, with ACs at the core, surrounded by a layer of PCs, surrounded by ECs (Fig. 5.8).
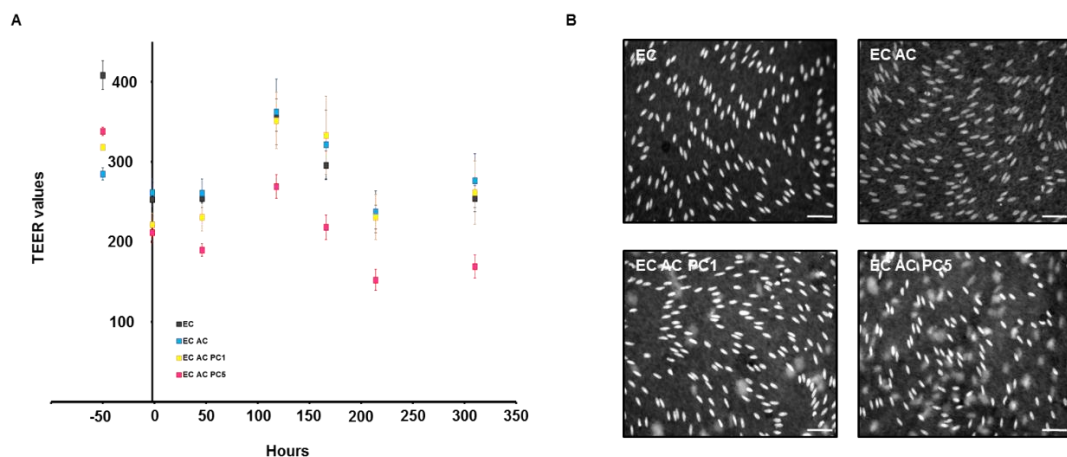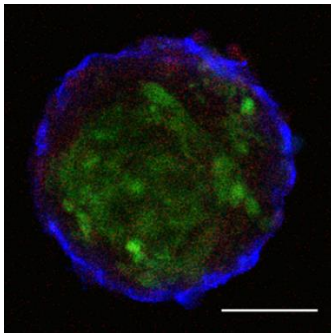


**Figure 5.8. Preliminary characterisation of multicellular *in vitro* spheroidal blood-brain barrier model**
Multicellular spheroidal BBB models were assembled, fixed and stained for confocal microscopy. Shown is an image of representative spheroid model comprised of projections of adjacent overlapping 0.35 µm sections at the centre of the spheroid. Scale bar = 50 µm.

## 5.4 Discussion

Transport across the BBB is more restricted than in other vascular beds, even basal levels of permeability are comparably low. In light of the findings in the first results chapter, that there is an apparent duality in the nature of the permeability response at the BBB following LPC treatment, I endeavoured to uncover more about transcellular transport in this setting using a range of mediators. It is widely accepted that transport across the BBB is limited primarily to highly regulated paracellular junctions and, when transcellular, is solely via specific transporters or receptor proteins (Abbott et al. 2010). There is a growing body of evidence, direct and indirect, that suggests transcellular transport is an important route for permeability responses if not the more important route in relation to disease and inflammation.

In non-neural vascular beds, caveolae have been found to sense mechanical pressure (Cheng et al. 2015). They have also been implicated in the permeability response to vasoactive mediators as when caveolin-1 knockout mice were treated with VEGF-A, leakage was attenuated (Chang et al. 2009). They have been found to be essential for lipid transport into the cell and have been found to rapidly transport caveolae targeted antibodies across the ECs of wildtype mice, but not caveolin-1 knockout mice (Shvets et al. 2015, Oh et al. 2007). Furthermore, caveolae form signalling platforms within ECs for proteins implicated in permeability *i.e.* eNOS, which is of particular importance as it has been suggested that NO signalling could link paracellular transport with transcellular transport (Duran et al. 2010, Goddard and Iruela-Arispe 2013).

Within neural vascular beds, increased expression of caveolin-1 occurs in conjunction with early brain oedema, VEGF-A increased both pinocytic vesicular transport in the BRB and caveolae-mediated transcellular pathway in the blood-tumor barrier of gliomas (Nag, Venugopalan and Stewart 2007, Hofman et al. 2000, Zhao et al. 2011). In terms of a combinatorial response to insult, akin to that seen for LPC treatment, a rodent stroke model was found to display early BBB permeability

via increased caveolae and transcytosis while the most profound disruption to tight junctions occurred 48 h later (Knowland et al. 2014). Work previously published by the lab found that MET induced permeability in a monocellular model of brain MVECs via unidentified intracellular structures (Martins et al. 2013). This chapter extended these observations to include other mediators as well as piloting work developing multicellular BBB models.

In this chapter, I provided preliminary functional and visual evidence for transcellular transport within brain MVECs, using a monoculture model, following treatment with endogenous and exogenous mediators. In a non-directional assay measuring HRP uptake, all of MET, DEOX, BK and LPA significantly enhanced uptake. While BK and LPA are known to effect junctional permeability, MET's effects on cell-cell junctions were investigated further, by immunocytochemistry, TEM and TEER measurements, with no indications of such an effect observed. Since this time, conflicting data has been published, indicating that MET decreases TEER about one fifth from control values following an incubation time 3 h post addition, before which there was no effect on TEER reported (Coelho-Santos et al. 2015).

I then proceeded to test whether these mediators increased complete transcellular transcytosis with a 1 h treatment timeframe, as opposed to uptake alone. This also allowed me to test VEGF-A, which exacts its permeability effects from the parenchymal side of the barrier (Hudson et al. 2014). All five mediators significantly enhanced HRP flux from the apical to basal side of the barrier, although each to relatively different extents, indicating some level of transcellular transport, *i.e.* caveolae or clathrin-coated vesicles, that can be regulated by exterior influences. However, this result conflicts with much of the known literature, which is firmly of the position that caveolae-mediated transport is extraneous to BBB permeability, and so it was highly desirable to be able to visualise the compartments into which the HRP was taken up (Rippe et al. 2002, Simionescu, Gafencu and Antohe 2002).

A set of HRP flux experiments were repeated for subsequent transmission EM processing and visualisation. While all five mediators enhanced the appearance of

non-HRP containing structures, four of the five (LPA excluded) enhanced the appearance of HRP containing structures. Furthermore, it was clear that the pattern, morphology and frequency of the structures varied between differently treated samples. There were clear differences between mediators based on the numbers of pits visible at the luminal or abluminal membranes. Without a significant amount of further experimentation, which was unfeasible within the timeframe available, it would be difficult to know for sure what these structures were. Working towards the smaller end of the scale in relation to diameter, it is possible that these structures are caveolae, or even another variety of endocytic vesicle independent of both caveolae and clathrin (Johannes et al. 2015, McMahon and Boucrot 2011). Caveolae are typically 50-100 nm in diameter and measurements in the current setting reveal that, while there are a number of structures about 50 nm in diameter, such as within MET, DEOX or VEGF-A treated samples, there are just as many structures that are in the 20nm range, especially within BK and LPA treated samples. There is further variation in the shape of the HRP containing structures, with some spherical and others oblong. As clathrin aids in normalising endocytic structure size, these results reinforce the possibility that these structures could be clathrin-independent, and also indicates that additional hypothetical shapes may not been fully realised by the current experimental approach (Johannes, Wunder and Bassereau 2014). Finally, there are great differences in relation to the number of pits visible at the membranes of differently treated samples, with far more found following BK, MET and LPA treatment when compared with DEOX and VEGF-A treated samples. Most notably the number of visible pits is greatest for LPA treated cells, unusual considering the known role LPA has within paracellular mediated transport but perhaps is indicative of alternative LPA-induced transport mechanisms. As the endogenous mediators used within these studies are more commonly known to be contributors to pathophysiological permeability via cell-cell junctions, the current results demonstrate a second distinct contribution via increased transcytosis. For the exogenous mediators, these studies demonstrate a role for MET besides its psychostimulant and neurotoxic features, that is promoting transcellular transport within brain MVEC, a role which is embodied by DEOX.

It is important to recognise a limitation of the approaches used, in that here, transcellular transport has been indirectly shown to occur within brain MVECs. Both macromolecular uptake and flux have been demonstrated functionally, as well as the intracellular structures which may facilitate macromolecular transport visualised. However, direct visualisation or tracking of the movement of intracellular structures containing macromolecular cargo from apical to basal sides of brain MVECs has not been performed. Recent developments in microscopy techniques could enable this, and simultaneously reinforce the data presented here but were not possible to pursue with the facilities available and within the timeframe remaining. Super-resolution microscopy can be performed in live cells, such as structured illumination microscopy, or SIM. Final super-resolution images are reconstructed from multiple images (9-15 depending on dimension of interest) taken from different phase positions and angles through a fine grating. While the relatively minimal number of images required translates into minimal impact on live cells, there are photo-toxicity risks associated with higher laser powers if using shorter exposures (Cox 2015). In addition, alternative fluorescent macromolecular tracers from the HRP employed in the present study would have to be used. Another potential approach is correlative light and electron microscopy, or CLEM. CLEM images combine data illustrating protein dynamics and protein complexes in living cells with their ultrastructural details, by performing live confocal microscopy followed by EM. However, this can be restrictive in terms of the need for the labelling required to be compatible across both microscopy approaches (Liss et al. 2015, Hell et al. 2015).

Recent literature has indicated that some of the intrinsic characteristics of the BBB and BRB, such as the highly regulated nature of transport across the endothelium, are imparted by other members of the neurovascular unit, particularly pericytes (Daneman et al. 2010). For example, it has been shown that MFSD2A, a protein whose expression is largely restricted to the neural vasculature, may suppress transcellular transport at the BBB while its expression is regulated by pericytes (Ben-Zvi et al. 2014). With this in mind, it was important to be able to exclude the possibility that the lack of the other members of the neurovascular unit was

173

responsible for results presented earlier (Helms et al. 2016). I proceeded to establish two multicellular *in vitro* BBB models within the lab to similarly provide functional and visual evidence of transcellular transport within brain MVECs when part of a simulated neurovascular unit. Within the time available it was possible to develop and characterise a functional co-culture model as well as developing the protocol for preparing the spheroidal model. More characterisation of the latter would be ideal before proceeding with intended aims however, such as establishing working functional and transmission EM experiments. Pilot *ex vivo* work performed within the lab extended the *in vitro* observation that MET increased transcellular transport at the BBB to the intact NVU (Chang and Turowski, unpublished observation).

# Chapter 6   Results

**VEC internalisation at neural microvascular barriers**

## 6.1     Contribution of Authors

**Figure 6.1. The role for endothelial MAPKs following ICAM-1 engagement**

(A) Hudson, N

(B) Hudson, N

(C) Hudson, N

**Figure 6.2. ICAM-1 mediates VEC internalisation in a JNK dependent manner in GPNT cells**

(A) Kenny, BA

(B) Kenny, BA

**Figure 6.3. ICAM-1 mediates VEC internalisation in a JNK dependent manner in D3 cells**

(A) Kenny, BA

(B) Kenny, BA

**Figure 6.4. Visualisation of ICAM-1 mediated VEC internalisation in D3 cells**

(A) Kenny, BA

(B) Kenny, BA

(C) Kenny, BA

(D) Kenny, BA

**Figure 6.5. VEC internalisation in response to a range of vascular mediators, and ICAM-1 ligation, in D3 cells**

(A) Kenny, BA and Burgoyne, T

(B) Kenny, BA and Burgoyne, T

(C) Kenny, BA and Burgoyne, T

(D) Kenny, BA and Burgoyne, T

(E) Kenny, BA

## 6.2 Introduction

As the previous chapter's investigation of transcellular transport at neural vascular barriers indicated the presence of a vesicular process, I became involved with a project which was exploring the outcome of ICAM-1 signalling at cell-cell junctions in the context of lymphocyte TEM and the AJ protein VEC. From the outset, it was evident that ICAM-1 signalling and subsequent lymphocyte TEM was mediated, in part, by the MAPK protein JNK (detailed in Fig. 6.1). At sites of inflammation and tissue damage, a series of steps delivers circulating leukocytes to the parenchyma of post-capillary venules (Muller 2014). Leukocyte TEM is a feature of both the adaptive and innate immune responses as well as immune surveillance (Wittchen 2009). During instances of inflammation, mediators promoting increased EC permeability such as histamine are released while the arrival and extravasation of leukocytes occurs later indicating disparity between both (MAJNO and PALADE 1961). However, the observation that AJs are disrupted during both TEM *in vitro* and endothelial permeability events also indicates a level of similarity between mechanisms (Alcaide et al. 2008). Leukocyte TEM can be described as a series of consecutive adhesive and signalling steps: capture from blood flow, rolling adhesion to the required site mediated by selectins, activation of the leukocyte triggered by cytokines, firm adhesion (or arrest) mediated by integrins and TEM, either paracellularly or transcellularly (Wittchen 2009, Muller 2014). These steps require the appropriate coordinated response between leukocytes and ECs, with ECs releasing an array of mediators to stimulate receptor exocytosis at the cell surface and thus promote leukocyte capture for example (Muller 2014). VCAM-1 and ICAM-1 are critical for leukocyte rolling along the EC and subsequent firm adhesion. A key role for ICAM-1 following leukocyte adhesion is to subsequently initiate outside-in signalling which facilitates leukocyte TEM via an array of mediators (Wittchen 2009, Hubbard and Rothlein 2000). One of the intracellular effects of ICAM-1 signalling is VEC phosphorylation mediated by intracellular $Ca^{2+}$ and NO (Turowski et al. 2008, Martinelli et al. 2009). Furthermore, while VEC internalisation has been observed in relation to both EC permeability as well as

leukocyte TEM, the role this plays in relation to each process is not yet clear *i.e.* whether VEC is targeted for degradation, recycling or dynamic rearrangements facilitating AJ disruption (Gavard and Gutkind 2006, Orsenigo et al. 2012, Yamamoto et al. 2015).

In this chapter VEC internalization in response to ICAM-1 ligation was explored, work that originated within a larger collaborative project in the lab. Here quantitative data indicates internalization in response to ICAM-1 ligation, in both rat and human brain MVEC lines, that is dependent on JNK. Two methods were then employed to identify the location and dynamics of VEC internalization with resulting data unable to confirm VEC's exact intracellular course, although further supporting internalization in response to different vasoactive stimuli.

## 6.3    Results

### 6.3.1    The role for endothelial MAPKs following ICAM-1 engagement

Adhesion of activated PLNCs to GPNTs, a rat brain MVEC line, was performed to study levels of MAPK activation by immunoblot analysis (Fig. 6.1A). A statistically significant, two-fold increase in activation was observed for ERK, JNK and p38 following 15 min of co-culture and this effect persisted for at least 1 h (Fig. 6.1A). Next, as antibody-mediated cross-linking of ICAM-1 on the cell surface is known to mimic the ICAM-1 response to lymphocyte adhesion, it was tested whether these three MAPKs would be similarly activated by ICAM-1 cross-linking (Martinelli et al. 2009). When compared with ERK and JNK, phosphorylation of p38 was induced more rapidly and persisted over the length of the time course (Fig. 6.1B). Phosphorylation of ERK peaked at 15 min cross-linking while JNK phosphorylation first peaked with statistical significance at 5 min cross-linking, with a second significant peak at 30 min (Fig. 6.1B). Extending PLNC adhesion data to TEM, MAPK inhibitors were used to determine MAPK involvement in TEM (Fig. 6.1C). Inhibition of ERK (with inhibitor designated UO) had no effect on lymphocyte TEM. Inhibition of p38 (with inhibitor designated SB) had a statistically significant effect on lymphocyte TEM, reducing TEM levels by 10% from that of non-treated co-cultures. JNK inhibition (with inhibitor designated SP) had the greatest effect on lymphocyte TEM, reducing it by 50% from that of non-treated co-cultures.
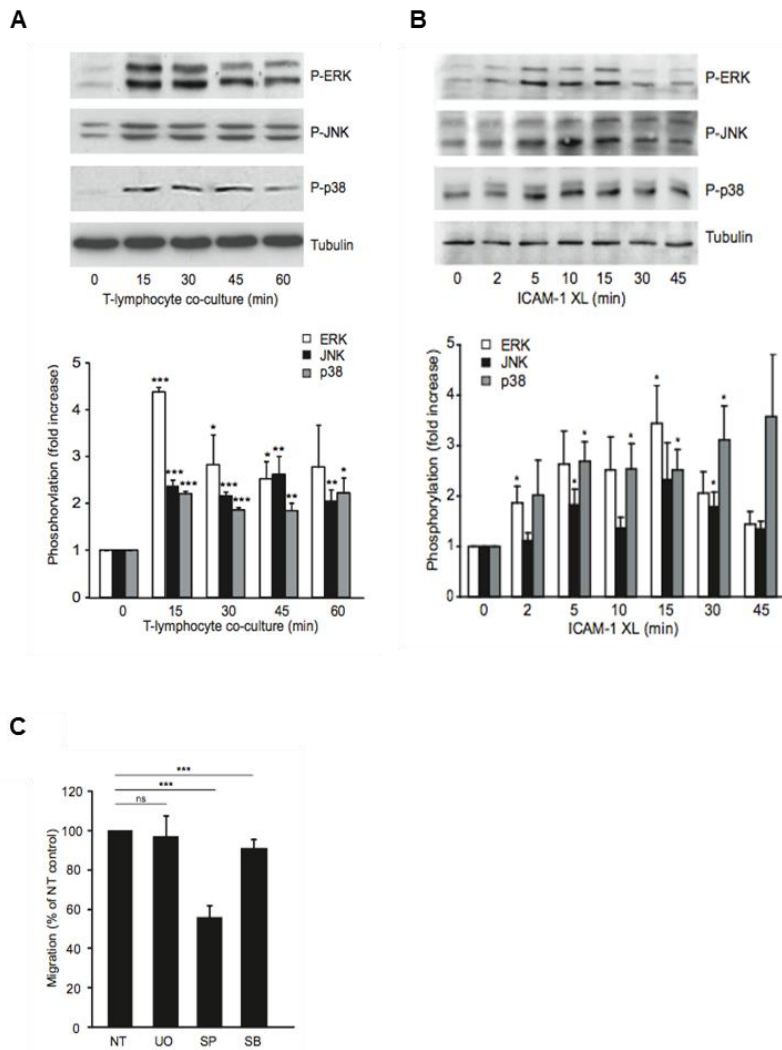
**Figure 6.1. The role for endothelial MAPKs following ICAM-1 engagement**

MAPKs were activated in response to GPNT co-culture with concanavalin A-activated rat PLNCs. Briefly, peripheral lymph node cells (PLNCs) taken from female Lewis rats were activated with 5 µg/mL of concanavalin-A and fluorescently labelled with 1 µm calcein-AM. PLNCs were then resuspended in EC-conditioned, serum-free growth medium and incubated with GPNT monolayers for the times indicated. For immunoblot analysis, PLNCs were extensively washed off with ice-cold PBS to restrict analysis to ECs. Shown are representative immunoblots of MAPK activation alongside tubulin loading controls and their normalized densitometric quantification (means ± SEM, n = 3) (A). GPNTs were subjected to ICAM-1 cross-linking (XL) for the indicated length of time and MAPK phosphorylation analysed. Shown are representative immunoblots of MAPK activation alongside tubulin loading controls and their normalized densitometric quantification (means ± SEM, n = 3)

180

(B). Data were compared with the corresponding time 0 controls and significant differences determined by one-way ANOVA followed by Student's t-test (*, $p < 0.05$; **, $0.001 < p < 0.01$; ***, $p < 0.001$). GPNT monolayers were pretreated or not (NT) with either 50 µm U0126 (UO), SP600125 (SP) or SB202190 (SB) for 1 h prior to a 30 min TEM assay. For U0126, inhibitor was not washed out and maintained throughout the experiment. Data sets were compared to NT controls and analysed by ANOVA and Student's t-test (ns, not significant; ***, $p < 0.001$).

### 6.3.2 ICAM-1 mediates VEC internalization in a JNK dependent manner

Lymphocyte TEM has been shown to occur in conjunction with VEC internalization (Yamamoto et al. 2015). GPNTs were used to test whether ICAM-1 ligation caused VEC internalization. The amount of full length VEC, that resistant to extracellular trypsin when withdrawn internally to the cell, was measured by immunoblot and, as it corresponds to the amount of VEC internalized, used to study the effect of ICAM-1 ligation times on VEC internalization (Fig. 6.2A). A highly significant, three-fold increase in the level of trypsin-resistant VEC, when compared with a trypsin treated control (without any other chemical treatment *i.e.* ICAM-1 ligation), was seen following 5 min of ICAM-1 ligation (Fig. 6.2B). This level corresponds to the internalization of approximately 4% of the VEC found in non-trypsin treated control cells. With decreasing significance, both 15 min and 30 min of ICAM-1 ligation also increased the level of trypsin-resistant VEC from that of the trypsin treated control (Fig. 6.2B). As the project had a particular focus on paxillin, JNK and their involvement in ICAM-1 ligation induced VEC internalization, the chemical inhibitor, SP600125, was used to inhibit JNK within this experimental setup and its use significantly prevented increased VEC internalization mediated by 5 min of ICAM-1 ligation (Fig. 6.2B).
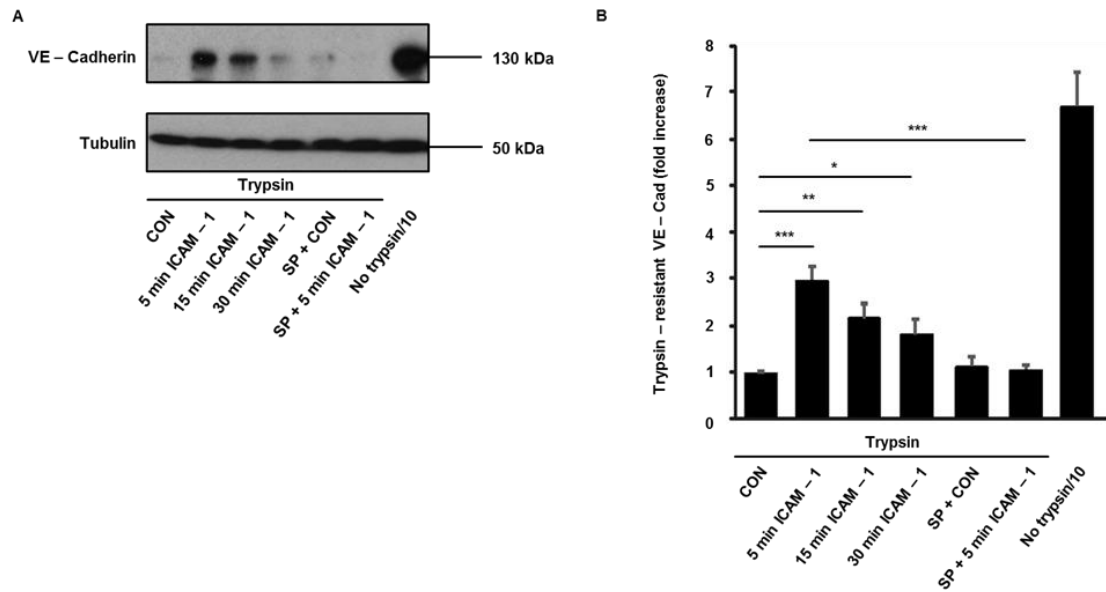
**Figure 6.2. ICAM-1 mediates VEC internalisation in a JNK dependent manner in GPNT cells**

Post-confluent, serum starved GPNTs were pre-treated with SP600125 (50 µm) for 1 h where indicated, treated with anti-ICAM-1 (5 µg/mL) for the times indicated, treated with trypsin on ice, pelleted and levels of trypsin-resistant (internalized) VEC determined by western blotting. Representative blot (A) and densitometric quantifications of trypsin-resistant VEC compared to cellular tubulin content (B) shown (means ± SEM, n = 3). One-way ANOVA followed by Student's t-test indicates significant differences between control (trypsin) and 5 min ICAM-1 (***, p < 0.001), between control (trypsin) and 15 min ICAM-1 (**, p < 0.01), between control (trypsin) and 30 min ICAM-1 (*, p < 0.05) and between 5 min ICAM-1 and SP600125 + 5 min ICAM-1 (***, p < 0.001). Total VEC content revealed by loading one tenth of non-treated control cell extract (no trypsin/10).

D3 cells, a human brain MVEC line, were next used to extend the prior observations to human physiology using the same assay, comparing levels of trypsin-resistant VEC for different treatments. When compared with a trypsin treated control a significant increase in the level of trypsin-resistant VEC was found following 5 min of ICAM-1 ligation, with the change characterising an increase from control levels by half (Fig. 6.3A and B). Furthermore, this 5 min of ICAM-1 ligation stimulated

increase was completely, and significantly, prevented by JNK inhibition using SP600125 (Fig. 6.3A and B).
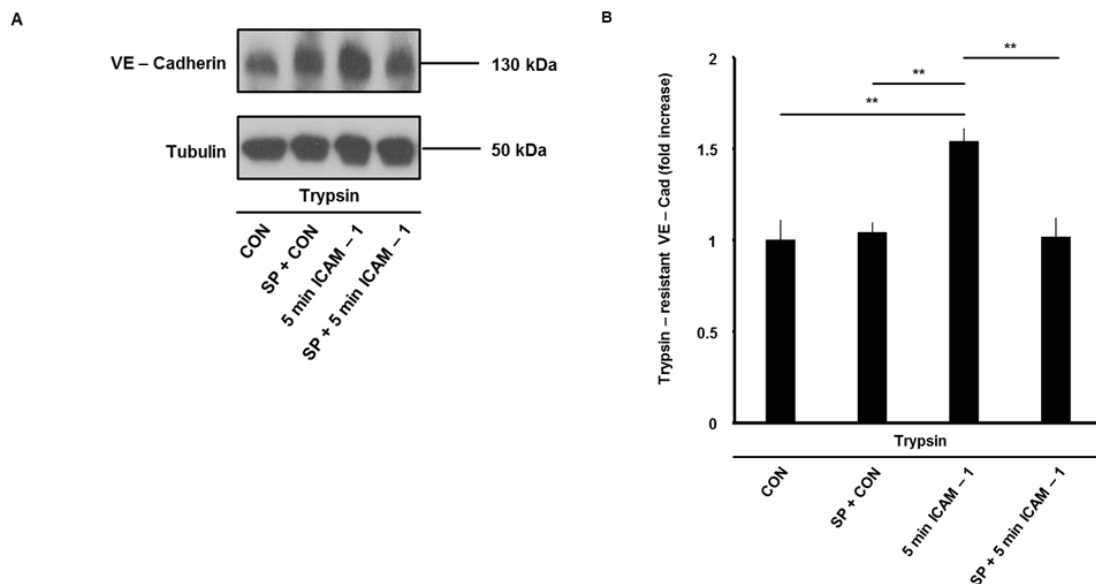


**Figure 6.3. ICAM-1 mediates VEC internalisation in a JNK dependent manner in D3 cells**

Post-confluent, serum starved D3s were pre-treated with SP600125 (50 µm) for 1 h where indicated, treated with anti-ICAM-1 (5 µg/mL) for the times indicated, treated with trypsin on ice, pelleted and levels of trypsin-resistant (internalized) VEC determined by western blotting. Representative blot (A) and densitometric quantifications of trypsin-resistant VEC compared to cellular tubulin content (B) shown (means ± SEM, n = 4). One-way ANOVA with Bonferroni post-hoc test indicates significant differences between control and 5 min ICAM-1 (**, p < 0.01), between SP600125 + control and 5 min ICAM-1 (**, p < 0.01) and between 5 min ICAM-1 and SP600125 + 5 min ICAM-1 (**, p < 0.01).

### 6.3.3 Visualisation of ICAM-1 mediated VEC internalization

To visualize VEC internalization using D3 cells, the extracellular domain of VEC was tagged with FITC labelled antibodies before treating cells with either 5 min or 15 min of ICAM-1 ligation (or not, as indicated, for controls). The cells were then washed with an acid before fixation (or not, as indicated), application of a nuclear

stain (DAPI) and visualization by confocal microscopy. Without any acid wash, full length VEC can be clearly visualized along cell-cell contacts of untreated cells (Fig. 6.4A). When untreated cells, with FITC-tagged VEC, underwent an acid wash before fixation, junctional fluorescence cannot be seen but only sporadic FITC staining throughout the field of view, indicating that VEC located at the cell-cell junctions had been removed by the treatment (Fig. 6.4B). Cells that were treated to either 5 min or 15 min of ICAM-1 ligation followed by acid wash had higher levels of FITC staining compared with the acid wash control, with 5 min of ICAM-1 ligation more potent than 15 min of ICAM-1 ligation (Fig. 6.4C and D respectively). The staining pattern resulting from 5 min of ICAM-1 ligation did not resemble that of the non-acid wash control. While the non-acid wash control staining was mostly junctional, 5 min of ICAM-1 ligation resulted in intracellular punctate staining resembling vesicles. 15 min of ICAM-1 ligation staining pattern was similar but less potent.
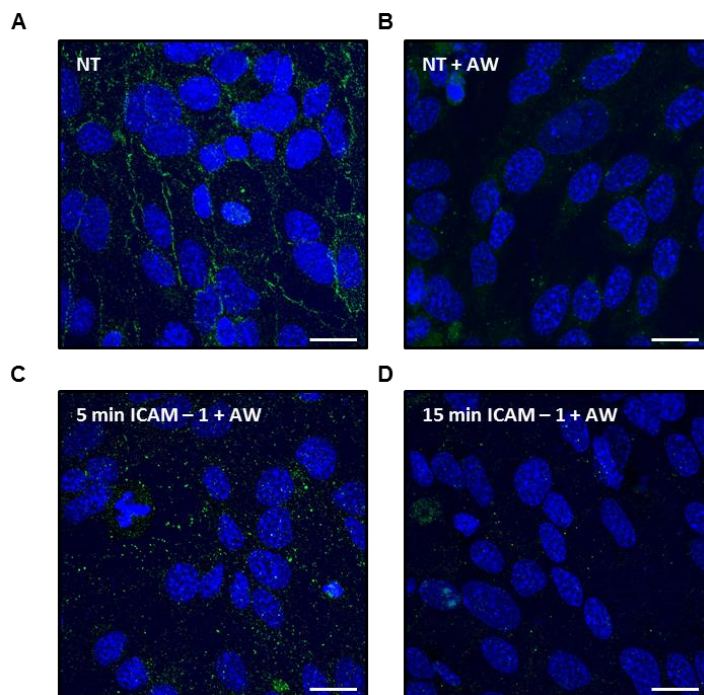


**Figure 6.4. Visualisation of ICAM-1 mediated VEC internalisation in D3 cells**
Post-confluent, serum starved D3s were treated with anti-VEC-FITC (5 µg/mL) for 1 h on ice (4°C) to tag the extracellular tail of VEC. Cells were then either untreated or treated with anti-ICAM-1 (5 µg/mL) for times indicated, before either fixation or 15 min of acid wash

(AW) followed by fixation, NT (A), NT + AW (B), 5 min ICAM-1 + AW (C), 15 min ICAM-1+ AW (D). Cells were stained with nuclear DAPI stain and analysed by confocal microscopy. Scale bar = 10 µm.

### 6.3.4   VEC internalization in response to a couple of vascular mediators, and ICAM-1 ligation

D3 cells were used to pin point the localization of VEC internalization using an immune-EM approach. To provide a multifaceted outlook on the internal course of VEC a range of vascular mediators were used, namely BK, VEGF-A and ICAM-1. Two different VEC antibodies, one targeting the extracellular domain of VEC (TEA 1.31), and another targeting the intracellular domain of VEC (C-19) were used. Cells were either untreated or treated with BK, VEGF-A or ICAM-1 for 5 min, followed by fixation for immune-EM preparation and visualization. As it was not possible at that time to target VEC using both antibodies simultaneously within a sample, representative images depict staining for either the extracellular domain (TEA 1.31) or the intracellular domain of VEC (C-19) and a box plot created to quantitatively compare staining across all samples and stains.

For untreated cells (Fig. 6.5A), VEC antibody staining (denoted by black arrowhead) can be clearly seen in the vicinity of cell-cell junctions (denoted by white arrowhead with black border) for both the extracellular domain targeting antibody (TEA 1.31) and the intracellular domain targeting antibody (C-19). Cells treated with ICAM-1 antibody for 5 min had a slightly different staining pattern when compared with untreated cells (Fig. 6.5B). When stained for either the extracellular domain (TEA 1.31) or the intracellular domain of VEC (C-19) it is clear that a certain proportion of VEC remains in the vicinity of the cell-cell junctions however another proportion is relatively removed from this area (Fig. 6.5B). 5 min of BK treatment had a more pronounced effect on VEC localization, for both the extracellular domain targeting antibody (TEA 1.31) and the intracellular domain targeting antibody (C-19) there was little VEC to be found within the vicinity of cell-cell junctions (Fig. 6.5C).

Overall there was relatively less VEC staining when compared with other treatments and when it was found, VEC location was further removed from the cell perimeter than that found following ICAM-1 ligation (Fig. 6.5C). Following treatment with 5 min of VEGF-A (Fig. 6.5D), a combination of VEC staining was observed, both in the vicinity of the cell-cell junctions as well as clear staining further within the cell body for both the extracellular domain targeting antibody (TEA 1.31) and the intracellular domain targeting antibody (C-19). In relation to VEC localization removed from the cell perimeter for VEGF-A treated samples, for both antibodies, VEC localization can be clearly observed on vesicular structures less than 100 nm in diameter, within images where a number of such vesicular structures can be seen (Fig. 6.5D).

Online software, BoxPlotR, was used to graphically represent the distance of the gold particles in each sample from a cell-cell junction (Fig. 6.5E and Table 6.1). In terms of overall number of gold particles visible for counting in each treatment, staining for both BK treated samples (158 average) was far less than that observed for CON, ICAM-1 or VEGF-A treated samples (236, 239 and 344 average respectively). When comparing overall median antibody distances from cell-cell junctions, the distances of both VEC domains from cell-cell junctions following ICAM-1 treatment were highly significant when compared with control samples, for C-19 staining, $p < 0.0001$ and for TEA 1.31 staining, $p < 0.001$. This was also the case for both VEC domains following BK treatment, $p < 0.0001$ for C-19 staining and $p < 0.0001$ for TEA 1.31 staining. Only VEC stained for the intracellular domain (C-19) was highly significant following VEGF-A treatment, with $p < 0.0001$, VEC stained for the extracellular domain (TEA 1.31) was not significantly removed from the cell-cell junctions following VEGF-A treatment.

**Table 6.1: BoxPlotR data**

|  | CON | | ICAM-1 | | BK | | VEGF-A | |
| --- | --- | --- | --- | --- | --- | --- | --- | --- |
|  | C-19 | TEA 1.31 | C-19 | TEA 1.31 | C-19 | TEA 1.31 | C-19 | TEA 1.31 |
| Median | 19.29 | 32.01 | 93.04 | 88.21 | 141.41 | 142.07 | 152.08 | 62.13 |
| Data point no. | 173 | 63 | 61 | 178 | 74 | 84 | 210 | 134 |
| Average data points per treatment | 236 | | 239 | | 158 | | 344 | |

A
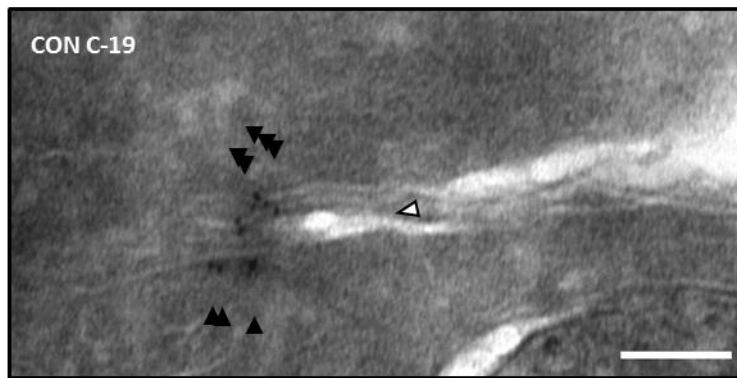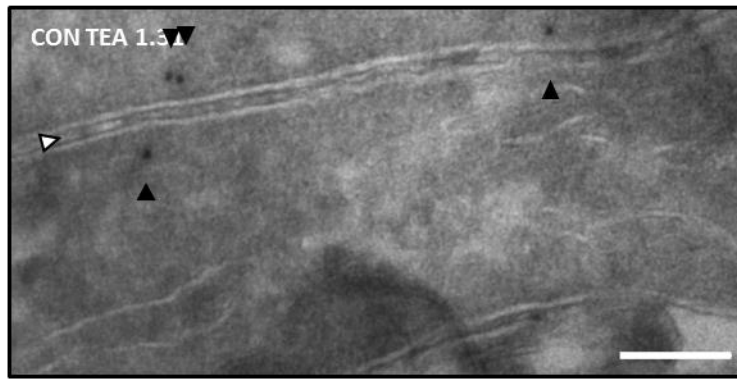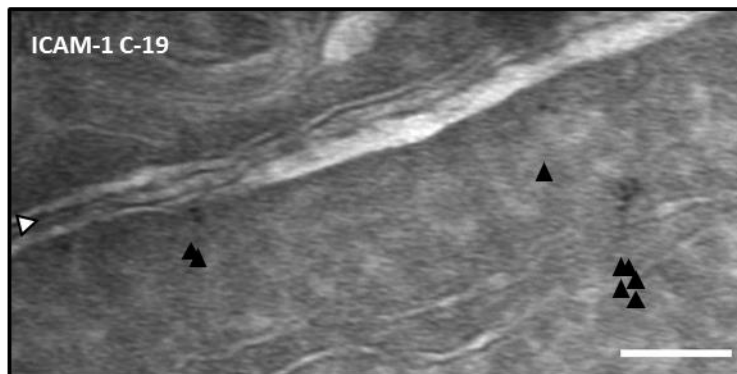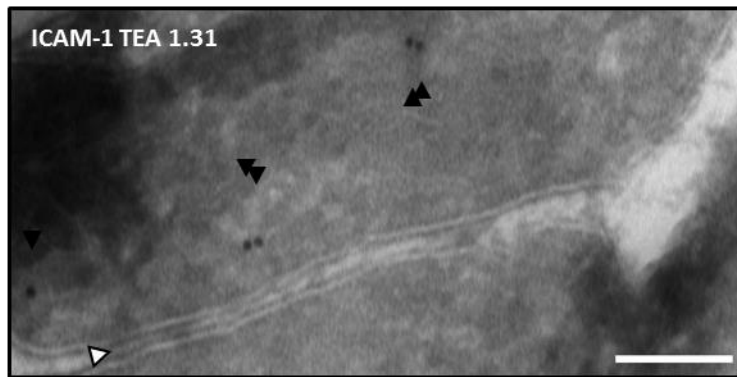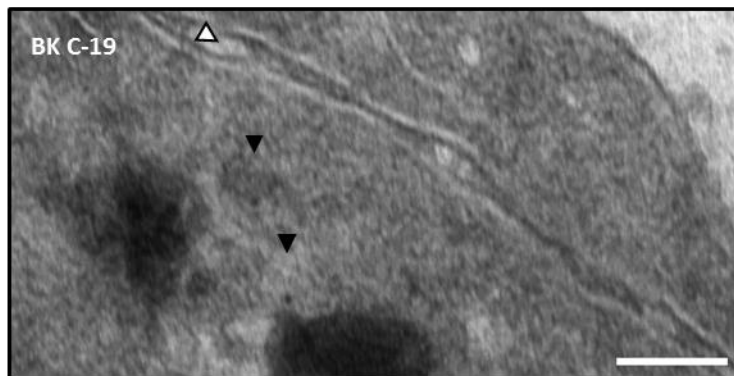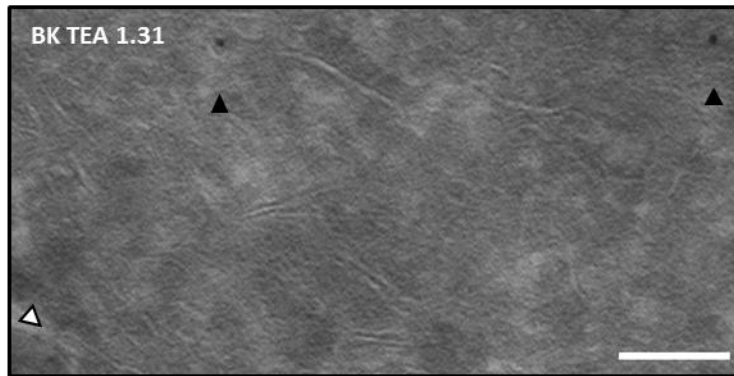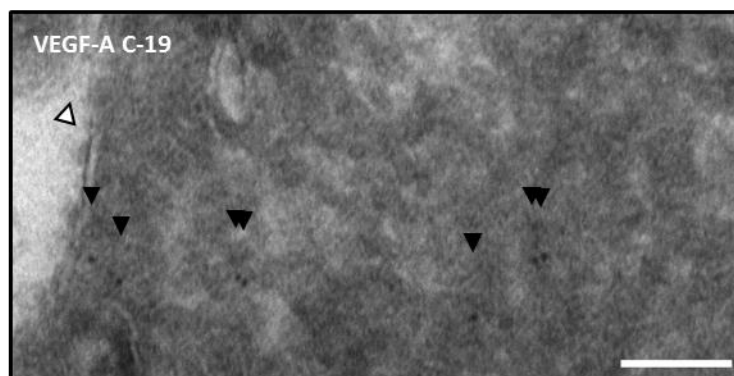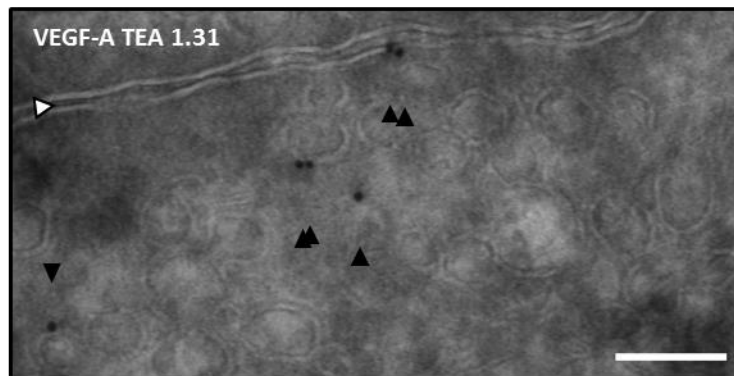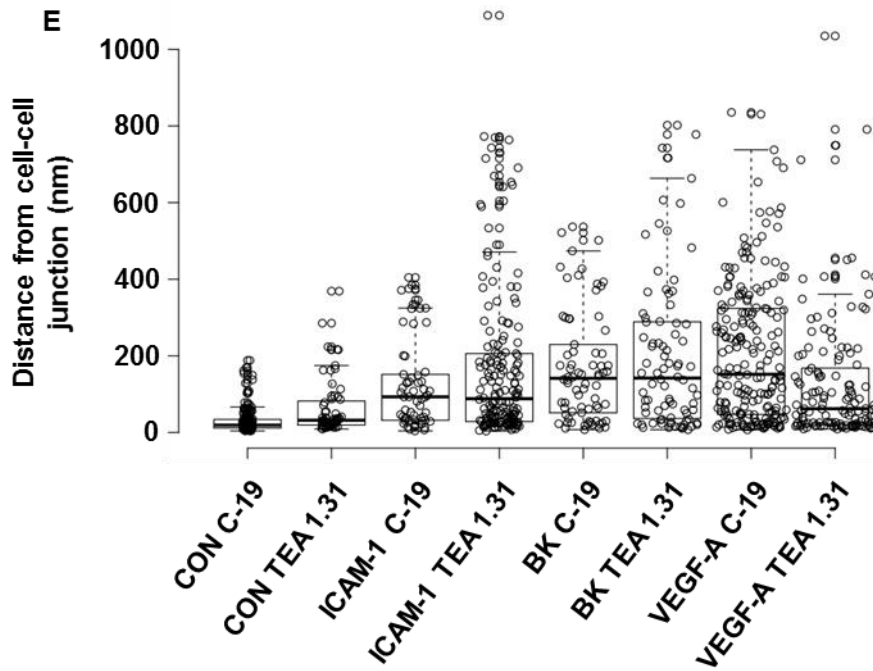


CON TEA 1.31

CON C-19

B



ICAM-1 TEA 1.31

ICAM-1 C-19

188

C



BK TEA 1.31



BK C-19

D



VEGF-A TEA 1.31



VEGF-A C-19

189

**Figure 6.5. VEC internalisation in response to a range of vascular mediators, and ICAM-1 ligation, in D3 cells**

Post-confluent, serum starved D3s were either untreated (A) or treated with anti-ICAM-1 (B), bradykinin (C) or VEGF-A (D) for 5 min before fixation and preparation for immune-EM analysis of VEC localization. Briefly, grids containing sections cut at -120°C were stored on 2.3 M sucrose, 2% methylcellulose glass slides. Grids of interest were extracted and twice incubated with 10-20 mM glycine for 5 min, to quench free aldehyde groups. Sections were twice incubated with 0.1% Aurion in wash buffer for 2 min, to prevent non-specific binding. Primary antibodies were prepared in wash buffer and sections incubated for at least 20 min before rinsing twice with wash buffer. This was followed by similar incubations with bridging antibody (30 min) and then Protein A-Gold (45 min). Sections were rinsed with PBS four times for 2 min and then fixed with 1% glutaraldehyde in PBS for 5 min before multiple rinses with distilled water. Gold particles, indicating the location of either extracellularly labelled VEC (TEA 1.31) or intracellularly labelled VEC (C-19), are designated by black arrowheads. White arrowheads with black border designate areas of cell perimeter or cell-cell junctions. Scale bar = 100 nm. BoxPlotR was used to generate a boxplot from data measurements taken using ImageJ software. Distances between gold particles and the nearest cell-cell junction, drawn and measured in ImageJ, were collated and uploaded to BoxPlotR. A boxplot and related descriptive statistics were then generated (E).

190

When comparing within antibody stains, for C-19, one-way ANOVA with Bonferroni post-hoc test indicates significant differences between control and 5 min BK ($p < 0.0001$), between control and 5 min ICAM-1 ($p < 0.0001$) and between control 5 min VEGF-A ($p < 0.0001$). For TEA 1.31, one-way ANOVA with Bonferroni post-hoc test indicates significant differences between control and 5 min BK ($p < 0.0001$) and between control and 5 min ICAM-1 ($p < 0.001$).

## 6.4    Discussion

Dynamic cell-cell endothelial junctions are required to maintain barrier function relying on both AJs and TJs to ensure the correct balance between stability and controlled remodelling (Gavard 2013). Key roles for VEC, the major component of AJs, have been established over the last decade in relation to barrier function with VEC internalisation found to occur during increased EC permeability changes in haemodynamic forces, actomyosin contraction and also during TEM (Gavard and Gutkind 2006, Orsenigo et al. 2012, Wessel et al. 2014, Sakurai et al. 2014, Dorland et al. 2016). A number of intracellular partners are known to interact with VEC, from its closest set of three proteins, β-catenin, p120 catenin and γ-catenin, to a wider range of supporting proteins including eplin, actin and α-catenin (Giannotta, Trani and Dejana 2013, Gavard 2013). An increasing subset of VEC's intracellular partners are being identified as key facilitators of VEC internalisation including β-catenin, β-arrestin-2, vinculin, α-catenin, AP-2 and p120 catenin (Chen et al. 2012, Huveneers et al. 2012, Wessel et al. 2014, Gavard, Patel and Gutkind 2008). However, the aggregated literature has not established a unified model of VEC internalisation with discrepancies in relation to pertinent binding partners, residue phosphorylation, mechanism of internalisation and particularly the fate of internalised VEC (Orsenigo et al. 2012, Wessel et al. 2014, Gavard and Gutkind 2006). As a preliminary expansion on a larger ongoing project within the lab, investigating MAPKs role within diapedesis-related and non-diapedesis-related processes during ICAM-1 ligation, I specifically set out to better define VEC internalisation in response to ICAM-1, BK and VEGF-A.

In this chapter, I first presented data showing that three MAPKs, ERK, p38 and JNK, were activated in response to ICAM-1 engagement on rat brain MVECs (GPNTs), either by lymphocyte adhesion or by ICAM-1 cross-linking. Results previously published by the lab had found that cross-linking of ICAM-1 mimicked the ICAM-1 response to lymphocyte adhesion (Martinelli et al. 2009). I then presented data from the same project which found that lymphocyte TEM across GPNTs, and also across

primary rat brain MVECs, was reduced by almost 50% following JNK inhibition, but not following ERK or p38 inhibition (all data generated by Hudson, N). From the literature, JNK is activated downstream of Src, Rho GTPase and PKC, all of which are known to be involved in TEM regulation across both the neural microvasculature and the microvasculature of other vascular beds (Etienne et al. 1998, Adamson et al. 1999, Etienne-Manneville et al. 2000, Yang et al. 2006). These signalling patterns suggest a pivotal role for JNK in an extensive signalling pathway leading to leukocyte TEM.

As mentioned earlier, the intracellular mechanisms leading to TEM are closely related to that of EC permeability and involve disruption of cell-cell junctions, specifically AJs and VEC. I proceeded to find ICAM-1 mediated VEC internalisation in GPNTs following ICAM-1 ligation through the measurement of trypsin-resistant VEC, with the strongest effect seen following 5 min of ligation. A similar result had been found when peripheral lymph node cells (PLNCs) were co-cultured with the same cell line, indicating ICAM-1 ligation stimulated VEC internalisation, and without the need for ICAM-1 cross-linking (data not shown, generated by Hudson, N). To determine whether VEC internalisation resulted directly from ICAM-1 engagement signalling via JNK, JNK inhibition was used and was found to completely prevent VEC internalisation, again as measured by trypsin-resistant VEC. These results were extended to a human brain MVEC line (D3s) where 5 min of ICAM-1 ligation significantly increased VEC internalisation, and the effect was also prevented by JNK inhibition.

Due to antibody restrictions, extending the observations to D3 cells enabled an acid wash experiment to visualise internalisation of immuno-stained VEC. While non-treated, non-acid wash cells had junctional VEC staining, 5 min of ICAM-1 ligation generated an intracellular signal which was punctate and did not adhere closely to cell-cell junctions. When 15 min of ICAM-1 ligation was used, the level of staining was similar to non-treated, acid washed cells, perhaps indicating a timeframe for VEC internalisation and subsequent degradation, or recycling to the cell surface. The

literature is divisive about the compartment into which VEC is internalised, how far away from the cell-cell junctions it is moved when internalised and whether or not is degraded (Orsenigo et al. 2012, Xiao et al. 2005). Although the current acid wash approach is limited in that it does not reveal precise intracellular locations towards which VEC is taken when internalised.

To overcome this, immune-EM was performed (in collaboration with Burgoyne, T) using D3 cells either non-treated or treated with ICAM-1 ligation, BK or VEGF-A for 5 min. The movement of VEC was then captured using two antibodies targeting distinct areas of the protein (C-19 or TEA 1.31). Representative images for each treatment and VEC stain already provide clear indications of different routes for VEC internalisation following mediator treatment. Most notably, within VEGF-A treated cells, VEC stained gold particles can be seen on intracellular vesicles ranging in size from 25-75 nm. All images were analysed by measuring the distance between gold particles and the nearest cell-cell junction and a boxplot summarising this data was generated using BoxPlotR (Spitzer et al. 2014). This confirmed observations based on the representative images and provided greater insight into VEC internalisation as it was clear that all three treatments caused more internalisation when compared with control. The observation that BK treated samples had less gold particle staining compared to CON, ICAM-1 and VEGF-A was confirmed by the boxplot. It is possible that the staining observed for BK treated samples represents a pathway for VEC internalization where the VEC epitopes are not accessible for staining *i.e.* VEC is taken into an inaccessible compartment or taken up for lysosomal degradation. The boxplot also confirmed the observation that, when compared with CON treatment, all three of ICAM-1 ligation, BK and VEGF-A treatment enhanced the level of VEC internalisation, and also that the internalisation process may be different for each. According to the boxplot, the distance VEC travelled from the cell-cell junction, when followed by either antibody, was very similar when comparing within ICAM-1 ligation, BK or control treatments. However, the distance VEC travelled according to the same two antibodies was markedly different following treatment with VEGF-A. This is unlike the

194

circumstances observed for BK, which had less staining and, excluding any potential unknown technical issues, I speculate as to whether there is some role for VEC that has been cleaved following VEGF-A treatment. I do not use the phrase soluble VEC as all measurements were taken from gold particles located within the cell but the literature shows data for the involvement of soluble VEC in EC barrier breakdown in systemic inflammation and sepsis (Flemming et al. 2015, Flemming et al. 2016).

The regulation of proteins at the cell surface is predominantly maintained by a balance of endocytosis and endosomal recycling pathways trafficking either endocytosed or newly formed proteins to the cell surface (Yan et al. 2016). Furthermore, recycling of proteins is known to increase when cell-cell contacts are disrupted, such as when exposed to vasoactive mediators (Le, Yap and Stow 1999, Stenmark 2009). As well as recycling, endocytosed proteins can be degraded in lysosomes (Xiao et al. 2005). Finally, and originally investigated in relation to VEC, exo-endocytosis between cells may also occur, the direct exchange of proteins between adjacent cells (Sakurai et al. 2014). As there may be a variety of mechanisms characterising VEC internalisation, it was interesting to see variations when comparing only three vasoactive mediators. Regardless of whether internalisation is clathrin independent (*i.e.* caveolae) or clathrin dependent, pathways generally feed vesicles into early endosomes, if not returned to the cell surface through a rapid recycling pathway (Grant and Donaldson 2009). Both early endosomes and recycling endosomes can be characterised primarily by their expression of proteins, the Ras-related proteins in brain (Rab) GTPases. Rab proteins coordinate "membrane trafficking, cargo selection, vesicle budding, moving, tethering, docking and targeting" (Yan et al. 2016). Specifically, early endosomes are associated with the expression of Rab5, which regulates membrane docking and fusion as well as endosome motility along microtubules, and when the endosome transforms, into either a recycling compartment or multivesicular body, Rab5 expression decreases as Rab11 expression increases (Nielsen et al. 1999, Grant and Donaldson 2009). Internalisation of glycosphingolipids and receptors such as transferrin has been associated with a rapid recycling pathway, and early endosomes

returning to the cell surface found to express Rab4 and Rab35 (Grant and Donaldson 2009, van der Sluijs et al. 1992, Choudhury et al. 2004). Interestingly, rapid recycling has also been indicated to be involved in T cell function (Patino-Lopez et al. 2008). More recently, VEC has been found to localise with Rab5 GTPase expressing endosomes, a small fraction with Rab4 expressing endosomes, indicating rapid recycling but not in Rab11 recycling endosomes (Sakurai et al. 2014, Dorland et al. 2016, Yamamoto et al. 2015). Opposing this, Rab11 mediated VEC recycling has also recently been found to be required for AJ formation and the restoration of EC barrier function (Yan et al. 2016). Although the current work has not elucidated exact compartments to which VEC is being internalised either, it has established an alternative approach for doing so. Similar work has been performed relating to AJs within other vascular beds, *i.e.* the coronary artery, and using other vascular mediators, *i.e.* doxycycline (Le Bihan et al. 2015). Despite this, the current findings are quite novel and provide a new dynamic in relation to the study of VEC internalisation at the BBB.

# Chapter 7   FINAL CONCLUSIONS AND FUTURE WORK

## 7.1   Summary of Conclusions and Final Remarks

During my PhD, my aim has been to explore different aspects of transport across the neural microvasculature, as measured in response to different vasoactive mediators, with an interest for the roles played by both paracellular and transcellular routes across neural MVEC barriers.

My LPC research contributed to a study demonstrating that the inhibition of its generating enzyme, Lp-PLA$_2$, effectively prevented BRB dysfunction resulting from diabetes in an animal model and that the mode of action involved LPC acting via VEGFR2 transactivation at the BRB. While the initial transport route affected was determined to be paracellular, this research also generated data indicating that a transcellular element plays a part, perhaps progressing from the initial junctional component.

Pursuing VEGFR2 transactivation, my research revealed two other vasoactive mediators, THR and LPA which act, at least partly, via this mechanism at neural microvascular barriers, thus increasing paracellular permeability.

Related to the finding that LPC's actions appear to affect both paracellular and transcellular permeability, I also investigated transcellular transport at the BBB more specifically. This research contributed to a study demonstrating that MET induced the production of NO and increased vesicular transport at the BBB. Furthermore, this research revealed additional vasoactive mediators triggering differentially enhanced transcellular transport and led to the development and preliminary characterisation of two multicellular *in vitro* BBB models.

Lastly, my research into VEC internalisation at neural microvascular barriers has also contributed to a study (in preparation) demonstrating that the activation of JNK, via ICAM-1 ligation such as during lymphocyte TEM, led to phosphorylation of

paxillin (a cytoskeletal scaffolding protein), its association with VEC and subsequent VEC internalisation. This research also revealed distinctive enhancement of VEC internalisation in response to different vasoactive mediators.

My thesis findings have made a significant contribution towards the field of neural microvascular biology. My work investigating LPC research has contributed to a peer-reviewed primary research paper (Canning et al. 2016). My work investigating transcellular transport at the BBB contributed to a peer-reviewed primary research paper and a peer-reviewed review article (Martins et al. 2013, Turowski and Kenny 2015). My work investigating VEC internalisation has been included in a manuscript in preparation for submission by remaining members of the group (see **Appendix** – co-authored publications). Further research building on the work described in this thesis is outlined in the following section.

## 7.2 Future Work

### 7.2.1 Define LPC receptor and characterise signalling pathway

Having established that LPC functions as a novel permeability mediator at both the BBB and BRB operating through VEGFR2 transactivation from the luminal side of the vasculature, future work could investigate the receptor that triggers this signalling network. There is no receptor confirmed as of yet but LPC is known to interact with a number of proteins, has a transporter across the BBB and BRB and, in relation to neuronal cells, incorporates into phospholipid bilayers (Qiao et al. 2006, Maingret et al. 2000, Chen et al. 2002, Pirillo et al. 2013, Ueno et al. 2016, Vladykovskaya et al. 2011, Stewart et al. 2010, Carneiro et al. 2013). Preliminary future experiments could identify receptors in PT2 cells using chemical or knockdown approaches targeting putative proteins followed by immunoblotting with VEGFR2 phosphorylation as a known downstream outcome. This could be followed by functional experiments performed in primary cells, such as TEER measurements, using inhibitors directed at identified targets.

### 7.2.2 Investigate the signalling network contributing to VEGFR2 transactivation and enhanced permeability

Alongside LPC, there are other components of the diabetic microenvironment contributing to cellular dysautoregulation with altered inflammatory and oxidative states leading to BBB and BRB dysfunction. For example, both fluid shear stress and ROS generated from hyperglycemia are also known to transactivate VEGFR2 (Warren et al. 2014, Jin et al. 2003). These studies indicated the involvement of Src kinases, eNOS, PI3K and Akt, intracellular mediators which would be good starting points to elucidate the intermediaries within the VEGFR2 transactivation network. Similar to the previous section, future experiments performed could identify mediators in PT2 cells using chemical approaches followed by immunoblotting with VEGFR2 phosphorylation as a known downstream outcome. ROS could be measured using an assay with a fluorescent indicator following LPC stimulation in conjunction with appropriate inhibitors. This could also be followed by functional experiments performed in primary cells, such as TEER measurements, using inhibitors directed at identified targets

### 7.2.3 Characterisation of vesicular pattern, morphology and frequency following vasoactive stimuli

In conjunction with performing more replicates for EM and subsequent statistical analysis, to better understand the transcellular transport occurring in response to vasoactive stimuli, characterising the pattern, morphology and frequency of vesicles and pits would be an ideal starting point for future experiments. Once sufficient replicates involving cell culture, HRP transport, EM preparation and imaging were gathered, this could be achieved using ImageJ software.

### 7.2.4 Utilisation of multicellular models

To address whether or not the observed increase in transcellular transport is an artefact of the monoculture *in vitro* BBB model, future experiments would involve

utilising the multicellular models developed within the current thesis. As it has been characterised, experiments using the co-culture model would be similar to those performed for the monoculture model, allowing a direct comparison between results of both models. Future experiments would include functional assays measuring transcellular HRP flux followed by the preparation of corresponding samples for EM analysis. The spheroidal model on the other hand may provide a truer representation of the *in vivo* setting – as the cell types would be in direct contact with each other, but it would require the establishment of novel assays. An initial experimental approach could involve the treatment of spheroidal cultures in the presence of HRP and a vasoactive mediator (similar to TW models), followed by gentle harvesting and pelleting of cultures with washing in order to remove extracellular HRP followed by cell lysis to measure intracellular, and intra-spheroidal, levels of HRP by reaction with OPD and hydrogen peroxide as normal. In a manner similar to TW models, spheroidal cultures treated in the presence of HRP and a vasoactive mediator could be directly harvested for subsequent DAB reaction, EM processing and analysis to reveal both interactions between cells and the presence of intracellular vesicles.

### 7.2.5 Characterisation of the vesicular compartment VEC internalises to in response to a range of vasoactive stimuli

Having established an approach visualising VEC internalisation in response to vasoactive stimuli, future work could investigate the intracellular compartments into which VEC may be internalised to. This would involve using immune-EM in conjunction with a combination of markers for VEC, C-19 or TEA 1.31, and for components of different vesicular and endosomal compartments such as caveolin-1, Rab4, Rab5, Rab11 and Rab35 (Nielsen et al. 1999, van der Sluijs et al. 1992, Grant and Donaldson 2009, Yamamoto et al. 2015, Choudhury et al. 2004, Yan et al. 2016, Dorland et al. 2016, Sakurai et al. 2014, Nag et al. 2007). Furthermore, given the specialisations of the neural microvasculature, it would be of interest to determine whether these observations extend to other vascular beds and additional future experiments could be performed in relevant cell lines, such as HUVEC or DMEC.

### 7.2.6 Investigate the signalling network contributing to differential VEC internalisation

Complementary to section 7.2.5, future work could also investigate the signalling network mediating differential VEC internalisation following ICAM-1 ligation. This could include experiments investigating further the intracellular partners upstream of VEC, a number of which have already been indicated to be involved to some extent, such as β-catenin, p120 catenin, β-arrestin-2, vinculin, AP-2, α-catenin, Src, RhoGTPase, eNOS and PKC (Etienne et al. 1998, Wessel et al. 2014, Chen et al. 2012, Huveneers et al. 2012, Adamson et al. 1999, Yang et al. 2006, Etienne-Manneville et al. 2000, Gavard et al. 2008). Preliminary experiments, such as measurement of trypsin-resistant VEC could be performed using appropriate chemical inhibitors. Aiding this would be an approach investigating the relevant VEC residues phosphorylated during differentially mediated internalisation, as it has been found to characterise ICAM-1 stimulation and leukocyte adherence on microvascular ECs (Yuan et al. 2012, Turowski et al. 2008). Future experiments, such as measurement of trypsin-resistant VEC, could be performed using VEC mutants with altered amenability to phosphorylation. Ultimately it would be ideal to confirm results in immune-EM experiments.

# Chapter 8   BIBLIOGRAPHY

Abbott, N. J. (2000) Inflammatory mediators and modulation of blood-brain barrier permeability. *Cell Mol Neurobiol,* 20**,** 131-47.

Abbott, N. J. & A. Friedman (2012) Overview and introduction: the blood-brain barrier in health and disease. *Epilepsia,* 53 Suppl 6**,** 1-6.

Abbott, N. J., C. C. Hughes, P. A. Revest & J. Greenwood (1992) Development and characterisation of a rat brain capillary endothelial culture: towards an in vitro blood-brain barrier. *J.Cell Sci.,* 103 ( Pt 1)**,** 23-37.

Abbott, N. J., A. A. Patabendige, D. E. Dolman, S. R. Yusof & D. J. Begley (2010) Structure and function of the blood-brain barrier. *Neurobiol.Dis.,* 37**,** 13-25.

Abbott, N. J., L. Ronnback & E. Hansson (2006) Astrocyte-endothelial interactions at the blood-brain barrier. *Nat.Rev.Neurosci.,* 7**,** 41-53.

Acharya, N. K., E. C. Levin, P. M. Clifford, M. Han, R. Tourtellotte, D. Chamberlain, M. Pollaro, N. J. Coretti, M. C. Kosciuk, E. P. Nagele, C. Demarshall, T. Freeman, Y. Shi, C. Guan, C. H. Macphee, R. L. Wilensky & R. G. Nagele (2013) Diabetes and hypercholesterolemia increase blood-brain barrier permeability and brain amyloid deposition: beneficial effects of the LpPLA2 inhibitor darapladib. *J Alzheimers Dis,* 35**,** 179-98.

Adamson, P., S. Etienne, P. O. Couraud, V. Calder & J. Greenwood (1999) Lymphocyte migration through brain endothelial cell monolayers involves signaling through endothelial ICAM-1 via a rho-dependent pathway. *J.Immunol.,* 162**,** 2964-2973.

Aijaz, S., M. S. Balda & K. Matter (2006) Tight junctions: molecular architecture and function. *Int Rev Cytol,* 248**,** 261-98.

Aird, W. C. (2005) Spatial and temporal dynamics of the endothelium. *J Thromb Haemost,* 3**,** 1392-406.

--- (2007) Phenotypic heterogeneity of the endothelium: I. Structure, function, and mechanisms. *Circ Res,* 100**,** 158-73.

Alcaide, P., G. Newton, S. Auerbach, S. Sehrawat, T. N. Mayadas, D. E. Golan, P. Yacono, P. Vincent, A. Kowalczyk & F. W. Luscinskas (2008) p120-Catenin regulates leukocyte transmigration through an effect on VE-cadherin phosphorylation. *Blood,* 112**,** 2770-9.

Allt, G. & J. G. Lawrenson (2001) Pericytes: cell biology and pathology. *Cells Tissues Organs,* 169**,** 1-11.

Alvarez, J. I., R. Cayrol & A. Prat (2011) Disruption of central nervous system barriers in multiple sclerosis. *Biochim Biophys Acta,* 1812**,** 252-64.

Argaw, A. T., L. Asp, J. Zhang, K. Navrazhina, T. Pham, J. N. Mariani, S. Mahase, D. J. Dutta, J. Seto, E. G. Kramer, N. Ferrara, M. V. Sofroniew & G. R. John (2012) Astrocyte-derived VEGF-A drives blood-brain barrier disruption in CNS inflammatory disease. *J Clin Invest,* 122**,** 2454-68.

Armulik, A., G. Genove & C. Betsholtz (2011) Pericytes: developmental, physiological, and pathological perspectives, problems, and promises. *Dev Cell,* 21**,** 193-215.

Armulik, A., G. Genove, M. Mae, M. H. Nisancioglu, E. Wallgard, C. Niaudet, L. He, J. Norlin, P. Lindblom, K. Strittmatter, B. R. Johansson & C. Betsholtz (2010) Pericytes regulate the blood-brain barrier. *Nature,* 468**,** 557-61.

Artus, C., F. Glacial, K. Ganeshamoorthy, N. Ziegler, M. Godet, T. Guilbert, S. Liebner & P. O. Couraud (2014) The Wnt/planar cell polarity signaling pathway contributes to the integrity of tight junctions in brain endothelial cells. *J Cereb Blood Flow Metab,* 34**,** 433-40.

Attwell, D., A. M. Buchan, S. Charpak, M. Lauritzen, B. A. Macvicar & E. A. Newman (2010) Glial and neuronal control of brain blood flow. *Nature,* 468**,** 232-43.

Balda, M. S., C. Flores-Maldonado, M. Cereijido & K. Matter (2000) Multiple domains of occludin are involved in the regulation of paracellular permeability. *J.Cell Biochem.,* 78**,** 85-96.

Ballmer-Hofer, K., A. E. Andersson, L. E. Ratcliffe & P. Berger (2011) Neuropilin-1 promotes VEGFR-2 trafficking through Rab11 vesicles thereby specifying signal output. *Blood,* 118**,** 816-26.

Bamforth, S. D., S. L. Lightman & J. Greenwood (1997) Ultrastructural analysis of interleukin-1 beta-induced leukocyte recruitment to the rat retina. *Invest Ophthalmol.Vis.Sci.,* 38**,** 25-35.

Barber, A. J. & D. A. Antonetti (2003) Mapping the blood vessels with paracellular permeability in the retinas of diabetic rats. *Invest Ophthalmol Vis Sci,* 44**,** 5410-6.

Beckman, J. A., M. A. Creager & P. Libby (2002) Diabetes and atherosclerosis: epidemiology, pathophysiology, and management. *JAMA,* 287**,** 2570-81.

Begley, D. J. & M. W. Brightman (2003) Structural and functional aspects of the blood-brain barrier. *Prog Drug Res,* 61**,** 39-78.

Bellomo, R. & D. D. Giantomasso (2001) Noradrenaline and the kidney: friends or foes? *Crit Care,* 5**,** 294-8.

Ben-Zvi, A., B. Lacoste, E. Kur, B. J. Andreone, Y. Mayshar, H. Yan & C. Gu (2014) Mfsd2a is critical for the formation and function of the blood-brain barrier. *Nature,* 509**,** 507-11.

Bergmann, S. R., T. B. Ferguson & B. E. Sobel (1981) Effects of amphiphiles on erythrocytes, coronary arteries, and perfused hearts. *Am J Physiol,* 240**,** H229-37.

Betsholtz, C. (2004) Insight into the physiological functions of PDGF through genetic studies in mice. *Cytokine Growth Factor Rev,* 15**,** 215-28.

Blanco, R. & H. Gerhardt (2013) VEGF and Notch in tip and stalk cell selection. *Cold Spring Harb Perspect Med,* 3**,** a006569.

Bolduc, V., N. Thorin-Trescases & E. Thorin (2013) Endothelium-dependent control of cerebrovascular functions through age: exercise for healthy cerebrovascular aging. *Am J Physiol Heart Circ Physiol,* 305**,** H620-33.

Boo, Y. C., G. Sorescu, N. Boyd, I. Shiojima, K. Walsh, J. Du & H. Jo (2002) Shear stress stimulates phosphorylation of endothelial nitric-oxide synthase at Ser1179 by Akt-independent mechanisms: role of protein kinase A. *J Biol Chem,* 277**,** 3388-96.

Borbiev, T., A. Birukova, F. Liu, S. Nurmukhambetova, W. T. Gerthoffer, J. G. Garcia & A. D. Verin (2004) p38 MAP kinase-dependent regulation of endothelial cell permeability. *Am J Physiol Lung Cell Mol Physiol,* 287, L911-8.

Borbiev, T., A. D. Verin, A. Birukova, F. Liu, M. T. Crow & J. G. Garcia (2003) Role of CaM kinase II and ERK activation in thrombin-induced endothelial cell barrier dysfunction. *Am J Physiol Lung Cell Mol Physiol,* 285, L43-54.

Bos, C. L., D. J. Richel, T. Ritsema, M. P. Peppelenbosch & H. H. Versteeg (2004) Prostanoids and prostanoid receptors in signal transduction. *Int J Biochem Cell Biol,* 36, 1187-205.

Bouchard, P., L. D. Ghitescu & M. Bendayan (2002) Morpho-functional studies of the blood-brain barrier in streptozotocin-induced diabetic rats. *Diabetologia,* 45, 1017-25.

Boulant, J. A. (2006) Neuronal basis of Hammel's model for set-point thermoregulation. *J Appl Physiol (1985),* 100, 1347-54.

Boulay, A. C., S. Cisternino & M. Cohen-Salmon (2016) Immunoregulation at the gliovascular unit in the healthy brain: A focus on Connexin 43. *Brain Behav Immun,* 56, 1-9.

Brasch, J., O. J. Harrison, B. Honig & L. Shapiro (2012) Thinking outside the cell: how cadherins drive adhesion. *Trends Cell Biol,* 22, 299-310.

Brault, S., F. Gobeil, A. Fortier, J. C. Honoré, J. S. Joyal, P. S. Sapieha, A. Kooli, E. Martin, P. Hardy, A. Ribeiro-da-Silva, K. Peri, P. Lachapelle, D. Varma & S. Chemtob (2007) Lysophosphatidic acid induces endothelial cell death by modulating the redox environment. *Am J Physiol Regul Integr Comp Physiol,* 292, R1174-83.

Braverman, I. M. (1989) Ultrastructure and organization of the cutaneous microvasculature in normal and pathologic states. *J Invest Dermatol,* 93, 2S-9S.

Brozovich, F. V., C. J. Nicholson, C. V. Degen, Y. Z. Gao, M. Aggarwal & K. G. Morgan (2016) Mechanisms of Vascular Smooth Muscle Contraction and the Basis for Pharmacologic Treatment of Smooth Muscle Disorders. *Pharmacol Rev,* 68, 476-532.

Bruns, R. R. & G. E. Palade (1968) Studies on blood capillaries. II. Transport of ferritin molecules across the wall of muscle capillaries. *J Cell Biol,* 37, 277-99.

Burridge, K. & E. S. Wittchen (2013) The tension mounts: stress fibers as force-generating mechanotransducers. *J Cell Biol,* 200, 9-19.

Bushong, E. A., M. E. Martone, Y. Z. Jones & M. H. Ellisman (2002) Protoplasmic astrocytes in CA1 stratum radiatum occupy separate anatomical domains. *J Neurosci,* 22, 183-92.

Butt, A. M. (1995) Effect of inflammatory agents on electrical resistance across the blood-brain barrier in pial microvessels of anaesthetized rats. *Brain Res,* 696, 145-50.

Bělohlávek, J., V. Dytrych & A. Linhart (2013) Pulmonary embolism, part I: Epidemiology, risk factors and risk stratification, pathophysiology, clinical

presentation, diagnosis and nonthrombotic pulmonary embolism. *Exp Clin Cardiol,* 18**,** 129-38.

Canning, P., B. A. Kenny, V. Prise, J. Glenn, M. H. Sarker, N. Hudson, M. Brandt, F. J. Lopez, D. Gale, P. J. Luthert, P. Adamson, P. Turowski & A. W. Stitt (2016) Lipoprotein-associated phospholipase A2 (Lp-PLA2) as a therapeutic target to prevent retinal vasopermeability during diabetes. *Proc Natl Acad Sci U S A,* 113**,** 7213-8.

Cardillo, C., S. S. Nambi, C. M. Kilcoyne, W. K. Choucair, A. Katz, M. J. Quon & J. A. Panza (1999) Insulin stimulates both endothelin and nitric oxide activity in the human forearm. *Circulation,* 100**,** 820-5.

Carman, C. V., P. T. Sage, T. E. Sciuto, M. A. de la Fuente, R. S. Geha, H. D. Ochs, H. F. Dvorak, A. M. Dvorak & T. A. Springer (2007) Transcellular diapedesis is initiated by invasive podosomes. *Immunity,* 26**,** 784-97.

Carneiro, A. B., B. M. Iaciura, L. L. Nohara, C. D. Lopes, E. M. Veas, V. S. Mariano, P. T. Bozza, U. G. Lopes, G. C. Atella, I. C. Almeida & M. A. Silva-Neto (2013) Lysophosphatidylcholine triggers TLR2- and TLR4-mediated signaling pathways but counteracts LPS-induced NO synthesis in peritoneal macrophages by inhibiting NF-κB translocation and MAPK/ERK phosphorylation. *PLoS One,* 8**,** e76233.

Cattaneo, F., G. Guerra, M. Parisi, M. De Marinis, D. Tafuri, M. Cinelli & R. Ammendola (2014) Cell-surface receptors transactivation mediated by g protein-coupled receptors. *Int J Mol Sci,* 15**,** 19700-28.

Chang, S. H., D. Feng, J. A. Nagy, T. E. Sciuto, A. M. Dvorak & H. F. Dvorak (2009) Vascular permeability and pathological angiogenesis in caveolin-1-null mice. *Am J Pathol,* 175**,** 1768-76.

Charkoudian, N. (2003) Skin blood flow in adult human thermoregulation: how it works, when it does not, and why. *Mayo Clin Proc,* 78**,** 603-12.

Chehade, J. M., M. J. Haas & A. D. Mooradian (2002) Diabetes-related changes in rat cerebral occludin and zonula occludens-1 (ZO-1) expression. *Neurochem Res,* 27**,** 249-52.

Chen, M., T. Masaki & T. Sawamura (2002) LOX-1, the receptor for oxidized low-density lipoprotein identified from endothelial cells: implications in endothelial dysfunction and atherosclerosis. *Pharmacol Ther,* 95**,** 89-100.

Chen, X. L., J. O. Nam, C. Jean, C. Lawson, C. T. Walsh, E. Goka, S. T. Lim, A. Tomar, I. Tancioni, S. Uryu, J. L. Guan, L. M. Acevedo, S. M. Weis, D. A. Cheresh & D. D. Schlaepfer (2012) VEGF-induced vascular permeability is mediated by FAK. *Dev Cell,* 22**,** 146-57.

Cheng, J. P., C. Mendoza-Topaz, G. Howard, J. Chadwick, E. Shvets, A. S. Cowburn, B. J. Dunmore, A. Crosby, N. W. Morrell & B. J. Nichols (2015) Caveolae protect endothelial cells from membrane rupture during increased cardiac output. *J Cell Biol,* 211**,** 53-61.

Chew, S. S., C. S. Johnson, C. R. Green & H. V. Danesh-Meyer (2010) Role of connexin43 in central nervous system injury. *Exp Neurol,* 225**,** 250-61.

Choudhury, A., D. K. Sharma, D. L. Marks & R. E. Pagano (2004) Elevated endosomal cholesterol levels in Niemann-Pick cells inhibit rab4 and perturb membrane recycling. *Mol Biol Cell,* 15**,** 4500-11.

Cines, D. B., E. S. Pollak, C. A. Buck, J. Loscalzo, G. A. Zimmerman, R. P. McEver, J. S. Pober, T. M. Wick, B. A. Konkle, B. S. Schwartz, E. S. Barnathan, K. R. McCrae, B. A. Hug, A. M. Schmidt & D. M. Stern (1998) Endothelial cells in physiology and in the pathophysiology of vascular disorders. *Blood,* 91**,** 3527-61.

Cipolla, M. 2009. *The Cerebral Circulation*. Morgan & Claypool Life Sciences.

Ciulla, T. A., R. M. Hussain, L. M. Ciulla, B. Sink & A. Harris (2015) RANIBIZUMAB FOR DIABETIC MACULAR EDEMA REFRACTORY TO MULTIPLE PRIOR TREATMENTS. *Retina*.

Coelho-Santos, V., R. A. Leitão, F. L. Cardoso, I. Palmela, M. Rito, M. Barbosa, M. A. Brito, C. A. Fontes-Ribeiro & A. P. Silva (2015) The TNF-α/NF-κB signaling pathway has a key role in methamphetamine-induced blood-brain barrier dysfunction. *J Cereb Blood Flow Metab,* 35**,** 1260-71.

Coomber, B. L. & P. A. Stewart (1986) Three-dimensional reconstruction of vesicles in endothelium of blood-brain barrier versus highly permeable microvessels. *Anat Rec,* 215**,** 256-61.

Cox, S. (2015) Super-resolution imaging in live cells. *Dev Biol,* 401**,** 175-81.

Curry, F. E. & C. C. Michel (1980) A fiber matrix model of capillary permeability. *Microvasc Res,* 20**,** 96-9.

Curtis, T. M., T. A. Gardiner & A. W. Stitt (2009) Microvascular lesions of diabetic retinopathy: clues towards understanding pathogenesis? *Eye (Lond),* 23**,** 1496-508.

Daneman, R. (2012) The blood-brain barrier in health and disease. *Ann Neurol,* 72**,** 648-72.

Daneman, R., L. Zhou, A. A. Kebede & B. A. Barres (2010) Pericytes are required for blood-brain barrier integrity during embryogenesis. *Nature,* 468**,** 562-6.

Davis, M. J. & M. A. Hill (1999) Signaling mechanisms underlying the vascular myogenic response. *Physiol Rev,* 79**,** 387-423.

De Spiegelaere, W., C. Casteleyn, W. Van den Broeck, J. Plendl, M. Bahramsoltani, P. Simoens, V. Djonov & P. Cornillie (2012) Intussusceptive angiogenesis: a biologically relevant form of angiogenesis. *J Vasc Res,* 49**,** 390-404.

de Vries, H. E., M. C. Blom-Roosemalen, M. van Oosten, A. G. de Boer, T. J. van Berkel, D. D. Breimer & J. Kuiper (1996) The influence of cytokines on the integrity of the blood-brain barrier in vitro. *J Neuroimmunol,* 64**,** 37-43.

Dejana, E. (2004) Endothelial cell-cell junctions: happy together. *Nat.Rev.Mol.Cell Biol.,* 5**,** 261-270.

Dejana, E. & F. Orsenigo (2013) Endothelial adherens junctions at a glance. *J Cell Sci,* 126**,** 2545-9.

Dejana, E., E. Tournier-Lasserve & B. M. Weinstein (2009) The control of vascular integrity by endothelial cell junctions: molecular basis and pathological implications. *Dev Cell,* 16**,** 209-21.

Deli, M. A. (2009) Potential use of tight junction modulators to reversibly open membranous barriers and improve drug delivery. *Biochim Biophys Acta,* 1788**,** 892-910.

Deli, M. A., C. S. Abrahám, Y. Kataoka & M. Niwa (2005) Permeability studies on in vitro blood-brain barrier models: physiology, pathology, and pharmacology. *Cell Mol Neurobiol,* 25**,** 59-127.

Direk, N., H. S. Perez, S. Akoudad, B. F. Verhaaren, W. J. Niessen, A. Hofman, M. W. Vernooij, M. A. Ikram & H. Tiemeier (2016) Markers of cerebral small vessel disease and severity of depression in the general population. *Psychiatry Res,* 253**,** 1-6.

Dobrivojevic, M., K. Spiranec & A. Sindic (2015) Involvement of bradykinin in brain edema development after ischemic stroke. *Pflugers Arch,* 467**,** 201-12.

Dore-Duffy, P. & J. C. LaManna (2007) Physiologic angiodynamics in the brain. *Antioxid Redox Signal,* 9**,** 1363-71.

Dorland, Y. L., T. S. Malinova, A. M. van Stalborch, A. G. Grieve, D. van Geemen, N. S. Jansen, B. J. de Kreuk, K. Nawaz, J. Kole, D. Geerts, R. J. Musters, J. de Rooij, P. L. Hordijk & S. Huveneers (2016) The F-BAR protein pacsin2 inhibits asymmetric VE-cadherin internalization from tensile adherens junctions. *Nat Commun,* 7**,** 12210.

Drozdzik, M., M. Bialecka, K. Mysliwiec, K. Honczarenko, J. Stankiewicz & Z. Sych (2003) Polymorphism in the P-glycoprotein drug transporter MDR1 gene: a possible link between environmental and genetic factors in Parkinson's disease. *Pharmacogenetics,* 13**,** 259-63.

Duncker, D. J. & R. J. Bache (2000) Regulation of coronary vasomotor tone under normal conditions and during acute myocardial hypoperfusion. *Pharmacol Ther,* 86**,** 87-110.

--- (2008) Regulation of coronary blood flow during exercise. *Physiol Rev,* 88**,** 1009-86.

Dupuis, J., F. Harel & Q. T. Nguyen (2014) Molecular imaging of the pulmonary circulation in health and disease. *Clin Transl Imaging,* 2**,** 415-426.

Duran, W. N., J. W. Breslin & F. A. Sanchez (2010) The NO cascade, eNOS location, and microvascular permeability. *Cardiovasc Res,* 87**,** 254-61.

Easton, A. S. & N. J. Abbott (2002) Bradykinin increases permeability by calcium and 5-lipoxygenase in the ECV304/C6 cell culture model of the blood-brain barrier. *Brain Res,* 953**,** 157-69.

Ellis, C. G., J. Jagger & M. Sharpe (2005) The microcirculation as a functional system. *Crit Care,* 9 Suppl 4**,** S3-8.

Emerich, D. F., R. L. Dean, C. Osborn & R. T. Bartus (2001) The development of the bradykinin agonist labradimil as a means to increase the permeability of the blood-brain barrier: from concept to clinical evaluation. *Clin Pharmacokinet,* 40**,** 105-23.

Etienne, S., P. Adamson, J. Greenwood, A. D. Strosberg, S. Cazaubon & P. O. Couraud (1998) ICAM-1 signaling pathways associated with Rho activation in microvascular brain endothelial cells. *J.Immunol.,* 161**,** 5755-5761.

Etienne-Manneville, S., J. B. Manneville, P. Adamson, B. Wilbourn, J. Greenwood & P. O. Couraud (2000) ICAM-1-coupled cytoskeletal rearrangements and transendothelial lymphocyte migration involve intracellular calcium signaling in brain endothelial cell lines. *J.Immunol.,* 165**,** 3375-3383.

Faraci, F. M. (2011) Protecting against vascular disease in brain. *Am J Physiol Heart Circ Physiol,* 300**,** H1566-82.

Faraci, F. M. & D. D. Heistad (1990) Regulation of large cerebral arteries and cerebral microvascular pressure. *Circ Res,* 66**,** 8-17.

Farooqui, A. A. & L. A. Horrocks (2006) Phospholipase A2-generated lipid mediators in the brain: the good, the bad, and the ugly. *Neuroscientist,* 12**,** 245-60.

Feigl, E. O. (1983) Coronary physiology. *Physiol Rev,* 63**,** 1-205.

Feletou, M., Y. Huang & P. M. Vanhoutte (2010) Vasoconstrictor prostanoids. *Pflugers Arch,* 459**,** 941-50.

Figueroa, X. F. & B. R. Duling (2009) Gap junctions in the control of vascular function. *Antioxid Redox Signal,* 11**,** 251-66.

Filosa, J. A., H. W. Morrison, J. A. Iddings, W. Du & K. J. Kim (2016) Beyond neurovascular coupling, role of astrocytes in the regulation of vascular tone. *Neuroscience,* 323**,** 96-109.

Fishman, A. P. (1982) Endothelium: a distributed organ of diverse capabilities. *Ann N Y Acad Sci,* 401**,** 1-8.

Fleming, I. & R. Busse (2003) Molecular mechanisms involved in the regulation of the endothelial nitric oxide synthase. *Am J Physiol Regul Integr Comp Physiol,* 284**,** R1-12.

Flemming, S., N. Burkard, M. Renschler, F. Vielmuth, M. Meir, M. Schick, C. Wunder, C.-T. Germer, V. Spindler, J. Waschke & N. Schegel. 2016. Soluble VE-cadherin contributes to loss of VE-cadherin-mediated adhesion and endothelial barrier function. The FASEB Journal.

Flemming, S., N. Burkard, M. Renschler, F. Vielmuth, M. Meir, M. A. Schick, C. Wunder, C. T. Germer, V. Spindler, J. Waschke & N. Schlegel (2015) Soluble VE-cadherin is involved in endothelial barrier breakdown in systemic inflammation and sepsis. *Cardiovasc Res,* 107**,** 32-44.

Florey (1966) The endothelial cell. *Br Med J,* 2**,** 487-90.

Ford, J. A., N. Lois, P. Royle, C. Clar, D. Shyangdan & N. Waugh (2013) Current treatments in diabetic macular oedema: systematic review and meta-analysis. *BMJ Open,* 3.

Franco, M., P. Roswall, E. Cortez, D. Hanahan & K. Pietras (2011) Pericytes promote endothelial cell survival through induction of autocrine VEGF-A signaling and Bcl-w expression. *Blood,* 118**,** 2906-17.

Fraser, P. A. (2011) The role of free radical generation in increasing cerebrovascular permeability. *Free Radic Biol Med,* 51**,** 967-77.

Fraser, P. A., A. D. Dallas & S. Davies (1990) Measurement of filtration coefficient in single cerebral microvessels of the frog. *J Physiol,* 423**,** 343-61.

Fujita, Y., M. Yoshizumi, Y. Izawa, N. Ali, H. Ohnishi, Y. Kanematsu, K. Ishizawa, K. Tsuchiya & T. Tamaki (2006) Transactivation of fetal liver kinase-1/kinase-insert domain-containing receptor by lysophosphatidylcholine induces vascular endothelial cell proliferation. *Endocrinology,* 147**,** 1377-85.

Fulton, D., J. P. Gratton, T. J. McCabe, J. Fontana, Y. Fujio, K. Walsh, T. F. Franke, A. Papapetropoulos & W. C. Sessa (1999) Regulation of endothelium-derived nitric oxide production by the protein kinase Akt. *Nature,* 399**,** 597-601.

Förstermann, U. & W. C. Sessa (2012) Nitric oxide synthases: regulation and function. *Eur Heart J, 33*, 829-37, 837a-837d.

Gavard, J. (2013) Endothelial permeability and VE-cadherin: a wacky comradeship. *Cell Adh Migr, 7*, 455-61.

Gavard, J. & J. S. Gutkind (2006) VEGF controls endothelial-cell permeability by promoting the beta-arrestin-dependent endocytosis of VE-cadherin. *Nat.Cell Biol., 8*, 1223-1234.

Gavard, J., V. Patel & J. S. Gutkind (2008) Angiopoietin-1 prevents VEGF-induced endothelial permeability by sequestering Src through mDia. *Dev Cell, 14*, 25-36.

Gerhardt, H., M. Golding, M. Fruttiger, C. Ruhrberg, A. Lundkvist, A. Abramsson, M. Jeltsch, C. Mitchell, K. Alitalo, D. Shima & C. Betsholtz (2003) VEGF guides angiogenic sprouting utilizing endothelial tip cell filopodia. *J Cell Biol, 161*, 1163-77.

Giannotta, M., M. Trani & E. Dejana (2013) VE-cadherin and endothelial adherens junctions: active guardians of vascular integrity. *Dev Cell, 26*, 441-54.

Girouard, H. & C. Iadecola (2006) Neurovascular coupling in the normal brain and in hypertension, stroke, and Alzheimer disease. *J Appl Physiol (1985), 100*, 328-35.

Goddard, L. M. & M. L. Iruela-Arispe (2013) Cellular and molecular regulation of vascular permeability. *Thromb Haemost, 109*, 407-15.

Gomez-Nicola, D. & V. H. Perry (2015) Microglial dynamics and role in the healthy and diseased brain: a paradigm of functional plasticity. *Neuroscientist, 21*, 169-84.

Gourlaouen, M., J. C. Welti, N. S. Vasudev & A. R. Reynolds (2013) Essential role for endocytosis in the growth factor-stimulated activation of ERK1/2 in endothelial cells. *J Biol Chem, 288*, 7467-80.

Grant, B. D. & J. G. Donaldson (2009) Pathways and mechanisms of endocytic recycling. *Nat Rev Mol Cell Biol, 10*, 597-608.

GROTTE, G., R. C. KNUTSON & J. L. BOLLMAN (1951) The diffusion of dextrans of different molecular sizes to lymph and urine. *J Lab Clin Med, 38*, 577-82.

Guillemot, L., S. Paschoud, P. Pulimeno, A. Foglia & S. Citi (2008) The cytoplasmic plaque of tight junctions: a scaffolding and signalling center. *Biochim Biophys Acta, 1778*, 601-13.

Gunzel, D. & A. S. Yu (2013) Claudins and the modulation of tight junction permeability. *Physiol Rev, 93*, 525-69.

Guo, V. Y., B. Cao, X. Wu, J. J. Lee & B. C. Zee (2016) Prospective Association between Diabetic Retinopathy and Cardiovascular Disease-A Systematic Review and Meta-analysis of Cohort Studies. *J Stroke Cerebrovasc Dis, 25*, 1688-95.

Hall, C. N., C. Reynell, B. Gesslein, N. B. Hamilton, A. Mishra, B. A. Sutherland, F. M. O'Farrell, A. M. Buchan, M. Lauritzen & D. Attwell (2014) Capillary pericytes regulate cerebral blood flow in health and disease. *Nature, 508*, 55-60.

Hara, Y., Y. Kusumi, M. Mitsumata, X. K. Li & M. Fujino (2008) Lysophosphatidylcholine upregulates LOX-1, chemokine receptors, and activation-related transcription factors in human T-cell line Jurkat. *J Thromb Thrombolysis,* 26**,** 113-8.

Harhaj, N. S., E. A. Felinski, E. B. Wolpert, J. M. Sundstrom, T. W. Gardner & D. A. Antonetti (2006) VEGF activation of protein kinase C stimulates occludin phosphorylation and contributes to endothelial permeability. *Invest Ophthalmol Vis Sci,* 47**,** 5106-15.

Harris, T. J. & U. Tepass (2010) Adherens junctions: from molecules to morphogenesis. *Nat Rev Mol Cell Biol,* 11**,** 502-14.

Hawkins, B. T., Y. H. Gu, Y. Izawa & G. J. del Zoppo (2015) Dabigatran abrogates brain endothelial cell permeability in response to thrombin. *J Cereb Blood Flow Metab,* 35**,** 985-92.

Hayashi, R., N. Yamashita, S. Matsui, T. Fujita, J. Araya, K. Sassa, N. Arai, Y. Yoshida, T. Kashii, M. Maruyama, E. Sugiyama & M. Kobayashi (2000) Bradykinin stimulates IL-6 and IL-8 production by human lung fibroblasts through ERK- and p38 MAPK-dependent mechanisms. *Eur Respir J,* 16**,** 452-8.

Hell, S. W., S. J. Sahl, M. Bates, X. Zhuang, R. Heintzmann, M. J. Booth, J. Bewersdorf, G. Shtengel, H. Hess, P. Tinnefeld, A. Honigmann, S. Jakobs, I. Testa, L. Cognet, B. Lounis, H. Ewers, S. J. Davis, C. Eggeling, D. Klenerman, K. I. Willig, G. Vicidomini, M. Castello, A. Diaspro & T. Cordes. 2015. The 2015 super-resolution microscopy roadmap. Journal of Physics D: Applied Physics.

Helms, H. C., N. J. Abbott, M. Burek, R. Cecchelli, P. O. Couraud, M. A. Deli, C. Förster, H. J. Galla, I. A. Romero, E. V. Shusta, M. J. Stebbins, E. Vandenhaute, B. Weksler & B. Brodin (2016) In vitro models of the blood-brain barrier: An overview of commonly used brain endothelial cell culture models and guidelines for their use. *J Cereb Blood Flow Metab,* 36**,** 862-90.

Hirano, A., T. Kawanami & J. F. Llena (1994) Electron microscopy of the blood-brain barrier in disease. *Microsc Res Tech,* 27**,** 543-56.

Hofman, P., H. G. Blaauwgeers, M. J. Tolentino, A. P. Adamis, B. J. Nunes Cardozo, G. F. Vrensen & R. O. Schlingemann (2000) VEGF-A induced hyperpermeability of blood-retinal barrier endothelium in vivo is predominantly associated with pinocytotic vesicular transport and not with formation of fenestrations. Vascular endothelial growth factor-A. *Curr Eye Res,* 21**,** 637-45.

Holash, J., S. Davis, N. Papadopoulos, S. D. Croll, L. Ho, M. Russell, P. Boland, R. Leidich, D. Hylton, E. Burova, E. Ioffe, T. Huang, C. Radziejewski, K. Bailey, J. P. Fandl, T. Daly, S. J. Wiegand, G. D. Yancopoulos & J. S. Rudge (2002) VEGF-Trap: a VEGF blocker with potent antitumor effects. *Proc Natl Acad Sci U S A,* 99**,** 11393-8.

Huang, F., P. V. Subbaiah, O. Holian, J. Zhang, A. Johnson, N. Gertzberg & H. Lum (2005) Lysophosphatidylcholine increases endothelial permeability: role of PKCalpha and RhoA cross talk. *Am J Physiol Lung Cell Mol Physiol,* 289**,** L176-85.

Hubbard, A. K. & R. Rothlein (2000) Intercellular adhesion molecule-1 (ICAM-1) expression and cell signaling cascades. *Free Radic.Biol.Med.,* 28**,** 1379-1386.

Hudson, N., M. B. Powner, M. H. Sarker, T. Burgoyne, M. Campbell, Z. K. Ockrim, R. Martinelli, C. E. Futter, M. B. Grant, P. A. Fraser, D. T. Shima, J. Greenwood & P. Turowski (2014) Differential apicobasal VEGF signaling at vascular blood-neural barriers. *Dev Cell,* 30**,** 541-52.

Huiban, M., C. Coello, K. Wu, Y. Xu, Y. Lewis, A. P. Brown, M. Buraglio, C. Guan, S. Shabbir, R. Fong, J. Passchier, E. A. Rabiner & A. Lockhart (2017) Investigation of the Brain Biodistribution of the Lipoprotein-Associated Phospholipase A2 (Lp-PLA2) Inhibitor [(18)F]GSK2647544 in Healthy Male Subjects. *Mol Imaging Biol,* 19**,** 153-161.

Hulpiau, P. & F. van Roy (2009) Molecular evolution of the cadherin superfamily. *Int J Biochem Cell Biol,* 41**,** 349-69.

Huveneers, S., J. Oldenburg, E. Spanjaard, G. van der Krogt, I. Grigoriev, A. Akhmanova, H. Rehmann & J. de Rooij (2012) Vinculin associates with endothelial VE-cadherin junctions to control force-dependent remodeling. *J Cell Biol,* 196**,** 641-52.

Iwase, M., K. Sonoki, N. Sasaki, S. Ohdo, S. Higuchi, H. Hattori & M. Iida (2008) Lysophosphatidylcholine contents in plasma LDL in patients with type 2 diabetes mellitus: relation with lipoprotein-associated phospholipase A2 and effects of simvastatin treatment. *Atherosclerosis,* 196**,** 931-6.

Jain, R. K. (2003) Molecular regulation of vessel maturation. *Nat Med,* 9**,** 685-93.

Jakobsson, L., J. Kreuger, K. Holmborn, L. Lundin, I. Eriksson, L. Kjellén & L. Claesson-Welsh (2006) Heparan sulfate in trans potentiates VEGFR-mediated angiogenesis. *Dev Cell,* 10**,** 625-34.

Jessen, N. A., A. S. Munk, I. Lundgaard & M. Nedergaard (2015) The Glymphatic System: A Beginner's Guide. *Neurochem Res,* 40**,** 2583-99.

Jeynes, B. & J. Provias (2011) The case for blood-brain barrier dysfunction in the pathogenesis of Alzheimer's disease. *J Neurosci Res,* 89**,** 22-8.

Jiang, Z. Y., Y. W. Lin, A. Clemont, E. P. Feener, K. D. Hein, M. Igarashi, T. Yamauchi, M. F. White & G. L. King (1999) Characterization of selective resistance to insulin signaling in the vasculature of obese Zucker (fa/fa) rats. *J Clin Invest,* 104**,** 447-57.

Jin, Z. G., H. Ueba, T. Tanimoto, A. O. Lungu, M. D. Frame & B. C. Berk (2003) Ligand-independent activation of vascular endothelial growth factor receptor 2 by fluid shear stress regulates activation of endothelial nitric oxide synthase. *Circ Res,* 93**,** 354-63.

Johannes, L., R. G. Parton, P. Bassereau & S. Mayor (2015) Building endocytic pits without clathrin. *Nat Rev Mol Cell Biol,* 16**,** 311-21.

Johannes, L., C. Wunder & P. Bassereau (2014) Bending "on the rocks"--a cocktail of biophysical modules to build endocytic pathways. *Cold Spring Harb Perspect Biol,* 6.

Johnson, J. M., C. T. Minson & D. L. Kellogg (2014) Cutaneous vasodilator and vasoconstrictor mechanisms in temperature regulation. *Compr Physiol,* 4**,** 33-89.

Jones, S. & J. Z. Rappoport (2014) Interdependent epidermal growth factor receptor signalling and trafficking. *Int J Biochem Cell Biol,* 51**,** 23-8.

Junge, C. E., C. J. Lee, K. B. Hubbard, Z. Zhang, J. J. Olson, J. R. Hepler, D. J. Brat & S. F. Traynelis (2004) Protease-activated receptor-1 in human brain: localization and functional expression in astrocytes. *Exp Neurol,* 188**,** 94-103.

Katan, M., Y. P. Moon, M. C. Paik, R. L. Wolfert, R. L. Sacco & M. S. Elkind (2014) Lipoprotein-associated phospholipase A2 is associated with atherosclerotic stroke risk: the Northern Manhattan Study. *PLoS One,* 9**,** e83393.

Kety, S. S. & C. F. Schmidt (1948) THE EFFECTS OF ALTERED ARTERIAL TENSIONS OF CARBON DIOXIDE AND OXYGEN ON CEREBRAL BLOOD FLOW AND CEREBRAL OXYGEN CONSUMPTION OF NORMAL YOUNG MEN. *J Clin Invest,* 27**,** 484-92.

Kim, B. J., B. M. Hancock, A. Bermudez, N. Del Cid, E. Reyes, N. M. van Sorge, X. Lauth, C. A. Smurthwaite, B. J. Hilton, A. Stotland, A. Banerjee, J. Buchanan, R. Wolkowicz, D. Traver & K. S. Doran (2015) Bacterial induction of Snail1 contributes to blood-brain barrier disruption. *J Clin Invest,* 125**,** 2473-83.

Kim, S. & H. Iwao (2000) Molecular and cellular mechanisms of angiotensin II-mediated cardiovascular and renal diseases. *Pharmacol Rev,* 52**,** 11-34.

Klaassen, I., C. J. Van Noorden & R. O. Schlingemann (2013) Molecular basis of the inner blood-retinal barrier and its breakdown in diabetic macular edema and other pathological conditions. *Prog Retin Eye Res,* 34**,** 19-48.

Knowland, D., A. Arac, K. J. Sekiguchi, M. Hsu, S. E. Lutz, J. Perrino, G. K. Steinberg, B. A. Barres, A. Nimmerjahn & D. Agalliu (2014) Stepwise recruitment of transcellular and paracellular pathways underlies blood-brain barrier breakdown in stroke. *Neuron,* 82**,** 603-17.

Kusters, Y. H. & E. J. Barrett (2016) Muscle microvasculature's structural and functional specializations facilitate muscle metabolism. *Am J Physiol Endocrinol Metab,* 310**,** E379-87.

La, M. & J. J. Reid (1995) Endothelin-1 and the regulation of vascular tone. *Clin Exp Pharmacol Physiol,* 22**,** 315-23.

Lampugnani, M. G., F. Orsenigo, M. C. Gagliani, C. Tacchetti & E. Dejana (2006) Vascular endothelial cadherin controls VEGFR-2 internalization and signaling from intracellular compartments. *J Cell Biol,* 174**,** 593-604.

Lanahan, A. A., K. Hermans, F. Claes, J. S. Kerley-Hamilton, Z. W. Zhuang, F. J. Giordano, P. Carmeliet & M. Simons (2010) VEGF receptor 2 endocytic trafficking regulates arterial morphogenesis. *Dev Cell,* 18**,** 713-24.

Laughlin, M., R. Korthuis, D. Duncker & R. Bache. 2011. Control of Blood Flow to Cardiac and Skeletal Muscle During Exercise. Comprehensive Physiology.

Lavi, S., J. P. McConnell, C. S. Rihal, A. Prasad, V. Mathew, L. O. Lerman & A. Lerman (2007) Local production of lipoprotein-associated phospholipase A2 and lysophosphatidylcholine in the coronary circulation: association with early coronary atherosclerosis and endothelial dysfunction in humans. *Circulation,* 115**,** 2715-21.

Le Bihan, O., M. Decossas, E. Gontier, M. C. Gerbod-Giannone & O. Lambert (2015) Visualization of adherent cell monolayers by cryo-electron microscopy: A snapshot of endothelial adherens junctions. *J Struct Biol,* 192**,** 470-7.

Le, T. L., A. S. Yap & J. L. Stow (1999) Recycling of E-cadherin: a potential mechanism for regulating cadherin dynamics. *J Cell Biol,* 146**,** 219-32.

Leckband, D. & A. Prakasam (2006) Mechanism and dynamics of cadherin adhesion. *Annu Rev Biomed Eng,* 8**,** 259-87.

Lee, K. R., N. Kawai, S. Kim, O. Sagher & J. T. Hoff (1997) Mechanisms of edema formation after intracerebral hemorrhage: effects of thrombin on cerebral blood flow, blood-brain barrier permeability, and cell survival in a rat model. *J Neurosurg,* 86**,** 272-8.

Lee, S., T. T. Chen, C. L. Barber, M. C. Jordan, J. Murdock, S. Desai, N. Ferrara, A. Nagy, K. P. Roos & M. L. Iruela-Arispe (2007) Autocrine VEGF signaling is required for vascular homeostasis. *Cell,* 130**,** 691-703.

Lehmann, R., H. Franken, S. Dammeier, L. Rosenbaum, K. Kantartzis, A. Peter, A. Zell, P. Adam, J. Li, G. Xu, A. Königsrainer, J. Machann, F. Schick, M. Hrabé de Angelis, M. Schwab, H. Staiger, E. Schleicher, A. Gastaldelli, A. Fritsche, H. U. Häring & N. Stefan (2013) Circulating lysophosphatidylcholines are markers of a metabolically benign nonalcoholic fatty liver. *Diabetes Care,* 36**,** 2331-8.

Levick, J. R. (1991a) Capillary filtration-absorption balance reconsidered in light of dynamic extravascular factors. *Exp Physiol,* 76**,** 825-57.

Levick, J. R. & C. C. Michel (2010) Microvascular fluid exchange and the revised Starling principle. *Cardiovasc Res,* 87**,** 198-210.

Levick, R. 1991b. *An Introduction to Cardiovascular Physiology*. Butterworth-Heinemann Ltd.

Ley, K., C. Laudanna, M. I. Cybulsky & S. Nourshargh (2007) Getting to the site of inflammation: the leukocyte adhesion cascade updated. *Nat Rev Immunol,* 7**,** 678-89.

Li, F., Y. Lan, Y. Wang, J. Wang, G. Yang, F. Meng, H. Han, A. Meng & X. Yang (2011) Endothelial Smad4 maintains cerebrovascular integrity by activating N-cadherin through cooperation with Notch. *Dev Cell,* 20**,** 291-302.

Li, X., N. Padhan, E. O. Sjöström, F. P. Roche, C. Testini, N. Honkura, M. Sáinz-Jaspeado, E. Gordon, K. Bentley, A. Philippides, V. Tolmachev, E. Dejana, R. V. Stan, D. Vestweber, K. Ballmer-Hofer, C. Betsholtz, K. Pietras, L. Jansson & L. Claesson-Welsh (2016) VEGFR2 pY949 signalling regulates adherens junction integrity and metastatic spread. *Nat Commun,* 7**,** 11017.

Liebner, S., M. Corada, T. Bangsow, J. Babbage, A. Taddei, C. J. Czupalla, M. Reis, A. Felici, H. Wolburg, M. Fruttiger, M. M. Taketo, H. von Melchner, K. H. Plate, H. Gerhardt & E. Dejana (2008) Wnt/beta-catenin signaling controls development of the blood-brain barrier. *J Cell Biol,* 183**,** 409-17.

Lin, H. & J. Trejo (2013) Transactivation of the PAR1-PAR2 heterodimer by thrombin elicits β-arrestin-mediated endosomal signaling. *J Biol Chem,* 288**,** 11203-15.

Lin, M. I., J. Yu, T. Murata & W. C. Sessa (2007) Caveolin-1-deficient mice have increased tumor microvascular permeability, angiogenesis, and growth. *Cancer Res,* 67**,** 2849-56.

Liss, V., B. Barlag, M. Nietschke & M. Hensel (2015) Self-labelling enzymes as universal tags for fluorescence microscopy, super-resolution microscopy and electron microscopy. *Sci Rep,* 5**,** 17740.

Liu, X., X. Zhou & W. Yuan (2014) The angiopoietin1-Akt pathway regulates barrier function of the cultured spinal cord microvascular endothelial cells through Eps8. *Exp Cell Res,* 328**,** 118-31.

Lizama, C. O. & A. C. Zovein (2013) Polarizing pathways: balancing endothelial polarity, permeability, and lumen formation. *Exp Cell Res,* 319**,** 1247-54.

Lo, E. H., T. Dalkara & M. A. Moskowitz (2003) Mechanisms, challenges and opportunities in stroke. *Nat Rev Neurosci,* 4**,** 399-415.

London, A., I. Benhar & M. Schwartz (2013) The retina as a window to the brain-from eye research to CNS disorders. *Nat Rev Neurol,* 9**,** 44-53.

Luchsinger, J. A. & D. R. Gustafson (2009) Adiposity, type 2 diabetes, and Alzheimer's disease. *J Alzheimers Dis,* 16**,** 693-704.

Maeda, Y., K. Hirano, J. Nishimura, T. Sasaki & H. Kanaide (2004) Endothelial dysfunction and altered bradykinin response due to oxidative stress induced by serum deprivation in the bovine cerebral artery. *Eur J Pharmacol,* 491**,** 53-60.

Maina, J. N. & J. B. West (2005) Thin and strong! The bioengineering dilemma in the structural and functional design of the blood-gas barrier. *Physiol Rev,* 85**,** 811-44.

Maingret, F., A. J. Patel, F. Lesage, M. Lazdunski & E. Honoré (2000) Lysophospholipids open the two-pore domain mechano-gated K(+) channels TREK-1 and TRAAK. *J Biol Chem,* 275**,** 10128-33.

Majesky, M. W., X. R. Dong, V. Hoglund, W. M. Mahoney & G. Daum (2011) The adventitia: a dynamic interface containing resident progenitor cells. *Arterioscler Thromb Vasc Biol,* 31**,** 1530-9.

MAJNO, G. & G. E. PALADE (1961) Studies on inflammation. 1. The effect of histamine and serotonin on vascular permeability: an electron microscopic study. *J Biophys Biochem Cytol,* 11**,** 571-605.

MAJNO, G., G. E. PALADE & G. I. SCHOEFL (1961) Studies on inflammation. II. The site of action of histamine and serotonin along the vascular tree: a topographic study. *J Biophys Biochem Cytol,* 11**,** 607-26.

Majno, G., S. M. Shea & M. Leventhal (1969) Endothelial contraction induced by histamine-type mediators: an electron microscopic study. *J Cell Biol,* 42**,** 647-72.

Mallette, M. M., G. J. Hodges, G. W. McGarr, D. A. Gabriel & S. S. Cheung (2016) Investigating the roles of core and local temperature on forearm skin blood flow. *Microvasc Res,* 106**,** 88-95.

Malpas, S. C. (1998) The rhythmicity of sympathetic nerve activity. *Prog Neurobiol,* 56**,** 65-96.

Manni, S., K. Kisko, T. Schleier, J. Missimer & K. Ballmer-Hofer (2014) Functional and structural characterization of the kinase insert and the carboxy terminal domain in VEGF receptor 2 activation. *FASEB J,* 28**,** 4914-23.

Martinelli, R., M. Gegg, R. Longbottom, P. Adamson, P. Turowski & J. Greenwood (2009) ICAM-1-mediated endothelial nitric oxide synthase activation via calcium and AMP-activated protein kinase is required for transendothelial lymphocyte migration. *Mol Biol Cell,* 20**,** 995-1005.

Martinez-Lemus, L. A. (2012) The dynamic structure of arterioles. *Basic Clin Pharmacol Toxicol,* 110**,** 5-11.

Martinez-Lemus, L. A., M. A. Hill & G. A. Meininger (2009) The plastic nature of the vascular wall: a continuum of remodeling events contributing to control of arteriolar diameter and structure. *Physiology (Bethesda),* 24**,** 45-57.

Martins, T., T. Burgoyne, B. A. Kenny, N. Hudson, C. E. Futter, A. F. Ambrosio, A. P. Silva, J. Greenwood & P. Turowski (2013) Methamphetamine-induced nitric oxide promotes vesicular transport in blood-brain barrier endothelial cells. *Neuropharmacology,* 65**,** 74-82.

Matoba, T., H. Shimokawa, H. Kubota, K. Morikawa, T. Fujiki, I. Kunihiro, Y. Mukai, Y. Hirakawa & A. Takeshita (2002) Hydrogen peroxide is an endothelium-derived hyperpolarizing factor in human mesenteric arteries. *Biochem Biophys Res Commun,* 290**,** 909-13.

Matsumoto, T., T. Kobayashi & K. Kamata (2007) Role of lysophosphatidylcholine (LPC) in atherosclerosis. *Curr Med Chem,* 14**,** 3209-20.

McEniery, C. M., I. B. Wilkinson & A. P. Avolio (2007) Age, hypertension and arterial function. *Clin Exp Pharmacol Physiol,* 34**,** 665-71.

McHowat, J. & P. B. Corr (1993) Thrombin-induced release of lysophosphatidylcholine from endothelial cells. *J Biol Chem,* 268**,** 15605-10.

McIntyre, T. M., G. A. Zimmerman & S. M. Prescott (1999) Biologically active oxidized phospholipids. *J Biol Chem,* 274**,** 25189-92.

McMahon, H. T. & E. Boucrot (2011) Molecular mechanism and physiological functions of clathrin-mediated endocytosis. *Nat Rev Mol Cell Biol,* 12**,** 517-33.

Mehta, D., S. Gupta, S. N. Gaur, S. V. Gangal & K. P. Agrawal (1990) Increased leukocyte phospholipase A2 activity and plasma lysophosphatidylcholine levels in asthma and rhinitis and their relationship to airway sensitivity to histamine. *Am Rev Respir Dis,* 142**,** 157-61.

Mehta, D. & A. B. Malik (2006) Signaling mechanisms regulating endothelial permeability. *Physiol Rev,* 86**,** 279-367.

Melega, W. P., A. K. Cho, D. Harvey & G. Laćan (2007) Methamphetamine blood concentrations in human abusers: application to pharmacokinetic modeling. *Synapse,* 61**,** 216-20.

Meng, L., W. Hou, J. Chui, R. Han & A. W. Gelb (2015) Cardiac Output and Cerebral Blood Flow: The Integrated Regulation of Brain Perfusion in Adult Humans. *Anesthesiology,* 123**,** 1198-208.

Michel, C. C. & F. E. Curry (1999) Microvascular permeability. *Physiol Rev,* 79**,** 703-61.

Miller, J. W., C. J. Le, E. C. Strauss & N. Ferrara (2013) Vascular endothelial growth factor a in intraocular vascular disease. *Ophthalmology,* 120**,** 106-114.

Montagne, A., S. R. Barnes, M. D. Sweeney, M. R. Halliday, A. P. Sagare, Z. Zhao, A. W. Toga, R. E. Jacobs, C. Y. Liu, L. Amezcua, M. G. Harrington, H. C. Chui, M. Law & B. V. Zlokovic (2015) Blood-brain barrier breakdown in the aging human hippocampus. *Neuron,* 85**,** 296-302.

Moolenaar, W. H., L. A. van Meeteren & B. N. Giepmans (2004) The ins and outs of lysophosphatidic acid signaling. *Bioessays,* 26**,** 870-81.

Muller, W. A. (2011) Mechanisms of leukocyte transendothelial migration. *Annu Rev Pathol,* 6**,** 323-44.

--- (2014) How endothelial cells regulate transmigration of leukocytes in the inflammatory response. *Am J Pathol,* 184**,** 886-96.

Murakami, T., E. A. Felinski & D. A. Antonetti (2009) Occludin phosphorylation and ubiquitination regulate tight junction trafficking and vascular endothelial growth factor-induced permeability. *J Biol Chem,* 284**,** 21036-46.

Mustafa, A. K., G. Sikka, S. K. Gazi, J. Steppan, S. M. Jung, A. K. Bhunia, V. M. Barodka, F. K. Gazi, R. K. Barrow, R. Wang, L. M. Amzel, D. E. Berkowitz & S. H. Snyder (2011) Hydrogen sulfide as endothelium-derived hyperpolarizing factor sulfhydrates potassium channels. *Circ Res,* 109**,** 1259-68.

Muñoz-Chápuli, R., A. R. Quesada & M. Angel Medina (2004) Angiogenesis and signal transduction in endothelial cells. *Cell Mol Life Sci,* 61**,** 2224-43.

Nag, S., R. Venugopalan & D. J. Stewart (2007) Increased caveolin-1 expression precedes decreased expression of occludin and claudin-5 during blood-brain barrier breakdown. *Acta Neuropathol,* 114**,** 459-69.

Nagy, J. A., L. Benjamin, H. Y. Zeng, A. M. Dvorak & H. F. Dvorak (2008) Vascular permeability, vascular hyperpermeability and angiogenesis. *Angiogenesis,* 11**,** 109-119.

Nagyoszi, P., I. Wilhelm, A. E. Farkas, C. Fazakas, N. T. Dung, J. Haskó & I. A. Krizbai (2010) Expression and regulation of toll-like receptors in cerebral endothelial cells. *Neurochem Int,* 57**,** 556-64.

Nakagawa, S., M. A. Deli, H. Kawaguchi, T. Shimizudani, T. Shimono, A. Kittel, K. Tanaka & M. Niwa (2009) A new blood-brain barrier model using primary rat brain endothelial cells, pericytes and astrocytes. *Neurochem Int,* 54**,** 253-63.

Nguyen, L. N., D. Ma, G. Shui, P. Wong, A. Cazenave-Gassiot, X. Zhang, M. R. Wenk, E. L. Goh & D. L. Silver (2014) Mfsd2a is a transporter for the essential omega-3 fatty acid docosahexaenoic acid. *Nature,* 509**,** 503-6.

Nielsen, E., F. Severin, J. M. Backer, A. A. Hyman & M. Zerial (1999) Rab5 regulates motility of early endosomes on microtubules. *Nat Cell Biol,* 1**,** 376-82.

Nilsson, A. L. (1987) Blood flow, temperature, and heat loss of skin exposed to local radiative and convective cooling. *J Invest Dermatol,* 88**,** 586-93.

Obermeier, B., R. Daneman & R. M. Ransohoff (2013) Development, maintenance and disruption of the blood-brain barrier. *Nat Med,* 19**,** 1584-96.

Oei, H. H., I. M. van der Meer, A. Hofman, P. J. Koudstaal, T. Stijnen, M. M. Breteler & J. C. Witteman (2005) Lipoprotein-associated phospholipase A2 activity is associated with risk of coronary heart disease and ischemic stroke: the Rotterdam Study. *Circulation,* 111**,** 570-5.

Oh, P., P. Borgström, H. Witkiewicz, Y. Li, B. J. Borgström, A. Chrastina, K. Iwata, K. R. Zinn, R. Baldwin, J. E. Testa & J. E. Schnitzer (2007) Live dynamic imaging of caveolae pumping targeted antibody rapidly and specifically across endothelium in the lung. *Nat Biotechnol,* 25**,** 327-37.

Olsson, A. K., A. Dimberg, J. Kreuger & L. Claesson-Welsh (2006) VEGF receptor signalling - in control of vascular function. *Nat.Rev.Mol.Cell Biol.,* 7**,** 359-371.

On, N. H., S. Savant, M. Toews & D. W. Miller (2013) Rapid and reversible enhancement of blood-brain barrier permeability using lysophosphatidic acid. *J Cereb Blood Flow Metab,* 33**,** 1944-54.

Oresic, M., S. Simell, M. Sysi-Aho, K. Näntö-Salonen, T. Seppänen-Laakso, V. Parikka, M. Katajamaa, A. Hekkala, I. Mattila, P. Keskinen, L. Yetukuri, A. Reinikainen, J. Lähde, T. Suortti, J. Hakalax, T. Simell, H. Hyöty, R. Veijola, J. Ilonen, R. Lahesmaa, M. Knip & O. Simell (2008) Dysregulation of lipid and amino acid metabolism precedes islet autoimmunity in children who later progress to type 1 diabetes. *J Exp Med,* 205**,** 2975-84.

Orsenigo, F., C. Giampietro, A. Ferrari, M. Corada, A. Galaup, S. Sigismund, G. Ristagno, L. Maddaluno, G. Y. Koh, D. Franco, V. Kurtcuoglu, D. Poulikakos, P. Baluk, D. McDonald, M. Grazia Lampugnani & E. Dejana (2012) Phosphorylation of VE-cadherin is modulated by haemodynamic forces and contributes to the regulation of vascular permeability in vivo. *Nat Commun,* 3**,** 1208.

Palade, G. E. (1953) An electron microscope study of the mitochondrial structure. *J Histochem Cytochem,* 1**,** 188-211.

Palmer, R. M., A. G. Ferrige & S. Moncada (1987) Nitric oxide release accounts for the biological activity of endothelium-derived relaxing factor. *Nature,* 327**,** 524-6.

Pappenheimer, J. R., E. M. Renkin & L. M. Borrero (1951) Filtration, diffusion and molecular sieving through peripheral capillary membranes; a contribution to the pore theory of capillary permeability. *Am J Physiol,* 167**,** 13-46.

Patel, K. D., S. L. Cuvelier & S. Wiehler (2002) Selectins: critical mediators of leukocyte recruitment. *Semin Immunol,* 14**,** 73-81.

Patino-Lopez, G., X. Dong, K. Ben-Aissa, K. M. Bernot, T. Itoh, M. Fukuda, M. J. Kruhlak, L. E. Samelson & S. Shaw (2008) Rab35 and its GAP EPI64C in T cells regulate receptor recycling and immunological synapse formation. *J Biol Chem,* 283**,** 18323-30.

Perez-Moreno, M. & E. Fuchs (2006) Catenins: keeping cells from getting their signals crossed. *Dev Cell,* 11**,** 601-12.

Perriere, N., P. Demeuse, E. Garcia, A. Regina, M. Debray, J. P. Andreux, P. Couvreur, J. M. Scherrmann, J. Temsamani, P. O. Couraud, M. A. Deli & F. Roux (2005) Puromycin-based purification of rat brain capillary endothelial

cell cultures. Effect on the expression of blood-brain barrier-specific properties. *J.Neurochem.,* 93**,** 279-289.

Petreaca, M. L., M. Yao, Y. Liu, K. Defea & M. Martins-Green (2007) Transactivation of vascular endothelial growth factor receptor-2 by interleukin-8 (IL-8/CXCL8) is required for IL-8/CXCL8-induced endothelial permeability. *Mol Biol Cell,* 18**,** 5014-23.

Pirillo, A., G. D. Norata & A. L. Catapano (2013) LOX-1, OxLDL, and atherosclerosis. *Mediators Inflamm,* 2013**,** 152786.

Pober, J. S. & W. C. Sessa (2007) Evolving functions of endothelial cells in inflammation. *Nat Rev Immunol,* 7**,** 803-15.

Pokutta, S. & W. I. Weis (2007) Structure and mechanism of cadherins and catenins in cell-cell contacts. *Annu Rev Cell Dev Biol,* 23**,** 237-61.

Prasain, N. & T. Stevens (2009) The actin cytoskeleton in endothelial cell phenotypes. *Microvasc Res,* 77**,** 53-63.

Predescu, D. & G. E. Palade (1993) Plasmalemmal vesicles represent the large pore system of continuous microvascular endothelium. *Am J Physiol,* 265**,** H725-33.

Predescu, S. A., D. N. Predescu & A. B. Malik (2007) Molecular determinants of endothelial transcytosis and their role in endothelial permeability. *Am J Physiol Lung Cell Mol Physiol,* 293**,** L823-42.

Pries, A. R. & T. W. Secomb (2009) Origins of heterogeneity in tissue perfusion and metabolism. *Cardiovasc Res,* 81**,** 328-35.

Pugsley, M. K. & R. Tabrizchi (2000) The vascular system. An overview of structure and function. *J Pharmacol Toxicol Methods,* 44**,** 333-40.

Qiao, J., F. Huang, R. P. Naikawadi, K. S. Kim, T. Said & H. Lum (2006) Lysophosphatidylcholine impairs endothelial barrier function through the G protein-coupled receptor GPR4. *Am J Physiol Lung Cell Mol Physiol,* 291**,** L91-101.

Quinton, M. S. & B. K. Yamamoto (2006) Causes and consequences of methamphetamine and MDMA toxicity. *AAPS J,* 8**,** E337-47.

Rabini, R. A., R. Galassi, P. Fumelli, N. Dousset, M. L. Solera, P. Valdiguie, G. Curatola, G. Ferretti, M. Taus & L. Mazzanti (1994) Reduced Na(+)-K(+)-ATPase activity and plasma lysophosphatidylcholine concentrations in diabetic patients. *Diabetes,* 43**,** 915-9.

Rahman, A., K. N. Anwar, S. Uddin, N. Xu, R. D. Ye, L. C. Platanias & A. B. Malik (2001) Protein kinase C-delta regulates thrombin-induced ICAM-1 gene expression in endothelial cells via activation of p38 mitogen-activated protein kinase. *Mol Cell Biol,* 21**,** 5554-65.

Raleigh, D. R., D. M. Boe, D. Yu, C. R. Weber, A. M. Marchiando, E. M. Bradford, Y. Wang, L. Wu, E. E. Schneeberger, L. Shen & J. R. Turner (2011) Occludin S408 phosphorylation regulates tight junction protein interactions and barrier function. *J Cell Biol,* 193**,** 565-82.

Raymond, J. J., D. M. Robertson & H. B. Dinsdale (1986) Pharmacological modification of bradykinin induced breakdown of the blood-brain barrier. *Can J Neurol Sci,* 13**,** 214-20.

Regina, A., I. A. Romero, J. Greenwood, P. Adamson, J. M. Bourre, P. O. Couraud & F. Roux (1999) Dexamethasone regulation of P-glycoprotein activity in an immortalized rat brain endothelial cell line, GPNT. *J.Neurochem.,* 73**,** 1954-1963.

Reitsma, S., D. W. Slaaf, H. Vink, M. A. van Zandvoort & M. G. oude Egbrink (2007) The endothelial glycocalyx: composition, functions, and visualization. *Pflugers Arch,* 454**,** 345-59.

Revenu, C., R. Athman, S. Robine & D. Louvard (2004) The co-workers of actin filaments: from cell structures to signals. *Nat Rev Mol Cell Biol,* 5**,** 635-46.

Rippe, B. & B. Haraldsson (1994) Transport of macromolecules across microvascular walls: the two-pore theory. *Physiol Rev,* 74**,** 163-219.

Rippe, B., B. I. Rosengren, O. Carlsson & D. Venturoli (2002) Transendothelial transport: the vesicle controversy. *J Vasc Res,* 39**,** 375-90.

Rist, R. J., I. A. Romero, M. W. Chan, P. O. Couraud, F. Roux & N. J. Abbott (1997) F-actin cytoskeleton and sucrose permeability of immortalised rat brain microvascular endothelial cell monolayers: effects of cyclic AMP and astrocytic factors. *Brain Res,* 768**,** 10-8.

Rosenberg, R. D. & W. C. Aird (1999) Vascular-bed--specific hemostasis and hypercoagulable states. *N Engl J Med,* 340**,** 1555-64.

Rosenegger, D. G. & G. R. Gordon (2015) A slow or modulatory role of astrocytes in neurovascular coupling. *Microcirculation,* 22**,** 197-203.

Rothe, C. F. (1983) Reflex control of veins and vascular capacitance. *Physiol Rev,* 63**,** 1281-342.

Sakurai, T., M. J. Woolls, S. W. Jin, M. Murakami & M. Simons (2014) Inter-cellular exchange of cellular components via VE-cadherin-dependent trans-endocytosis. *PLoS One,* 9**,** e90736.

Sandoo, A., J. J. van Zanten, G. S. Metsios, D. Carroll & G. D. Kitas (2010) The endothelium and its role in regulating vascular tone. *Open Cardiovasc Med J,* 4**,** 302-12.

Sarker, M. H., A. S. Easton & P. A. Fraser (1998) Regulation of cerebral microvascular permeability by histamine in the anaesthetized rat. *J.Physiol,* 507 ( Pt 3)**,** 909-918.

Sarker, M. H., D. E. Hu & P. A. Fraser (2010) Regulation of cerebromicrovascular permeability by lysophosphatidic acid. *Microcirculation.,* 17**,** 39-46.

Saunders, N. R., R. Daneman, K. M. Dziegielewska & S. A. Liddelow (2013) Transporters of the blood-brain and blood-CSF interfaces in development and in the adult. *Mol Aspects Med,* 34**,** 742-52.

Saunders, N. R., C. J. Ek, M. D. Habgood & K. M. Dziegielewska (2008) Barriers in the brain: a renaissance? *Trends Neurosci,* 31**,** 279-86.

Sawamiphak, S., S. Seidel, C. L. Essmann, G. A. Wilkinson, M. E. Pitulescu, T. Acker & A. Acker-Palmer (2010) Ephrin-B2 regulates VEGFR2 function in developmental and tumour angiogenesis. *Nature,* 465**,** 487-91.

Schaeffer, D. F., M. Riazy, K. S. Parhar, J. H. Chen, V. Duronio, T. Sawamura & U. P. Steinbrecher (2009) LOX-1 augments oxLDL uptake by lysoPC-stimulated murine macrophages but is not required for oxLDL clearance from plasma. *J Lipid Res,* 50**,** 1676-84.

Schelbert, H. R. (2010) Anatomy and physiology of coronary blood flow. *J Nucl Cardiol,* 17**,** 545-54.

Schleich, J. 2002. Development of the human heart: days 15–21. 487. Heart.

Schleicher, M., J. Yu, T. Murata, B. Derakhshan, D. Atochin, L. Qian, S. Kashiwagi, A. Di Lorenzo, K. D. Harrison, P. L. Huang & W. C. Sessa (2009) The Akt1-eNOS axis illustrates the specificity of kinase-substrate relationships in vivo. *Sci Signal,* 2**,** ra41.

Schulze, C., C. Smales, L. L. Rubin & J. M. Staddon (1997) Lysophosphatidic acid increases tight junction permeability in cultured brain endothelial cells. *J Neurochem,* 68**,** 991-1000.

Scott, A. & H. Mellor (2009) VEGF receptor trafficking in angiogenesis. *Biochem Soc Trans,* 37**,** 1184-8.

Shibasaki, M., T. E. Wilson & C. G. Crandall (2006) Neural control and mechanisms of eccrine sweating during heat stress and exercise. *J Appl Physiol (1985),* 100**,** 1692-701.

Shima, D. T., A. P. Adamis, N. Ferrara, K. T. Yeo, T. K. Yeo, R. Allende, J. Folkman & P. A. D'Amore (1995) Hypoxic induction of endothelial cell growth factors in retinal cells: identification and characterization of vascular endothelial growth factor (VEGF) as the mitogen. *Mol Med,* 1**,** 182-93.

Shimada, H. & L. E. Rajagopalan (2010) Rho-kinase mediates lysophosphatidic acid-induced IL-8 and MCP-1 production via p38 and JNK pathways in human endothelial cells. *FEBS Lett,* 584**,** 2827-32.

Shue, E. H., E. B. Carson-Walter, Y. Liu, B. N. Winans, Z. S. Ali, J. Chen & K. A. Walter (2008) Plasmalemmal vesicle associated protein-1 (PV-1) is a marker of blood-brain barrier disruption in rodent models. *BMC Neurosci,* 9**,** 29.

Shvets, E., V. Bitsikas, G. Howard, C. G. Hansen & B. J. Nichols (2015) Dynamic caveolae exclude bulk membrane proteins and are required for sorting of excess glycosphingolipids. *Nat Commun,* 6**,** 6867.

Simionescu, M., A. Gafencu & F. Antohe (2002) Transcytosis of plasma macromolecules in endothelial cells: a cell biological survey. *Microsc Res Tech,* 57**,** 269-88.

Simionescu, M., N. Ghinea, A. Fixman, M. Lasser, L. Kukes, N. Simionescu & G. E. Palade (1988) The cerebral microvasculature of the rat: structure and luminal surface properties during early development. *J Submicrosc Cytol Pathol,* 20**,** 243-61.

Simo, R., J. M. Sundstrom & D. A. Antonetti (2014) Ocular Anti-VEGF therapy for diabetic retinopathy: the role of VEGF in the pathogenesis of diabetic retinopathy. *Diabetes Care,* 37**,** 893-9.

Sit, S. T. & E. Manser (2011) Rho GTPases and their role in organizing the actin cytoskeleton. *J Cell Sci,* 124**,** 679-83.

Sorkin, A. & L. K. Goh (2009) Endocytosis and intracellular trafficking of ErbBs. *Exp Cell Res,* 315**,** 683-96.

Sorokin, L. (2010) The impact of the extracellular matrix on inflammation. *Nat Rev Immunol,* 10**,** 712-23.

Spitzer, M., J. Wildenhain, J. Rappsilber & M. Tyers (2014) BoxPlotR: a web tool for generation of box plots. *Nat Methods,* 11**,** 121-2.

Spyridopoulos, I., C. Luedemann, D. Chen, M. Kearney, D. Chen, T. Murohara, N. Principe, J. M. Isner & D. W. Losordo (2002) Divergence of angiogenic and vascular permeability signaling by VEGF: inhibition of protein kinase C suppresses VEGF-induced angiogenesis, but promotes VEGF-induced, NO-dependent vascular permeability. *Arterioscler Thromb Vasc Biol,* 22**,** 901-6.

Stafforini, D. M. (2009) Biology of platelet-activating factor acetylhydrolase (PAF-AH, lipoprotein associated phospholipase A2). *Cardiovasc Drugs Ther,* 23**,** 73-83.

Stamatovic, S. M., R. F. Keep & A. V. Andjelkovic (2008) Brain endothelial cell-cell junctions: how to "open" the blood brain barrier. *Curr Neuropharmacol,* 6**,** 179-92.

Stanimirovic, D. B. & A. Friedman (2012) Pathophysiology of the neurovascular unit: disease cause or consequence? *J Cereb Blood Flow Metab,* 32**,** 1207-21.

Steed, E., M. S. Balda & K. Matter (2010) Dynamics and functions of tight junctions. *Trends Cell Biol.,* 20**,** 142-149.

Stefanovska, A. & M. Bracic. 1999. Physics of the human cardiovascular system. 31-55. Contemporary Physics.

Steinberg, D. (1997) Low density lipoprotein oxidation and its pathobiological significance. *J Biol Chem,* 272**,** 20963-6.

Stenmark, H. (2009) Rab GTPases as coordinators of vesicle traffic. *Nat Rev Mol Cell Biol,* 10**,** 513-25.

Stewart, C. R., L. M. Stuart, K. Wilkinson, J. M. van Gils, J. Deng, A. Halle, K. J. Rayner, L. Boyer, R. Zhong, W. A. Frazier, A. Lacy-Hulbert, J. El Khoury, D. T. Golenbock & K. J. Moore (2010) CD36 ligands promote sterile inflammation through assembly of a Toll-like receptor 4 and 6 heterodimer. *Nat Immunol,* 11**,** 155-61.

Stitt, A. W., T. M. Curtis, M. Chen, R. J. Medina, G. J. McKay, A. Jenkins, T. A. Gardiner, T. J. Lyons, H. P. Hammes, R. Simó & N. Lois (2016) The progress in understanding and treatment of diabetic retinopathy. *Prog Retin Eye Res,* 51**,** 156-86.

Stossel, T. P., C. Chaponnier, R. M. Ezzell, J. H. Hartwig, P. A. Janmey, D. J. Kwiatkowski, S. E. Lind, D. B. Smith, F. S. Southwick & H. L. Yin (1985) Nonmuscle actin-binding proteins. *Annu Rev Cell Biol,* 1**,** 353-402.

Sugawara, J., Y. Saito, S. Maeda, M. Yoshizawa, H. Komine, M. Nakamura, R. Ajisaka & H. Tanaka (2014) Lack of changes in carotid artery compliance with systemic nitric oxide synthase inhibition. *J Hum Hypertens,* 28**,** 494-9.

Sumpio, B. E., J. T. Riley & A. Dardik (2002) Cells in focus: endothelial cell. *Int J Biochem Cell Biol,* 34**,** 1508-12.

Sun, M. K. (1995) Central neural organization and control of sympathetic nervous system in mammals. *Prog Neurobiol,* 47**,** 157-233.

Sun, Z., X. Li, S. Massena, S. Kutschera, N. Padhan, L. Gualandi, V. Sundvold-Gjerstad, K. Gustafsson, W. W. Choy, G. Zang, M. Quach, L. Jansson, M. Phillipson, M. R. Abid, A. Spurkland & L. Claesson-Welsh (2012) VEGFR2 induces c-Src signaling and vascular permeability in vivo via the adaptor protein TSAd. *J.Exp.Med.,* 209**,** 1363-1377.

Sundd, P., M. K. Pospieszalska, L. S. Cheung, K. Konstantopoulos & K. Ley (2011) Biomechanics of leukocyte rolling. *Biorheology,* 48**,** 1-35.

Sweeney, M. D., S. Ayyadurai & B. V. Zlokovic (2016) Pericytes of the neurovascular unit: key functions and signaling pathways. *Nat Neurosci,* 19**,** 771-83.

Sylvester, J. T., L. A. Shimoda, P. I. Aaronson & J. P. Ward (2012) Hypoxic pulmonary vasoconstriction. *Physiol Rev,* 92**,** 367-520.

Taddei, A., C. Giampietro, A. Conti, F. Orsenigo, F. Breviario, V. Pirazzoli, M. Potente, C. Daly, S. Dimmeler & E. Dejana (2008) Endothelial adherens junctions control tight junctions by VE-cadherin-mediated upregulation of claudin-5. *Nat Cell Biol,* 10**,** 923-34.

Takahashi, H. & M. Shibuya (2005) The vascular endothelial growth factor (VEGF)/VEGF receptor system and its role under physiological and pathological conditions. *Clin.Sci.(Lond),* 109**,** 227-241.

Tanimoto, T., Z. G. Jin & B. C. Berk (2002) Transactivation of vascular endothelial growth factor (VEGF) receptor Flk-1/KDR is involved in sphingosine 1-phosphate-stimulated phosphorylation of Akt and endothelial nitric-oxide synthase (eNOS). *J Biol Chem,* 277**,** 42997-3001.

Thompson, A., P. Gao, L. Orfei, S. Watson, E. Di Angelantonio, S. Kaptoge, C. Ballantyne, C. P. Cannon, M. Criqui, M. Cushman, A. Hofman, C. Packard, S. G. Thompson, R. Collins, J. Danesh & L.-P. S. Collaboration (2010) Lipoprotein-associated phospholipase A(2) and risk of coronary disease, stroke, and mortality: collaborative analysis of 32 prospective studies. *Lancet,* 375**,** 1536-44.

Thuringer, D., L. Maulon & C. Frelin (2002) Rapid transactivation of the vascular endothelial growth factor receptor KDR/Flk-1 by the bradykinin B2 receptor contributes to endothelial nitric-oxide synthase activation in cardiac capillary endothelial cells. *J Biol Chem,* 277**,** 2028-32.

Thygesen, K., J. S. Alpert, A. S. Jaffe, M. L. Simoons, B. R. Chaitman, H. D. White & T. F. f. t. U. D. o. M. Infarction (2012) Third universal definition of myocardial infarction. *Nat Rev Cardiol,* 9**,** 620-33.

Tietz, S. & B. Engelhardt (2015) Brain barriers: Crosstalk between complex tight junctions and adherens junctions. *J Cell Biol,* 209**,** 493-506.

Tiruppathi, C., W. Yan, R. Sandoval, T. Naqvi, A. N. Pronin, J. L. Benovic & A. B. Malik (2000) G protein-coupled receptor kinase-5 regulates thrombin-activated signaling in endothelial cells. *Proc Natl Acad Sci U S A,* 97**,** 7440-5.

Tomas, A., S. O. Vaughan, T. Burgoyne, A. Sorkin, J. A. Hartley, D. Hochhauser & C. E. Futter (2015) WASH and Tsg101/ALIX-dependent diversion of stress-internalized EGFR from the canonical endocytic pathway. *Nat Commun,* 6**,** 7324.

Tsukasaki, Y., K. Kitamura, K. Shimizu, A. H. Iwane, Y. Takai & T. Yanagida (2007) Role of multiple bonds between the single cell adhesion molecules, nectin and cadherin, revealed by high sensitive force measurements. *J Mol Biol,* 367**,** 996-1006.

Tsukita, S., M. Furuse & M. Itoh (2001) Multifunctional strands in tight junctions. *Nat Rev Mol Cell Biol,* 2**,** 285-93.

Turowski, P. & B. A. Kenny (2015) The blood-brain barrier and methamphetamine: open sesame? *Front Neurosci,* 9, 156.

Turowski, P., R. Martinelli, R. Crawford, D. Wateridge, A. P. Papageorgiou, M. G. Lampugnani, A. C. Gamp, D. Vestweber, P. Adamson, E. Dejana & J. Greenwood (2008) Phosphorylation of vascular endothelial cadherin controls lymphocyte emigration. *J.Cell Sci.,* 121, 29-37.

Ueno, M., Y. Chiba, K. Matsumoto, R. Murakami, R. Fujihara, M. Kawauchi, H. Miyanaka & T. Nakagawa (2016) Blood-brain barrier damage in vascular dementia. *Neuropathology,* 36, 115-24.

Urich, E., C. Patsch, S. Aigner, M. Graf, R. Iacone & P. O. Freskgard (2013) Multicellular self-assembled spheroidal model of the blood brain barrier. *Sci Rep,* 3, 1500.

van den Berg, B. M., H. Vink & J. A. Spaan (2003) The endothelial glycocalyx protects against myocardial edema. *Circ Res,* 92, 592-4.

van der Sluijs, P., M. Hull, P. Webster, P. Male, B. Goud & I. Mellman (1992) The small GTP-binding protein rab4 controls an early sorting event on the endocytic pathway. *Cell,* 70, 729-40.

van Hinsbergh, V. W. & G. P. van Nieuw Amerongen (2002) Intracellular signalling involved in modulating human endothelial barrier function. *J Anat,* 200, 549-60.

Van Itallie, C. M. & J. M. Anderson (2014) Architecture of tight junctions and principles of molecular composition. *Semin Cell Dev Biol,* 36, 157-65.

van Nieuw Amerongen, G. P., S. van Delft, M. A. Vermeer, J. G. Collard & V. W. van Hinsbergh (2000) Activation of RhoA by thrombin in endothelial hyperpermeability: role of Rho kinase and protein tyrosine kinases. *Circ Res,* 87, 335-40.

Van Teeffelen, J. W., J. Brands, E. S. Stroes & H. Vink (2007) Endothelial glycocalyx: sweet shield of blood vessels. *Trends Cardiovasc Med,* 17, 101-5.

Vestweber, D. (2007) Adhesion and signaling molecules controlling the transmigration of leukocytes through endothelium. *Immunol Rev,* 218, 178-96.

Vito, R. P. & S. A. Dixon (2003) Blood vessel constitutive models-1995-2002. *Annu Rev Biomed Eng,* 5, 413-39.

Vladykovskaya, E., E. Ozhegov, J. D. Hoetker, Z. Xie, Y. Ahmed, J. Suttles, S. Srivastava, A. Bhatnagar & O. A. Barski (2011) Reductive metabolism increases the proinflammatory activity of aldehyde phospholipids. *J Lipid Res,* 52, 2209-25.

von Wedel-Parlow, M., S. Schrot, J. Lemmen, L. Treeratanapiboon, J. Wegener & H. J. Galla (2011) Neutrophils cross the BBB primarily on transcellular pathways: an in vitro study. *Brain Res,* 1367, 62-76.

Wagner, R. C. & S. C. Chen (1991) Transcapillary transport of solute by the endothelial vesicular system: evidence from thin serial section analysis. *Microvasc Res,* 42, 139-50.

Walsh, M. P. & W. C. Cole (2013) The role of actin filament dynamics in the myogenic response of cerebral resistance arteries. *J Cereb Blood Flow Metab,* 33**,** 1-12.

Wang, W. Y., J. Zhang, W. Y. Wu, J. Li, Y. L. Ma, W. H. Chen, H. Yan, K. Wang, W. W. Xu, J. H. Shen & Y. P. Wang (2011) Inhibition of lipoprotein-associated phospholipase A2 ameliorates inflammation and decreases atherosclerotic plaque formation in ApoE-deficient mice. *PLoS One,* 6**,** e23425.

Wang, Y., H. Miao, S. Li, K. D. Chen, Y. S. Li, S. Yuan, J. Y. Shyy & S. Chien (2002) Interplay between integrins and FLK-1 in shear stress-induced signaling. *Am J Physiol Cell Physiol,* 283**,** C1540-7.

Warren, C. M., S. Ziyad, A. Briot, A. Der & M. L. Iruela-Arispe (2014) A ligand-independent VEGFR2 signaling pathway limits angiogenic responses in diabetes. *Sci Signal,* 7**,** ra1.

Weibel, E. R. & G. E. Palade (1964) New Cytoplasmic Components in Arterial Endothelia. *J Cell Biol,* 23**,** 101-12.

Weinbaum, S., J. M. Tarbell & E. R. Damiano (2007) The structure and function of the endothelial glycocalyx layer. *Annu Rev Biomed Eng,* 9**,** 121-67.

Weis, S. M. & D. A. Cheresh (2005) Pathophysiological consequences of VEGF-induced vascular permeability. *Nature,* 437**,** 497-504.

Weksler, B., I. A. Romero & P. O. Couraud (2013) The hCMEC/D3 cell line as a model of the human blood brain barrier. *Fluids Barriers CNS,* 10**,** 16.

Weltzien, H. U. (1979) Cytolytic and membrane-perturbing properties of lysophosphatidylcholine. *Biochim Biophys Acta,* 559**,** 259-87.

Wessel, F., M. Winderlich, M. Holm, M. Frye, R. Rivera-Galdos, M. Vockel, R. Linnepe, U. Ipe, A. Stadtmann, A. Zarbock, A. F. Nottebaum & D. Vestweber (2014) Leukocyte extravasation and vascular permeability are each controlled in vivo by different tyrosine residues of VE-cadherin. *Nat Immunol,* 15**,** 223-30.

West, J. B. & O. Mathieu-Costello (1999) Structure, strength, failure, and remodeling of the pulmonary blood-gas barrier. *Annu Rev Physiol,* 61**,** 543-72.

Wilensky, R. L., Y. Shi, E. R. Mohler, D. Hamamdzic, M. E. Burgert, J. Li, A. Postle, R. S. Fenning, J. G. Bollinger, B. E. Hoffman, D. J. Pelchovitz, J. Yang, R. C. Mirabile, C. L. Webb, L. Zhang, P. Zhang, M. H. Gelb, M. C. Walker, A. Zalewski & C. H. Macphee (2008) Inhibition of lipoprotein-associated phospholipase A2 reduces complex coronary atherosclerotic plaque development. *Nat Med,* 14**,** 1059-66.

Williams, L. R. & R. W. Leggett (1989) Reference values for resting blood flow to organs of man. *Clin Phys Physiol Meas,* 10**,** 187-217.

Winkler, E. A., R. D. Bell & B. V. Zlokovic (2011) Central nervous system pericytes in health and disease. *Nat Neurosci,* 14**,** 1398-405.

Wittchen, E. S. (2009) Endothelial signaling in paracellular and transcellular leukocyte transmigration. *Front Biosci (Landmark Ed),* 14**,** 2522-45.

Wolburg, H., K. Wolburg-Buchholz & B. Engelhardt (2005) Diapedesis of mononuclear cells across cerebral venules during experimental autoimmune

encephalomyelitis leaves tight junctions intact. *Acta Neuropathol.(Berl),* 109**,** 181-190.

Wong, B. H., J. P. Chan, A. Cazenave-Gassiot, R. W. Poh, J. C. Foo, D. L. Galam, S. Ghosh, L. N. Nguyen, V. A. Barathi, S. W. Yeo, C. D. Luu, M. R. Wenk & D. L. Silver (2016) Mfsd2a Is a Transporter for the Essential ω-3 Fatty Acid Docosahexaenoic Acid (DHA) in Eye and Is Important for Photoreceptor Cell Development. *J Biol Chem,* 291**,** 10501-14.

Worzfeld, T. & M. Schwaninger (2015) Apicobasal polarity of brain endothelial cells. *J Cereb Blood Flow Metab*.

Xiao, K., J. Garner, K. M. Buckley, P. A. Vincent, C. M. Chiasson, E. Dejana, V. Faundez & A. P. Kowalczyk (2005) p120-Catenin regulates clathrin-dependent endocytosis of VE-cadherin. *Mol.Biol.Cell,* 16**,** 5141-5151.

Yamamoto, H., M. Ehling, K. Kato, K. Kanai, M. van Lessen, M. Frye, D. Zeuschner, M. Nakayama, D. Vestweber & R. H. Adams (2015) Integrin β1 controls VE-cadherin localization and blood vessel stability. *Nat Commun,* 6**,** 6429.

Yan, Z., Z. G. Wang, N. Segev, S. Hu, R. D. Minshall, R. O. Dull, M. Zhang, A. B. Malik & G. Hu (2016) Rab11a Mediates Vascular Endothelial-Cadherin Recycling and Controls Endothelial Barrier Function. *Arterioscler Thromb Vasc Biol,* 36**,** 339-49.

Yang, L., J. R. Kowalski, P. Yacono, M. Bajmoczi, S. K. Shaw, R. M. Froio, D. E. Golan, S. M. Thomas & F. W. Luscinskas (2006) Endothelial cell cortactin coordinates intercellular adhesion molecule-1 clustering and actin cytoskeleton remodeling during polymorphonuclear leukocyte adhesion and transmigration. *J Immunol,* 177**,** 6440-9.

Yau, J. W., S. L. Rogers, R. Kawasaki, E. L. Lamoureux, J. W. Kowalski, T. Bek, S. J. Chen, J. M. Dekker, A. Fletcher, J. Grauslund, S. Haffner, R. F. Hamman, M. K. Ikram, T. Kayama, B. E. Klein, R. Klein, S. Krishnaiah, K. Mayurasakorn, J. P. O'Hare, T. J. Orchard, M. Porta, M. Rema, M. S. Roy, T. Sharma, J. Shaw, H. Taylor, J. M. Tielsch, R. Varma, J. J. Wang, N. Wang, S. West, L. Xu, M. Yasuda, X. Zhang, P. Mitchell, T. Y. Wong & M.-A. f. E. D. M.-E. S. Group (2012) Global prevalence and major risk factors of diabetic retinopathy. *Diabetes Care,* 35**,** 556-64.

Yuan, L., A. Le Bras, A. Sacharidou, K. Itagaki, Y. Zhan, M. Kondo, C. V. Carman, G. E. Davis, W. C. Aird & P. Oettgen (2012) ETS-related gene (ERG) controls endothelial cell permeability via transcriptional regulation of the claudin 5 (CLDN5) gene. *J Biol Chem,* 287**,** 6582-91.

Yung, Y. C., N. C. Stoddard & J. Chun (2014) LPA receptor signaling: pharmacology, physiology, and pathophysiology. *J Lipid Res,* 55**,** 1192-214.

Zawieja, D. (2005) Lymphatic biology and the microcirculation: past, present and future. *Microcirculation,* 12**,** 141-50.

Zeng, G. & M. J. Quon (1996) Insulin-stimulated production of nitric oxide is inhibited by wortmannin. Direct measurement in vascular endothelial cells. *J Clin Invest,* 98**,** 894-8.

Zhao, L. N., Z. H. Yang, Y. H. Liu, H. Q. Ying, H. Zhang & Y. X. Xue (2011) Vascular endothelial growth factor increases permeability of the blood-tumor

barrier via caveolae-mediated transcellular pathway. *J Mol Neurosci,* 44**,** 122-9.

Zhao, P., M. Metcalf & N. W. Bunnett (2014) Biased signaling of protease-activated receptors. *Front Endocrinol (Lausanne),* 5**,** 67.

Zhou, Y., Y. Wang, M. Tischfield, J. Williams, P. M. Smallwood, A. Rattner, M. M. Taketo & J. Nathans (2014) Canonical WNT signaling components in vascular development and barrier formation. *J Clin Invest,* 124**,** 3825-46.

Zihni, C., C. Mills, K. Matter & M. S. Balda (2016) Tight junctions: from simple barriers to multifunctional molecular gates. *Nat Rev Mol Cell Biol,* 17**,** 564-80.

Zlokovic, B. V. (2008) The blood-brain barrier in health and chronic neurodegenerative disorders. *Neuron,* 57**,** 178-201.

# Chapter 9   APPENDIX

Martins T, Burgoyne T, **Kenny BA**, Hudson N, Futter CE, Ambrósio AF, Silva AP, Greenwood J, Turowski P. (2013) Methamphetamine-induced nitric oxide promotes vesicular transport in blood-brain barrier endothelial cells. *Neuropharmacology*. 65:74-82.

Turowski P, **Kenny BA**. (2015) The blood-brain barrier and methamphetamine: open sesame? *Frontiers in Neuroscience*. 5;9:156.

Canning P, **Kenny BA**, Prise V, Glenn J, Sarker MH, Hudson N, Brandt M, Lopez FJ, Gale D, Luthert PJ, Adamson P, Turowski P, Stitt AW. (2016) Lipoprotein-associated phospholipase A2 (Lp-PLA2) as a therapeutic target to prevent retinal vasopermeability during diabetes. *Proceedings of the National Academy of Sciences of the United States of America*. 113 (26): 7213-8.

Hudson N, Dragoni S, McKenzie JA, **Kenny BA**, Gill Y, Blaber R, Adamson P, Greenwood J, Turowski P. Endothelial MAPKs direct ICAM-1 signaling to divergent inflammatory functions. In preparation.